AUTHOR: OGBUKE, I.

TITLE: Preparation, characterization and testing of inorganic ceramic membranes.

YEAR: 2013

This work was submitted to- and approved by Robert Gordon University in partial fulfilment of the following degree:
Doctor of Philosophy, Faculty of Design and Technology, School of Engineering

PREPARATION, CHARACTERIZATION

AND

TESTING OF INORGANIC CERAMIC MEMBRANES

Ikechukwu(Iyke) Ogbuke

Thesis submitted for the degree of Doctor of Philosophy

The Robert Gordon University,

Faculty of Design and Technology,

School of Engineering,

Aberdeen, UK

Oct.,2013.

ABSTRACT

A novel approach to enhance the concentration of Carbon dioxide to economic scale using low efficient Inorganic Ceramic membranes has been proposed. This was achieved by the addition of second and third stage permeation trains to the existing low CO_2 recovering Ceramic Inorganic membranes. The Inorganic Ceramic membrane development involved modification of Alpha Alumina support with Gamma Alumina for improved surface area. Further modifications with Magnesium Oxide and Silicon Elastomer showed increase in the selectivity of Carbon dioxide molecules over Nitrogen, Methane, Argon, and Helium molecules, both in pure and mixture forms. A simulated flue gas feed concentration of CO_2-14% and N_2-86% was found to be concentrated more than 90% of CO_2. The Carbon dioxide permeability was found to decrease as the membrane thickness and number of dipping increased, whereas, the selectivity of the Carbon dioxide over Nitrogen, Argon, Helium and Methane molecules improved with the use of modified membranes compared to membrane support only. The testing of the fabricated membrane demonstrated that modified membrane at third stage permeation at a pressure drop of 9.00KPa and operating temperature of 296K was capable of recovering more than 90% of Carbon dioxide from a feed gas mixture of 14%-CO_2 and N_2-86%.The permeability of the Carbon dioxide gas molecules that was recovered at the above listed operating conditions was $4.26X10^{-12}$ (mol.m/m^2.s.Pa). This was achieved by surface flow mechanism and membrane pore sizes estimated were found to be macroporoes and mesopores with their EDXA and SEM images. A numerical algorithm was used to estimate the errors. The error was found to decrease as the permeation value increases.

DEDICATIONS

I dedicate this piece of work to my entire family members, my sponsors, especially to my wife, daughter and son, Mrs Uzoamaka Ogbuke, Miss Mesoma Favor Ogbuke and Master Kosisochukwu Andre Ogbuke for their family supports throughout the time of this work.

ACKNOWLEDGEMENTS

I would like to seize this opportunity to extend my profound greetings to my supervisor, Professor Edward Gobina, for his tireless and most professional supervisions and guidance offered to me during my entire year on this project.

My appreciations go to the entire technical teams of Robert Gordon University, especially, Bill Worker, and Steve who had just recently retired, for their understanding and support in sourcing most of my project resources. Also, my regards go to my colleagues, Abubakar Alkali and Mohammed Kajama, who are working on their various projects, for their advice and contributions during my research time.

NOMENCLATURES

A = Measured Value

B_O = Geometric factor of membrane due to viscous,

C = Concentration

D_S=Surface diffusion coefficient, (m^2/sec)

D_O=Outer diameter of the membrane, m

Ft= Permeance (mol/m^2.S.Pa)

F_T= Permeability denotation (mol.m/m^2.S.Pa)

J= flux, ($mol \cdot m^{-2} \cdot s^{-1}$)

Kn = Knudsen Number

K_S= tortuosity factor for the pores

K=permeability coefficient (mol.m/m^2.s.Pa),

K_o = Knudsen Flow, (mol/m^2.s)

L_O= Effective length of the membrane, m

L_p =length of the pore,

P = Pressure (Pascal) or (Bar)

Q = Volume Flow rate of the permeated gas through the membrane, m^3/s

R = Universal gas constant, (J/kg/K)

MW=Molecular weight of permeating gas, (kg/mole)

T=Absolute temperature, (K)

R_P =Membrane pore size, nm

r_p =pore radius, (nm)

N_S=amount of gas transported in unit time across the membrane by surface flow mechanism, kmol/s

N_t= total number pores, having a radii from zero to R_{max}

Ph= pressure on the high pressure side of the membrane, Pa.

P_F= Feed Pressure, Bar or Pascal

P_R=Retentate Pressure, Bar or Pascal

P_P= Permeate Pressure, Bar or Pascal

Pl= pressure on the low pressure side of the membrane, Pa

P_1= Feed pressure (Pascal or Bar)

P_2= Permeate Pressure (Pascal or Bar)

R_{max}= Maximum pore radius (m)

r_P= Membrane pore radius, m

V_O= Viscous flow contribution (mol/m^2s)

Greek Letters

σ = Thickness of the membrane material, m

η = coefficient of viscosity of gases, Pa.s

ΔHa= Heat of Adsorption, KJ/mol

Å= Angstrom

λ =mean free path of gases, m

ρ =True density (kg/m^3)

ΔA= Estimated Error

ΔP=pressure drop across membrane, (Pa)

ρ_{app} =apparent density of the membrane, kg/m^3

Δq/Δp=amount of gas adsorbed in a given amount of membrane material, kmol/kg

μ = Dynamic viscosity of permeating gas, (Pascal. Sec)

∞ = proportionality constant

NOTES

Mixture A: [CO_2-14%, N_2-86%]

Mixture B: [CO_2-30%, N_2-70%]

Mixture C: [CO_2-60%, N_2-40%]

Membrane Support: Commercially supplied Alpha Alumina

Membrane A: Gamma Alumina modified membrane

Membrane B: Magnesium modified membrane

Membrane C: Silicon Elastomer modified membrane

Membrane D: Silicon Elastomer modified membrane with different concentration

Solution 1: Solution of magnesium oxide

Solution 2: Solution of Silicon Elastomer (Sylgard 184) with Isopentane (9:1)

Solution 3: Solution of Silicon Elastomer (Sylgard 184) with Isopentane (8:2)

TABLE OF FIGURES

List of Tables

TABLE OF Contents

1 INTRODUCTION

The uncontrollable emission of Carbon dioxide into the atmosphere has been scientifically proved to be the principal cause of global warming [1]. In order not to allow it to get to a dangerous stage, at the last Kyoto Treaty on Carbon Emission, it was agreed that every company should adopt a less carbon dioxide emission process, as a method of reducing the atmospheric concentration of Carbon dioxide. Also by reducing the emission, the Carbon dioxide would be captured, transported and then stored in a suitable container, preferably, in a geological storage. There are a number of commercially available technologies and many under research and development, for capturing carbon dioxide molecules. The availability of the fossil has made industrialization to depend so much on them to meet its energy needs. As the demand for the fossil fuel drives the combustion of the fuel, this has resulted to enormous release of the gas combustion waste (flue gas) which has different concentrations of carbon dioxide to the atmosphere. For years before now, the common practice in the fossil fuel related industries had been to release much produced combustion waste to the atmosphere. The increase in the temperature has been scientifically linked to the uncontrollable level in the concentration of the greenhouse gases [2]. Greenhouse gases occur naturally, but they are mostly produced as waste gases whenever there is combustion of fuels such as wood, wood products, solid wastes and fossil fuels (oil, natural gas and coal). Examples of the greenhouse gases are Carbon dioxide, Methane, Water Vapour, Nitrous Oxide, Chlorofluorocarbons (CFCs) and the Ozone in the lower atmosphere. Coal fired power plants produce up to 83% electricity sector's CO_2 emission, with most of the remaining emissions from natural gas fired power plant [2].These emissions are as the results of supplying electricity to homes, businesses and industries.

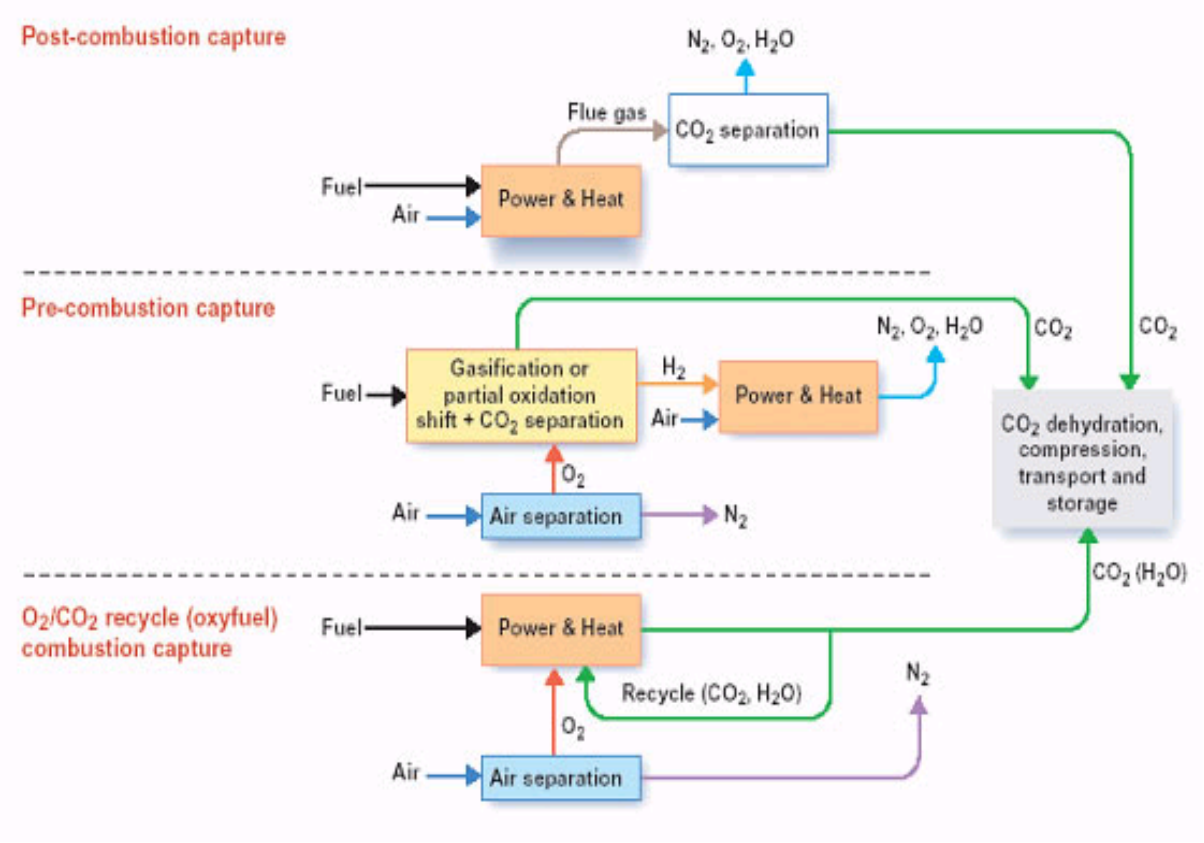

Figure 1:1 : Different CO_2 Capture Methods [2]

Figure 1:1 shows different Carbon dioxide capture methods. In post combustion method, Carbon dioxide molecules are capture after fossil fuel combustion, while in pre-combustion, the Carbon dioxide molecules are removed before combustion process take place [2].

Some methods of Carbon dioxide capture are already in commercial stage, while some are still under research and development stages. For instance, the CO_2 - Amine Absorption process has been in used by the industries for over two decades [3]. But because of high chemical usage and energy intensive nature of the process, there have been searches for a more efficient means of capturing Carbon dioxide from the industrial flue gas waste. This need for process efficiency has given birth to other capturing processes, for instance, Membrane Capturing process.

The application of the membrane materials depend on the operating condition of the process and the membrane process is categorized into two main groups: Organic membranes process and Inorganic membrane process [3]. Organic Membrane Carbon capture process has been developed with the membrane indicated high Carbon dioxide permeability and selectivity in a low temperature and non-acidic applications [5]. But because the compositions of the flue gas has the potential to form acids when in contact with associated flue gas water, the Organic membranes which have a low resistance to acids and low strength to withstand high temperature application will have limited opportunity to add to the efficiency of the Carbon dioxide capture [5]. This has limited the application of the Organic membranes suitable for Carbon dioxide capture from flue gas process. Recently, attention has been shifted to the Inorganic membrane process for capturing of Carbon dioxide from the flue gas. This is due to a high resistance to acids and ability to withstand elevated temperature application [5]. This research concentrated on the development of a Ceramic Inorganic membrane capable of capturing Carbon dioxide from the flue gas. These research ideas were started by Professor Edward Gobina and they contained in a US patent number 7,048,778 B2. The project was categorised into two phases: first stage involves fabrication of an Inorganic Ceramic membrane with a commercially available Alumina support; testing the membrane at a single staged processes; characterizing the developed membranes; modelling of the flow processes for membrane performance prediction. The second phase involves simulating a gas compressor in order to carry out permeation experiments in second and third stages. The simulated flue gas used throughout in this project has a composition of Carbon dioxide and Nitrogen only. The reason for this was because the flue gas produced from the power plant has both Carbon dioxide and Nitrogen as dominating compassions. The

first stage process involved concentrating the 14% of CO_2 in the feed up to 30%. The second and third stages involved in taking the 30% CO_2 as a feed concentration up to 60% and more, in the permeate section. The permeation experiments were conducted under different conditions, and the results were analysed and can be located in the later chapters.

2 LITERATURE REVIEW

2.1 INTRODUCTION

Since the introduction of Membrane technology to the processing industries, more attentions have been drawn to some engineering projects which were given little or no attention due to lack of ability by the existing technologies to harness them to their fullness. Some of the examples of the processes that gained increased attentions since the introduction of the Membrane Technology are development of Marginal fields, Natural Gas processing and Carbon dioxide capturing. The success of membrane technology as an effective means of treatment of fluids depends on ability of the membrane to satisfy applicable conditions. This means that the choice of a membrane is determined by the conditions of applications [5]. Some of the conditions to be considered in selecting membranes are as follows; temperature of the processing, the membrane mechanical strength, the Ph of the fluid and the affinity of the fluid to the membrane [5]. The first three conditions above are very important in selecting any membrane for effective application. Since the beginning of industrial revolution, the demand for fossil fuel has been on increase. This is due to the availability of the products in order to drive our industries to our much needed products. As the demand for the fossil fuel drive the combustion of the fuel which resulted to enormous release of the gas combustion waste to the atmosphere [6]. Fossil fuel is categorized into gas, oil and coal. Coal fired power plants produce up to 83% electricity sectors CO_2 emission, with most of the remaining emissions from natural gas fired power plant [6].These emissions were as the results of supplying electricity to homes, businesses and industries. Capturing of CO_2 from flue gases produced by the coal fired power plant has been in existence since the Carbon dioxide has been identified as one of the greenhouse gases with about 64%

greenhouse effect [6]. These methods of capture are categorised into pre-combustion capture, oxy-fuel combustion and post combustion capture. For Pre-combustion process, carbon is captured before combustion is taken place. In the Oxy fuel capture process, oxygen gas is used as the combustion gas instead of air.

This helps to increase the concentration of the Carbon dioxide in the flue gas which will make it easier to be removed from the mixture. For post combustion capture, the Carbon dioxide is captured after combustion process. Considering the existing facilities, post combustion is the only capture method with the capability to be retrofitted to the existing coal fired power plant. This formed the basis for the selection for this method. The technologies available, both existing and under research and development are as follows: Adsorption process; cryogenic separation; physical and chemical absorptions and membrane separation. Adsorption process involves high pressure which makes it challenging to apply to power plant flue gas separation as the carbon dioxide in the flue has a very low partial pressure [4]. For Cryogenic separation, the Carbon dioxide, as it concerns power plant flue, the maximum Carbon dioxide concentration was 15% [5]. So the technology is not suitable for the flue gas Carbon dioxide capture. Absorption process requires chemical to remove Carbon dioxide from the flue gas [6] [8]. Because of high consumption of the chemical and involvement of high pressure, flue gas application is not suitable for this process. For inorganic membrane process, this can be applied in a high temperature, low partial pressure stream, and it does not require any chemical for operating.

2.2 MEMBRANE SEPARATION TECHNOLOGY

2.2.1 Membranes: types and applications

Membrane can be natural or synthetic [6]. It can be thick or thin [6]. Its structure can be homogeneous or heterogeneous [6]. As such membrane can be classified according to different viewpoints. The first classification considered was by nature. Based on the classification by nature, membrane is divided into Biological membrane and Synthetic membrane [8]. A Biological membrane or a Bio-membrane is an enclosing or separating membrane that acts as a selective barrier, within or around a cell [6]. Also, a Synthetic membrane is an artificial membrane which is intended for separation purposes in the laboratory or industry [8]. This can further be divided into Organic (Polymeric or liquid) and Inorganic membranes (Ceramic, metal) [6]. Another means of classifying membrane is by morphology or structure [6]. These are Symmetric (Isotropic) and Asymmetric (anisotropic) [5]. Examples of Isotropic membranes are microporous membrane, Non-porous, Electrically-charged Membrane [12]. Also, examples of anisotropic membranes are Thin-Film (composite) membranes and Liquid membranes. The application of polymer membranes is generally temperature below $200^{O}C$ limited to and to the separation of mixtures that are chemically inert [14]. For high temperature operation and /or with chemically active mixtures, membrane made of inorganic materials can be used [5]. Examples of such membranes are Ceramic and metal [5]. This Inorganic membrane can be isotropic or anisotropic as mentioned earlier. Inorganic membranes can withstand very high temperatures up to $1100^{O}C$ [5].The high temperature resistance makes these membranes very attractive for gas separation operation, especially in combination with chemical reaction where the membrane is used as a catalyst as well as a selective barrier to remove one or more of the components which has been form [14]. The chemical stability of

existing polymeric materials is limited with respect to ph and Organic liquid [5]. The chemical stability of Inorganic materials is superior and is especially suitable for application in harsh environments [5]. Another important factor is the ease of cleaning for application under fouling conditions. For Inorganic membranes all kinds of cleaning agents can be used, allowing strong acid and alkali treatment [6]. Lastly, the lifetime of Inorganic membranes is generally greater than that of the Organic Polymeric membranes [5].

Isotropic membranes have a uniform composition structure throughout. The resistance to mass transfer in these membranes is determined by the total membrane thickness. A decrease in membrane thickness results in an increased permeation rate [5].

2.2.2 Micro porous Membrane

The simplest form of microporous membrane is a polymer film with cylindrical pores or capillaries [14]. However, more commonly microporous membranes have a more open and random structure, with interconnected pores. They are very similar in structure and function to conventional filters. However, in contrast with conventional filters, these pores are extremely small, on the order of 0.01 to 10 micrometer in diameter [15]. The separation of particles is mainly the function of molecular size and membrane pore size distribution [14].

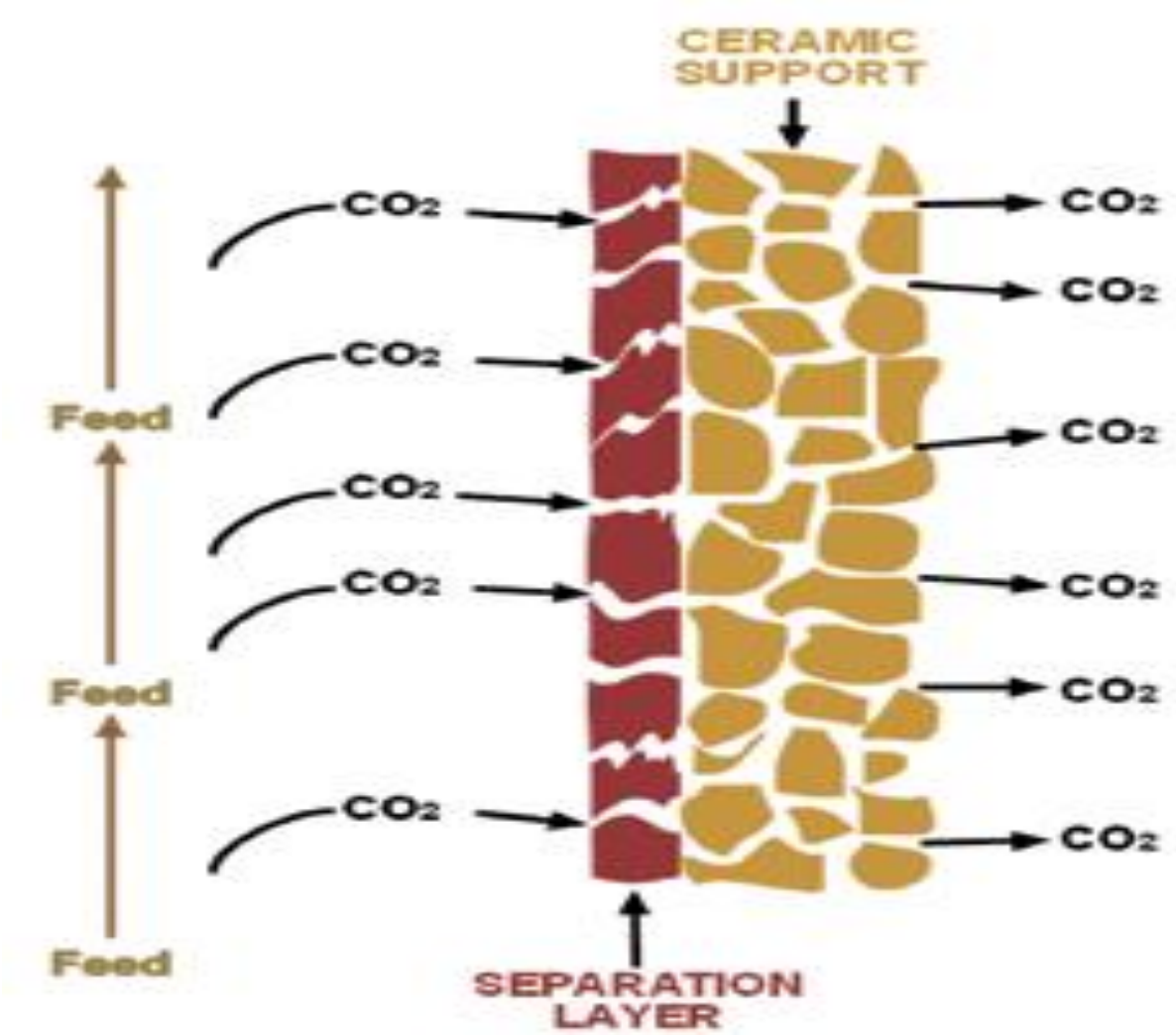

Figure 2:1: Inorganic hybrid membrane CO_2 separation technology [10].

Figure 2:1 is showing an internal view of a membrane support with diffusing Carbon dioxide gas molecules. All particles larger than the largest pores are completely rejected by the membrane [5].

In general, only molecules that differ considerably in size can be effectively separated by microporous membrane. These membranes are also as the substrate (support) layer in composite membranes and as a support matrix for liquid membranes [10].

2.2.3 Non-Porous, Dense Membranes

This type of membrane consist of a dense film through which permeates are transported by diffusion under the driving force of a pressure, concentration, or electrical potential gradient. The separation of various components of a mixture is related directly to their relative transport rates within the membrane, which are determined by their diffusivity and solubility in the membrane material [14] [5]. Thus, this type of membranes can separate permeates of similar size if their concentrations in the membrane material differ significantly. Dense membrane has the disadvantage of low flux unless they can be made extremely thin. For this reason dense membrane properties are incorporated into the top skin layers of asymmetric membranes [14]. Most gas separation, pervaporation, and reverse osmosis processes use dense membrane to perform the separation [13].

2.2.4 Electrically-Charged Membranes

These types of membranes are also referred to as Ion-Exchanged Membranes. They can be dense or microporous, but most commonly are very finely microporous, with the pore walls carrying fixed positively or negatively charged ions [15]. A membrane fixed with positively- charged ions is called an anion-exchanged membrane. This is because it binds anion in the surrounding fluid. The reverse is true for a cation-exchange membrane [16]. Separation is achieved mainly by exclusion of ions of the same charge as the fixed ones on the membrane structure, and is affected by the charge and concentration of ions in the solution. This type of membranes is used for processing electrolytes solutions in electro dialysis [17].

2.2.5 Anisotropic (Asymmetric) Membranes

These membranes consist of a number of layers, each with different structures and permeability. A typical anisotropic membrane has a relatively dense, extremely thin surface supported on an open, much thicker porous substructure. The separation properties and permeation rates are determined exclusively by the surface layer; and the substructure functions as mechanical support, with virtually no separating function. The resistance to mass transfer is determined largely or completely by the thin surface layer [14]. The membrane can be made thick enough to withstand the compressive forces used in the separation. The thin film is always on the high-pressure side of the membrane, that is, the feed side, since in this way maximum use of the support layer is made in stabilizing the thin film. These membranes had the advantage of higher fluxes, and almost all commercial processes use such membranes [9-10] [5].

2.2.6 Interfacial (Thin-film) Composite Membrane

This membrane consists of a thin dense film of highly cross-linked polymer formed on the surface of a thicker microporous support. The dense polymer layer is extremely thin, on the order of 0.1mm or less, so membrane permeability is high. Because it is highly cross- linked, its selectivity is also high [5] [14]. Interfacial composite membranes are widely used in reverse osmosis and nano-filtration application [18].

2.2.7 Solution-Coated Composite Membrane

This type of membrane is formed by solution coating a thin (0.5-2.0) micro meters selective layer on a suitable microporous support. Because the selective layer of

the composite membrane is often very thin and delicate, a sealing layer, also formed from a highly permeable material, is frequently used to protect such membranes [17]. The gutter layer acts as a conduit to transport material to the support membrane pores.

2.2.8 Liquid Membranes

Liquid membrane is a stable emulsion of an aqueous reagent solution and an immiscible hydrocarbon phase and is primary used in the separation of liquids [14]. The liquid membrane solution physically separates the feed solution from the permeate solution, as both solutions are immiscible in the liquid membrane. This has become increasingly significant in the context off facilitated transport, which utilizes carriers to selectively transport components such as metal ion at relatively high rate across the membrane interface. Liquid membranes are used on a pilot-plant scale for selective removal of heavy-metal ions and organic solvents from industrial waste streams [21] [20].

Membrane itself is the most important part of the separation. After a wide review of literatures, it was difficult to determine the exact definition of a membrane. This may be due to its vast application area, not only in gas separation, but also for liquid application. The reason for its wide application is that its functions depend on the structure as this essentially determines the mechanism of separation and thus the application [14]. A general definition that is often used for gas separation is "a membrane is a permeable or semi permeable phase, which restricts the motion of certain species and leads to a separation of components [5] [14]. Also, another definition of interest is that a membrane is a permeable or semi permeable phase, which acts as a selective barrier between two phases [21]. These phases can be in

the form of gas-gas phases, gas-liquid phases or liquid–liquid phase. The action of membrane processes is done by means of driving forces, which help to transport some of the multicomponent species through the membrane channels or could retain them in the membrane body itself. The membrane driving forces can be defined as forces acting on the molecules or particles which transport from one particular phase to another [5] [9] [14]. This movement that exists in the particles or molecules is determined by the gradients in the membrane driving forces. The driving forces are categorized into three types:

- Pressure (P)
- Concentration (C)
- Temperature(T)

Each driving force has a specific effect on the membrane transport [9].

Figure 2:2 below shows different driving forces, a membrane module and feed and permeate particles through the membrane.

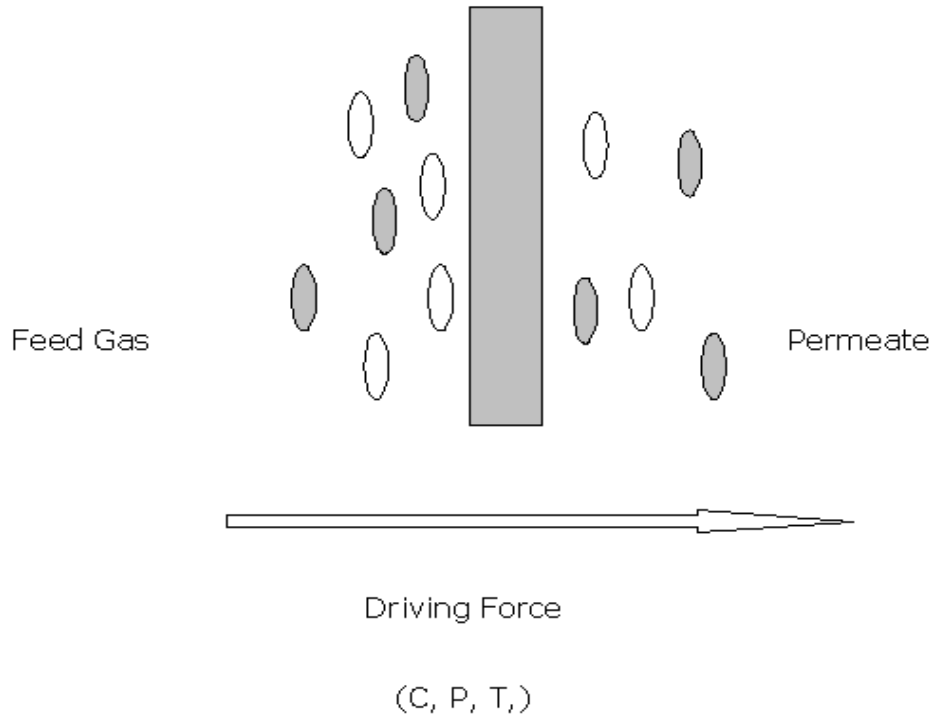

Figure 2:2: Membrane Gas Transports [5] [14]

2.2.9 Membrane Transport Models.

Various models have been used to explain the transport of fluids through a membrane. The model may act individually or in a combination with another model in order to give a complete explanation of the mass transport through a membrane. Some models are based on thermodynamics and statistical mechanical principles, whereas others are based on correlations between the observed transport phenomena and physical properties of the membrane material [9-10]. These transport models are classified according to the phase of the feed [5][13][14].Gas separation through membranes is primarily described by a single model or combination models as summarized in figure 2:3 below.

All the seven models are valid for liquid separation through membranes, whereas gas separation through membranes is best described by solution-diffusion model and solution-diffusion-imperfection model [4]. The solution-diffusion imperfection model includes various modifications applied to the solution-diffusion model. Two other models, namely irreversible thermodynamics and preferential sorption capillary flow model have been also used on a limited basis to describe gas transport through membrane [14]. As the present study is focused on gas transport through membranes, liquid theories are not covered in this piece of work.

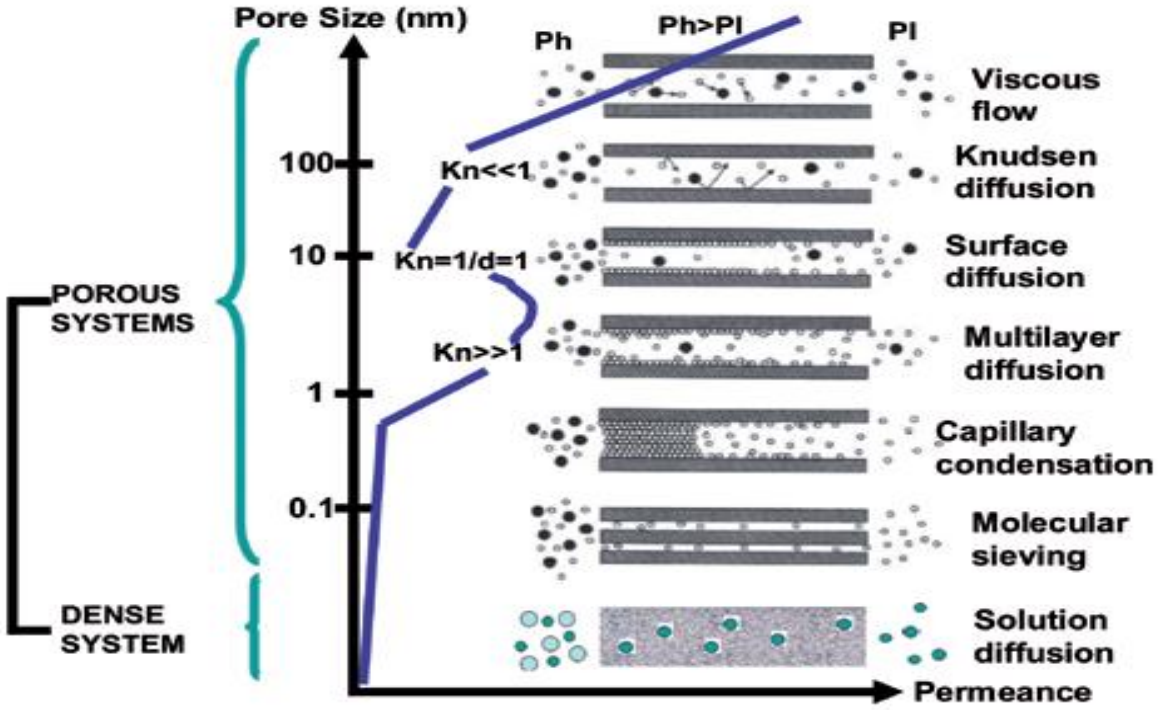

Figure 2:3: Various Transport Models for membrane Separation [9] [10]

Figure 2:3 above shows different transport models applicable for the movement of fluid through a membrane. From the above figure, it can be seen that the transport models are categorized into porous models and dense model. The porous models utilize the presence of pore size, mean free path and gas affinity to membrane

materials for the flow of gas through them [5][14].While dense model utilize the solubility of the permeating gas with the membrane material[5][9].

2.2.10 Solution Diffusion Model

The solution diffusion model describes the transport of gases through a membrane as a three steps process [14] (1) sorption of gas in the membrane, (2) diffusion through the membrane due to applied concentration gradient, and (3) desorption of the gas. Both the sorption/desorption and diffusion steps are dependent on the characteristics of the membrane materials and the gases, and are studied separately with various sorption and diffusion models [15]. While sorption models are based on the thermodynamics of the penetrant- membrane interaction, the diffusion is primarily modelled with Fick's laws of diffusion, presented in different forms [14]. Because this study is limited to porous membrane, the solution diffusion model will not be discussed in details here.

2.2.11 Pore Model

An early pore model was the preferential sorption-capillary flow (PSCF) model proposed [14]. This model assumes that the mechanism of separation is determined by the fluid transport through pores of the porous membrane [16] [10]. In contrast to solution diffusion model, the membrane is assumed to be microporous. The model states that the membrane barrier layer has chemical properties such that it has a preferential sorption for the solvent or preferential repulsion for the solute of free solution [9-10]. Also, gas transport through porous membrane can occur through a number of models, depending on the pore size of the membranes. The various types of flow theoretically characterize the gas

permeability across a porous membrane. This is shown graphically in figure 2:3 above.

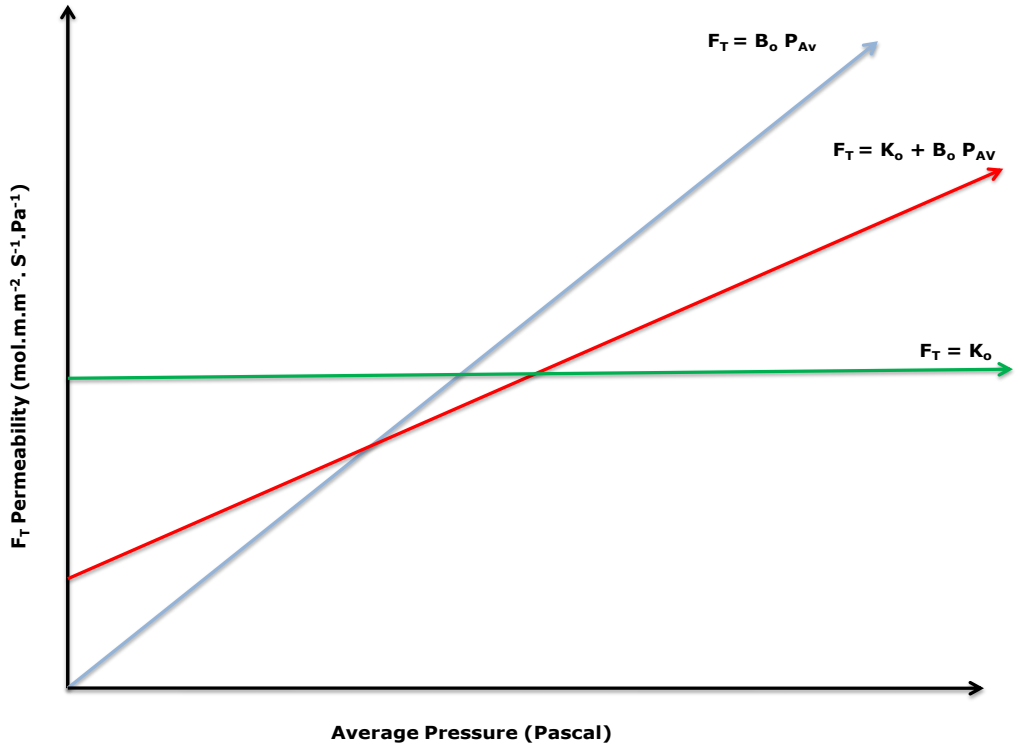

Figure 2:4: Straight line graphs defining the characteristics of flow through a membrane [5] [9-10] [14].

Principally, the porous ceramic support membrane that is used in this experiment should have one or a combination of these mechanisms. Figure 2:4 describes the simplest approximation where Knudsen and viscous flow may occur. Determining whether Knudsen or viscous flow is present in the transport mechanism depends both on the pore radius (rp) of the membrane and the mean free path (λ) of the molecules. The mean free path is defined as the average distance transverse by a molecule between collisions [9].

If the pore radius is smaller than the mean free path, Knudsen flow will predominate ($F_T=K_O$), as the collision between the gases molecules are less

frequent than the collisions with the pore walls [26]. Therefore, the permeation will be lower, and the gases will get separated better.

The Mean Free Path of the molecule and the pore radius of the membrane can be calculated using [14] [15] equation 1.0 and equation 1.1 below:

Hence,

$$\lambda = \frac{RT}{\sqrt{2.\pi\sigma^2}\mathrm{P}} \qquad 1.0$$

Where R= Universal gas constant (J/Mol.Kelvin), T = Absolute temperature (K), P= absolute Pressure (Pascal) and σ= collision diameter of the gas molecules (meters).

The Pore Radius can be calculated from the equation below:

$$r_p = \frac{16b\eta}{3a}\sqrt{\frac{8RT}{\pi M}} \qquad 1.1$$

Where

η = viscosity (Pas.sec) and M= molecular mass (Kg).

If the pore radius is larger than the mean free path, the flow will be classed as viscous flow ($F_T=B_OP$) as shown in figure 2:4. In this flow regime, the gas molecules collide entirely with each other and no separation is achieved among the various gases [14] [13]. Also, in Viscous flow regimes, high permeability through the membrane pores is observed with a little or no selectivity.

According to Hagen Poiseuille equation, the viscous flow is determined as

1.2

$$V_O = \frac{r_P{}^2(P_1^2 - P_2^2)}{16\delta\mu RT}$$

From the figure 2:4, one can deduct that the steeper the gradient of the line, the more viscous the flow becomes. Also, the shallower the gradient, the more Knudsen a flow becomes. Ideally, when $K_O=F_T$, the flow becomes total Knudsen and we achieve optimal separation [9] [5] [14].

2.2.12 Knudsen and Slip Flows

When the flow is in Knudsen flow regime, as mentioned above, the collision between the gas molecules and the pore walls of the membrane is more frequent than the collision among the molecules of the gas and the separation is based on the gas molecular weight. This gas molecule to membrane pore wall's behaviour determines the membrane flow characteristics. The flow is often occurred in microporous and mesoporous membranes [5] and is described by the Knudsen equation cited in equation 1.3 below.

$$F_{knudsen} = \frac{8r_p(P_1 - P_2)}{3\delta(2\Pi MRT)^{1/2}} \quad (mol/m^2s) \qquad 1.3$$

From the above equations, one can deduct that the free molecular diffusion is a selective mechanism, which means that the flux is inversely proportional to the square root of the molecular mass of the permeating gas. This is due to the decrease in the molecular velocity as a result of increase in the molecular weight of the permeating gases [16]. The decrease in flux as the temperature increases is because the concentration of the ideal gas (P/RT) decreases linearly with increase

in temperature, while the molecular velocity increases with the square root of the temperature [5, 9-10].

In figure 2:4, the three pore models used in this work were shown graphically. However, if the flow is predominately Knudsen, that is if the pore radius is smaller than the mean free path of the gas molecule, the flux through the membrane is mathematically represented above in equation 1.3. When the pore radius is larger than the mean free path, the flow will be governed by viscous flow [26].

$$F_{Viscous} = \frac{r_P{}^2(P_1^2 - P_2^2)}{16\delta\mu RT} \quad (mol/m^2s) \qquad 1.4$$

Acknowledging that equation 1.2 is equal to equation 1.4. The overall mathematical equation for pore flow for a gas flux through a porous membrane as limited to the above shown graph in figure 2:4 is then presented as:

$$F_t = F_{Knudsen} + F_{Viscous} \quad (mol/m^2s) \qquad 1.5$$

Putting equation 1.3 and equation 1.4 into equation 1.5 above, then equation 1.5 becomes

$$\Rightarrow F_t = \frac{8r_p(P_1 - P_2)}{3\delta(2\pi MRT)^{1/2}} + \frac{r_P{}^2(P_1^2 - P_2^2)}{16\delta\mu RT} \quad (mol/m^2s) \qquad 1.6$$

Multiplying equation 1.6 by $\frac{\delta}{(P_1 - P_2)}$ this gives

$$\frac{F_t\delta}{(P_1 - P_2)} = \frac{8r_p}{3(2\pi MRT)^{1/2}} + \frac{r_P{}^2(P_1 + P_2)}{16\delta\mu RT} \quad (mol/m^2SPa) \qquad 1.7$$

Where $\frac{Ft\delta}{(P_1 - P_2)}$ = F_T = Permeability

$$\Rightarrow \quad F_T = \frac{8r_p}{3(2\pi MRT)^{1/2}} + \frac{r_P{}^2(P_1 + P_2)}{16\delta\mu RT} \quad \text{(mol.m/m}^2\text{sPa)}$$

This can be re-written as:

$$F_T = \frac{8r_p}{3(2\pi MRT)^{1/2}} + \frac{r_p{}^2}{8\mu RT}\left[\frac{P_1 + P_2}{2}\right] \quad \text{(mol.m/m}^2\text{sPa)} \qquad 1.8$$

Or

$$F_T = K_O + B_O P_{Average} \qquad 1.9$$

Where

$$F_T = \frac{Ft\delta}{(P_1 - P_2)} \quad \text{(mol.m/m}^2\text{sPa)}$$

$$K_O = \frac{8r_p}{3(2\pi MRT)^{1/2}} \quad \text{(mol/m}^2\text{sPa)}$$

$$B_O = \frac{r_p{}^2}{8\mu RT} \quad \text{(mol/m}^2\text{sPa}^2\text{)}$$

$$P_{Average} = \frac{(P_1 + P_2)}{2} \quad \text{(Pascal)}$$

2.2.13 Molecular Sieving

This occurs when pore diameter are smaller enough to allow only smaller molecules to permeate, while larger ones are stopped from entering [14]. The limitation of the molecular sieving is that it compromises itself when the permeating gases have close particle size or kinetic diameter, which is the case in CO_2/N_2 permeation.

As shown in figure 2:4, one can easily deduct that the flow of gas through a membrane can be achieved by a single mechanism or a combination of mechanisms [14]. With respect to porous membrane permeation, quite a number of mechanisms which have already been explained in the previous pages of this work can actually act in a single or in combined form whenever gases are permeating through a porous membrane. But for the sake of this work, the mechanisms which were investigated for mass transport analyses are Knudsen mechanism, viscous mechanism and Surface Flow mechanism. The Knudsen and Viscous models are considered as pore flow mechanism, which are determined by the pore radius in equation 1.4 or by using membrane permeability data.

2.2.14 Contribution by the Surface Flow Mechanism

Surface flow mechanism comes in play when the permeating species are exhibiting an affinity to the membrane surface and there is adsorption of the gases (adsorbate) along the wall surface of the membrane (adsorbent) pores at a sufficiently low temperatures and / or high pressures [10]. For the surface flow to be contributory to the total flow or as a sole flow mechanism through the porous membrane pores, the adsorbed gases molecules must have exhibits enough adsorption energy capable of sticking it on the adsorbate and at the same time allowing it to flow along the pore channels of the inner structures of the membranes [16]. The rate of adsorption is however depends on the rate of the arrival of the molecule to the surface of the adsorbent and the proportion of the of the incident molecules which undergo adsorption [16]. This statement has an implication that adsorption occurs better at lower temperature and higher pressure. Also, it goes further to confirm that at high adsorption energy, high sticking effect

or probability occurs which retards the flow of molecules through the surface. This is due to the formation of a stronger bond being formed by the adsorbate and the adsorbent [10].

Considering total Surface flow mechanism, the theoretical surface flow is explained by using a modified Fick's law which is

$$F_{os}=\frac{F_s}{\Delta P}=\frac{\rho(1-\varepsilon)D_S}{K_S{}^2\delta}\frac{dq}{dP} \qquad 2.0$$

where ρ is the true density of the medium (kg/m^3), D_S the surface diffusion coefficient (m^2/sec), ($\mu_s=1/K_s$) is the shape factor, K_s is the tortuosity of the surface, dq/dP is the concentration gradient of the adsorbed species, ε is the porosity of the membrane medium and δ is the thickness of the membrane in meters.

The mechanism of surface flow is rather complicated. This subject has been treated in many papers extensively in [11-13] [27] [30]. For low surface concentrations the most general description is the two-dimensional form of Ficks' law: the surface permeability *F,* (mol/ m^{2}sec) equals

$$F_s=-\rho(1-\varepsilon)\frac{D_S}{K_S{}^2}\frac{dq}{dP} \qquad 2.1$$

This is given by the adsorption isotherm, such as Henry Isotherms. For Henry Isotherms,

$$n=KP \qquad 2.2$$

Where K is the Henry's constant (mol.kg^{-1}.Pa^{-1}), P is the pressure (Pa) and n is the amount adsorbed (mol.kg).

2.2.15 The Heat of Adsorption;-Δ*Ha*

The temperature dependence on the gas permeance is shown by the Arrhenius equation 2.5 [14] [31] below.

$$P = P_0 \exp\left(\frac{\Delta H_a}{RT}\right) \qquad 2.3$$

Putting equation 2.3 above into linear form, we have $\ln P = \ln P_0 + \frac{\Delta H_a}{RT}$

Then, plotting ln (permeance) and Temperature Resistance (1/T) has $\frac{\Delta H_a}{R}$ as the slope and $\ln P_0$ as the intercept. Where ΔH_a is the heat of adsorption and R is the universal gas constant (8.3145 J/mol.K).

Then, $\frac{\Delta H_a}{R}$ = slope

Δ*H*a = slope x 8.3145KJ/mol

2.2.16 Contribution by Capillary Condensation

In this type of flow mechanism, the pore is small enough to force the vapour to condense into liquid for separation of a mixture to occur.

2.3 MEMBRANE CHARACTERIZATION

2.3.1 Introduction

Because of the wide range of application area associated with membrane and a verse type of membranes available for application, there is a need to determine the structural properties of membranes in order to improve on the efficiency of membrane selection. This knowledge of the membrane structure will provide a greater understanding of separation problems and possibly predict the kind of structure needed for a given separation [33]. Membrane needs to be characterized to ascertain which may be used for a certain separation or class of separations [48]. The characterization of a membrane would lead to the determination of the structural and morphological properties of a given membrane [33]. According to the IUPAC Classification, porous membrane can be classified as:

i. macroporoes > 50nm

ii. mesopores > 2nm < pore size < 50nm

iii. micropores < 2nm

Note: 1nm =10Å

The pore size classification given here is referred to a pore diameter or more arbitrarily a pore width [10]. This implies that microfiltration membranes are porous media containing macropores and ultrafiltration membranes are also porous with mesopores in the top layer. With membranes of this type, it is not the membrane material which is characterized but the pores in the membrane [10]. Here the pore size and pore size distribution mainly determine which particles or molecules are retained and which will pass through the membrane [33]. On the other hand, with dense pervaporation/gas separation membranes, no fixed pores

are present and now the material itself mainly determines the performance [37]. In general, a membrane characterization is designed for two main purposes:

i. To determine the structural related parameters of the membrane. Example of such parameters are pore size, pore size distribution, top layer thickness and membrane surface porosity.

ii. To determine the permeation related parameters. Example of the permeation related parameters are determination of the actual separation parameters using solutes that are more or less retained by the membrane (cut-off measurements) [40].

There are a number of characterization techniques available for characterizing porous membrane. These are follows:

i. Scanning Electron Microscope (SEM)

ii. Bubble- Point Method

iii. Mercury Intrusion Porosimetry

iv. Adsorption- Desorption Method

v. Permeation Measurement

vi. Gas Liquid Equilibrium Method

vii. Liquid Displacement Permporometry (LDP)

viii. Diffusional Permoporometry (DP)

ix. Liquid Solid Equilibrium Method

x. Wide Angle X-Ray Scattering(WAXS)

xi. Atomic Force Microscopy

The methods listed above are either applied to determine the surface related parameters of the membrane or the permeation related. Only the ones used in my project were discussed in full.

2.3.2 Scanning Electron Microscopy (SEM)

This is conveniently used to characterize and investigate the porous structure of a microfiltration membrane. The membrane with the pore sizes ranging between 0.1 to 10μm [12]. The resolution limit of a simple microscope lies in the 0.01μm (10nm) range, whereas the pore diameters of microfiltration membranes are in the 0.1 to 10μm range [26]. The resolution of about 5 nm (0.005 μm) can be reached with more sophisticated microscopes [33]. This allows a clear view of the overall structure of the membrane structure; the top surface, the cross-section, and the bottom surface can all be observed.

2.4 MEMBRANE PREPARATION

Membrane preparation consists of two categories: the membrane support section and the thin film surface section. The membrane support (Alumina) used in this work was commercially supplied. The supports were modified in order to provide answers to research questions. Several routes can be utilized in modifying a membrane for a specific function [5].The method used will depend on the application needs for the membrane [5]. Sol-gel technique was used 100% in this work because it gave the provision of having a unique control over the membrane support pore size, which therefore minimize pore size distribution. Other membrane fabrication techniques one could use are thin-film deposition method, control pyrolysis, electro less coating, chemical vapour deposition [5] [14]. Only the technique used in this work was explained in detailed form.

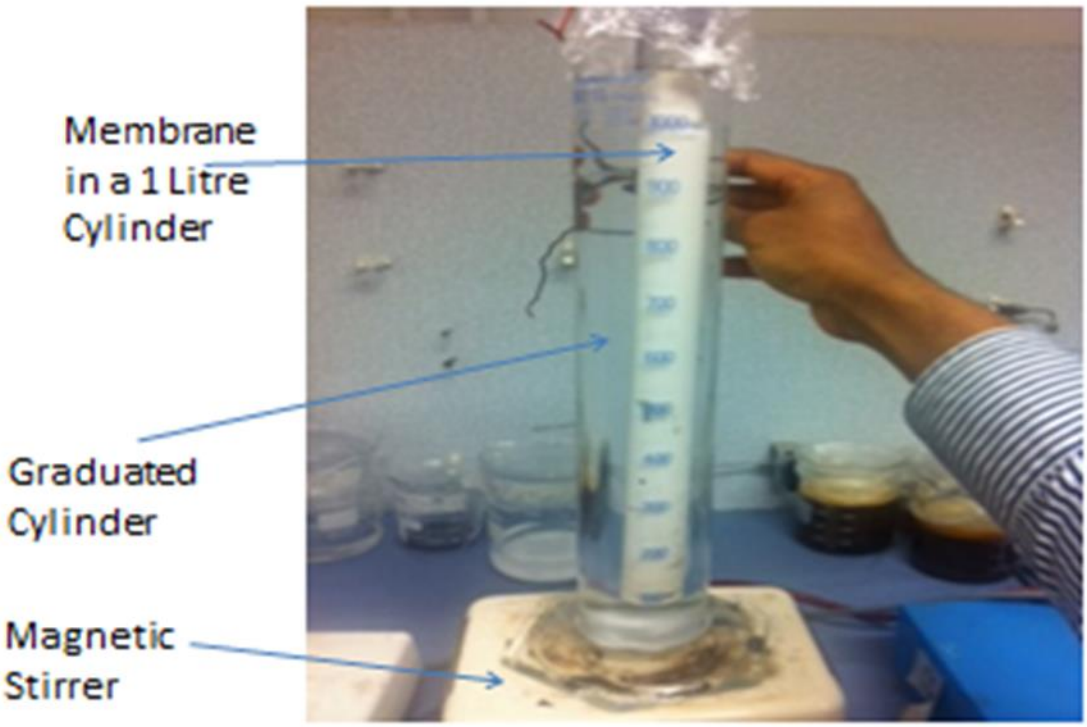

Figure 2:5: Experiment Dipping Set Up

2.4.1 Sol-Gel Dipping Method

This was the technique used in creating active layers on the surface of the membrane support. The technique is advantageous over others due to the fact that it allows access to better control of the membrane pore size and minimization of pore size distribution [5]. Once the solution is made, the membrane support with known weight and pore size is immersed completely for a thin film surface formation [5]. The coating can be done by inside - outside, outside only or inside coating [5]. Each dipping is dried to dryness and then oven treated for a particular temperature [5]. The detail of this will be found in the succeeding chapter.

2.5 EFFECT OF OPERATING CONDITIONS ON MEMBRANE PERMEABILITY

Membrane permeability is one of the important properties of membrane to be considered during membrane selection for industrial application [45]. Permeability is used to characterize the rate of permeation [5] [14] [33]. This is usually calculated by the equation below

$$P = \frac{Q.\delta}{A.t.(P_1 - P_2)} \qquad 2.4$$

Where, P is the permeability for a given membrane, Q is the volume of gas which penetrates through the membrane. δ is the thickness of the membrane, A is the area of membrane, t is the time, P_1 is the partial pressure of the gas on the higher pressure side of the membrane, and P_2 is the partial pressure of the gas on the lower pressure side of the membrane [33].The value of permeability of a membrane can be affected by a number of factors; either in normalization strength or by changing its form [5]. Some of the factors are as follows:

1. Type of Gas
2. Type of Membrane Materials
3. Temperature of the operation
4. Pressure of the gas
5. Thickness of the membrane
6. Area of the Membrane

2.5.1 Type of Gas

The type of gas affects the diffusivity of gas through a membrane. This equally affects the solubility of gas as concern dense membrane [48]. Diffusivity heavily

depends on the particle sizes of the diffusing gas molecules. The larger the particle size, the slower the diffusion of the gas molecules through the membrane [5] [9] [14]. So, gases which have large sizes are likely to experience low permeability with a membrane unless there is another prevailing factor other than that of the particle size effect [5]. The permeability of a membrane is affected by different gas type [5]. The Different gases have different permeability

2.5.2 Type of Membrane Materials

The material composition is equally established to have a link with the difference in the permeability of gases [5]. Some materials possess high permeability properties than other. So, if a material with high gas permeability is used as a membrane material, if everything being equal, the permeability of the membrane will be high as well. As it regards my project, Silicon Elastomer was selected as my membrane precursor due to the fact that it demonstrated a high permeability index to acidic gases like carbon dioxide as contained in US Patent 7,048,778 B2 [5]. The high permeability attributed to Silicon Elastomer may be due to the fact that the molecules of silicon are fully bounded by low intermolecular forces and relatively unhindered single bonds between silicon and oxygen backbone chain atoms together [5]. This resulted in a higher than normal amount of free volume and a high degree of chain mobility [13].

2.5.3 Temperature of the Operation

Temperature is known to increase the entropy of the gas molecules [7]. As the temperature of the process increased, gases in the confined place experience increased in their kinetic energy which results in gases diffusing through a membrane less than they normally do [7]. For silicon, its free volume depends on temperature, the lower the temperature, the less the free volume which results in slower permeability and more selective flow [28].

From equation 2.4, the value of permeability is independent of the pressure of the permeating gas. This means that membrane permeability is normalized by pressure. However, the amount of gas which diffuses through a membrane does depend on the pressure [13]. A lower pressure differential equates to less gas diffusing through the membrane [9]. When gas is a mixture, the calculation of permeability in equation 2.4 is based on the partial pressures of the individual gases in the mixture [5].

2.5.4 Membrane Thickness

Permeability is normalized by thickness of the membrane. The thickness of the membrane normalises the values of the membrane permeability but it directly proportional to the resistance provided by the membrane substance to the flow of gas through the membrane [5] [9-10] [14]. However, the amount of gas that diffuses through the membrane does depend on the thickness of the membrane. The effect of the resistance to the flow will be shown in the later chapter.

2.5.5 Area of the Membrane

The area of the membrane has a normalized effect on the membrane permeability. Once, a membrane area is defined, it does not change throughout the operating life of a membrane.

2.6 FACTORS AFFECTING MEMBRANE PERMEABILITY

The selection of gases by membrane depends on a number of factors [13]. The factors may act in a single or combination form in order for a membrane gas selection to be fully understood. Among the controlling operating conditions is temperature, particle size of gas, affinity of gas to material.

2.6.1 Temperature

Generally, increase in temperature reduces the selectivity of gas by the membrane. This is connected to the fact that at high temperature gas kinetic energy is high, thereby making gases to interact with each other more in a confined volume. This interaction makes it difficult for a particular gas to be selected by a membrane [5]. This selectiveness of a membrane is shown clearly in the successive chapters.

2.6.2 Affinity

Affinity of the membrane material to a particular gas contributed greatly in the separation of gases with close kinetic diameter and molecular weight. Gases which have affinity with membrane are preferentially selected (adsorbed) over other with absolutely no or weak affinity [10]. The adsorption of the gases molecules on the surface of the membrane material provided opportunity for the separation of the two gases mixtures with closed kinetic diameter [26]. CO_2 being acid gas will

adsorb more on the basic surface. The effect of basic magnesium (MgO) modified membrane has shown an increase in the adsorption rate of CO_2 about a 10 wt. % used in adsorbs 10 wt. % CO_2 at ambient temperature and 20torr CO_2 after 15 minutes [10]. Also, CaO showed an adsorption rate of 3.5 wt. % with carbon dioxide at ambient temperature and 10 torr of CO_2 after 15minutes [10]. These attractions of the acid gas to basic metals have encouraged the flow of carbon dioxide gas preferentially selected over light gases on basic metal modified membrane [10]. At ambient condition, MgO physisorbs [10] [16] or weakly chemisorbs CO_2 [10]. The energy required for the Carbodioxide to adsorb on the metal oxide depends on the basicity of the alkaline earth oxides, [10] [16] which increase with the period of the metal (that is, MgO is less basic than CaO and SrO is less basic than BaO, et cetera) [10]. Rare earth oxides have a stronger binding energy and adsorbed higher concentration of CO_2 than alkaline earth oxides [10]. Magnesium oxide was selected as a metal oxide with fit into the requirement to attract CO_2 molecules to enhance gas separation. The magnesium modified membrane will allow more CO_2 gas molecules to adsorb more frequently on the surface of the membrane and transported into the pore via a surface–diffusion mechanism. This evidence has been demonstrated in the later chapters.

2.6.3 Gas Particle Size/Weight or Kinetic Diameter

The selectivity of a particular gas to a membrane may be affected by the gas particle sizes as compared to the membrane pore sizes. Gases which are high in molecular weight are generally delayed from permeating through a membrane than light ones. This gaseous behaviour is better explained by the Knudsen mechanism. According to Knudsen flow mechanism, the flux is directly proportional to the

inverse of the square root of the molecular weight of the gas [5] [14]. Mathematically,

$$F_T \quad \propto \quad \frac{1}{\sqrt{MW}} \qquad 2.5$$

Table 2:1: Gases with their Kinetic Diameters and Molecular Weight [10][9].

Molecules	Molecular Weight(g/mol)	Kinetic Diameter(Å)
CO_2	44	3.3
N_2	28	3.64
O_2	32	3.46
H_2O	18	2.65
CH_4	16	3.8
H_2	2	2.89

From the equation 2.5, we can deduct that the flux through the membrane increases with decrease in the molecular weight of gas and decrease with increase in the molecular weight of gas [5]. There are some exceptions to this; some gases which are heavier are preferentially selected over lighter gases. In this case, Knudsen is limited.

The ceramic membrane pores could come in different arrangements and they can be highly connected to one pore to another, tortuous or non-connected or straight in arrangements [5]. Based on the IUPACK pore size classification of the ceramic membrane, membrane with pore sizes greater than 500 Angstrom (>500Å) are classified as macro porous, mesoporous (500-20 Å) or micro porous (<20 Å) [15].

The permeation data generated experimentally were based on the following assumptions:

(a) The membrane surface is consisting of bundle of asymmetric capillary tubes.

(b) The molecules adsorbed on the membrane surface and walls of the membrane pores are assumed to be mobile.

Based on these above mentioned assumptions, the transport of the gases through capillary tubes can be described based on Kinetic theory of gases.

Three mechanisms have been tested in this work to explain the gas transport through the porous membrane, namely: (1) Knudsen Flow (2) Surface Flow and (3) Viscous Flow. For a single capillary, it has been found that, depending on the relative magnitudes of pore radius, r_p, and mean free path, λ, of the gas, gas molecules passes through capillary by one or more mechanisms listed above. According to Liepmann, when the $(r_p/\lambda) < 0.05$, Knudsen type is predominant. According to Li, slip flow occur in the range $(r_p/\lambda) = 0.05$ to 3 and viscous flow is occurs when $(r_p/\lambda)>3$.

2.7 CAPTURING OF CARBON DIOXIDE

Attentions have been drawn over an increase in the concentration of Carbon dioxide in the atmosphere and its effect on global climate change [1] [6]. This concern has prompted an increase in the carbon awareness and investigation for reducing Carbon dioxide emissions. Carbon Capture could be defined as a process by which Carbon dioxide stream is concentrated for transportation to the suitable storage facility or for a further industrial utilization [41]. Because most of the

mitigation methods require Carbon dioxide in a more concentrated form, the CO_2 must be concentrated first in order to either store it or for other purposes [26].

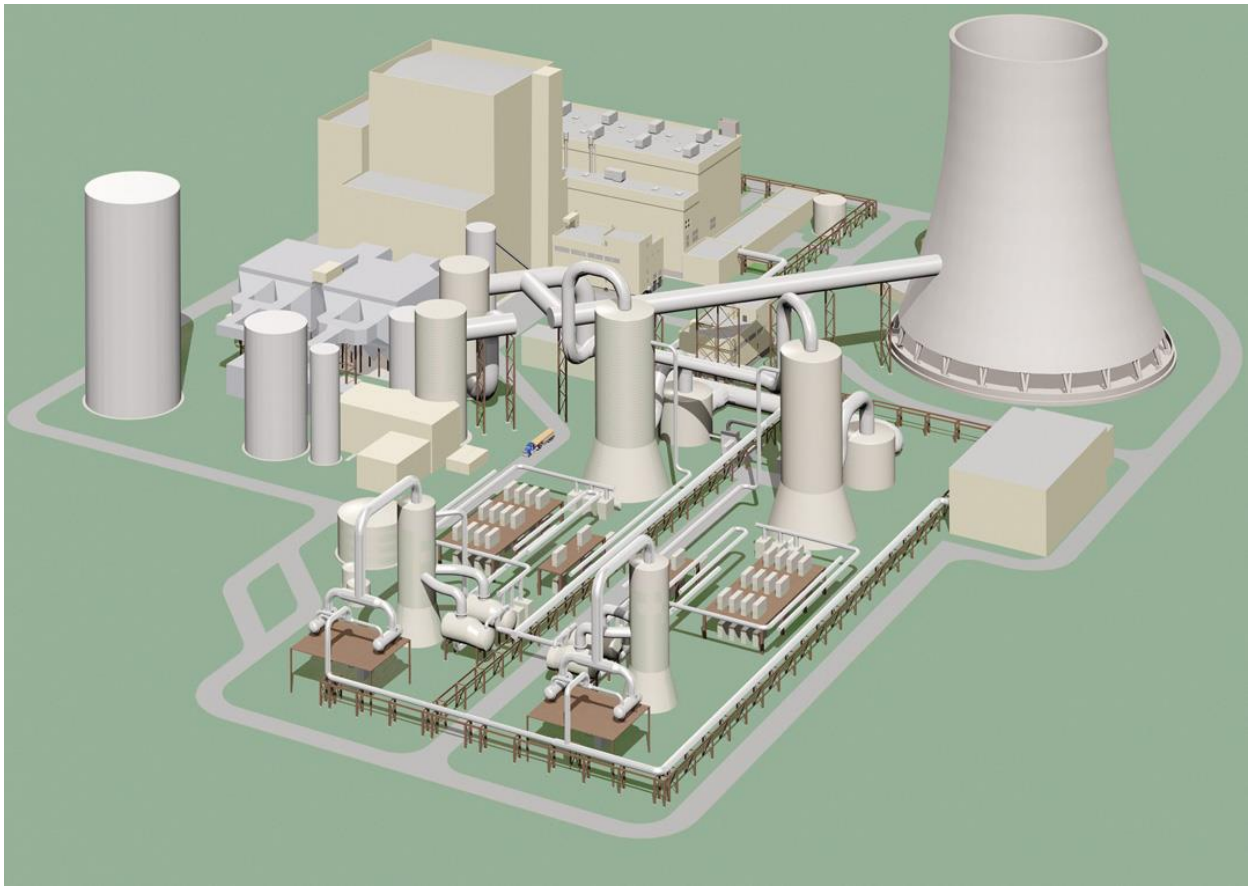

Figure 2:6: layout for a steam power plant with retrofitted CO_2 capture and compression [45] [61].

Figure 2:6 above shows a simulated layout of a power plant with fitted Carbon dioxide capture facility and compressor. The compressor is used to increase the partial pressure of Carbon dioxide molecules.

2.7.1 Categories of Carbon Capture Methods

Carbon Capture is categorized into four capturing systems: Post-combustion capture system; Oxy-fuel combustion Capture system; Pre-combustion captures system and Capture from industrial process streams [25] [61].

2.7.2 Capture from Industrial Process Streams

Carbondioxide has been captured and vented to the atmosphere from the industrial process streams do to the fact that there was no requirement for storage or as an incentive [18]. Some of the examples of the industrial process that involved carbon dioxide capture from process streams are purification of natural gas and production of hydrogen-containing synthesis gas for the manufacture of ammonia, alcohols and synthetic liquid fuels [18]. This method of capture is similar to the technology utilized in the Pre combustion capture system [45].

2.7.3 Pre-Combustion Capture System

In Pre-combustion capture system, oxygen or air and /or steam is reacted with fossil fuel to give mainly a synthesis gas (syngas) or fuel gas which consist of carbon monoxide and hydrogen [41]. The carbon monoxide is then reacted with steam in a catalytic reactor called a shift converter, to give carbon dioxide and more hydrogen [41]. The process is typically occurred at high pressure (20atm) [26]. The carbon dioxide produced is either separated by physical or chemical process and the enriched hydrogen is used as fuel in boilers, furnaces, gas turbines, engines and fuel cells [18].

2.7.4 Oxy-Fuel Combustion Capture

In this combustion capture, high graded oxygen is used for combustion instead of air, resulting in a flue gas that is mainly Carbon dioxide and water being produced [10]. When fuel with high-grade oxygen is burnt, the flame generated is excessively high, but the Carbon dioxide and /or water rich flue gas can be recycled to the combustor to moderate this [29].

2.7.5 Post- Combustion Capture System

In Post-combustion capture system, the flue gases produced from the combustion of fossil fuels and biomass are captured instead of being discharged to the atmosphere [41]. The produced flue gases are directed into a facility where the carbon dioxide part of the flue is captured and further conditioned for either geological storage or industrial utilization [26]. This type of capture system has different categories which are either at commercial level or under research and development [26]. Some of the methods are as follows:

i. Chemical Absorption

ii. Physical Absorption Method

iii. Physical Adsorption Method

iv. Cryogenic Separation Method

v. Membrane Technology Method

2.7.6 Chemical Absorption Method

This post-combustion method uses MEA (Monoethanolamine) as the sorbent in separating Carbon dioxide from flue gas [41]. This was originally employed to remove carbon dioxide from other gas mixtures such as methane, hydrogen, etc. The gas separation is achieved by considering different relativities of different gases with the chemical sorbents [5]. The reactions that exist between the gases and the sorbent chemical is reversible, hence, regeneration can be achieved [18]. The strong binding that exists between the carbon dioxide molecules and the sorbent offers a quick and effective recovery of the carbon dioxide in one stage, but

this equally causes high regeneration energy requirement [31]. Also, the control of impurities and miner components in the flue gas which have the capability of degrading the sorbent is very poor. Finally, the most sorbents used are very corrosive; they are to be used in a low concentration (around 18%) in order to avoid sudden failure of the facility [41]. The equation below shows the reaction between carbon dioxide in the flue gas and the sorbent chemical.

$$CO_2 + 2\ MEA \Leftrightarrow MEACOO^- + MEAH^+ \qquad 2.6$$

Figure 2:7 below is a typical process flow diagram of the AMEA process [62]. Carbon dioxide molecules are chemically absorbed from a stream of gas by a constantly moving Amine in a contacting tower.

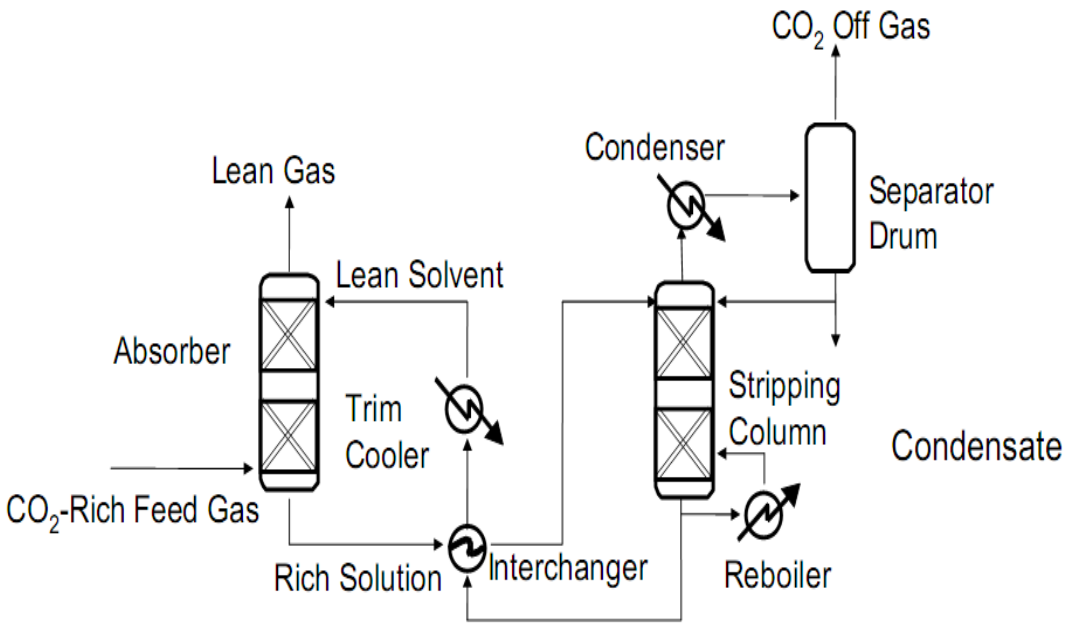

Figure 2:7: Process flow diagram for MEA captures [61] [62].

2.7.7 Physical Absorption Method

In physical absorption process, the carbon dioxide dissolved in a liquid solvent, and no chemical reaction takes place [26]. Since there is no chemical reaction involved in this process, the binding force that exist between the carbon dioxide molecules

and the solvent are rather weaker than that of the chemical absorption process [26]. The amount of gas absorbed is linearly proportional to its partial pressure (Henry's law) [26].

Thus, the physical absorption is more effective when the partial pressure of the gas to be absorbed is high [26]. Also, the absorption rate of the gas equally depends on the temperature of the process, the lower the temperature, the high the absorption rate [20]. Examples of the solvent used in physical absorption process are methanol, glycol dimethyl ether, propylene carbonate and sulfolane [13]. After gas absorption, desorption can be achieved either by lowering of the pressure as in the pressure swing absorption (PSA), or by raising the temperature as in the temperature swing absorption (TSA) [13]

2.7.8 Physical Adsorption Method

In physical Adsorption process, gas is adsorbed on the solid surface by Van der Waals force [46]. In this process, the gas separation is based on the difference in the gas molecular sizes.(Steric Effect), or different binding forces between gas species and the adsorbent (Equilibrium Effect or Kinetic Effect) [26]. Pressure Swing Adsorption and Temperature Swing Adsorption are applicable in this process, this is because the gas molecules are attached on the surface of the solid and therefore, form mono or multi-layers in the process [21]. Despite large surface area per unit volume presence in physical adsorption process, the gas loading capacity could still be lower than in physical absorption process [15]. Because of the large amount of carbon dioxide in the flue gas, physical adsorption might not be effective or an economic method for recovering carbon dioxide from flue gas,

but in a combination with other capture methods the physical adsorption process has shown a promising trend [56].

2.7.9 Cryogenic Separation Methods

This separation method uses the difference in boiling points of various gas species to achieve separation with the fact that each gas specie has a distinctive boiling temperature [26]. At the temperature between the critical temperature and triple point, carbon dioxide can be liquefied by compression and cooling [26]. This process is a high energy intensive process, therefore is not cost effective process [26]. As the concentration of the carbon dioxide in the flue gas is up to 15% , the energy used to compress the rest 85% of the flue is substantial[10]. A simple calculation for energy requirement for liquefying carbon dioxide by isothermally compressing the flue gas near the critical temperature to 74 Bar would spend about 30% total power output in compressing 85% of the remaining gases, and this is about 50% more than MEA process [26]. This is a very energy intensive process unless there is a novel process developed its application in capturing carbon dioxide can never be competitive [45].

2.7.10 Membrane Process Method

Membranes were fabricated by manufacturers for specific purposes [29]. They allow selective permeation of gas through them. The performance of membrane is classified by the permeability and selectivity [26]. The membrane selectivity to different gases is particularly depends on the nature of the material, but the flow of gas through the membrane is usually driven by the pressure drop across the membrane [26]. Therefore high pressure streams are usually preferred for

membrane separations [26]. There are different kinds of membranes as mentioned in the previous pages in this work. The Polymeric membrane as mentioned early in this work has been successful in various capacities [5]. These membranes have shown both high selectivity and permeability in natural gas process, but due to the fact that the flue gas composition has the potential to form acidic, the polymeric materials which are non-resistance to acid attack would not be suitable for the process [13]. Another reason polymeric is getting replaced for carbon dioxide capturing is that the membrane when absorbed water molecules swollen up. This typically affects the structural profile of the membrane, therefore compromising the membrane morphology [26].

In order to provide a membrane which will not only withstand the corrosive nature of the gas, but to provide a high permeability and selectivity, Professor Edward Gobina, in his United State Patent no: 7,048,778 B2 proposed an inorganic (Ceramic) membrane for the separating acidic gas from gas mixtures [5] [9-10][14].

In general, Inorganic membrane has greater thermal and chemical stabilities. Inorganic membranes are attractive for capture of carbon dioxide.

Figure 2:8-- below shows a proposed schematic of a coal combustion power plant with a tested Ceramic membrane capture facility fitted to it with the results of reduced emission. From the diagram below, the flue gas was found to have only 1.4% of CO_2 after being passed through a Ceramic Inorganic membrane. This represented more than 90% of 14% CO_2 being recovered from the flue gas source.

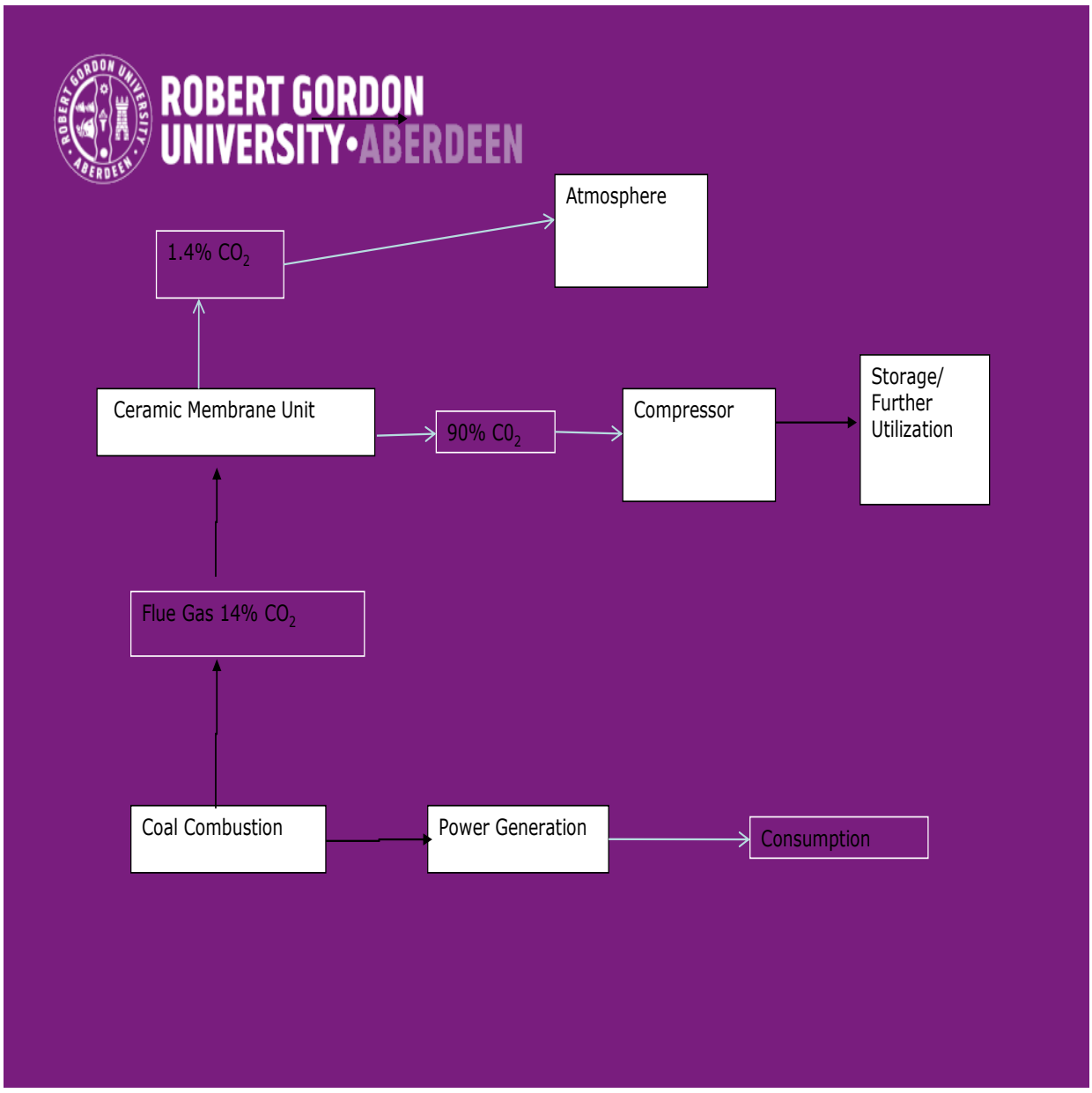

Figure 2:8: Proposed Schematic Representation of a CO_2 balance from a conventional power plant with CO_2 capture facility.

Ceramic membranes have several advantages over organic membrane as follows: chemical Resistant-in almost all cases, any chemical interaction between the membrane and the fluid is undesirable; thermally stable than most other membranes; materials like oil are much easier to filter at high temperatures as their viscosity decreases ;mechanical Strength- the membranes of ceramics are of high physical strength than others. They are capable of withstanding high pressure.

Ceramic membranes do not absorb water, so swelling is not a problem with a ceramic membrane as it is commonly with polymeric membrane [20]. Finally, ceramic membranes are very stable and have great longevity.

2.8 INDUSTRIAL APPLICATION OF THE HYBRID INORGANIC CERAMIC MEMBRANES

Due to limitations faced by organic membranes in the processing or gases, particularly acidic gases, has given rise for the development of Inorganic ceramic membranes. Hybrid inorganic ceramic membranes which have ability to withstand high temperature, high pressure and corrosive chemicals have provided opportunities for the membrane market which suffered huge set back due to the challenges and limitations that confronting the organic membranes. The inorganic membranes with high resistance to corrosive chemicals, high mechanical strength, high temperature and low energy demand offer opportunity to replace the Glycol Absorption process which requires high energy for regeneration and chemical gas processing. Some of the industrial application points for high hybrid inorganic ceramic membranes are:

1. Urea Plant which produces a waste stream with CO_2 volume percent of 8% [57].
2. Hydrogen Plant which produces a waste stream with CO_2 volume percent of 12% [58].
3. CO_2 removal in the Iron and Steel Industry with a waste stream of CO_2 volume percent of 20%, 24 % and 44% (Conventional Blast Furnace) , (Corex) and (CCF) respectively[59].
4. Cement Kiln Flue gas recovering Scrubber for CO_2 volume per cent of 19% [59].

All the above mentioned processes can utilize the application of inorganic ceramic membrane due to the fact that the membrane application has ability to handle varying concentration of the carbon dioxide which has been demonstrated in the experimental and results sections of this project.

3 EXPERIMENTAL WORK

3.1 APPARATUS:

Most of the experimental apparatus used in this product were based fundamentally on the US Patent number 7,048,778 B2 invented by Professor Edward Gobina. The skeleton of the experimental rig and stainless steel reactors which were both designed by Professor Edward Gobina were used throughout the experimental process in this project. These reactors were capable of withstanding pressures up to 50 bar [5] [14]. Although this experimental work was limited to 0.1 (Bar) Gauge pressure, the experimental rig and set up could be used for a pressure of up to 50 bar gauge pressure [14] [5]. The reactor used was of size ID25-L650.

All the membrane units of the membrane sizes are in millimetres. The reactors used have three sections: Feed Section, Permeate Stream section and Retentate section. Figure 3:1 and figure 3:2 show the diagrammatic representations of the membrane reactors used in my projects for high and low temperature operations. The reactor was designed in such a way that there is a direct fluid communication between the feed stream and the retentate stream. A retentate stream is gases which are unable to pass through the membrane pores [5] [14], while the permeate stream is gases which pass through the membrane pores [5] [9].

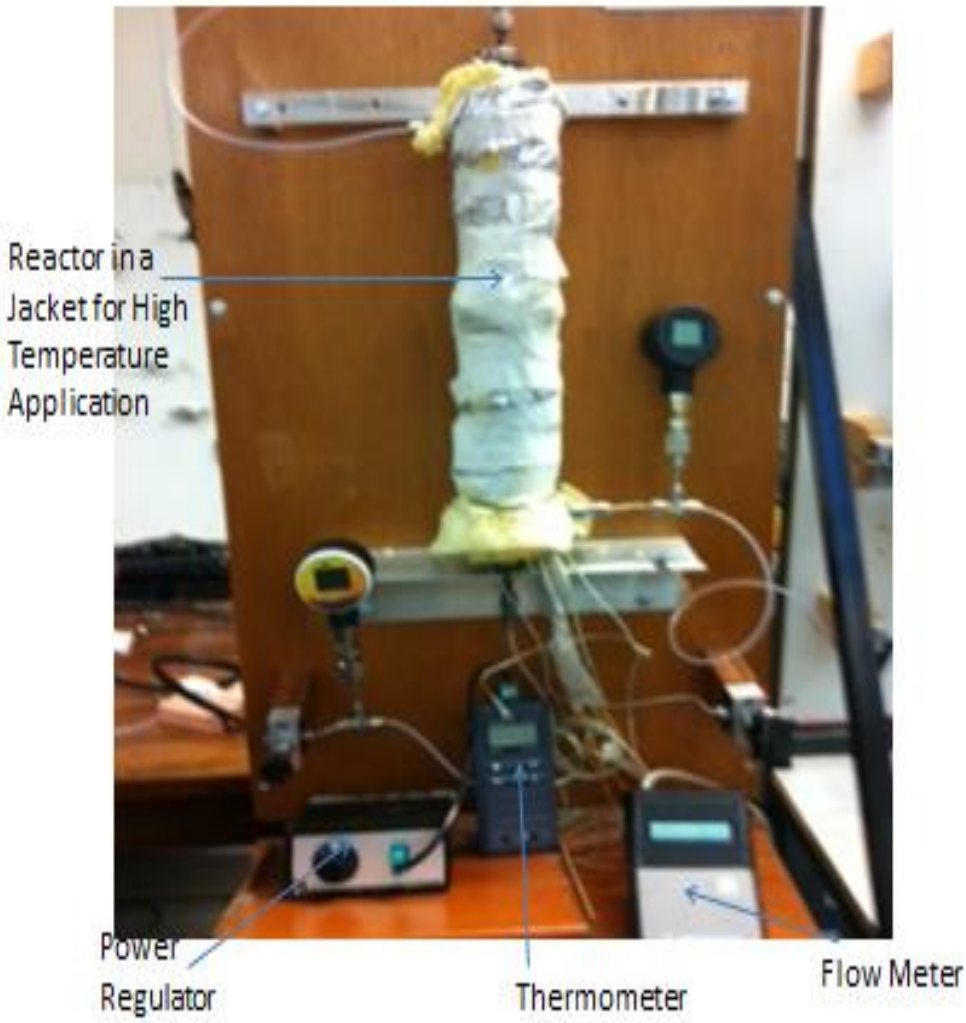

Figure 3:1: Pictorial representation of the Reactor used with high temperature application Jacket

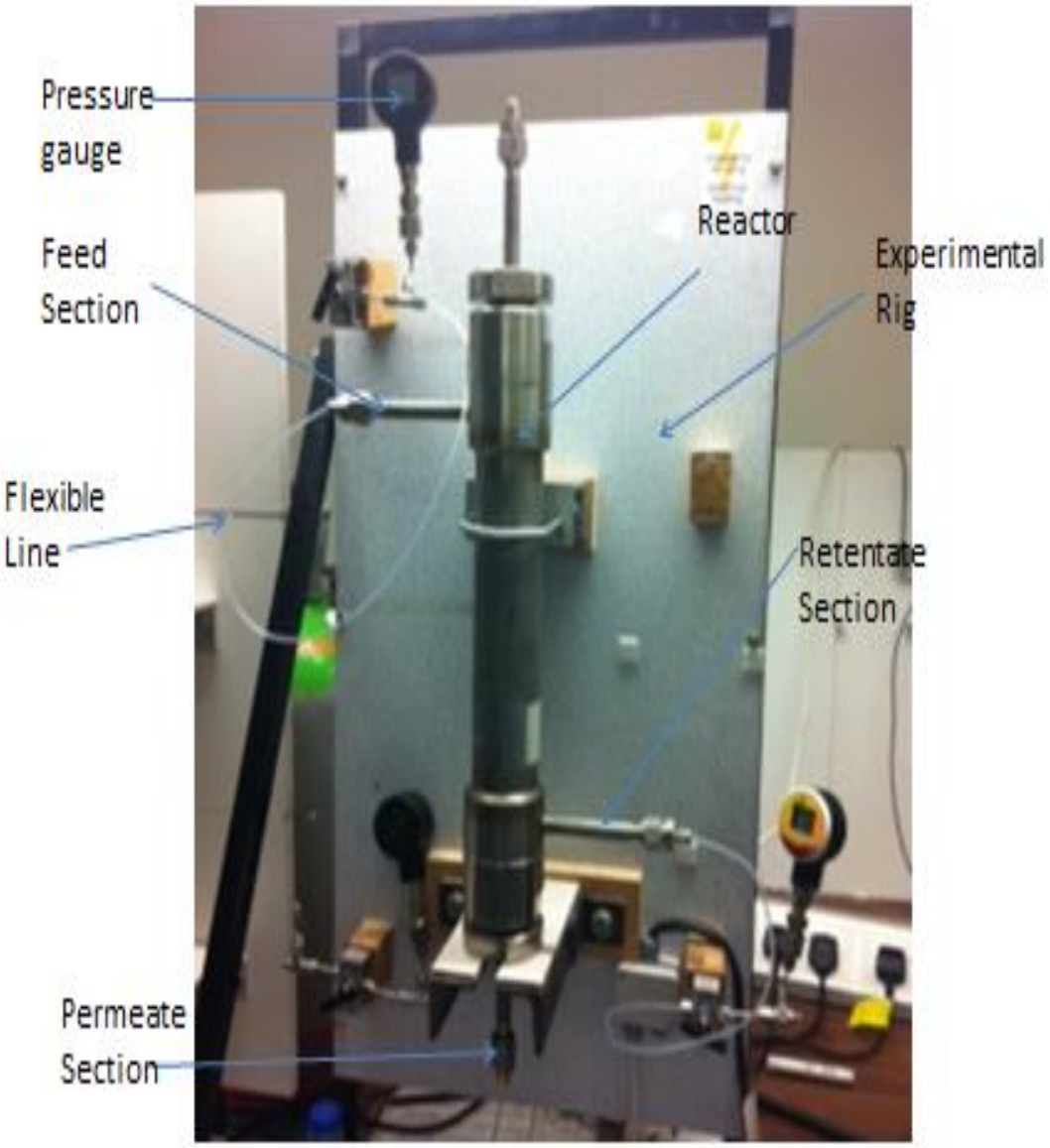

Figure 3:2: Showing the Reactor used at room/low temperature operation

Other experimental apparatus used in this work are follows

i. Membrane Support

ii. Graphite Seal

iii. CO_2 Mass Flow Controller(Sierra)

iv. Nitrogen Mass Flow Controller(Sierra)

v. Flow Meter Agilent Technologies(ADM1000, Capacity 1 litre/min)

vi. Carborite Furnace (Temp Max. 1100^0C)

vii. Carborite Oven(Temp Max. 300^0C)

viii. Power Regulator (Barnstead Electro Thermal)

ix. Thermocouples (RS)

x. Heating Tapes

xi. Swagelok Fittings

xii. Gas Chromatography(CP-3800 Varian)

xiii. Various Gas Cylinder (Air Bottle)

xiv. Veneer Calliper

xv. Beakers

xvi. Magnetic Stirrer

xvii. Weighing Balance

xviii. A lab Built bubble Point Testing Kit

xix. Thermometer

xx. Pressure Gauge

xxi. Fume Cupboard

The permeation experiment set up is categorized into Feed Section, Reactor Section and the Analytical Section. The figure 3:3 shows the schematic diagram of the feed system, membrane reactor system and the analytical section of the permeation experimental set up.

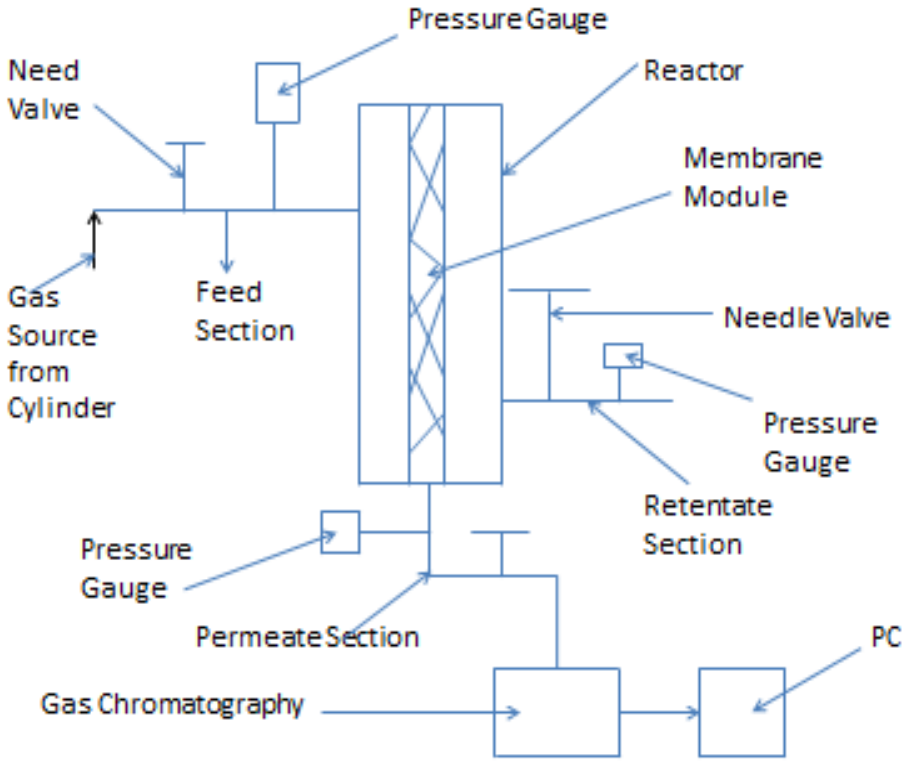

Figure 3:3: Schematic diagram of the feed, reactor and analytical section.

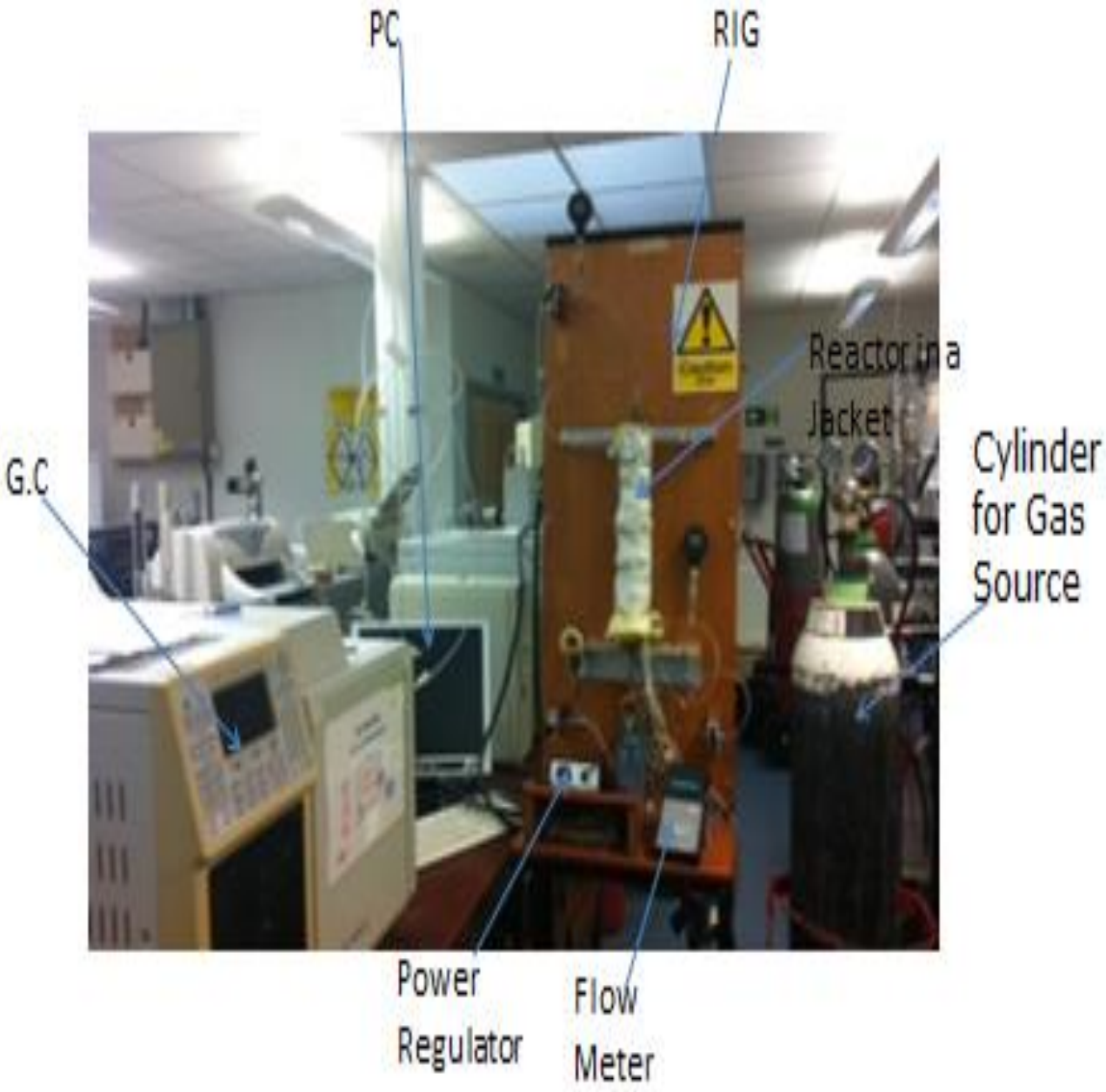

Figure 3:4: Pictorial View of the Experimental Set Up

3.1.1 Feed Delivery Section

The feed section of the permeation experimental set up consists of various gas cylinders from Air Liquid. The cylinders were specifically of different mixtures and pure gases, ranging from 14%-CO_2/N_2-86% [mixture A], 30%-CO_2/70%-N_2 [mixture B], 60%-CO_2/40%-N_2 [mixture C], pure CO_2, pure N_2, pure Argon (Arg), pure Helium, and pure Methane bottles. Each gas cylinder was provided with pressure regulators. Mass flow controller was used as a part of the feed delivery system. This was used to achieve desired mixtures from the supplied single gas cylinder bottles. In this project, the gases used were supplied in pure state and in mixtures. In order to make a mixture, the supplied pure gases will be connected to the mass flow controller and desired gas concentration will be achieved, by the help of the needle valve in the mass flow controller. It is only when the amount of feed flow is defined in terms of volume flow rate that mass flow controller is useful. This metery gadget was situated between the gas bottles and the membrane section.

Figure 3:5: Pictorial view of the source gas

Figure 3:5 shows the feed delivery system of the experimental set up. The figure shows the gas bottles and the regulator point used in this project as the source gas. The bottles were supplied pre- made as single and mixtures from the Air Liquid. The experimental procedure is explained in more details at the later part of this chapter. The gas cylinder regulators were supplied together with the cylinders.

Figure 3:6: Membrane in the Oven

The figure 3:6 above shows the support in the Carbolite Oven. The oven has a maximum operating temperature of 330^0C. The oven was used to dry the dipped membrane at 65^0C for 2 hours, after the membranes have been taken through the Motor powered Rig shown in figure 3:14. The dried membrane is removed from the Carbolite Oven and allowed to cool to room before the gain will be determined.

3.1.2 Reactor System

The reactor system used in this project was made of stainless steel material with welds at all the needed joints. The reactor has three segments: the feed side, the retentate section and the permeate side. Figure 3:7 show a typical membrane reactor with the three sections. The reactor in figure 3:7 below was used to carry out different permeation experiment at room temperature, low and high pressure condition only. At elevated temperature process, the reactor in jacket which is

shown in figure 3:1 was used. The jacket was to optimize the heat distribution and for safety needs. In figure 3:8, the reactor is showing a hollow part which houses the membrane during permeation experiments. The shape of the reactors used in this project determined the shape of the membrane support used. This project only limited the reactor housing to a hollow unit. Each reactor end was provided with a graphite seal; to create a seal between the membrane support and the internal end surface of the membrane reactor. The graphite seals were ordered from GeeGrahite and they were designed to withstand high temperature (up 800^0C) [5] and acidic and high pressure operation.

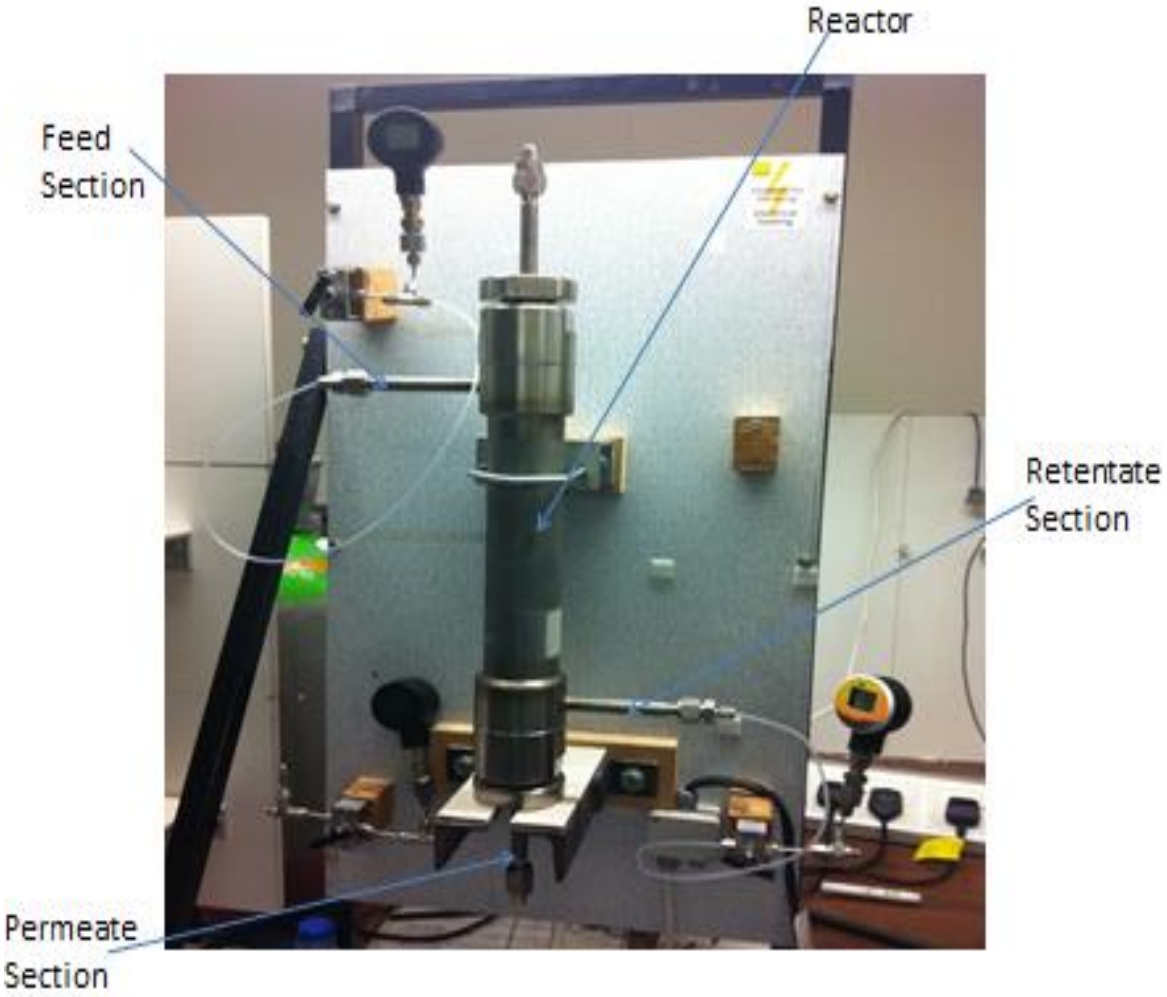

Figure 3:7: Membrane Reactor with Section

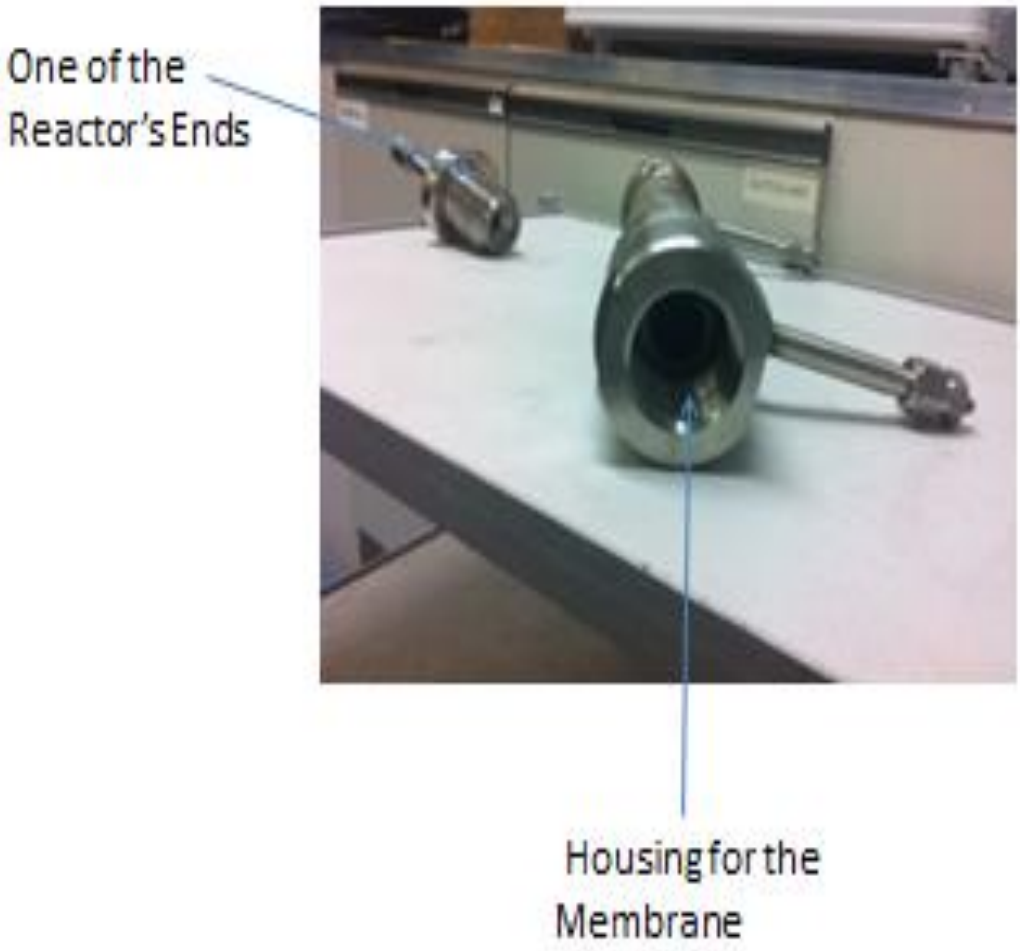

Figure 3:8: Reactor showing the Membrane Housing Unit

Figure 3:9: Pictorial Diagram of the Analytical Section

The Analysis system consists of Gas Chromatograph and the Computer set. The Gas chromatograph of Variant type was always calibrated before any analysis was conducted. This was to ensure that the machine was in a good working condition. This has a gas inlet and out let pots for gas mass transfer through the system. The gas analysis was achieved on a 2 metre long stainless steel column packed with porapak QS 50-80 mesh and 2 metre x 1/8 inches x 2 mm stainless steel column packed with molecular sieve 13x mesh, using a thermal conductivity detector[5]. The Air was used to activate the valves of the chromatograph while Helium or Argon was used as a carrier gas. The gas analysed is displayed on the computer in a graphical presentation called Peaks. Each gas peak represents the amount of gas in a particular stream of the gas mixture being injected into the gas

chromatograph. The results of the analysis are based on a percentage composition of all the gases present in the inlet gas stream.

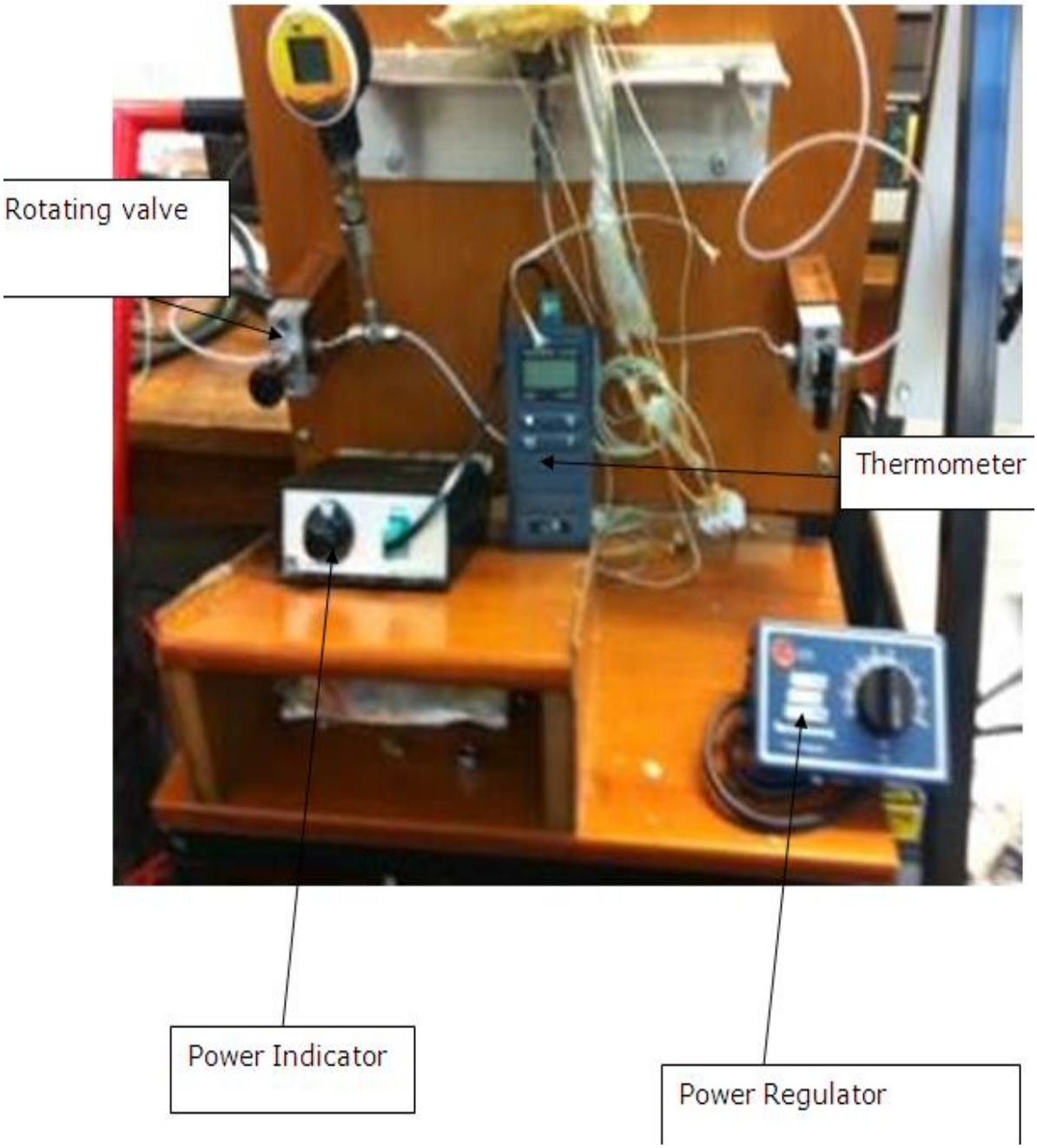

Figure 3:10: Reactor Heating System and Control

The figure 3.10 shows different experimental apparatus that used in heating and controlling the reactor during permeation experiment. In high temperature

permeation, the heating effect was supplied from the power mains, which was regulated by the power regulator shown in figure 3:10 above. The pressure gauge is used to monitor the gauge pressure of the gas. The thermocouple transmits the heating effect to the power indicator.

3.2 MATERIAL

3.2.1 Gases

i) Carbon dioxide

Carbon dioxide supplied was categorized into two groups: the single gas and mixtures. The single gas carbon dioxide was supplied 99.8 % pure by Air Liquid with maximum pressure at 288.5 K of 50Bar. For Carbon dioxide mixtures, below is the table of all the mixtures of the Carbon dioxide used in this investigation.

Table 3:1: Different CO_2 gas mixtures

Carbon dioxide and Nitrogen	Gas Mixtures
14% CO_2 86% Nitrogen	Mixture A
30% CO_2 70% Nitrogen	Mixture B
60% CO_2 40% Nitrogen	Mixture C

All these mixtures were supplied by Air Liquid with the same temperature and pressure as mentioned above.

ii) Nitrogen

Nitrogen of 99.97 % purity was supplied in cylinders by Air liquid with maximum pressure at 288.15 K of 230 Bar. No additional purification was required.

iii) Oxygen

Oxygen 99.5% was supplied from Air Liquid and this was used without further purification. Maximum delivery pressure was 230 Bar at 288.15 K

iv) Methane

Methane gas supplied was 99.9% pure. No further purification needed, and maximum operating pressure at 296K was 137 Bar. This was equally from Air Liquid.

v) Gases for Chromatograph

Helium, Argon and Air gases which were used as carrier gases and as an activation gas were equally supplied from Air Liquid with the same temperature and pressure condition with that of Nitrogen . All the gases used in this gas chromatograph were used one after the other to calibrate the GC.

3.2.2 Chemicals

i) Silicon Elastomer SYLGARD 184 from Dow Corning

ii) SYLGARD 184 Curing Agent Silicone Elastomer from Dow Corning

iii) 2- Methyl butane (Isopentane) from SIGMA-ALDRICH

iv) Aluminum Monohydrate (AlO (OH)) – Boehmite Powder. This was supplied by Alcan Chemical Europe.

v) Magnesium Oxide from SIGMA-ALDRICH, 98 % purity

3.2.3 Ceramic Support

The support used from this project was an alpha alumina tube with externally coated with Titania. This was supplied by Ceramiques Techniques et Industrielles (CTI SA) in France.

3.3 SAFTEY

3.3.1 Flame and Explosion

The gases used in this investigation were categorized into flammable and non-flammable gases. The experiments with any of the flammable gases were done with extreme care. The gas exhaust from the GC was always channelled to the Fume cardboard in order to minimize the gas concentration in the investigation Lab. No real flame was involved in the investigation.

3.4 SAFETY CHARACTERISTICS OF CARBON DIOXIDE

Carbon dioxide is a colourless gas or a colourless cryogenic liquid [6]. At low concentration, both the gas and liquid are odourless. At higher concentrations Carbon dioxide will have a sharp, acidic odour. Because of the risk of exposure of high concentration of carbon dioxide, the gas exist was connected to the fume cardboard which vent the excess carbon dioxide to the atmosphere. This has made it possible for the carbon dioxide to be regulated to allowable concentration. For explosion risk, carbon dioxide is considered safe in this regards.

3.4.1 Safety Characteristics of Nitrogen.

Nitrogen is already abundant in nature and its ability to not support combustion gave me a free hand to handle it without any concern. The Nitrogen was used in pure and mixture state.

3.4.2 Safety Characteristic of Methane

Methane gas is one of the top flammable gases used in this investigation. A lot of care was put in place each time methane gas was involved in the permeation experiment. Fume Cardboard was always on and the lab was ensured of heat free at every time permeation involved methane gas.

3.4.3 Safety Characteristic of Isopentane

This high volatile and high flammable liquid was given a special attention each time it was to be used in the investigation process. This volatile liquid was always kept in the refrigerator to ensure its safety. Direct contact with flame was completely discouraged throughout this investigation period.

3.4.4 Safety Characteristics of Boehmite Powder

Boehmite used in this project was supplied in a powdered form. This is one of the non-hazardous gases used in this project. There was no risk of explosion that was encountered as a result of using Boehmite.

3.4.5 Safety Characteristics of Magnesium Oxide.

The Magnesium Oxide could be poisonous if inhaled the burnt one. For this case, no direct heat was allowed with the magnesium powder used in this experiment.

3.5 MEMBRANE PREPARATIONS

3.5.1 Support Modification

The modification of the supports used in this investigation was done to create a more active surface for separation of gases from their mixtures. The supports were commercially supplied by CTI SA France. These consist of Alpha Alumina (α-alumina) structure washed coated externally with TiO_2 resulting in 77% α - alumina and 23% TiO_2. The support profile has an outer diameter (OD) of 25.81mm, inner diameter (ID) of 20.5mm and support thickness of 5 mm. All the supports used had the average pore sizes of 6000nm and a total length of 360.5mm each, with effective length 310.5mm. Figure 3.10 and figure 3.11 show typical example of the support profile used in this project.

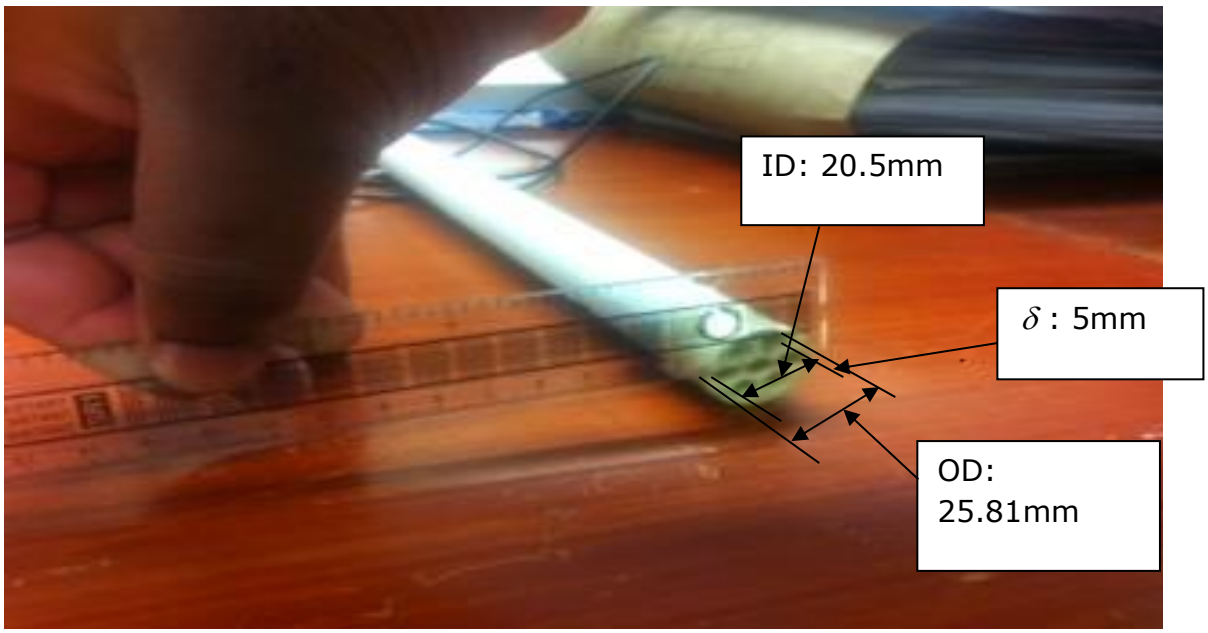

Figure 3:11: Pictorial front view of a Membrane Support

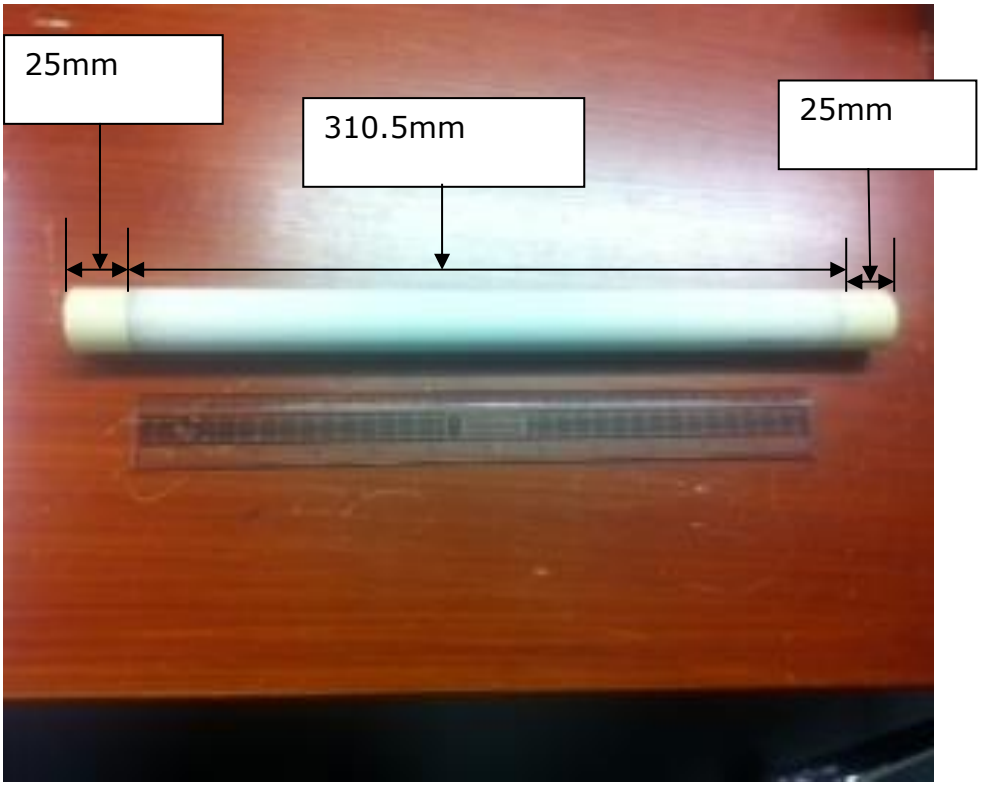

Figure 3:12: Pictorial side view of a Membrane Support

The figures 3:11 and figure 3:12 above show the pictorial diagrams of the front and side views of the membrane support. The support has permeating and non-

permeating section. The permeating section was 310.5mm long and non-permeating sections were 25mm long on each end.

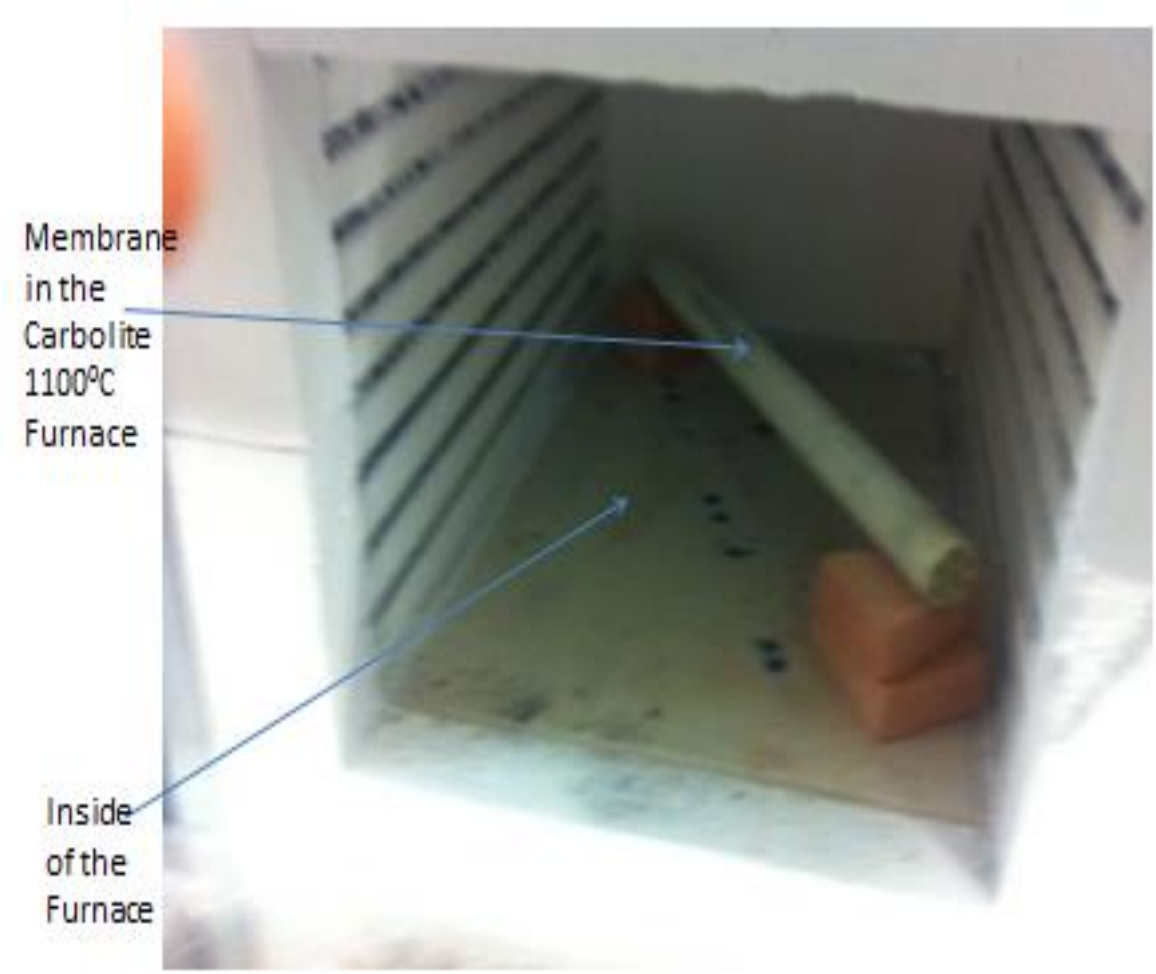

Figure 3:13: Carbolite Furnace (Max temperature= 1100^0C)

3.6 BOEHMITE PREPARATION

Before a sample of support was modified, the weight of the support was measured. After that a 0.6 mol/L Boehmite sol was prepared as an γ-alumina source. The support was then dipped in the prepared solution and both the internal and external surfaces of the support were exposed to the Boehmite solution for up to 20 minutes. At the end of the dipping, the membrane support was removed and air dried for 20 minutes motor powered rig before calcining in a 900K furnace for 5

hours program. Figure 3:14 and figure 3:15 below show the pictorial view of the rotating rig and the schematic diagram of the Calcination program, otherwise known as the Heat Treatment Profile.

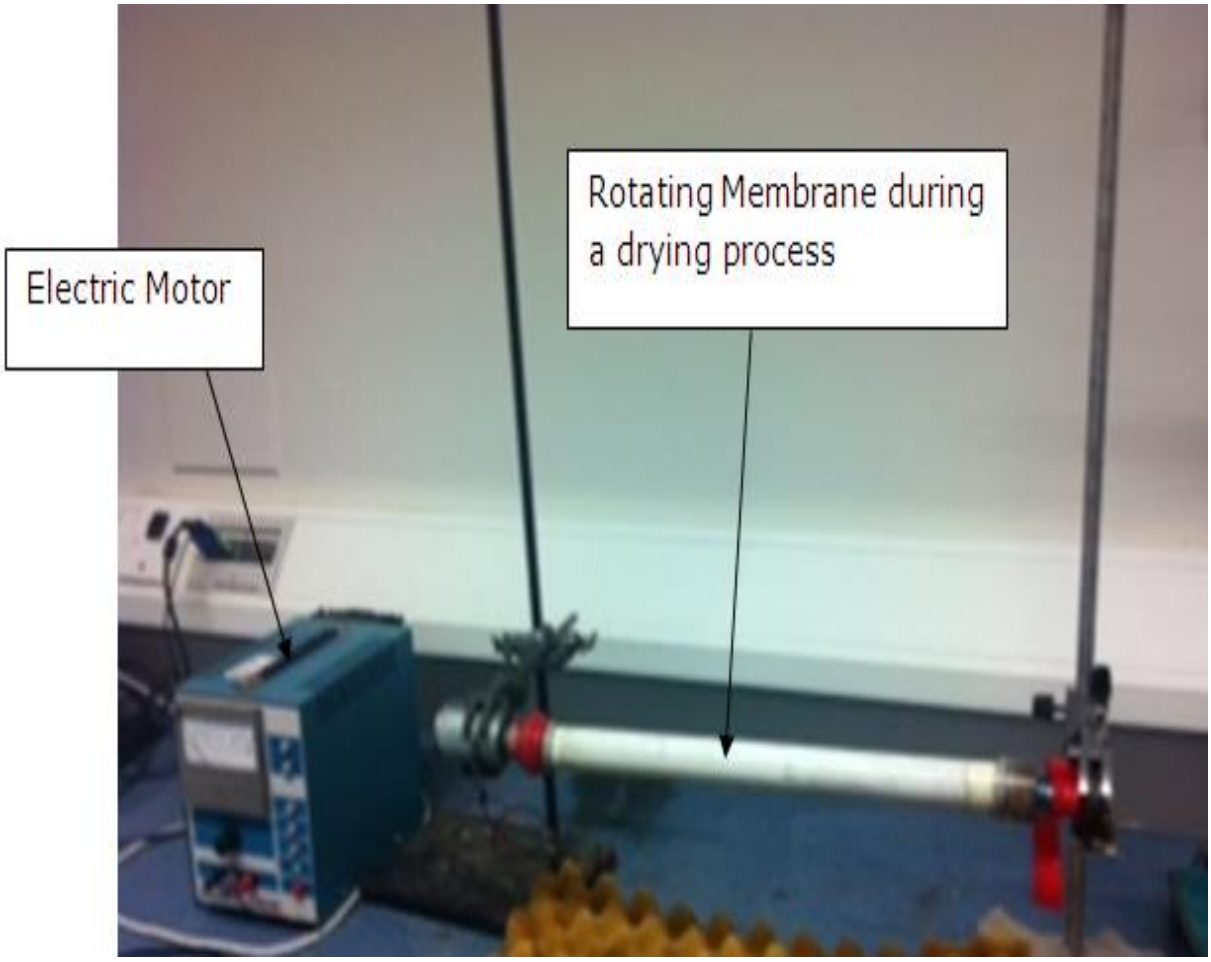

Figure 3:14: Motor powered Rig for uniform drying of the dipped membrane

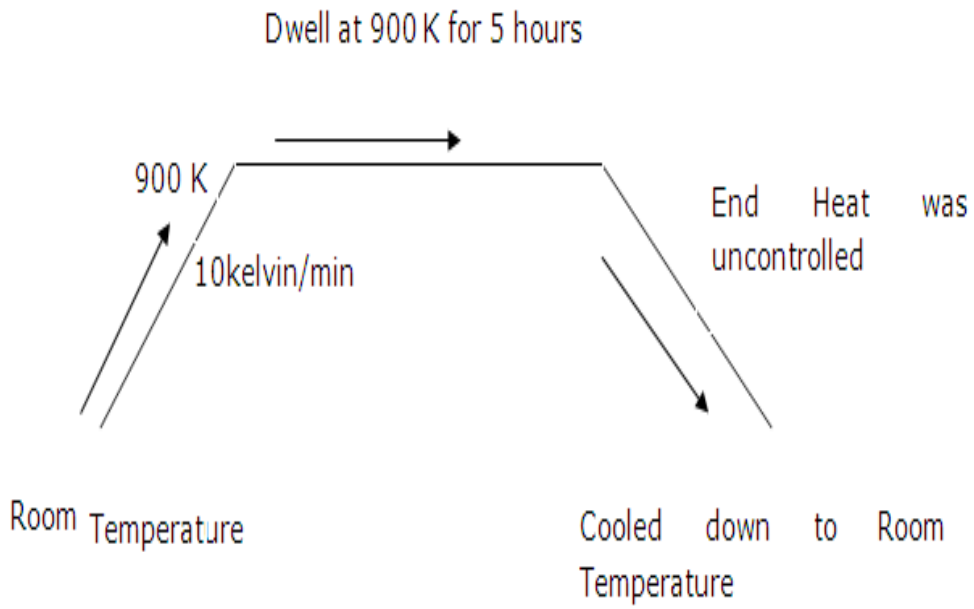

Figure 3:15: Calcination Program (Heat Treatment Profile) in Kelvin per minute

The membrane dipping was done more than once in order to achieve the desired level of gamma alumina thickness on and inside surfaces of the membrane.

3.7 MEMBRANE CHARACTERIZATION.

In order to view the surface morphology and inter structure of the developed ceramic membrane, the developed membranes were subjected to high resolution SEM machine. This Scanning Electron Microscope check was conducted by the help of Technicians in the Natural Science department. The pictures of the fabricated membrane which were checked under SEM are in figures 4:14 and figure 4:15 respectively.

3.8 PRODUCT IDENTIFICATION

Gas chromatography (GC) from Varian was used throughout this project to identify the gases from the membrane stream. As shown earlier in figure 3:9, the GC has an inlet and outlet ports where the gas from the membrane reactor goes in and out of the GC. The Chromatography used had a constant supply of a carrier gas, usually Helium, and air as an activation gas, which were permanently connected to the GC for the analysis to be done. Below is the pictorial view of the Varian GC 3800 used in the identification of the permeate results.

Figure 3:16: Schematic Diagram of Varian 3800 Gas Chromatography

The temperature of the GC was always 30^{O}C and the flow rates of the carrier gas and activation gas 12.5 ml/min each. All these operating conditions of the GC were part of the methods used in analyzing each gas stream. The methods used depend

on the gas to be analyzed. The GC was run in on line mode and was equipped with two air actuated automatic valves including a sampling and a bypassing valve, star work station for data collection and analysis. There was two isothermal (323.15) stainless steel columns, porapak QS and molecular sieve 13X equally was used. The GC was always calibrated prior to each analysis. This was to ensure that the machine was in the right working condition. The calibration involved injecting pure gases such as CO_2, CH_4, N_2, He, and Arg to obtain their retention times. Then, a known gas compositions was injected to obtain the area of the peaks. All the gases mentioned above were analyzed in the molecular sieve column except Carbon dioxide which was analyzed in the Porapak column. All the gas analysis used a thermal conductivity detector (TCD) was used to identify the gases exiting from both columns. Figure 3:17 below shows a typical N_2 and CO_2 peak generated by the GC 3800 used in this project.

3.8.1 GC Calibration

The calibration of the GC was always done before any new analysis was done with the GC. This was done by equating the gas composition obtained by the GC to be same as the supplied gas bottle for analysis. Calibration of G/C is an automated process.

Operator : ike
Workstation: RG02701
Instrument : varian star #1
Channel : Front = TCD

Detector Type: 3800 (10 Volts)
Bus Address : 44
Sample Rate : 10.00 Hz
Run Time : 5.495 min

** GC Workstation Multi Instrument Version 6.41 ** 01141-2588-C69-24B5 **

Chart Speed = 3.87 cm/min Attenuation = 38 Zero Offset = 4%
Start Time = 0.000 min End Time = 5.495 min Min / Tick = 1.00

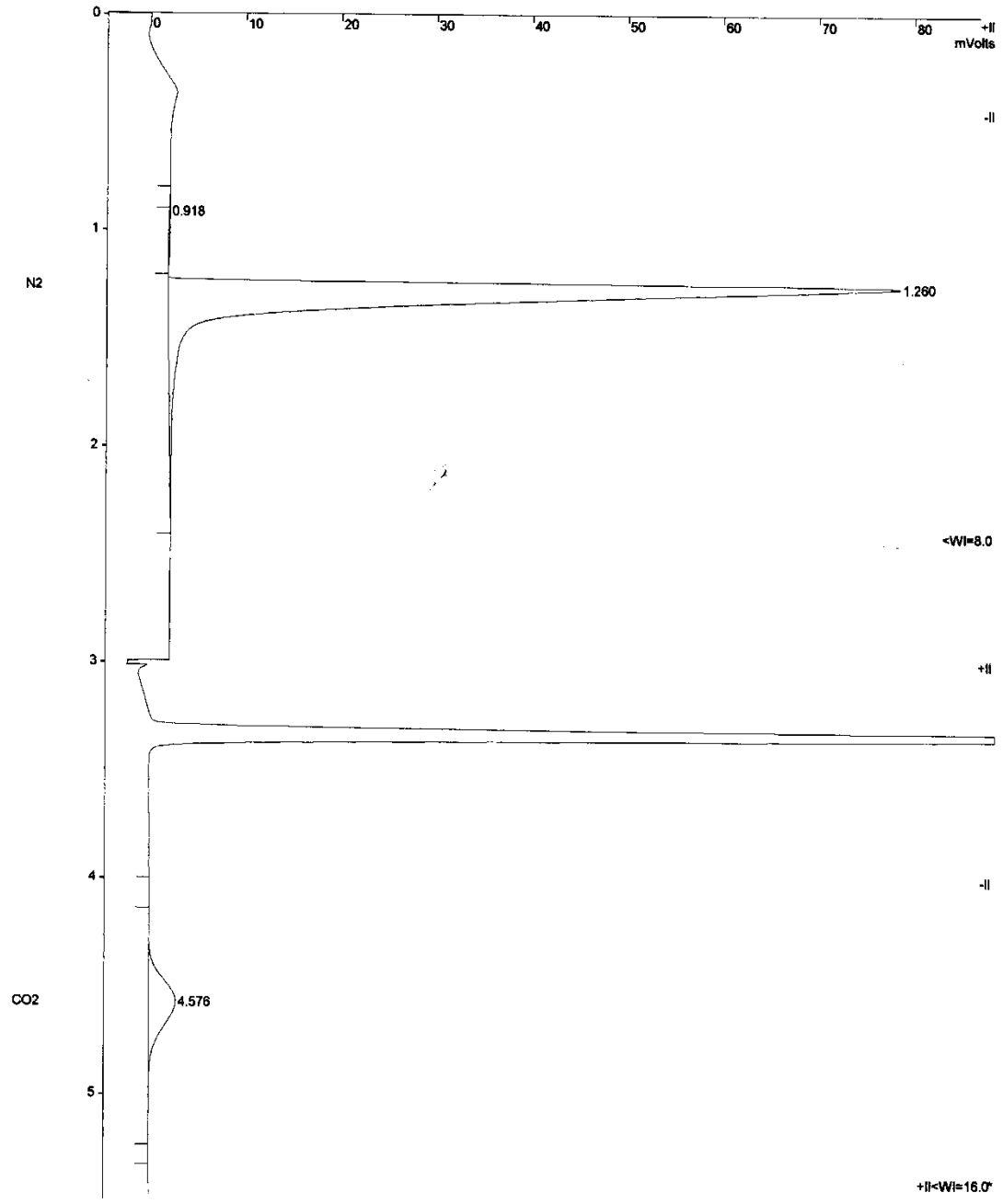

Figure 3:17: A typical GC Peak Graph showing CO_2 and N_2 Concentration

Table 3:2: GC Peak Table showing CO_2 Recovered at Third Stage Permeation

Print Date: Mon Jul 16 13:09:24 2012 Page 1 of 1

Title :
Run File : c:\star\data\3800.45079.run
Method File : C:\Star Data\CP3800\Methods\IKE UPDATED Method.mth
Sample ID : Manual Sample

Injection Date: 3/26/2012 1:26 PM Calculation Date: 3/26/2012 1:34 PM

Operator : RGU Detector Type: 3800 (10 Volts)
Workstation: ENGMA22PC15929ÿ□HÚ•8 Bus Address : 45
Instrument : Varian CP3800 Sample Rate : 10.00 Hz
Channel : Front = TCD Run Time : 8.492 min

** GC Workstation Multi Instrument Version 6.41 ** 01141-2588-C69-24B5 **

Run Mode : Analysis
Peak Measurement: Peak Area
Calculation Type: Percent

Peak No.	Peak Name	Result ()	Ret. Time (min)	Time Offset (min)	Area (counts)	Sep. Code	Width 1/2 (sec)	Group	Status Codes
1		1.1996	6.171	0.000	31318	BP	4.8	0	
2		4.0542	6.750	0.000	105844	PV	5.5	0	
3	N2	3.8439	7.047	0.000	100356	VV	17.5	0	
4	CO2	90.9023	7.419	-0.008	2373247	VB	15.3	0	
	Group 0	100.0000		-0.008	2610765				
	Totals:	100.0000		-0.008	2610765				

Total Unidentified Counts : 237519 counts

Detected Peaks: 4 Rejected Peaks: 0 Identified Peaks: 1

Multiplier: 1 Divisor: 1 Unidentified Peak Factor: 0

Baseline Offset: -59 microVolts LSB: 1 microVolts

Noise (used): 50 microVolts - monitored before this run

Manual injection

Data Handling: All Coefficients for All Peaks are Zero
Data Handling: Default to A%

3.9 SCREENING TESTS

A lot of preliminary different gas permeation tests were carried out with alpha alumina to determine the behaviour of the commercially supplied support (6000nm) to different gases. The trial experiments involved single and gas mixtures such as CO_2, He, Argon, N_2, and CH_4 under different pressure. No significant separation was identified during the trial stage. The results of the trial experiments can be located at the results section of this report.

3.10 SUPPORT MODIFICATION

After the preliminary experiments with the commercially supplied support, the supports were modified with gamma alumina in order to obtain the gamma crystal structure. The supports used were identified as support A, Support B, Support C and Support D. Support A, B and C were supplied with 6000nm mean pore sizes. All the supports used in this report were modified first with Boehmite suspension. The heat treatment of the supports was discussed in section 3 as shown in figure 3:15 in this report.

3.10.1 Membrane Solutions

3.10.1.1 Solution 1

Magnesium Oxide (MgO) Solution was the first solution prepared in this investigation project. The solution preparation and concentration achieved was similar to that of the Gamma Suspension in section 3.6 of this report. Permeation experiments carried out with this MgO modified membranes showed a rise in the flow rate of the carbon dioxide molecules more than Nitrogen molecules as shown in Table 8:42,8:43 and 8:44 in the result analysis section.

3.10.1.2 Solution 2

The solution 2 prepared was Silicon Elastomer (Sylgard 184) with Isopentane (2-methylbutane). The Isopentane was used as a solvent in 9:1 ratio with silicon elastomer. Also, a curing agent (Sylgard 184) was added into the solution after achieving a clear uniform state. This was added in a 9:1 ratio to the Silicon Elastomer (curry agent: 10 ml).The solution was kept in constant agitation with a magnetic stirrer during and after preparation except during membrane dipping.

3.10.1.3 Solution 3

The solution 3 prepared was Silicon Elastomer (Sylgard 184) with Isopentane (2-methylbutane). The Isopentane was used as a solvent in 4:1 ratio with silicon elastomer. Also, a curing agent (Sylgard 184) was added into the solution after achieving a clear uniform state. This was added in an 4:1 ratio to the Silicon Elastomer (curry agent: 20 ml).The solution was kept in constant agitation with a magnetic stirrer during and after preparation except during membrane dipping.

3.11 MEMBRANE COATING

As explained in the literature section, the coating method used in this investigation was Dipping Coating Technique. Four different membranes were produced in this project beside the commercially supplied alumina support. The membranes fabricated were numbered as Membrane A, Membrane B, Membrane C and Membrane D

3.11.1 Membrane A

Membrane A was prepared by dipping the dimensioned support A, which had 6000nm mean pore size and 25.81 mm outer diameter into a prepared suspension described in section 3 above. The membrane was heat treated (calcined) according to the heat treatment profile shown in figure 3:15.The membrane demonstrated better results than support A which had no coating on it.

3.11.2 Membrane B

Membrane B was combination of 6000nm mean pore size support, Gamma Alumina and Magnesium Oxide. This was prepared by the same procedure as discussed in section 3.10.2. Each section was heat treated according to the heat treatment profile shown in the figure 3:14 above. Also, membrane B showed an improvement on the $C0_2$ gas permeation compared to Membrane A (figure 8:43 and figure 8:44) in the analysis section.

3.11.3 Membrane C

Membrane C was prepared with a 25.81mm outer diameter support that had a 6000nm mean pore size. The support was dipped in a Gamma Alumina Suspension, solution 1 and solution 2 as discussed above in section 3.9.1.1 and 3.9.1.2 above. The results of the permeation experiments with Membrane demonstrated the highest performance with carbon dioxide compared to other membranes used in this investigation.

3.11.4 Membrane D

The Membrane D was prepared with a similar procedure to that of the Membrane C except that solution 3 was used instead of solution 2. There was no permeability result from this membrane as the concentration of the silicon elastomer was in excess; therefore it plugged the pores of the membrane which led to no permeation results with membrane D.

3.12 REACTOR AND MEMBRANE DESIGN

3.12.1 Reactor Design

The membrane reactors used in this investigation were designed by Professor Edward Gobina. The reactors were fabricated with high grade stainless steel which made them suitable for high temperature and high pressure applications. The shape of the reactors used determined the shape of the membrane modules used in this research. Reactors of two different sizes were used; Reactor A has a length of 450mm, outer Diameter of 70mm. As mentioned before in the previous section of this report, the reactors have three sections: the feed section, retentate section and permeate section. Each reactor has a housing (figure 3:8), which houses the

membrane module during permeation experiments. The membrane module was always sealed off at its two ends with graphite seals while in the housing.

3.12.2 Membrane Module Design

As mentioned above the shape of the membranes was determined by the reactor shape. The membrane was designed to be used for high temperature and high pressure processing application. Also, it was designed to be used for acid gas processing. Figure 3:11 and figure 3:12 show the profiles of a membrane module. The different channels help to support the entire membrane module mechanically. The design the membranes had gave them the ability to be used in carrying out investigations with different flow rates.

3.12.3 Flue Gas Design

As already mentioned in the previous chapters in this report, the flue gas used was simulated with different gas bottles supplied by BOC gas Ltd. Each composition was representations of industrial produced flue gas, which have undergo one or two stages in the compression stages. Full information on all the gases used for the investigation can be found in table 3:1.

3.13 INTRODUCTION OF SECOND AND THIRD STAGE IN THE PERMEATION TRAIN

As mentioned in the previous chapter, to achieve the recovering target, two more stages of equal recovering efficiency were introduced in series and one more extra membrane like membrane C was reproduced with the same reproduction steps discussed in the earlier chapters.

3.13.1 Second Stage Permeation and Recovering

In this stage, the gas stream which had CO_2-30% and N_2- 70% being the permeate composition of the gas stream recovered with the membrane C as the maximum recovering efficiency from the feed gas stream concentration of CO_2-14% and N_2-86%, was used as the feed gas stream for the second stage permeation. The results of the permeation showed a high rise in the selectivity of the carbon dioxide molecules and a drop in Nitrogen permeability contributed to the overall drop flow in by the membrane. This comply with the literature that the higher the concentration of the carbon dioxide in the feed gas, the more the partial pressure of the gas which give more mass transport of carbon dioxide through the ceramic inorganic membrane. The experiment demonstrated a positive result compared to the first stage permeation. The results of this are shown in the result and discussion section.

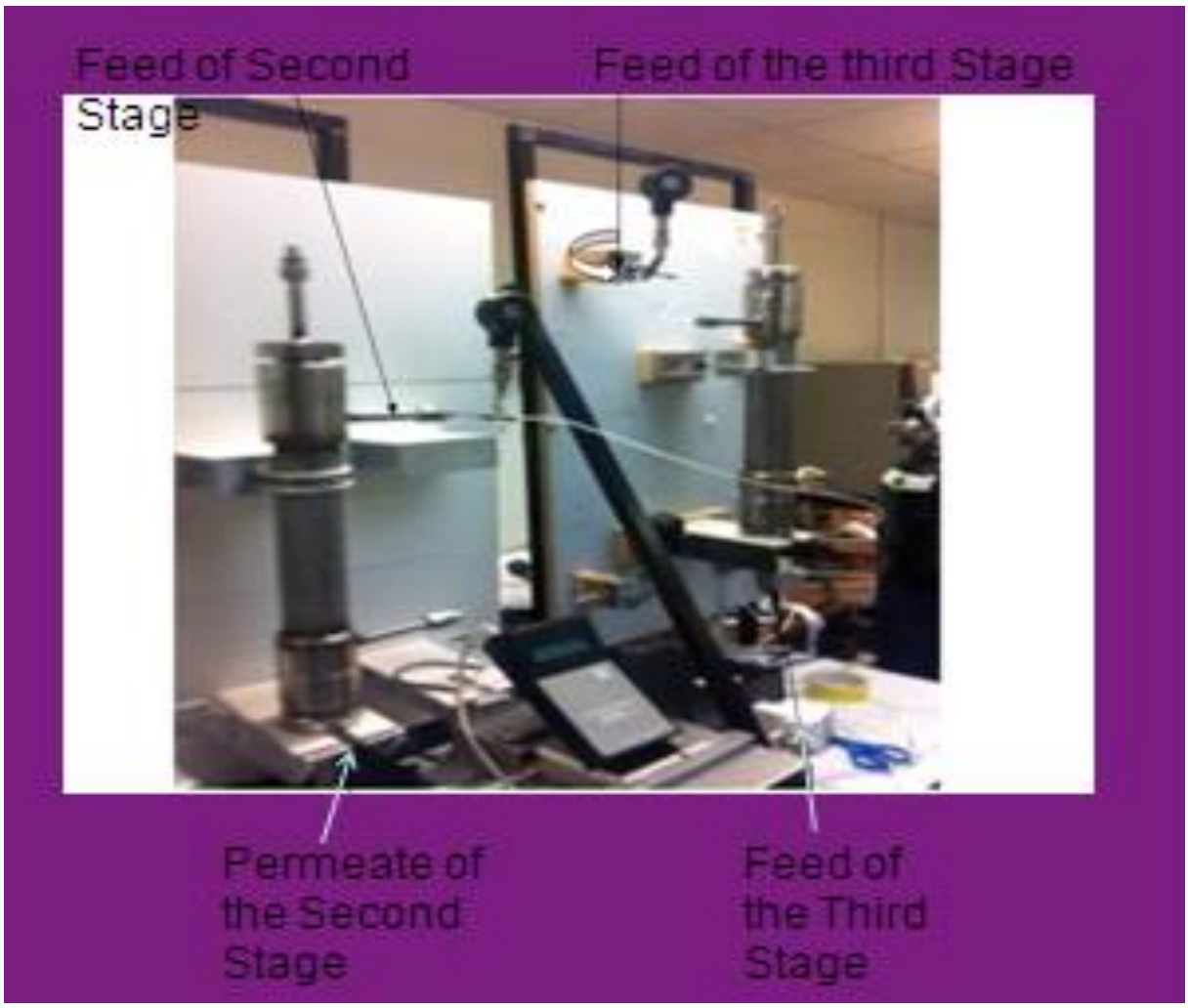

Figure 3:18: Showing Second Stage and Third Stage Permeation System

3.13.2 Third Stage Permeation and Recovering

In this permeation stage, the feed stream concentration was CO_2-60% and N_2-40% represented as mixture C, with a high partial pressure of the carbon dioxide gas stream. The same experimental conditions used at first and second stages were used in third stage permeation system. The overall permeability of the gas through the membrane was further reduced with a high recovery of the carbon dioxide gas molecules at the permeate side of the membrane. The pictorial representation of the second and third stage system is shown in figure 3:18 above.

4 RESULTS AND DISCUSSIONS

4.1 INTRODUCTION

This section contains the results and the discussions of the experimental data observed while varying different experimental parameters in order to determine the best approach, in using the Ceramic Membranes, for enhancing the concentration of the CO_2 from flue gas streams. The membranes fabricated in this project were tested with different gases and the maximum operating parameters of the permeation experiment and the operating limitation of Ceramic Inorganic Membranes were determined. The 6000nm average pore size, Alpha Alumina Supports (No Coat) which provided the mechanical strength to the membrane module were tested for permeation of gases at different conditions; the results indicated that the Carbon dioxide permeation rate was lower than the Nitrogen permeation rate in single gas permeation. The permeation of the mixture of CO_2/N_2, using no coated Alumina Membrane showed a higher permeation than with a pure CO_2 but there was no increase in the recovery of the CO_2 gas molecules. This comply with the literature that due to the sizes of the CO_2 and N_2 molecules as shown in (table 2:0), and there was no affinity attraction of either gases to the membrane support material, no difference was seen in the feed concentration of the CO_2/N_2 compared to the permeate concentration. This and other experimental results were discussed in more details below. The experiment equally found that counter current flow arrangement favoured N_2 permeation more than CO_2 permeation and there were no significant changes in the co current permeation arrangement of different gases. However, the membrane testing was focus on co current flow arrangement throughout the project time.

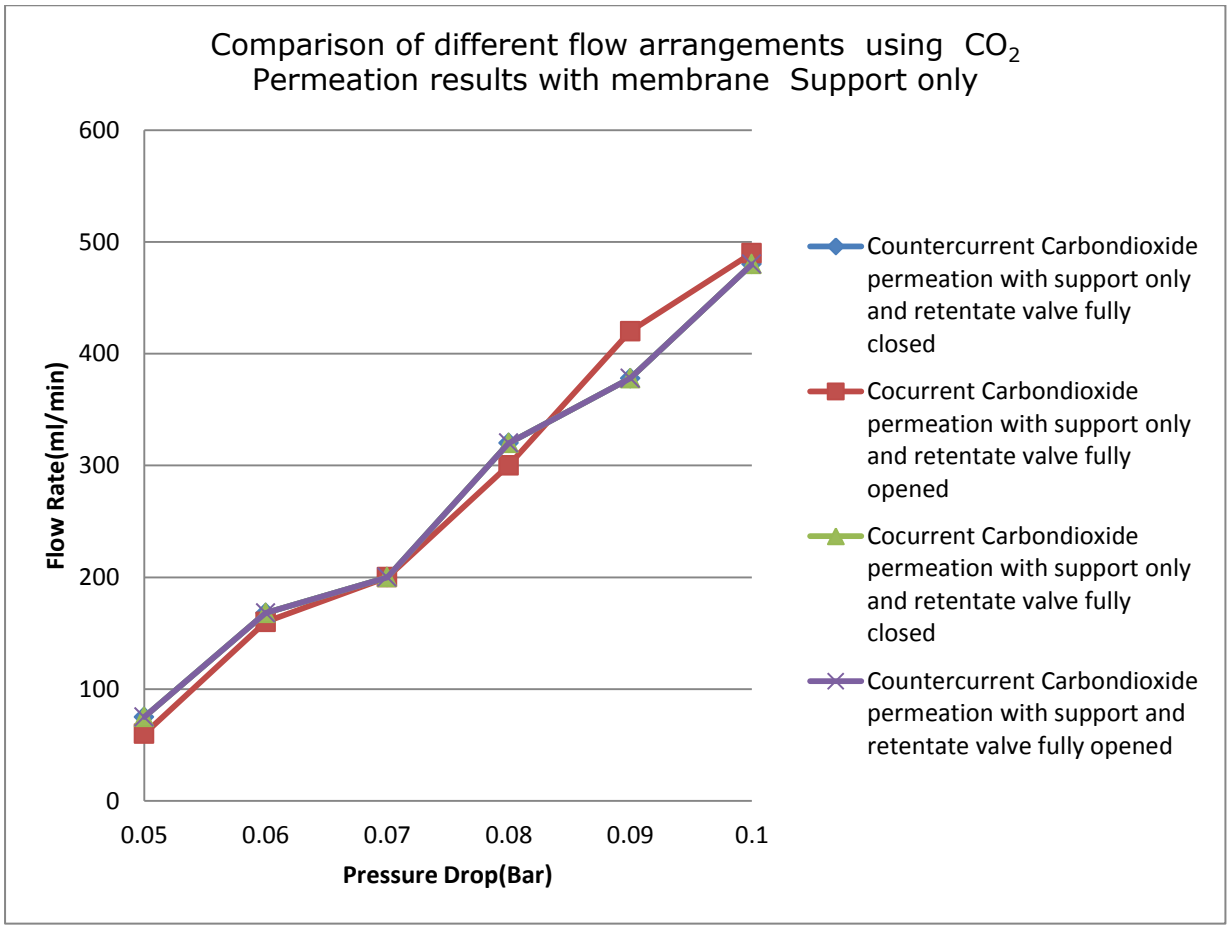

Figure 4:1: Comparison of different flow arrangements using CO_2 permeation results with a membrane support only

Figure 4:1 above shows different permeation arrangements of CO_2 permeation using Alpha Alumina support (no coat). Here, the graph indicated that no significant changes in the permeation arrangements with carbon dioxide molecules. But due to the high flow rate demonstrated by Nitrogen molecules using membrane support only, when in counter current position, as shown in figure 4:2 below, the Cocurrent flow arrangement with retentate valve fully closed was chosen as a suitable permeation arrangement for high CO_2 recovering using Inorganic Ceramic

membrane. The permeation results with the membrane support only favoured CO_2 more on co current arrangement than Nitrogen molecules which were higher than CO_2 permeation in counter current flow arrangement with retentate valve fully closed, as shown in figure 4:2 below. The pure Nitrogen and pure CO_2 permeations' experiments, in counter current flow arrangement gave a Nitrogen flow rate of 278 ml/min and CO_2 flow rate of 75 ml/min at a transmembrane pressure of 0.05 bar each, using membrane support only at 296K. But at the same operating conditions with co current flow arrangements, the Nitrogen flow rate was 90 ml/min and Carbon dioxide flow rate was 70 ml/min. These were shown in tables 8:6, 8:8, 8:10 and 8:11 respectively. The CO_2 permeation was lower than Nitrogen results in both permeation arrangements because according to relative molecular mass, Carbon dioxide which has a molecular mass of 44(g/mol) against Nitrogen of 28 (g/mole) may have experienced higher friction with the membrane support pore walls than that of the Nitrogen molecules. This was according to the gas transport properties shown in table 2:1, which was in agreement with Knudsen flow, expressed in equation 2.5.There was no modification what so ever on the membrane support at that point. The Nitrogen permeation flow was noticed to be more when the flow arrangement was in counter current mode due to more energy required for Carbondioxide to flow through the pores of the membrane support as already shown in figure 4:2 below.

As one of the interests in this project was centred on using the fabricated Ceramic Inorganic membranes to optimize carbon dioxide recovering from flue gas stream, up to an economic scale, Membrane A, which was modified with Gamma Alumina was fabricated, and then used in the permeation of different gases, like the one mentioned earlier. The results of this membrane, as seen in figure 4:3 below,

shows a rise in the Carbon dioxide permeation more than that of the results from the Alpha Alumina Support in figure 4:2. These results comply with the literature [3][5][15] confirmed that the Gamma Alumina which has more basic hydroxyl surface exhibited more attraction to acid gas(CO_2) than a neutral gas(N_2), although, Nitrogen still showed a good permeation rate because of its molecular weight factor as compared to that of the carbon dioxide molecules. The Gamma Alumina increases the area of the adsorbing site of the membrane, thereby making more sites available for Carbon dioxide adsorption as the electrical charge exhibits by the hydroxyl group increase as the acid-base interaction increase which was found to be higher in Gamma Alumina than Alpha Alumina, as confirmed in a study [10].

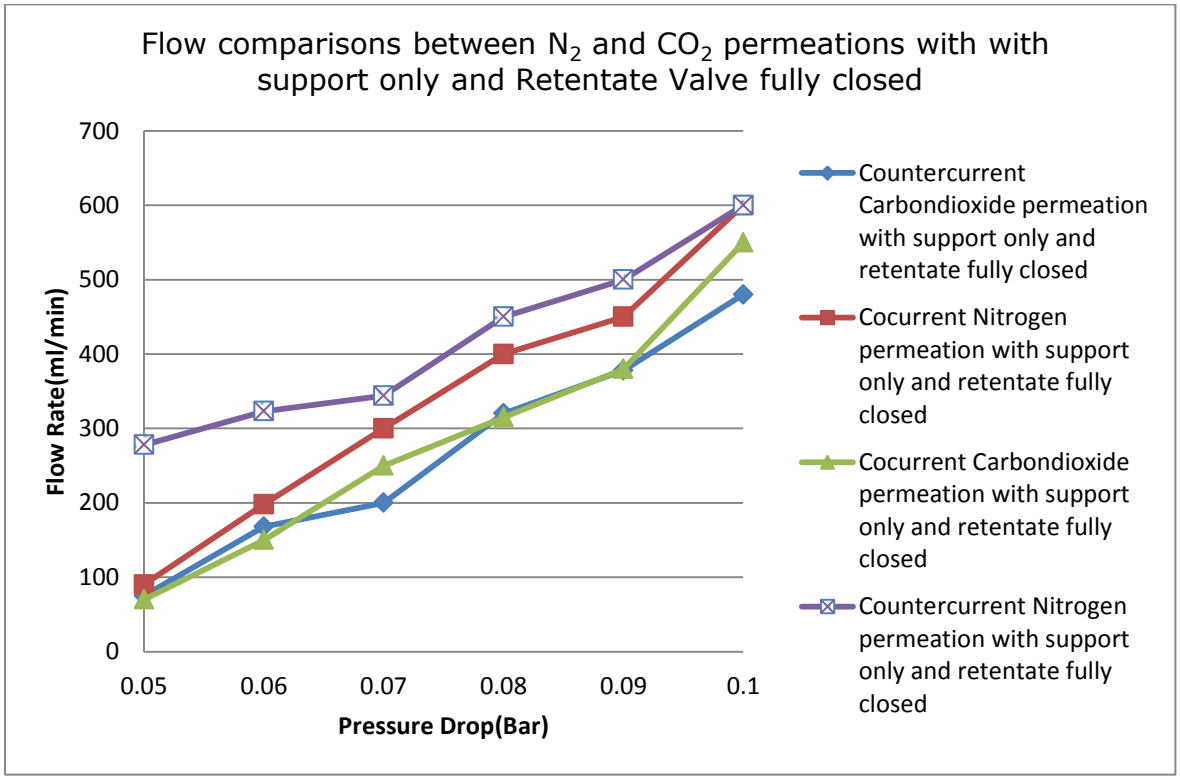

Figure 4:2: Showing different permeation arrangements of CO_2 and N_2 gas molecules with support only.

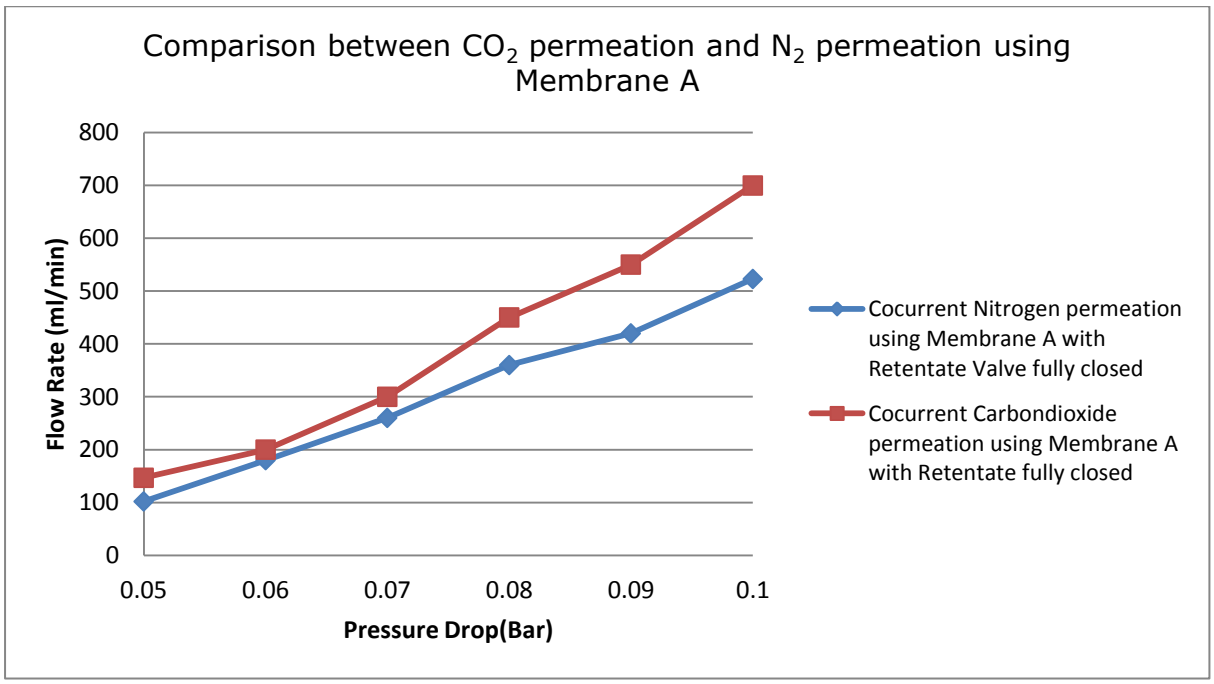

Figure 4:3: Comparison between CO_2 permeation and N_2 permeation using Membrane A

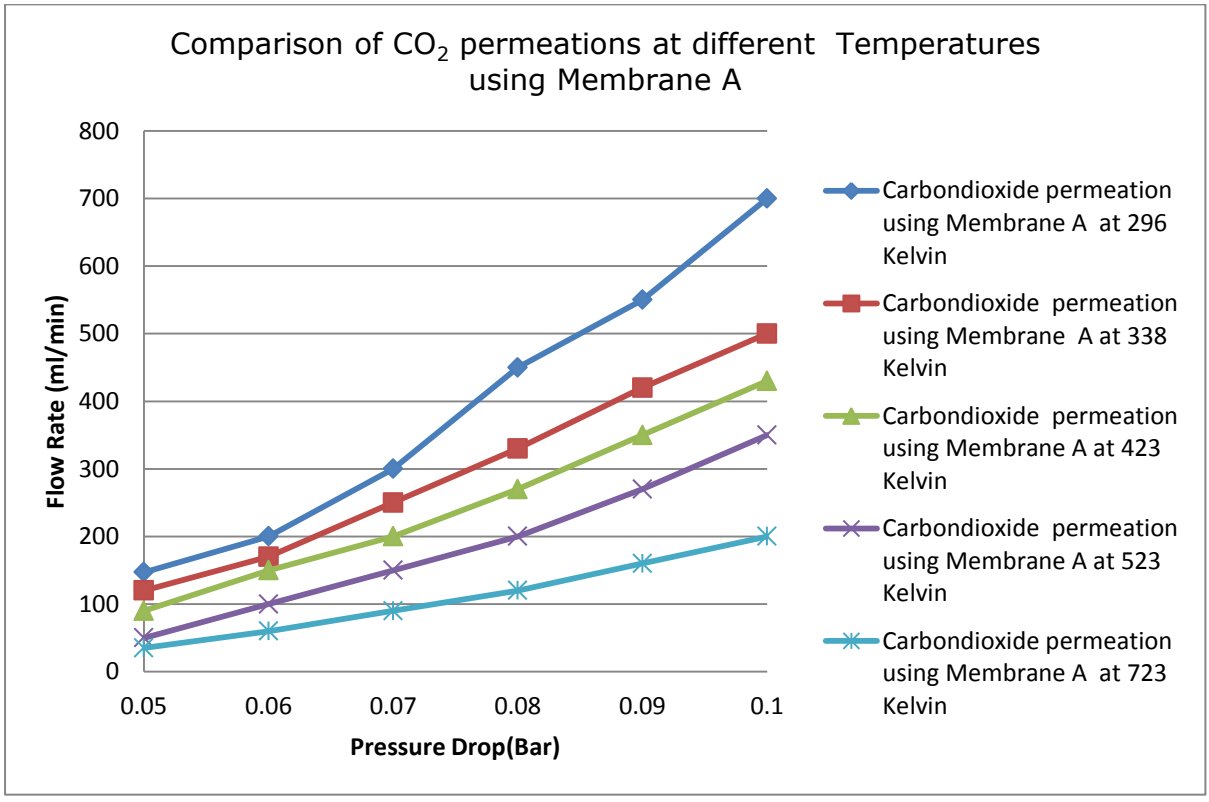

Figure 4:4: Comparison of CO_2 Permeations at different Temperatures using Membrane A

The figure 4:4 above is showing the permeation results of Membrane A after calcination at 900 K as described in the previous chapter. The above figure shows the behaviour of Carbon dioxide molecules at different temperatures using Membrane A at a transmembrane pressure range of between 0.05 bars to 0.1 bars. The membrane demonstrated high permeation rate of Carbon dioxide at 296K than at 723K. This was in line with the literature [26] where it was reported that the concentration of the ideal gas (P/RT) decreases linearly with increase in temperature. So at high temperature, fewer molecules of carbon dioxide were available to adsorb on the created adsorption site provided by calcination of membrane support. Also, at higher temperatures, molecule would be more energized, thereby making them more random in movement. This random motion makes it more difficult for the energized gas molecules to follow a defined path which resulted in reduction in the permeation of carbon dioxide molecules at 723K. The membrane A showed a decrease in the Carbon dioxide Permeance from 8.93E-07($mol.m^{-2}.s.Pa^{-1}$) at 296K to 2.13E-07($mol.m^{-2}.s.Pa^{-1}$) at 723K. The temperature effect on gas permeation using membrane A showed the same effect on the membrane B and C respectively as shown in tables 8:91 and table 8:95 for membrane B, and table 8:121 and table 8:126 for membrane C respectively. The recovery efficiency made by membrane A indicated no significant changes on the positive direction compared to Alpha Alumina Support.

From table 8:42 in the appendix section, the permeation and recovering of the CO_2 gas molecules from the mixture of CO_2/N_2 molecules. The feed concentration for CO_2/N_2 was CO_2-14% and N_2-86%. The membrane used was named as membrane B which was modified with magnesium oxide solution as discussed in the previous chapter, in order to increase the membrane adsorption sites which resulted in increasing the Carbon dioxide flow through the membrane. The table shows that up

to 25% of the Carbon dioxide was recovered by the membrane, making it a promising membrane for acidic gas purification.

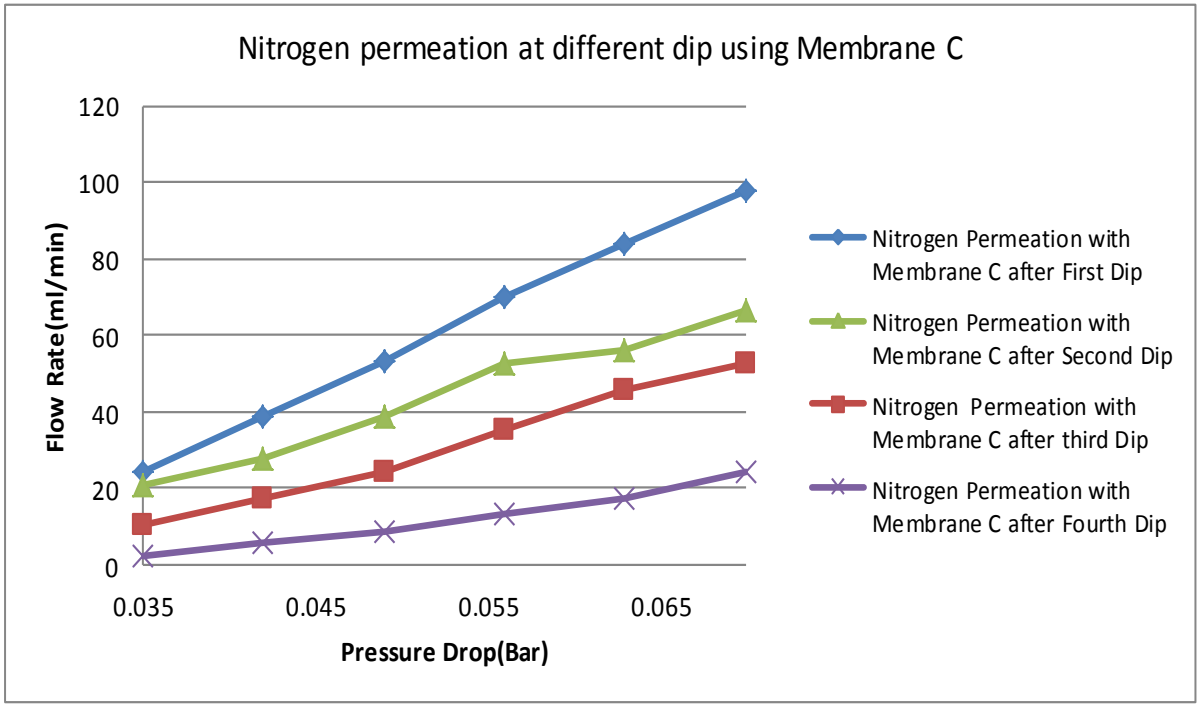

Figure 4:5: Nitrogen Permeation using Membrane C after different Dips

Figure 4:5 shows the reduction in the flow of the Nitrogen through Inorganic Ceramic membrane as the dipping number increases. The membrane permeation rate of the Nitrogen decreases as the dipping number of the membrane increases in the form 1st Dip>2nd Dip>third Dip>4th Dip. This was so because as the membrane dipping increases, more materials were found to be deposited on and inside the pore channels of the membrane surface, thereby lowering or even plugging the channels. As a result of this, gas flow resistance through the channels has increased significantly, resulting in lowering of the flow through the membrane channels.

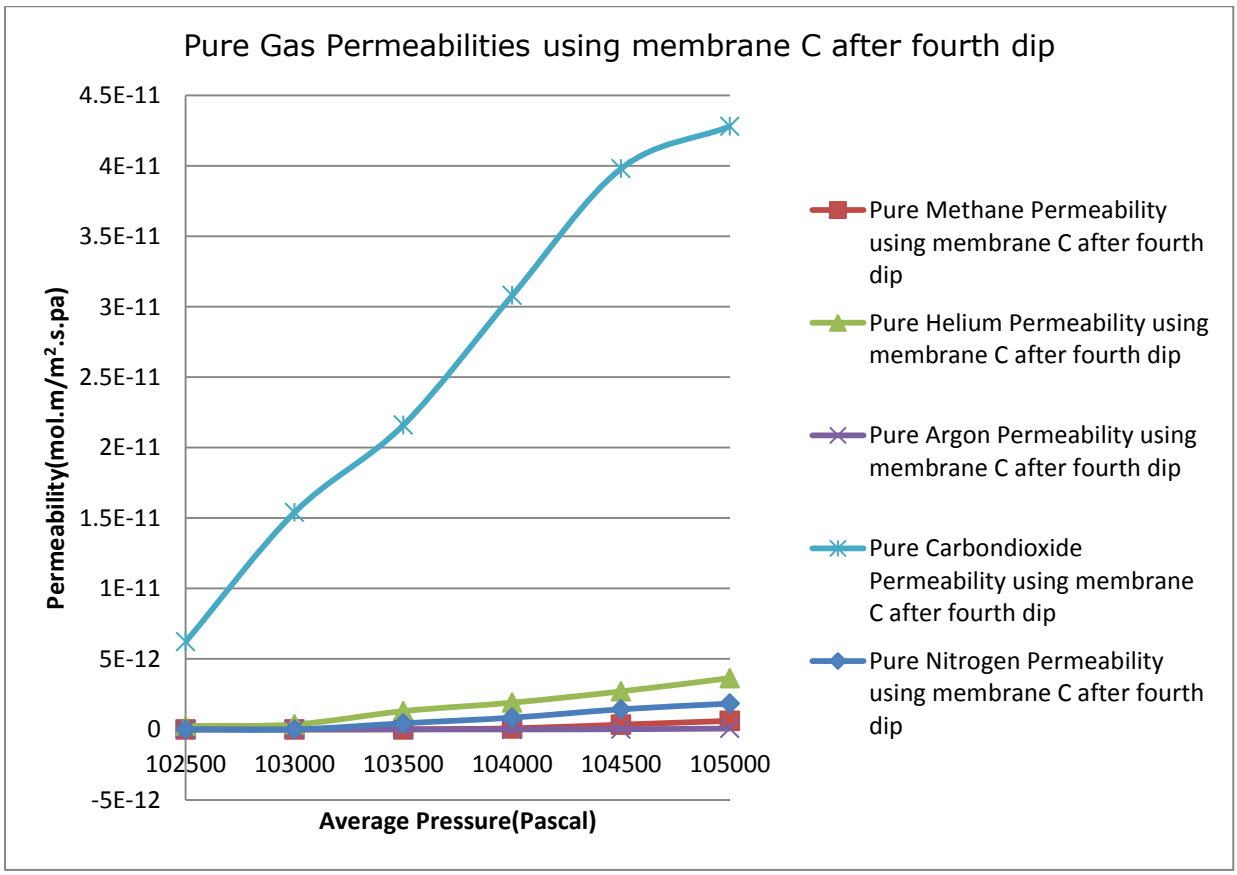

Figure 4:6: Comparison of different gas permeation using Membrane C after 4 Dips with Retentate Valve fully closed

In figure 4:6 above, different gases were tested using Membrane C after fourth Dip. The results above demonstrated that the membrane C was preferably selective to carbon dioxide more than every other gas tested on it. The Membrane C which combined the adsorption strength of the Magnesium oxide and silica demonstrated an enhanced affinity to Carbon dioxide. The experiment demonstrated that pure Argon was not permeable to the Membrane C up to 8KPa transmembrane pressure as shown in figure 8:79 and table 8:120. For pure methane gas molecule, the permeability of the gas at 5KPa and 6KPa transmembrane pressures were both(0) zero compared to over $6.22x10^{-12}$ ($mol.m.m^{-2}.s^{-1}.Pa^{-1}$) and $1.54x10^{-11}$($mol.m.m^{-2}.s^{-1}.Pa^{-1}$) of the Carbon dioxide molecules through the same membrane C at same

operating as shown in tables 8:116 and table 8:122 in appendix sections . For pure Nitrogen molecules permeability of membrane C, zero flows were recorded with the gas at transmembrane pressures of 5KPa and 6KPa respectively as shown in table 8:128. Also, for pure Helium gas molecules, the gas permeability through the membrane were $2.44x10^{-13}$(mol.m.m^{-2}.s^{-1}.Pa^{-1}) at 5KPa transmembrane pressure and $3.54x10^{-13}$ (mol.m.m^{-2}.s^{-1}.Pa^{-1}) as shown in table 8:118 in the appendix section. These above results were in compliance with the earlier studies in [[5] [7][15] [34]that the Silica membrane , in combination with magnesium oxide forms a stronger affinity to acid gas, in this case CO_2 molecules was favoured. Also, membrane C was unable to select Carbon dioxide 100% due to the involvement of other factors of diffusion which did not favour Carbon dioxide when compared to other gases [23]. Factors such as gas molecular weight, particles diameter, and pore size of the membrane affected the diffusion of gases through the membrane pores [23]. For mixture of gases, mixture A which consists of (14%- CO_2 and 86% N_2) as shown in table 3:1 in the chapter 2, was used for the permeation experiment. The permeability of the Nitrogen molecules through the membrane C at 3.01KPa transmembrane partial pressure was 4.24E-13(mol.m.m^{-2}.s^{-1}.Pa^{-1}) and at 3.1KPa transmembrane partial pressure was $1.10x10^{-12}$ (mol.m.m^{-2}.s^{-1}.Pa^{-1}) as shown in table 8:114. For Carbon dioxide molecules from mixture A using membrane C, the permeability at 1.05KPa transmembrane partial pressure was 5.20E-13(mol.m.m^{-2}.s^{-1}.Pa^{-1}) and at 1.06KPa transmembrane partial pressure was 1.38E-12 (mol.m.m^{-2}.s-1.Pa^{-1}) as shown in table 8:112. From the listed results, Membrane C was found to favour pure gas permeating through it than mixture of gases. These results were in line with the literature [15] which indicated that the presence of different gases can introduce a competition at the membrane adsorption site and in the pore channel, thereby creating a relative motion between

the gases which has a delay effect on the escaping velocity of the permeating gas. As a result of this, the overall permeability of the Carbon dioxide mixture was found to be less than that of the pure gas permeability using membrane C respectively.

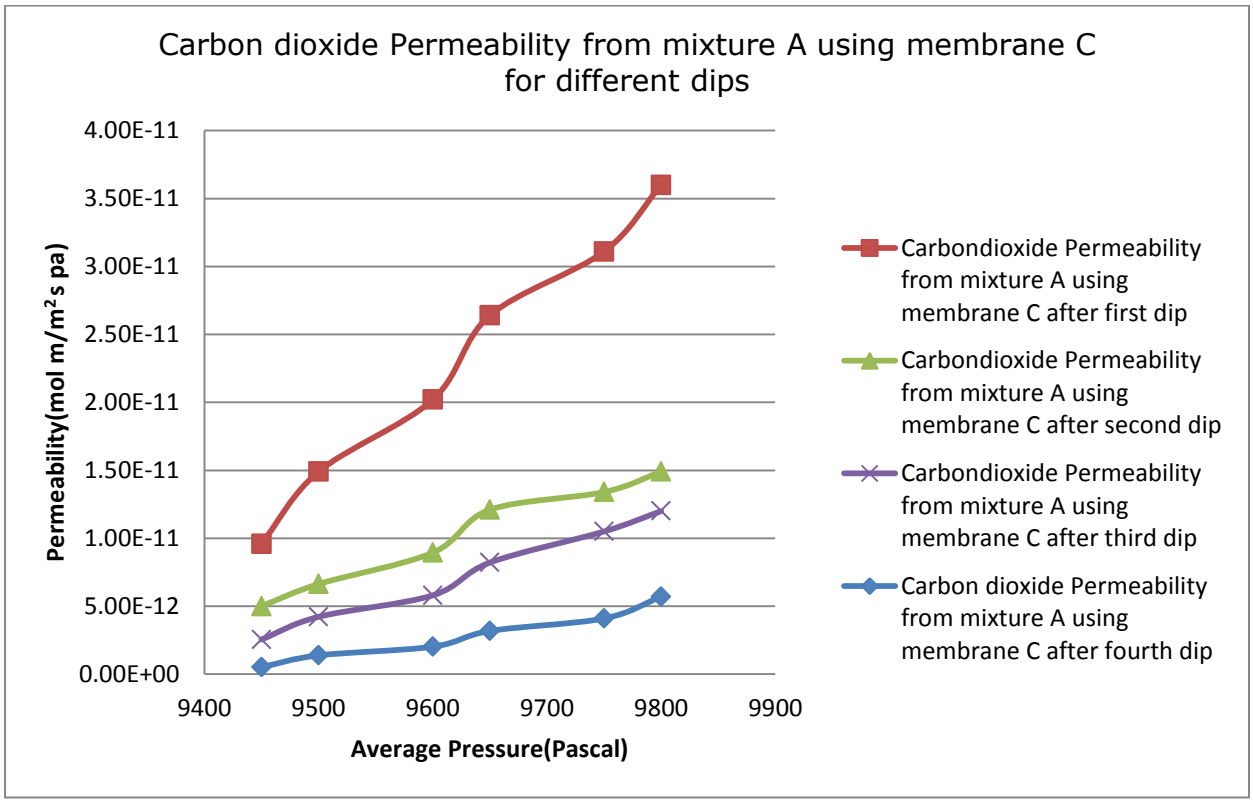

Figure 4:7: CO_2 Permeability from mixture A using Membrane C for different Dips

As was stated in the literature study, the permeability of the gas does not depend on the thickness of the membrane, but the thickness has a normalizing effect on the permeability [23] and does affect the diffusion of the gas through the membrane. In figure 4:7 above, Carbon dioxide was found to experience least permeability with membrane C after fourth dip with a membrane thickness of $2.00x10^{-4}$m. Here, as thickness affects the diffusion of the gas through a controlled pore, fewer gas were available to permeate through the membrane as can be seen in figure 4:7 above.

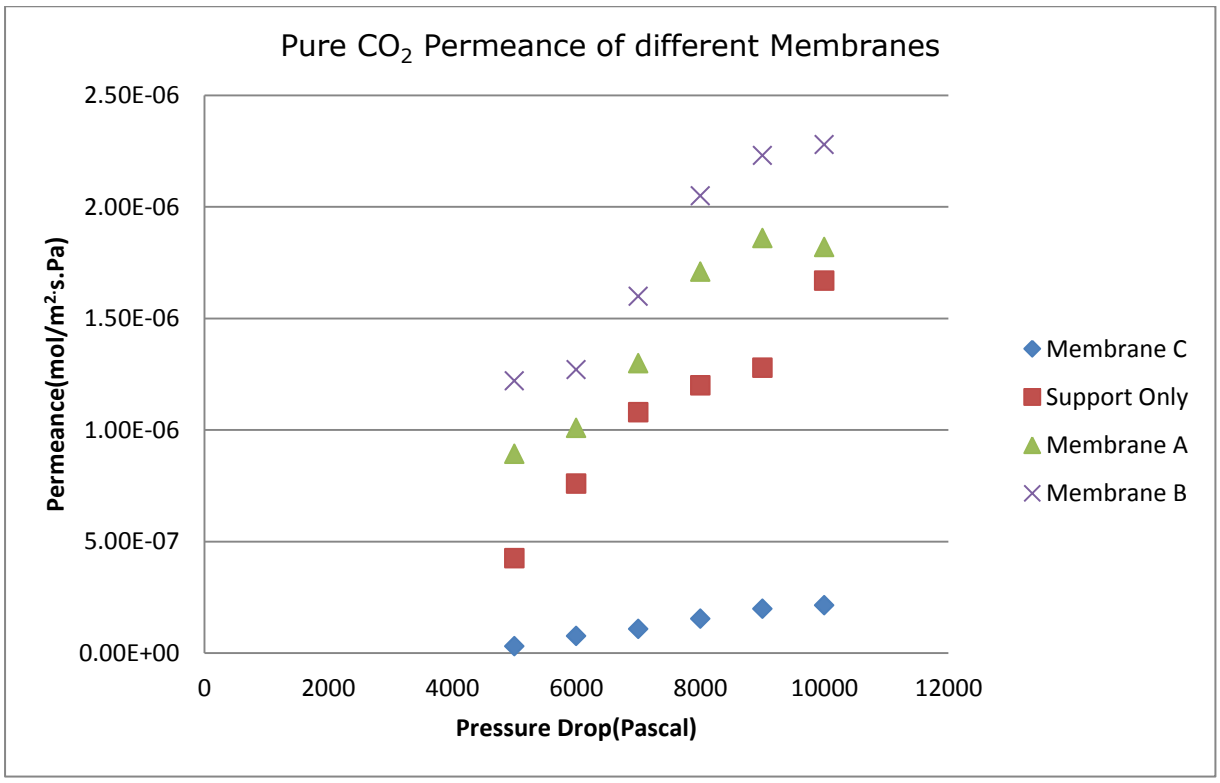

Figure 4:8 : Pure CO_2 Permeance using different Membranes

The figure above shows changes in the Carbon dioxide permeance with different membranes. The Membrane B was seen to favour pure Carbon dioxide permeance more than any other membrane used in this research as shown in figure 4:8. The least permeable membrane as shown above was membrane C which was modified by Gamma Alumina, Magnesium Oxide and Silica material. Membrane support was permeating more Nitrogen molecules than Carbon dioxide molecules as shown in table 4:1 below. Membrane A demonstrated a higher permeance as shown in figure 4:3 above and table 4:1 below. As mentioned before, the Membrane A with increased surface Area for the adsorbing site contributed in the increased flow of the Carbon dioxide molecules compared to support only at the same operating conditions. For membrane B the modification with magnesium oxide showed highest permeance of Carbon dioxide as shown in figure 4:8 above and table 4:1below. Here magnesium oxide as a strong base attracted Carbon dioxide

molecules more to itself by the utilising affinity factor. Magnesium oxide was found to be a stronger adsorbent than Gamma Alumina according to literature [9]; this may have contributed to higher permeance membrane B has shown to Carbon dioxide than Membrane A. Membrane C recorded the lowest permeance results to Carbon dioxide. Apart from the fact that silica and magnesium oxide were involved at this stage, diffusion played a significant part in the overall permeance of the membrane. As was mentioned earlier, the membrane C had a thickness of 2.0E-4m at fourth dip. This affected the diffusion of gas as fewer Carbon dioxide molecules were available for permeation through the membrane C.

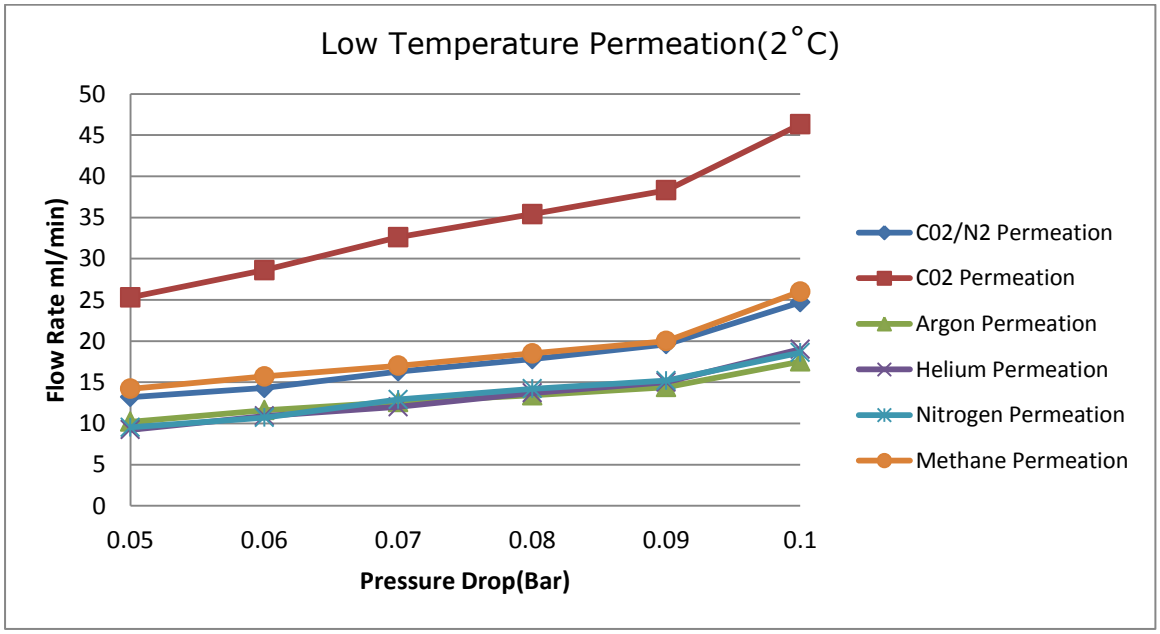

Figure 4:9: Low Temperature Permeations at (2^0C)

The figure 4:9 above represents the low temperature permeation experiment with membrane C, which complies with the earlier results of the membrane. The graph above indicated a high flow rate for carbon dioxide molecules compared to other gases. This is in line with the literature [23] that the adsorption of carbon dioxide molecules on the surface of the silica membrane is more favourable at low

temperature compared to high temperature permeation. This also, in agreement with the experimental results in figure 4:4 where the flow rate of the Carbon dioxide at 296K was higher compared to the Carbon dioxide flow rate at a higher temperature of 723K.

Table 4:1: Pure CO_2 Permeance using different membranes

Pressure Drop(Pascal)	Support only CO_2 Permeance (mol/m^2.s.Pa)	Membrane A CO_2Permeance (mol/m^2.s.Pa)	Membrane B CO_2 Permeance (mol/m^2.s.Pa)	Membrane C CO_2 Permeance (mol/m^2.s.Pa)
5000	4.25E-07	8.93E-07	1.22E-06	3.11E-08
6000	7.60E-07	1.01E-06	1.27E-06	7.69E-08
7000	1.08E-06	1.30E-06	1.60E-06	1.08E-07
8000	1.20E-06	1.71E-06	2.05E-06	1.54E-07
9000	1.28E-06	1.86E-06	2.23E-06	1.99E-07
10000	1.67E-06	1.82E-06	2.28E-06	2.14E-07

Table 4:1 shows different Carbon dioxide permeance using membrane support, Membrane A, Membrane B and Membrane C respectively. Membrane B was the most favoured for the permeation of the Carbon dioxide as discussed earlier.

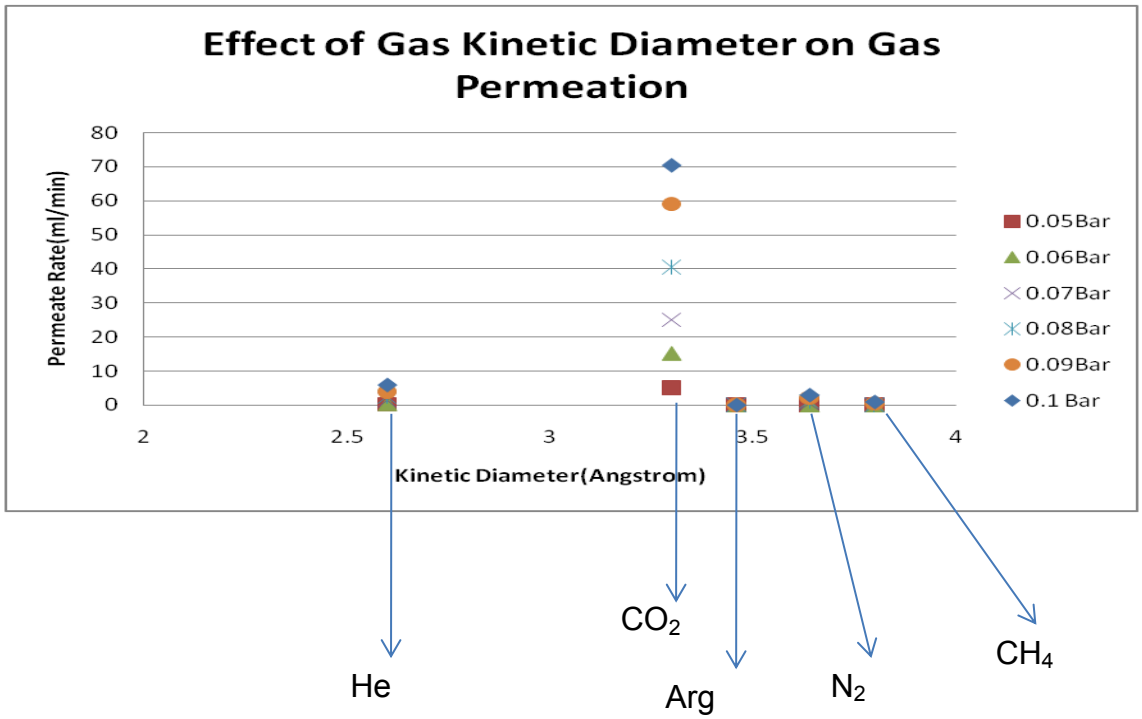

Figure 4:10 : Effect of gas kinetic Diameter on Gas Permeation

As mentioned in the literature [15], the gases with smaller kinetic diameter were expected to flow through membrane pore size easily compared to gases with larger kinetic diameter, but from the permeation experiments involving pure Helium, pure Carbon dioxide, pure Argon, pure Nitrogen and pure methane molecules as shown in table 8:145, 8:146, 8:147, 8:148, 8:149 and 8:150 respectively. Helium molecules with the smallest kinetic diameter (2.6Å) among the gases involved in the experiment showed a higher permeation flow than Argon with kinetic diameter (3.46Å). But when compared the permeation flow of Carbon dioxide with Helium gas molecules as shown in figure 4:1, the Carbon dioxide permeation flow with kinetic diameter (3.3Å) was found to permeate more than Helium with smaller kinetic diameter (2.6Å). This observation was in line with the literature [15] that suggested that factors such as affinity, gas molecular weight and membrane

thickness can equally affect the diffusion rate of the gas through a membrane pores.

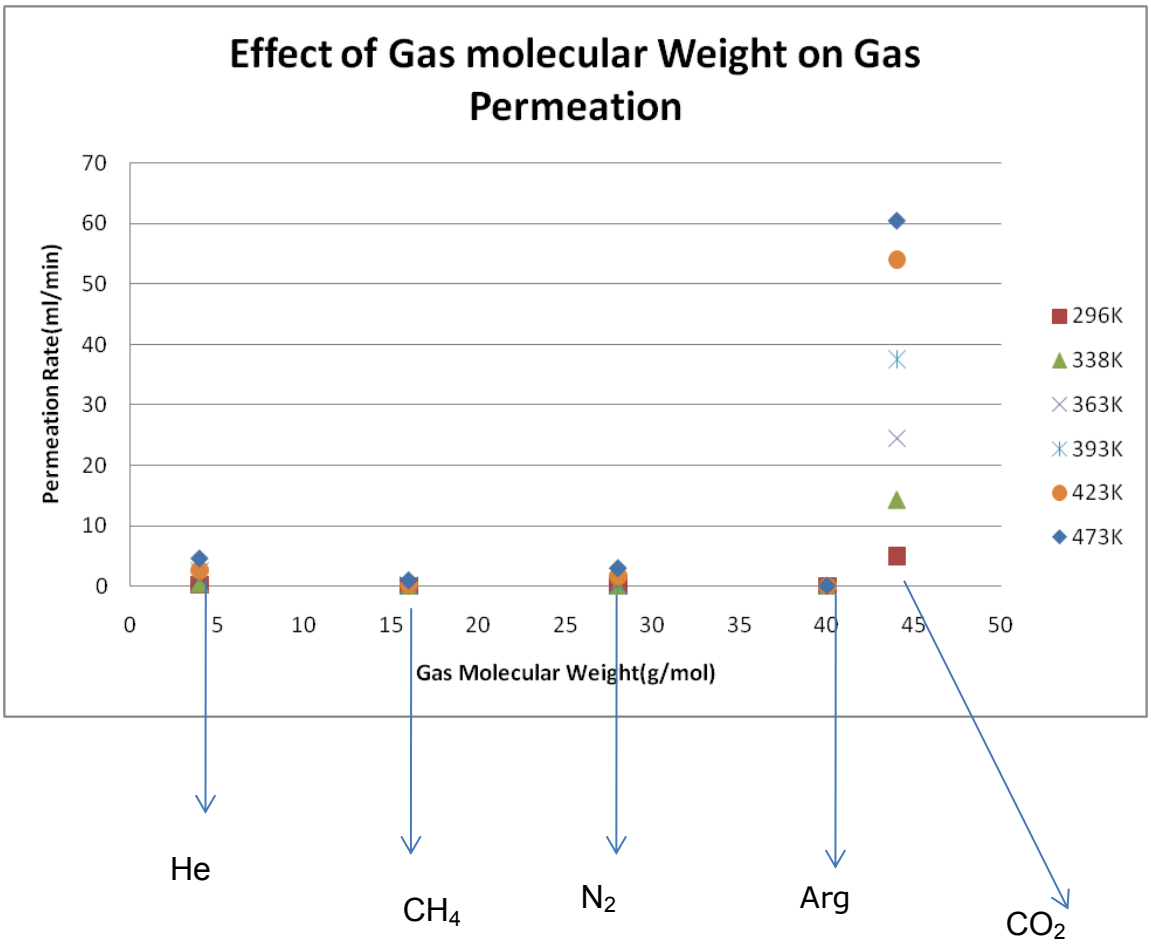

Figure 4:11 : Effect of Gas molecular Weight on gas permeation

Figure 4:11 is showing the effect on gas molecular weight on gas permeation through a ceramic membrane. According to Knudsen flow mechanism, the membrane flux is inversely proportional to the square root of the permeating gas molecules. So, as the molecular weight of gas increases, according to Knudsen mechanism, we expected to see a reduction in the permeation flux of the gas. But in the graph above, Carbon dioxide molecule with molecular weight of 44.0(g/mole) was observed to permeate more than Helium gas molecule with molecular weight

of 4.0(g/mole), Methane molecule with molecular weight of 16.0(g/mole), Nitrogen molecule with molecular weight of 28.0(g/mole) and Argon molecule with molecular weight of (40.1g/mole). The high permeation of Membrane C with Carbon dioxide was because of the affinity effect of the magnesium oxide and silica surface of the membrane C which created higher adsorption phenomenon for Carbon dioxide than any other gases involved in the experiment. The experimental results were shown in tables 8:152, table 8:153, table 8:154, table 8:155 and table 8:156 respectively in appendix section.

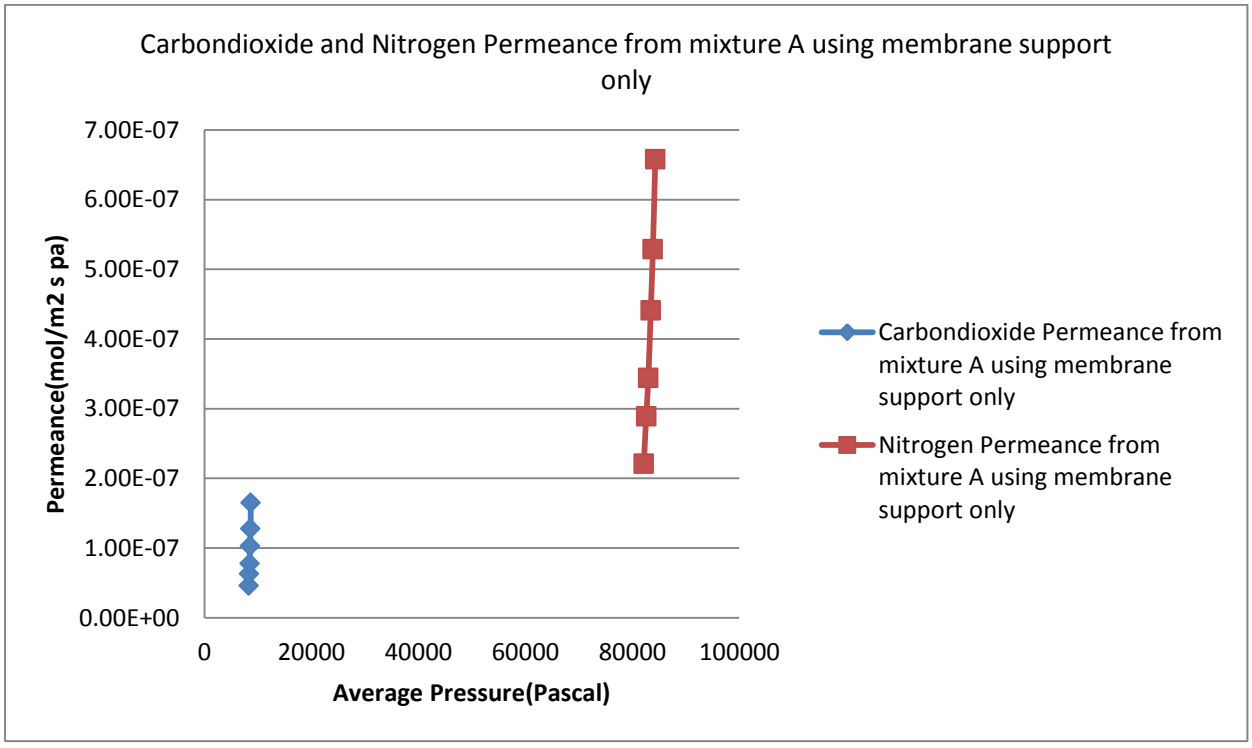

Figure 4:12: Carbon dioxide and Nitrogen Permeance from mixture A using membrane support only

In figure 4:12 above, before the modification of the membrane support, the permeation experiment conducted with a mixture A which had 86% Nitrogen in the

feed and 14% of Carbon dioxide in the feed gas favoured Nitrogen molecule more than the Carbon dioxide. The membrane support was used as it was supplied without any modification. The permeance of the Carbondioxide at 12.7kPa transmembrane partial pressure was $4.61x10^{-08}$ ($mol.m^{-2}.s^{-1}.Pa^{-1}$) as shown in table 8:74, compared to the Nitrogen permeance of 2.21E-07 ($mol.m^{-2}.s^{-1}.Pa^{-1}$) at a transmembrane partial pressure of 16.34kPa as shown in table 8:75 in the appendix section. The results comply with the Knudsen mechanism as the Nitrogen molecules which are less in molecular weight (28g/mole) compares to Carbon dioxide molecules with (44.0g/mole) were expected to permeate more easily than the Carbon dioxide.

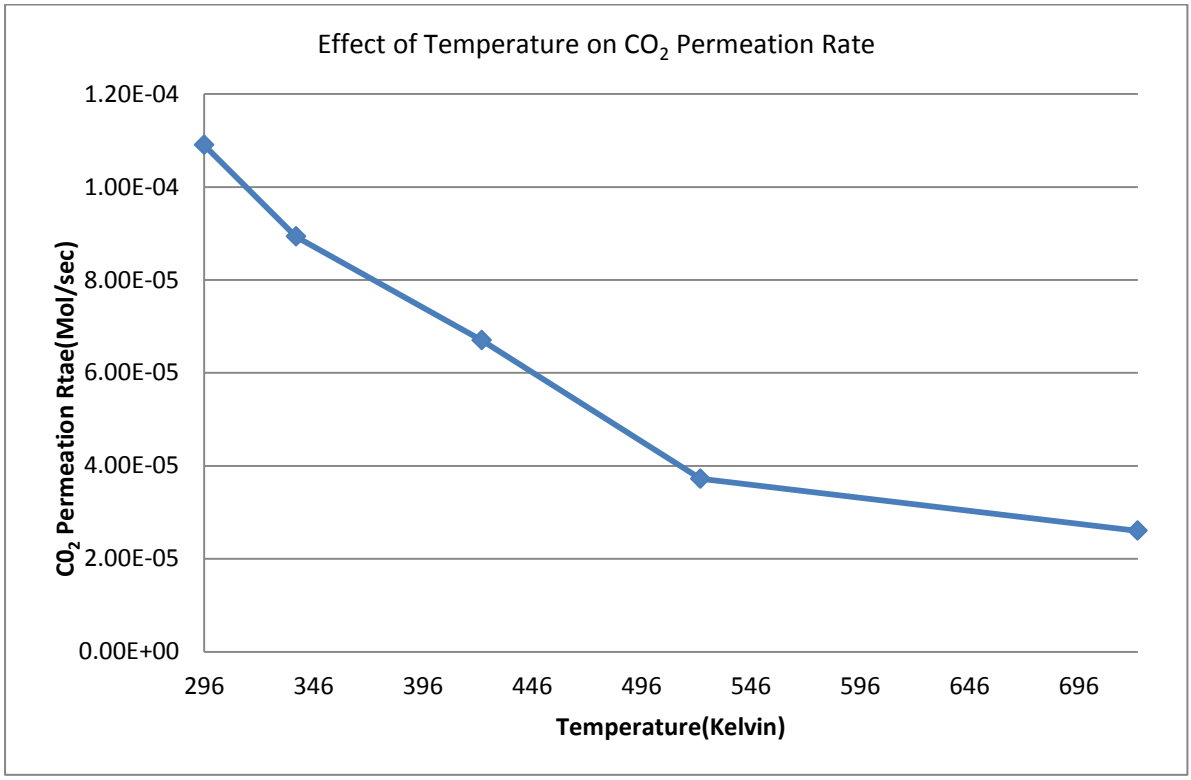

Figure 4:13: Effect of Temperature on CO_2 Permeation Rate

The graph above shows how the increase in the temperature of the permeation experiment affects the permeance of the gases, in this case, Carbon dioxide gas was used as shown in figure 4:13 above. As can be deducted from the above

figure, the increase in the temperature of the adsorption reduces the concentration of the adsorbate thereby limiting the amount ready for adsorption process as was sited in literature [15]. This therefore affects the permeance or permeability of the adsorbing gas through a membrane. This had already been explained in more details using figure 4:4 above.

4.2 MASS TRANSFER MECHANISMS

The permeability through the fabricated and tested membranes was done by the help of the mechanism or mechanisms discussed earlier in the previous chapters. The overall mechanism equation constitutes the free pore diffusion and surface diffusion mechanisms.

For pore diffusion, the gas diffusion was characterised by Knudsen and viscous flow discussed in the previous chapters. Recalling equation 1.4, 1.5 for the pore model and equation 2.4 for surface flow model, as described in details in chapter two, then, total flux through the membrane is calculated with the equation 3.3 below. Hence,

$$F_T = \frac{8r_p}{3(2\pi MRT)^{1/2}} + \frac{r_p^{\,2}}{8\mu RT}\frac{[P_1 + P_2]}{2} + \frac{\rho(1-\varepsilon)D_S}{K_S^{\,2}\delta}\frac{dq}{dP} \qquad 3.3$$

Or

$$F_T = K_O + B_O P_{average} + F_{OS} \qquad 3.4$$

Applying equation 3.3 and 3.4 above to the permeability data from the experiment, pore sizes of the membrane C were calculated at different dips. The detailed pore size calculation is located in section 4.3 below.

4.3 FLOW PREDICTION AND PORE SIZE ESTIMATION.

As earlier mentioned in the previous chapter, the total flow of gas through a porous membrane could be achieved by a number of mechanisms, either in a contributing or acting as a sole mechanism. Since the mechanisms applicable to porous flow are characterised by the pore size or pore diameter of the membranes, the mean free path of the permeating gas molecules and the affinity between the gas molecules and the membrane materials [26]. Estimations on how much each mechanism contributed to the flow through the membrane were determined.

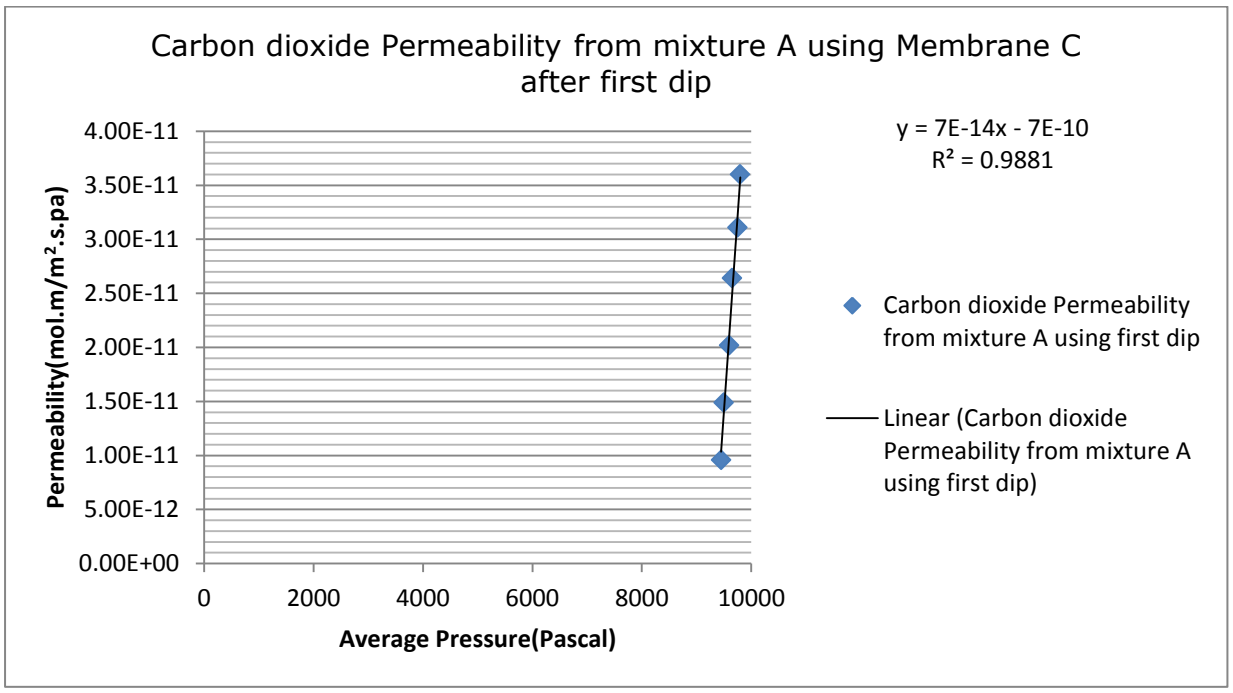

Figure 4:14: Carbondioxide Permeability from mixture A using mixture C after first dip

From the figure 8:84 above, Slope= 7.0E-14 $\frac{mol.m}{m^2.s.Pa^2}$

Then, the intercept =-7.00E-10(mol.m/m^2.s.Pa).

Recalling equation 1.9, Bo= Slope= $\frac{r_p^{\ 2}}{8\mu RT}$ = 7.0E-14, when the flow is Viscous flow $r_p = \sqrt{(8)(1.372E-5)(8.3145)(296)(7.0E-14)}$ = 1.38E-07 metres

where T is the absolute temperature in Kelvin

μ = $C0_2$ gas viscosity; 1.372E-5 (Pa. s)

T= 296 Kelvin

R= 8.3145J/mol.K

r_p= 1.38E-07 metres= 138 nm and also equals to 1380Å

For the Knudsen contribution, from the graph figure above, the intercept was recorded to be -7.0E-10(mol.m/m^2.s.Pa). This makes the Knudsen mechanism not applicable to the Carbon dioxide flow through the membrane C after first dip since Knudsen does not have a negative contribution to the gas flow.

The pore size of Membrane C after First Dip was 138nm or 1380 Å which was found to be a macro porous ceramic membrane based on the IUPACK pore size classification discussed in chapter 2. From the results above, the Viscous mechanism has a positive value, but because the viscous flow does not bring about separation of the gas and the membrane C recovering of the Carbondioxide from the mixture A after first dip was 30%. This confirmed that another mechanism was responsible for the flow of the Carbondioxide through membrane C after first dip.

The calculation of rest of the pore sizes were fully shown in appendix section, but the membrane pore sizes are shown in table 4:2 below .

Table 4:2: Membrane C Pore Sizes at different Dips

Membrane C Pore Sizes Calculated for Different Dips		Gas Molecules used	Pore Size from Viscous flow in nanometres	Pore Size from Viscous flow in Angstroms(Å)
			Pore Sizes, R_P (nm)	Pore Sizes (Å)
First Stage Permeation	Ist Dip	CO_2	276	2760
	2nd Dip	CO_2	180	1800
	Third Dip	CO_2	180	1800
	Fourth	CO_2	104	1040
Second Stage Permeation	After Fourth Dip	CO_2	57	570
Third Stage Permeation	After Fourth Dip	CO_2	46.4	464

From the table 4:2 above, the pore sizes of the membrane C at all the stages were displayed. The results above justified the Surface flow in Equation 3.23 which was the only applicable model to aid permeability of Carbon dioxide molecules through different stages of membrane C. It was clearly shown by the results that pore models were not contributing to the permeability of Carbon dioxide molecules from the mixture A, B and C using membrane C at different stages. Since membrane C at various stages and dipping, brought about separation of Carbon dioxide to different degrees of separations, a mechanism other than pore model was responsible for the flow of the separated carbon dioxide through the membrane C.

4.3.1 Flow Prediction

From the values of the membrane permeability, the Knudsen flow and viscous flow were found to be non-significant in contributing to the total flow of the fluid through the modified membrane. This was confirmed as the values of the Knudsen contribution were found to be negative. This contradicts the Knudsen flow contribution. Also, for the viscous mechanism, in this work, the values of the viscous flow were found to be positive, but the selectivity of the membrane indicated a separation for the membranes. Therefore, due to the fact that Viscous flow does not aid to separation of gases through a porous membrane. This confirmed that a surface flow mechanism was responsible for the flow of the gas through the modified membrane.

Considering total Surface flow mechanism, the theoretical surface flow is explained by using a modified Fick's law which is

$$F_{os} = \frac{F_s}{\Delta P} = \frac{\rho(1-\varepsilon)D_S}{K_S{}^2\delta}\frac{dq}{dP} \qquad 3.4$$

Where ρ is the true density of the medium (kg/m^3), D_s the surface diffusion coefficient (m^2/sec), ($\mu_s=1/K_s$) is the shape factor, K_s is the tortuosity of the surface, dq/dp is the concentration gradient of the adsorbed species, ε is the porosity of the membrane medium[11][15]. This subject has been treated in many papers [11] [13]**.** For low surface concentrations the most general description is the two-dimensional form of Ficks' law: the surface permeability *F,* (mol/ m^2-sec) equals

$$Fs = -\rho(1-\varepsilon)\frac{D_S}{K_S{}^2}\frac{dq}{dl} \qquad 3.5$$

where ρ is the true density of the medium (kg/m^3), D_s, the surface diffusion coefficient (m^2/sec), k_s^2, the tortuosity of the surface, dq/d*l* the concentration gradient of the adsorbed species, and q the amount of species adsorbed (mol/kg).

Assuming a linear pressure gradient and integrating the results of Eqn. (3.5)

in an expression for the surface permeability, one obtains

$$F_{OS} = \frac{F_s}{\Delta P} = \frac{\rho(1-\varepsilon)D_S}{K_S{}^2\delta}\frac{dq}{dP} \qquad 3.6$$

where *ΔP* is the pressure difference and *L or* δ *is the* thickness of the porous medium.

The term dq/dP is given by making it subject in equation 3.6 above and assuming the values of Ks and Ds. The equation (3.6) can be rewritten as

$$\frac{dq}{dp} = \frac{F_{os}\left(k_s{}^2\delta\right)}{\rho(1-\varepsilon)Ds} \qquad 3.7$$

Assuming that membrane surface tortuosity is 6.5[4][17][23] as an average value used in the literatures and the surface diffusion coefficient , Ds is assumed to range from 10-20E-09(m^2/Sec)[11][13][23][12] which often used as 11E-09(m^2/sec) and porosity, ε is ranged from 15% - 100%[23] [14].

Then, selecting values of Ds and ε from the above range of values for this application, we have ε = 0.52 after fourth dip and Ds=11E-09(m^2/sec) [12] [11].

4.3.1.1 Estimation of Theoretical Surface Flow using Henry Adsorption Isotherm

From the graph of adsorptions such as figure 8:101, 8:102, 8:103, 8:104,8:105,8:107 and 8:109 shown in appendix section 8.10, it was found that Henry Isotherm fitted more at 723k and 296k due to highest values of R^2. But because the amount of Carbon dioxide permeated using Silica membrane which was represented as membrane C was more at 296k compared to that at 723k, the model for Henry at 296k was selected.

Hence, recalling that n=KP, so the graph of n against P produced K as a slope which is the same as $\frac{\Delta q}{\Delta p}$. Applying this to the graph at 296k in the appendix section, we have Slope= 0.0135 ml STP g^{-1} Pa^{-1}.

Converting into $mol.kg^{-1}$, 1ml (STP) g^{-1} ≡ 0.045 $mol.kg^{-1}$, then for 0.0135 ml (STP) g^{-1} = 6.08E-04 $mol.kg^{-1}$

$\frac{\Delta q}{\Delta p}$ =6.08E-04 $mol.kg^{-1}$

Applying the selected values into equation 3.7 above resulted in the values of the Carbon dioxide adsorbed theoretically. The table 4:3 below shows the theoretical Surface flow permeability at 296k and 5000 Pascal transmembrane pressure using membrane C after fourth dip. From the table below, the values of the theoretical surface flow were seen to be the higher than the experimental surface flow contribution. This could be due to errors in the experimental measurement and control of the experimental parameters.

Table 4:3 Experimental and theoretical permeability for pure CO_2 using membrane C after fourth dip.

Pressure Drop (Pascal)	Experimental Permeability for Pure CO_2 Permeability through membrane C after fourth dip (mol.m/m^2.s.Pa)	$\frac{\Delta q}{\Delta P}$ (mol/kg)	Temperature in Kelvin	Theoretical Permeability for Pure CO_2 through membrane C after fourth dip (mol.m/m^2.s.Pa) $\frac{\rho(1-\varepsilon)\Delta_S \frac{\Delta q}{\Delta P}}{K_S{}^2 \delta}$
5000	6.22E-12	6.08E-04	296	3.91E-07
5000	4.86E-12	3.51E-04	338	2.26E-07
5000	3.88E-12	2.30E-04	423	1.48E-07
5000	3.52E-12	1.62E-04	523	1.04E-07
5000	1.70E-12	1.08E-04	723	6.95E-08

Table 4:4 : Values of the Heat of Adsorption on membrane A

Gas	P_o(molm^{-2} s^{-1} Pa^{-1})	ΔH_a(KJ mol^{-1})	Regression coefficient
CO_2	-16.49	6.79	0.9678
N_2	-15.708	3.633	0.9098

Table 4:5: Values of the Heat of Adsorption on membrane C

Gas	Ln P_o($molm^{-2}$ s^{-1} Pa^{-1})	ΔH_a(KJ mol^{-1})	Regression coefficient
CO_2	-16.49	6.53	0.9810
N_2	-15.708	17.45	0.8205

Tables 4:5 and 4:6 show the values of the Heat of Adsorption of Carbon dioxide and Nitrogen using membrane A and membrane C. For membrane A, the heat of adsorption for Carbon dioxide molecules was calculated to be 6.79(KJ mol^{-1}) and that of the Nitrogen molecules was calculated to be 3.633(KJ mol^{-1}).With the permeance of Carbon dioxide and Nitrogen using membrane A as 8.93E-07 $mol.m^{-2}.s^{-1}.Pa^{-1}$ and 6.20E-07 $mol.m^{-2}.s^{-1}.Pa^{-1}$ respectively. Also, the permeance of Carbon dioxide and Nitrogen using membrane C were recorded to be 3.11E-08 $mol.m^{-2}.s^{-1}$. Pa and 9.14E-09 ($mol.m^{-2}.s^{-1}.Pa^{-1}$) respectively. As discussed in the literature, the effect of heat of adsorption on the gas permeance depends on the model involves and the temperature with which the gas is permeating through the membrane [13]. If the permeance is achieved by surface flow mechanism, an increase in the heat of adsorption will bring a decrease in the overall permeance through the membrane [15]. But if there are other mechanisms that have contributed to a permeance of gas through a membrane, for instance, a molecular sieve, an increase in the heat of adsorption value might bring about an increase in the permeance of the gas through the membrane [15]. Relating the values of the heat of adsorption calculated in this work as shown in table 4:5 and table 4:6 above, the heat of adsorptions of Carbon dioxide and Nitrogen in table 4:6 above fit in to the explanation above as the 6.53KJ/mol of adsorption heat was required for pure 3.11E-09 $mol.m^{-2}.s^{-1}.Pa^{-1}$ of Carbon dioxide to permeate through membrane C. Also, 17.5KJ/mol of adsorption heat was equally required for 9.14E-09 $mol.m^{-2}.s^{-}$

$^{1}.Pa^{-1}$ pure Nitrogen to permeate through membrane C as well. These results show that at higher heat of adsorption, the permeance of the gas through the membrane is reduced, as along as the flow is governed by surface flow which was the case with the membrane C. For the results in table 4:5, the heat of adsorption of Carbon dioxide was higher than that of Nitrogen but, membrane A shows a relatively no difference in the permeance results of the Carbon dioxide and Nitrogen. This suggested that no clear model was responsible for the permeance of the either gas through membrane A. The detailed procedure for heat of adsorption calculations is located in the appendix section.

4.4 MEMBRANE CHARACTERIZATION

The membranes used in this project were characterized using permeation flow rate method as one of the characterization methods listed above. Some of the Scanning Electron Microscope (SEM) pictures of the fabricated membranes took were equally attached in this section as figures 4:15, 4:16 and EDXA pictures of the membrane analysis as shown in tables 4:7 and 4:8 respectively.

From the permeability and average pressure required for the flow through membrane C after each dip, mean pore radii of the membranes were estimated from the slope of the graphs listed above.

From the estimated pore radii, pore sizes or pore diameter were calculated for the membrane C using viscous flow models since Knudsen was found to be negative. The Viscous flow model used in estimating the membrane C pore radii is in agreement with the observation since the gas separation was achieved by surface flow mechanism.

The membrane classification, according to IUPACK specifications were as follows:

1. For membrane C after first dip, the pore size was calculated to be 276nm or 2760 Å, this was found to be macroporoes membrane based on IUPACK pore size classification.
2. After second dip, the pore size was found to be 180nm or 1800 Å, the membrane C at this stage was still in macroporoes region according to IUPACK pore size classification.
3. For Third Dip, the Membrane C pore size was 180 nm or 1800Å, which was found to be a macroporoes Ceramic Membrane based on the IUPACK pore size classification discussed in chapter 2.
4. For Fourth Dip, the Membrane C pore size was 104 nm or 1040Å, which was found to be a Macro porous Ceramic Membrane based on the IUPACK pore size classification discussed in chapter 2.

For second stage, the Membrane C pore size was 57 nm or 570Å, which was found to be a Macroporoes Ceramic Membrane based on the IUPACK pore size classification discussed in chapter 2.

For third stage, the Membrane C pore size was 46.4 nm or 464Å, which was found to be a Mesoporous Ceramic Membrane based on the IUPACK pore size classification discussed in chapter 2.

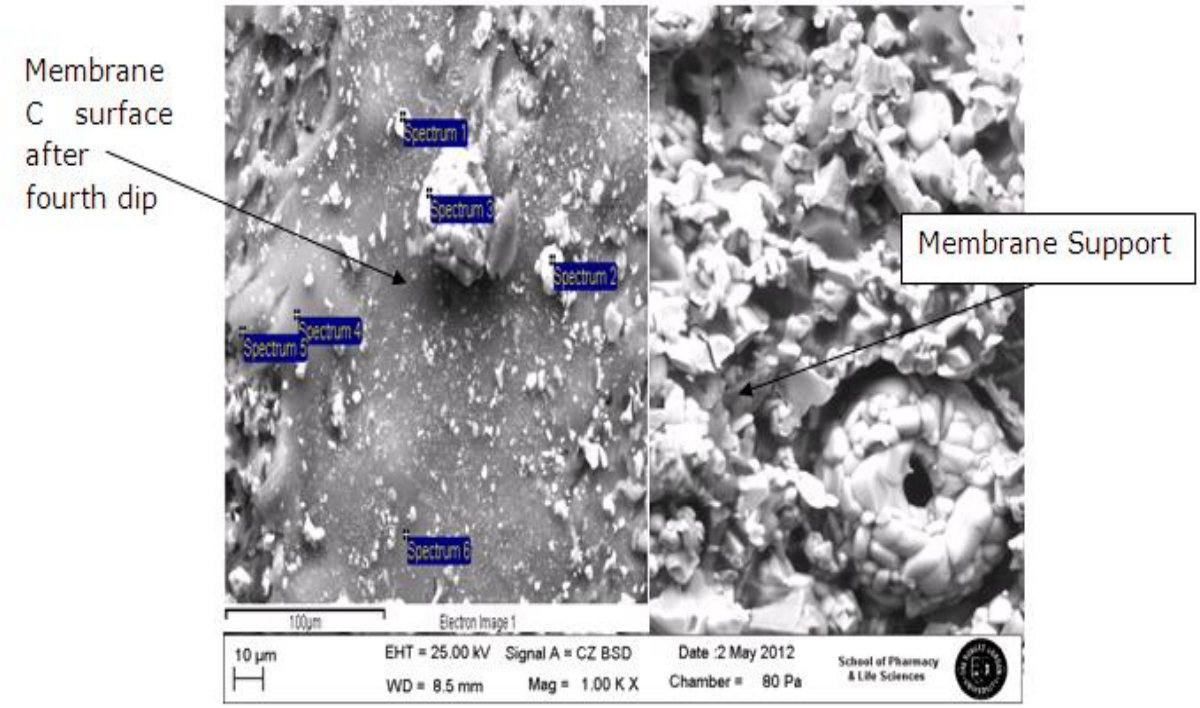

Figure 4:15: Outer section of Membrane C and membrane support x 1000

Figures 4:15 and figure 4:16 show the SEM images of the Membrane C and membrane support. The membrane support image indicates the large mean pore (6000nm) associated with the commercially supplied Alpha Alumina support. The EDXA analysis conducted on the support as contain in table 4:7 revealed low weight percentage of silica deposited on it at spectrum 1 point. Also, for Membrane C after fourth dip as shown in table 4:14 and table 4:15, the SEM image revealed fine smooth orientations which suggested modified pores. The EDXA analyses on the both images show an increase in the silica deposit weight percentage as shown in table 4:8.

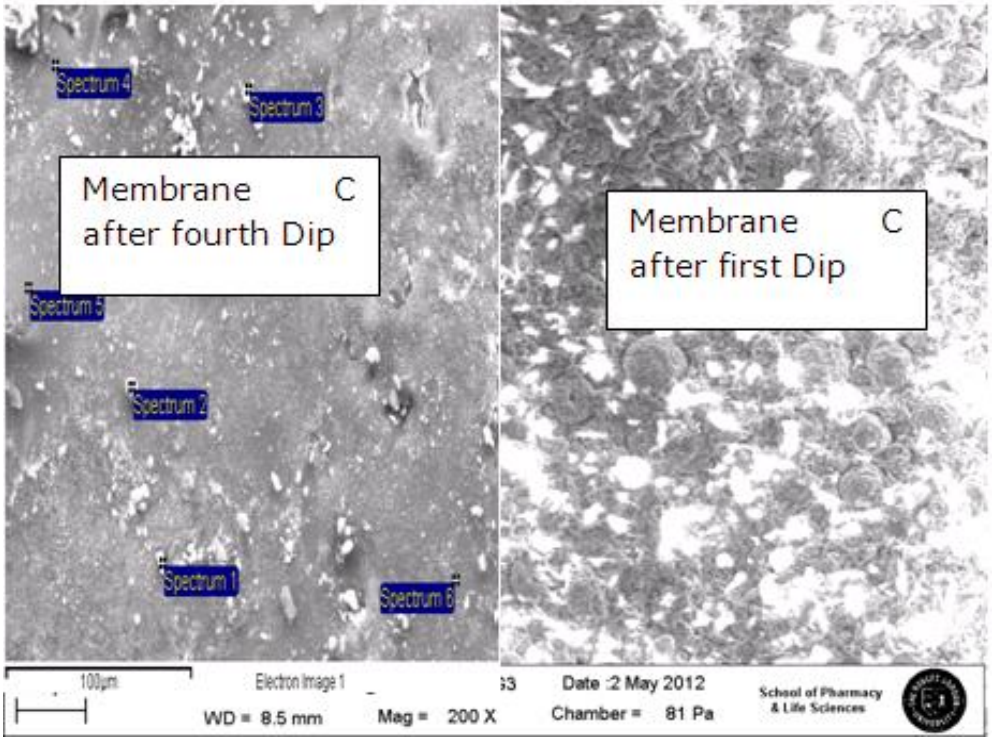

Figure 4:16: Cross Section of outer Membrane C after fourth and first dips magnification x 500

Table 4:6: EDXA analysis of the Membrane C after membrane support

Spectrum	In stats.	C	O	Al	Si	Ti	Zr	Total
Spectrum 1	Yes	5.47	45.94	2.12	0.84	44.85	0.78	100.00
Spectrum 2	Yes	7.08	37.98	3.45	1.46	49.04	0.99	100.00
Spectrum 3	Yes	4.58	40.99	2.74	0.92	49.96	0.82	100.00
Spectrum 4	Yes	7.83	49.56	29.29	1.11	12.21		100.00
Spectrum 5	Yes	11.46	48.15	28.30	2.31	9.78		100.00
Spectrum 6	Yes	9.09	48.18	29.28	1.11	12.34		100.00

Table 4:7: EDXA analysis of the Membrane C after fourth Dip

Spectrum	In stats.	C	O	Al	Si	Ti	Total
Spectrum 1	Yes	9.55	36.04	0.78	15.96	37.66	100.00
Spectrum 2	Yes	19.69	46.73	3.60	20.28	9.70	100.00
Spectrum 3	Yes	15.19	40.10	1.33	21.18	22.20	100.00
Spectrum 4	Yes	29.38	33.07	0.46	34.67	2.42	100.00
Spectrum 5	Yes	26.91	28.72	0.53	41.39	2.46	100.00
Spectrum 6	Yes	29.3	31.3	0.5	36.6	2.15	100.0

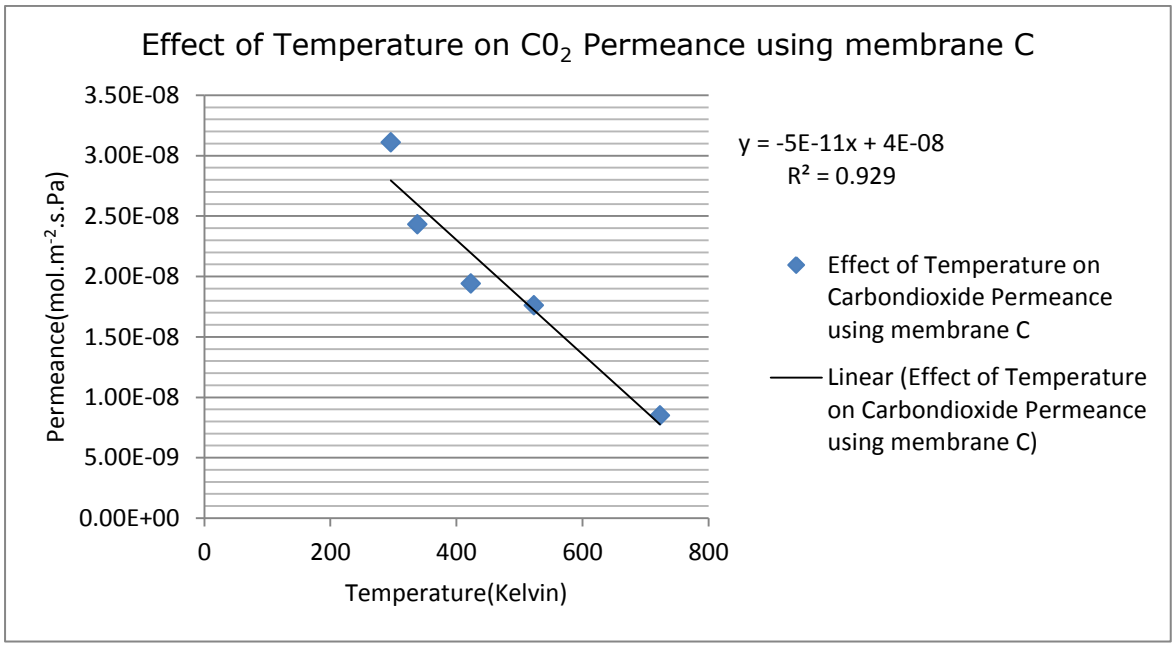

Figure 4:17: Effect of Temperature on CO_2 Permeance using Membrane C

The figure 4:17 was used to show the effect of temperature on membrane permeation using Carbon dioxide. Membrane C after fourth dip was subjected to different temperatures, ranging from 296K, 323K, 423K, 523K and 723K respectively. The membrane permeance at 296k was highest compared with the values at every other temperature. The permeance result was least at the 723K. This is in agreement with the literature [15] that adsorption of gas occurs better at the smallest temperature as shown in figure 4:19 below.

4.5 SELECTIVITY

The Selectivities for the fabricated membranes in this project were categorised into pure gas and mixed gas selectivities. All the membranes developed in this project were checked for their recovering efficiency with Membrane C revealed to show good recovering efficiencies to Carbon dioxide over Nitrogen, Methane, Helium and Argon both in pure and mixed gas permeation processes.

For the membrane support only, when the permeation was in cocurrent flow arrangement with retentate valve fully opened at 0.05bar pressure drop absolute value, the Selectivity to Carbon dioxide over Nitrogen α_{CO_2/N_2} was 0.71. This was increased to 0.78 when the retentate valve in the same cocurrent flow arrangement was fully closed. When the permeation arrangements were in counter current flow, the selectivity of the membrane support to Carbon dioxide over Nitrogen were recorded as 0.27 when retentate is fully closed and 0.22 when retentate is opened. This is low compared to the cocurrent flow arrangements. The reason for this is because membrane support permeated more Nitrogen than Carbon dioxide in counter current flow arrangement as shown in tables 8:8 and table 8:11 respectively.

For membrane Support with mixture A for feed, the selectivity was recorded to be 1. This means that the membrane support was neither selective to Carbondioxide nor Nitrogen at this stage.

For Membrane A, after calcination, which increased the surface area for adsorption, the selectivity of the Membrane A to Carbon dioxide over Nitrogen using mixture A was increased to 1.17 for cocurrent flow with retentate valve fully opened and 1.3 when the retentate valve is fully closed.

Also, for pure gas the selectivity of Membrane A to Carbon dioxide over Nitrogen was found to increase to 1.44.

For Membrane B after modification with Magnesium Oxide, the membrane selectivity to Carbon dioxide over Nitrogen was found to be 2.04 when the mixture A was used. The increase in the selectivity is because of the increase in the adsorption strength of the membrane which was added by the presence of Magnesium Oxide as discussed earlier.

For Membrane C after first dip using mixture A as feed, the selectivity of membrane C to Carbon dioxide was increased to 2.63 approximately 3. There was no further increment on the membrane C selectivity to Nitrogen from mixture A as the dipping number increased from two to 4. Carbon dioxide experienced more resistance to flow when in mixture A which has a low concentration compare to Nitrogen with high concentration. The Membrane C at this stage has shown its maximum recovering efficiency to Carbon dioxide in a mixture with Nitrogen at low Carbon dioxide concentration.

The pure gas selectivity determined with Membrane C after fourth dip revealed the capacity of the membrane in recovery Carbondioxide to other gases. The Membrane C selectivities to Methane, Argon and Nitrogen at 0.05 bar transmembrane pressure were recorded to be infinity values. At this point no flux was recorded for methane, Argon and Nitrogen molecules. Also, at 0.06 bar transmembrane pressure, the Membrane C selectivity to Carbon dioxide over Nitrogen was still infinity value. Membrane C has an approximated value of 26 for the Carbon dioxide to Helium selectivity at 0.05 bar transmembrane pressure and

10.24 for the Carbon dioxide to Nitrogen selectivity at 0.07 bar transmembrane pressure. The detailed calculation of this can be found in the appendix section.

4.5.1 Selectivity of Second and Third Stage Permeations

The low recovering efficiency of the Membrane C at first stage has to be improved on its recovering efficiency in order to make this approach a competitive alternative in Carbon dioxide concentration method. In view of this, second and third stages permeations were introduced into the existing permeation (first stage) train systems. The results of the membrane C selectivity to Carbon dioxide over Nitrogen revealed improved results of approximated value of 4 for the second stage permeation and a value of 6 for the third stage permeation. The mixture B was used for the second stage and mixture C was used for the third stage.

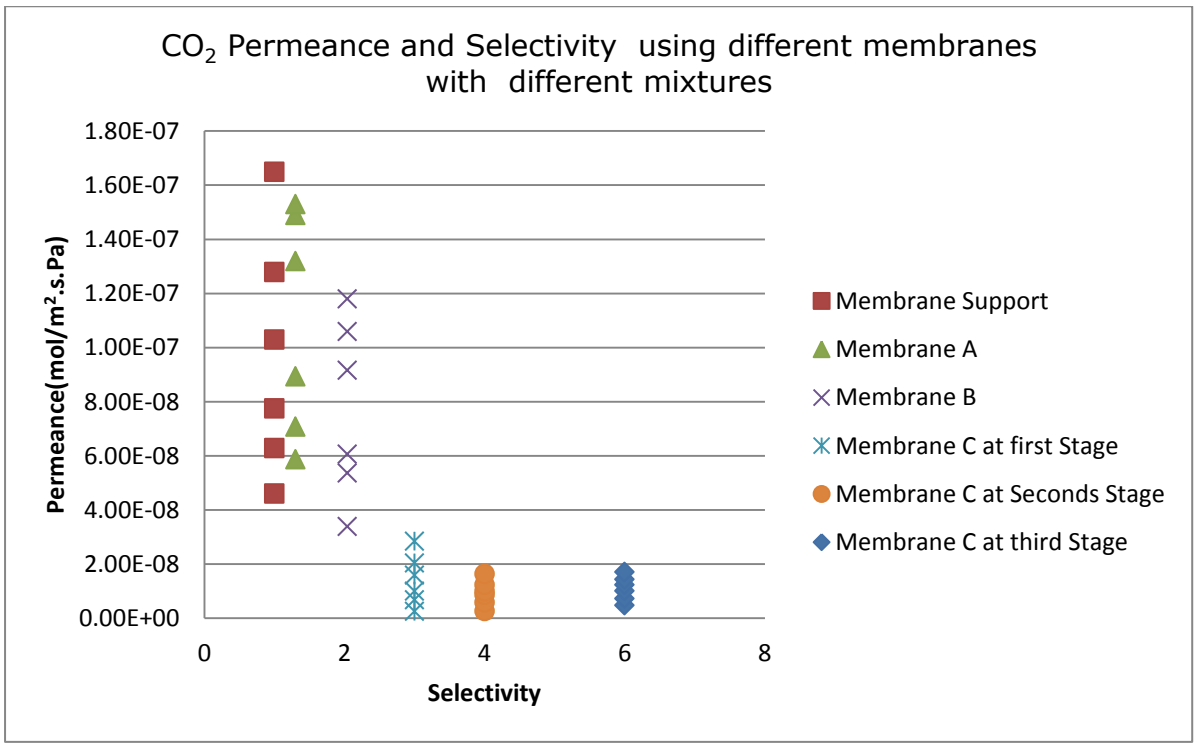

Figure 4:18: CO_2 Permeance and Selectivity using different membranes with different mixtures

Figure 4:18 above shows a trend in the permeance and selectivity of the different membranes to Carbon dioxide over different gases, ranging from membrane support, Membrane A, Membrane B and Membrane C respectively. The results in the figure above indicated that the Carbon dioxide permeance recorded highest values with membrane support and equally with the least values with Membrane C at third stage. As in line with the literature, due to the decrease in the pores sizes of the membrane due to modification of the membrane surface, this resulted in a rise in the selectiveness of the membrane to the preferred gas, the gas permeance of the membrane decreases as the selectivity increases. Carbon dioxide encountered less restriction as it tries to diffuse through the pore channels of the membrane support than when it is in the pore channels of the Membrane C at third stage. The figure 4:19 shows that increase in the adsorption volume of the Carbon

dioxide is affected by the temperature of the process. The adsorption volume which has a direct impact on the selectiveness of the membrane is affected by the temperature as shown in figure 4:19. The figure below shows that at 296K, the membranes experienced the highest values of their selectivity than at 723K which was the highest temperature at this study. The reason to this was explained in the earlier section.

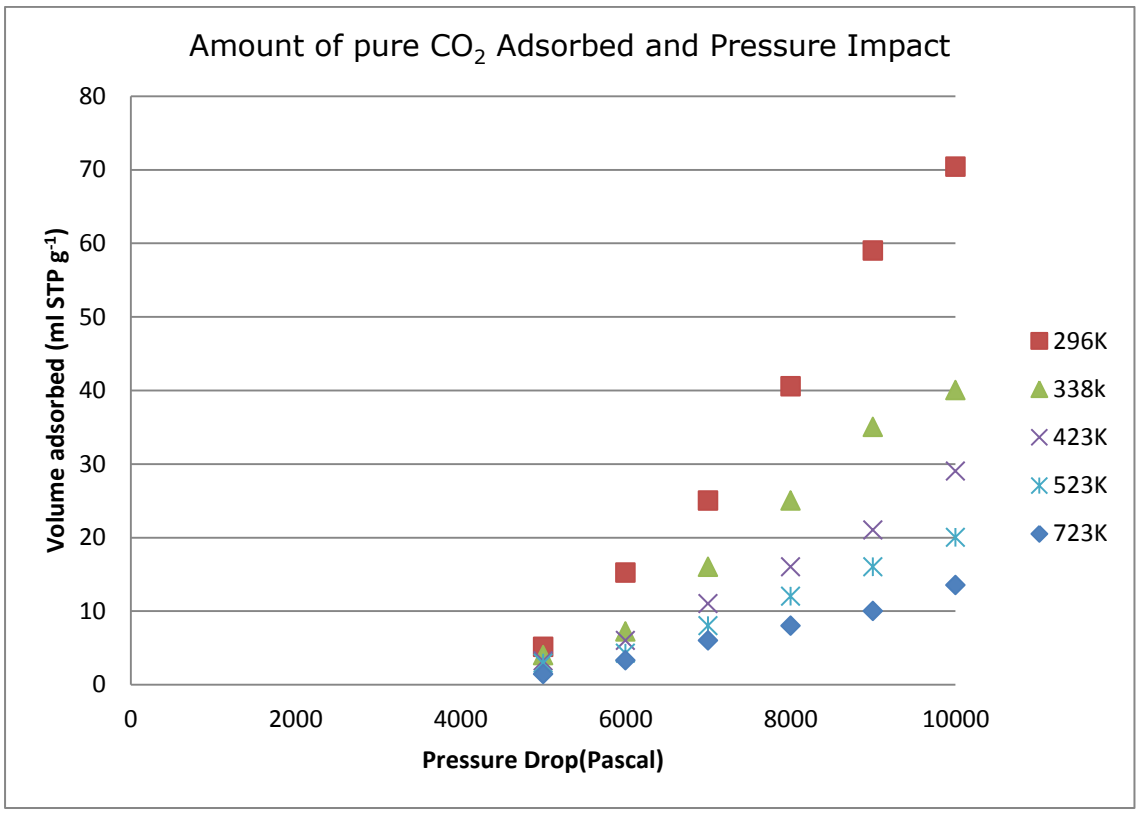

Figure 4:19: Amount of Pure CO_2 Adsorbed at different Temperatures

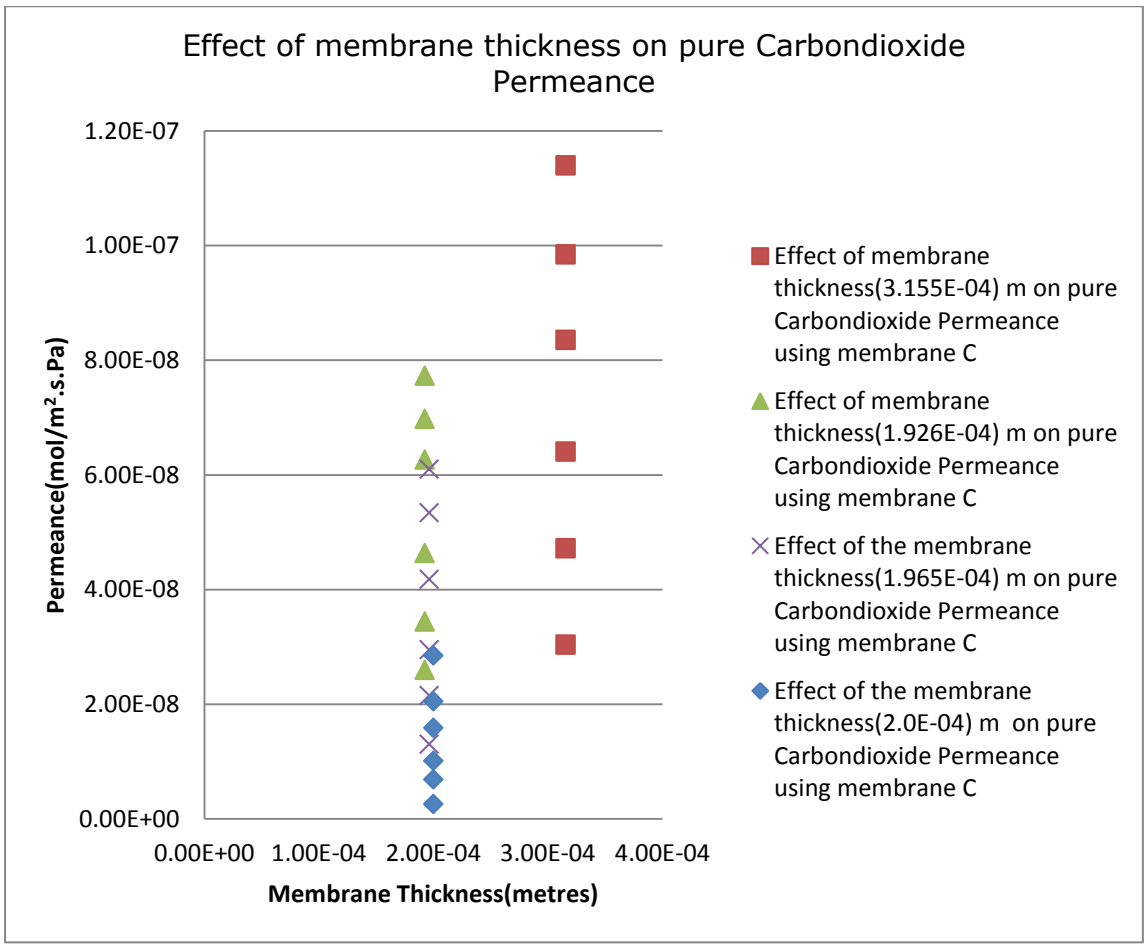

Figure 4:20: Effect of membrane thickness on pure Carbon dioxide Permeance

Permeance of the gases through the membrane are normalised by thickness [15]. However, the diffusion constants are directly affected by the thickness of the membrane [15]. In view of this the membrane results in figure 4:20 above shows that the membrane C at first dip with membrane thickness of 3.155E-04 metres permeated Carbon dioxide more than the membrane C after fourth dip with membrane thickness of 2.0E-04 metres. The explanation to these results is that at first dip, membrane C has provided less restriction to the diffusion of the Carbon dioxide molecules through the membrane than the diffusion resistance produced by the membrane C after fourth dip.

Table 4:8: Membrane thickness and number of dipping

Thickness(metres)	Number of Dipping
3.155E-04	1
1.926E-04	2
1.965E-04	3
2.00E-04	4

The table 4:9 and figure 4:21 show the effect of number of dipping on the membrane thickness. The results in table 4:9 indicated that there was a sharp decrease in the thickness of the membrane after the first dip and a continues increase as the dipping number increases. The reason for this could be that as the membrane was porous, the solution permeated more into the membrane pores at the first dip and as it became saturated, less solution was found to permeate into the pores, thereby creating a positive differential gain as the dipping number increases as shown on the table 4:9 above. Also, the graph of figure 4:21 shows that the membrane thickness has a poor linear relationship with number of dipping as indicated by the R^2 factor which is 0.5499 against a value of 1. The increase in the dipping number does bring about an increase in the membrane thickness, but the increase is not a linear function as shown in the figure 4:21 below.

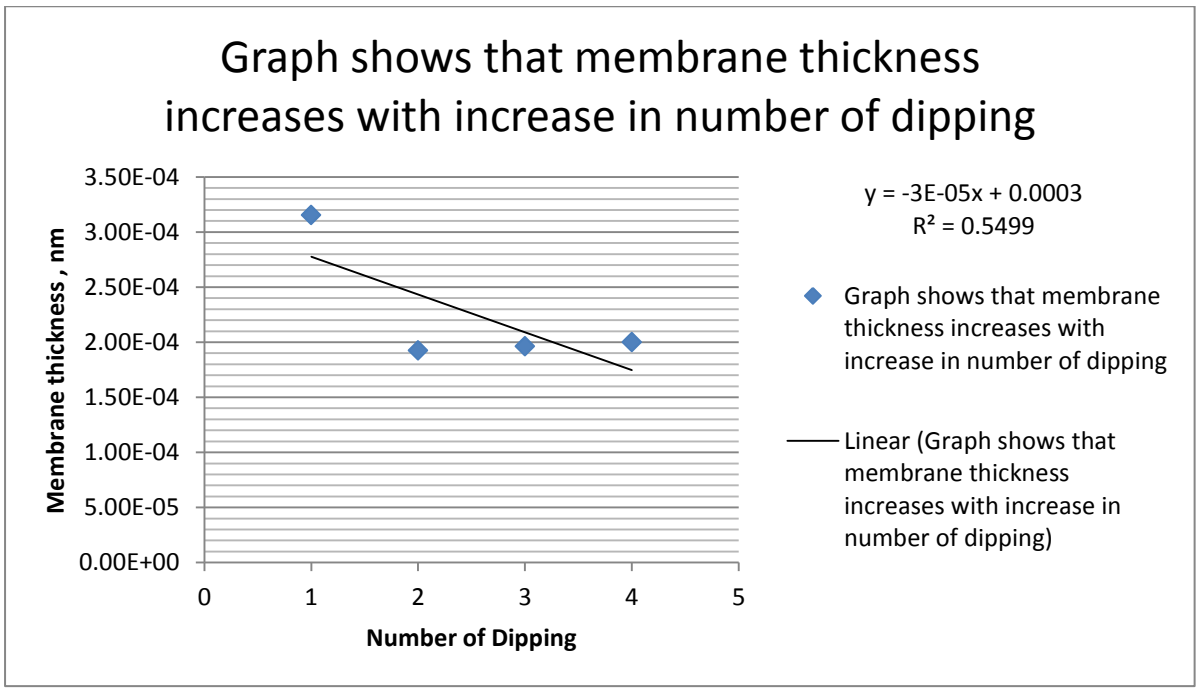

Figure 4:21: Shows membrane thickness increases with number of dipping

Table 4:9: Membrane pore size and number of dipping

Membrane Pore Size (nanometres)	Number of Dipping
276	1
180	2
180	3
104	4

The results of figure 4:22 and table 4:10 show that as the dipping number increases, the pore size reduction is equally the case with a mid linear relationship as shown in figure 4:22 with an R^2 factor of 0.894 against 1.

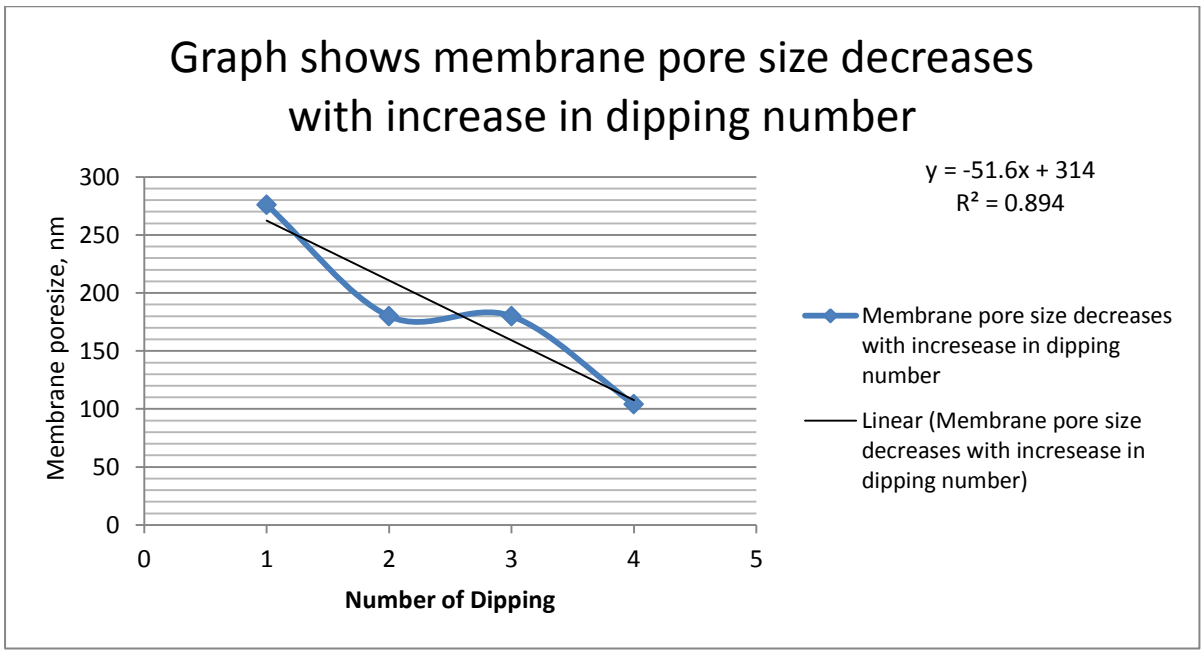

Figure 4:22: Membrane pore size and number of dipping

5 CONCLUSION

For decade of years now, Amine Absorption process has been one of the commercially proven approaches to capture Carbon dioxide from their mixture with Nitrogen, Water molecules, Oxygen and some particulates. But due to the involvement of chemicals and high energy requirement for regeneration process, there has been a need to develop a process which will be more energy efficiency and cost effective in capturing Carbon dioxide from its mixture.

Membrane approach was introduced as alternative for separating gases from their mixtures, because of their non-involvement with chemicals and their ability to be tailored to a particular gas and their low cost of maintenance. Organic membranes were first sets of membranes developed with the hope of separating gas from their mixtures. The organic membrane for example, Polymeric membrane has ability to produce high permeability and high selectivity to their gases of interest [13].But because its ability to fail in a presence of water, harsh chemicals and high temperature application, has put their application opportunity in gas processing on a serious decline. Searches for membranes with high selectivity and permeability of as the organic membrane with a resistance to high temperature, chemical and water has been on for a time now. Recently Professor Edward Gobina, in a patent number 7,048,778 B2, developed an approach by which an inorganic membrane with the desired specifications could be achieved. The research was centred on application of technology in the above mentioned patent to the recovering of the low Carbon dioxide from high concentration Nitrogen mixture.

The inorganic membranes used in this work were developed by Sol-Gel method which provided easy and better controlled approach to membrane preparation. The membranes were developed by modification of the commercially supplied 6000nm

Alpha Alumina supports. The Alpha Alumina Supports were modified first by Gamma Alumina for improved surface Area, followed by Magnesium oxide which increased the adsorption property of the membrane and finally with the Silica which in combination with the magnesium oxide increased the adsorption capacity of the membrane further. The preparation, characterization and testing of the ceramic inorganic membranes have given a further step in the acidic gas processing, such as Carbon dioxide recovery from a flue gas streams. The membranes were tested with simulated flue gas feed compositions: (CO_2-14%, N_2-86%) as mixture A, (CO_2-30%, N_2-70%) as mixture B and (CO_2-60%, N_2-70%) as mixture C respectively. The testing of the fabricated membranes with different gases at different operating parameters demonstrated maximum CO_2 recovery capacity with the membranes at different conditions. The testing indicated that the Carbon dioxide molecules demonstrated strong affinity to Magnesium Oxide and Silica resulted in improved selectivity towards the membrane than when tested with the Alpha Alumina and Gamma Alumina Supports. The testing also indicated that the CO_2 permeability decreases as the thickness of the membrane increases.

At the first stage of the permeation experiment, the maximum recovery efficiency of the fabricated membranes is 30% from a feed concentration of 14% CO_2 and 86% N_2. So in order to improve on the recovering efficiency of membrane towards CO_2 in the permeate, two additional stages were introduced in the permeation line and this resulted in a high CO_2 recovery efficiency of up to 90% at the permeate. The permeation experiment were carried out in four flow arrangements: cocurrent flow fully opened, cocurrent flow fully closed, counter current flow fully opened and counter current flow fully closed, but cocurrent flow arrangement was chosen as the most suitable method for Carbon dioxide recovery as the counter current flow

results favoured Nitrogen flow. The cocurrent flow arrangement used in this project was chosen after the initial experimental results with the Alpha Alumina support demonstrated improved flow of carbon dioxide more than with Nitrogen molecule gas. Membrane C demonstrated that as the thickness of membranes increases, the diffusion of gas through the pore channels reduces thereby reducing the overall permeability of the membrane to individual gas. This clearly demonstrated and explained more in the discussion section. Also, membrane C was used to show the effect of temperature to membrane permeability and selectivity and this proved that at high temperature, the permeability of membrane to gas is lower, but its selectivity is favoured. This was explained and demonstrated in the results and discussion section. The characterization of the prepared membranes equally revealed that the membranes were macro porous and mesoporous according to the permeation data characterization by IUPAC Classification discussed in chapter 2. From the total permeability of the membrane, it was proved that neither Knudsen nor Viscous flow mechanisms was responsible for the flow of Carbon dioxide molecules through the membrane C, Surface Flow was most suitable based on the adsorption effect. The pore sizes estimated were too large to aid for a separation of Carbon dioxide (3.3Å) from Nitrogen (3.64Å) from their mixtures. The achieved surface flow model was confirmed by the Adsorption Heat of the Carbon dioxide and Nitrogen as Nitrogen exhibited a higher Adsorption Heat which confirms its poor adsorption quality ability than Carbondioxide molecules. The introduction of the second and third stage permeation experiment added improvement to the selectivity of the membrane C to Carbon dioxide up to the value of 6 for gas mixtures and up to infinity values for pure Nitrogen, Argon and Methane gas gases at 5kPascal transmembrane pressure. The membrane C at third Stage permeation at a partial transmembrane pressure of 9KPascal and operating temperature of 296

K was capable of recovering up to 90% of carbon dioxide from a feed mixture of 60% CO_2 and 40% Nitrogen. The permeability of the carbon dioxide gas molecule that was recovered at the above listed operating conditions was 9.72E-13 (mol.m/m^2.s.Pa). The membrane C at this permeability produced a selectivity of 6 compared to 2.04 given by membrane B and a value of 3 given by membrane C after fourth dip. These represent a significant improvement in the research history of acidic gas separation using inorganic ceramic membranes.

Finally, the experimental results demonstrated that the fabricated membranes may be used as a competitive option in the concentrating of Carbon dioxide from different feed concentrations as low as 14% as shown in proceeding chapters.

6 RECOMMENDATIONS FOR FUTURE WORK

The recommendations for future work on this project were formed based on the limitations and challenges encountered during fabrication, characterization and testing stages of this project. The flue gas used in this project was limited to Carbon dioxide and Nitrogen molecules mixtures. There are other vital constituents of flue gas which might have impacts on the permeability and selectivity of ceramic membrane studies. Substances like oxygen molecules, Water molecules, SO_X and NO_X would definitely change the experimental design and it might be important to investigate the transport impact of each substance on Carbon dioxide recovering. One vital limitation in this stage of experiment was the control of the membrane thickness. It will be very helpful, for the purpose of future investigation, if equipment or a model is developed for predicting the required membrane thickness. For the characterization stage, all membrane produced were broken in order to carry out SEM imaging on them. This process was the only available method of imaging the surface of the membrane structures. It might worth research to see if an alternative method for surface imaging could be developed without being destructive in order to capture the membrane surface. Also, the amount of then surface Area improve by the modification of the membrane support with Gamma Alumina could not be determined as at the time of this project. Further investigation might be needed to determine the amount of the Surface Area being created using Surface Area Analyser which was out of service at this point.

For the testing of the fabricated membranes, especially in the areas of low temperature application, there should be a proper provision of equipment to achieve a low temperature state, as low as standard condition. In this work, iced blocks were used to achieve the low temperature which gave a lot of challenges.

7 REFERENCES

[1] EIA (Energy Information Administration), Emissions Greenhouse Gases Report, US Department of Energy Report, DOE/EIA-0573(2006), (2007).

[2] Canada's Emission Outlook: An update; (Dec 1999); Available at http://www.nrcan.gc.ca/es/ceo/update.htm

[3] Howard Herzog, Jerry Meldon and Alan Hatton, *Advanced Post-Combustion CO_2 Capture by clean Air Task force* April 2009.

[3] Liu, S. M. and Li, K., *Preparation of TiO_2/Al_2O_3 composite hollow fibre membranes.* Journal of Membrane Science, 218 (1–2): 269–277 (2003).

[4] Weaver, J. A. and Metzer, A. B., *The surface transport of adsorbed molecules*. American Institute of Chemical Engineers Journal, 12: 655–661 (1966).

[5] E.Gobina, A method to separate at least one acidic gas from a mixture comprising the at least one acidic gas and at least one non-acidic gas, US Patent N 7,048,778 B2.

[6] *Ceramic asymmetric hollow fibre membranes-one step fabrication process*, Wei, Chiao Chien; Chen, oi Yee; Liu, Y.; Li, K., p . 191-197

[7] Okazaki, M., Tamon, H. and Toel, R., *Interpretation of surface flow phenomenon of adsorbed gases by hopping model*. American Institute of Chemical Engineers Journal, 27 (2): 262–270 (1981).

[8] Uhlhorn, R. J. R., Keizer, K. and Burggraaf, A. J., *Gas transport and separation with ceramic membranes*. Part I. *Multilayer diffusion and capillary condensation*. Journal of Membrane Science, 66 (2–3): 259–269 (1992).

[9] Andrew Ohwoka, Iyke Ogbuke and Edward Gobina., *Performance of pure and mixed gas transport in reconfigured hybrid inorganic membrane.* Journal of Membrane Technology, Part 1. Page (7-12) June 2012.

[10] Andrew Ohwoka, Iyke Ogbuke and Edward Gobina., *Performance of pure and mixed gas transport in reconfigured hybrid inorganic membrane.* Journal of Membrane Technology, Part 2. Page (7-12) July 2012.

[11] Rao A, Rubin E. *A technical, economic and environmental assessment of amine-based $C0_2$ captures technology for power plant greenhouse gas control*. Environ Sci Technol 2002; 36:4467-4475.

[12] Ponzi, M., Papa, J., Rivarola, J. B. P. and Zgrablich, G., *Surface-diffusion of absorbable gases through porous-media*. American Institute of Chemical Engineers Journal, 23: 347–352 (1977).

[13] Rangarajan, R., Mazid, M. A., Matsuura, T. and Sourirajan, S., *Permeation of pure gases under pressure through asymmetric porous membranes – membrane characterization and prediction of performance*. Industrial and Engineering Chemistry Process Design and Development, 23 (1): 79–87 (1984).

[14] Gobina, E., *Apparatus and Method for Separating Gases*, granted US Patent 7048778, 23 May 2006

[15] Keizer, K., Uhlhorn, R. J. R., van Vuren, R. J. and Burggraaf, A. J., *Gas separation mechanisms in microporous modified [gamma]-Al2O3 membranes*. Journal of Membrane Science, 39 (3): 285–300 (1988).

[16] Tamura, H.; Katayama, N.; Furuichi, R. Modeling of ion exchange reactions on metal oxides with the frumkin isotherm: 1*. Acid–base and charge characteristics*

of MnO_2, TiO_2, Fe_3O_4, and Al_2O3 surfaces and adsorption affinity of alkali metal ıon. Environ. Sci. Technol. 1996, 30(4), 1198–1204.

[17] Uhlhorn, R. J. R., Keizer, K. and Burggraaf, A. J., *Gas and surface diffusion in modified [gamma]- alumina systems. Journal of Membrane Science*, 46 (2–3): 225–241 (1989).

[18] de Vos, R. M. and Verweij, H., *Improved performance of silica membranes for gas separation*. Journal of Membrane Science, 143 (1–2): 37–51 (1998).

[19] Favre E. Carbon dioxide recovery from post-combustion process: Can gas permeation membranes compete with absorption? J Membrane Sci 2007; 294:50-59.

[20] Gouzinis, A. and Tsapatsis, M., *on the preferred orientation and microstructural manipulation of molecular sieve films prepared by secondary growt*

[21] *Koros, W.J. and G.K. Fleming, Membrane-Based Gas Separation, Journal of Membrane Science, 1993, **83**(1), 1-80 h*. Chemistry of Materials, 10 (9): 2497–2504 (1998)

[22] Reed, J. S., *Principles of Ceramic Processing*. 2nd edn. (1995) New York: John Wiley & Sons, Inc.

[23] Ronald Wincek, Chunshan Song, and John M. Anderson, *Separation of CO_2 from Power Plant Flue Gas Using a Novel CO_2 'Molecular Basket Adsorbent'*, fuel Chemistry Division Preprints 2003, 48(1)

[24] Tan, X., Liu, S. and Li, K., *Preparation and characterization of inorganic hollow fibre membranes*. Journal of Membrane Science, 188 (1): 87–95 (2001).

[25] Liu, S., Li, K. and Hughes, R., *Preparation of porous aluminium oxide (Al2O3) hollow fibre membranes by a combined phase-inversion and sintering method*. Ceramics International, 29: 875–881 (2003)

[26] *Cross linking poly1-(trimethylsily)-1-propynel and its effect on physical* stability, Kelman, scott D.; Rowe, Brandon W.; Bielawski, Christopher W.; et al., p.123-134

[27] Julbe, A. and Ramsay, J. D. F., *Methods for the characterisation of porous structure in membrane materials, in Fundamentals of Inorganic Membrane Science and Technology*, Burggraaf, A. J. and Cot, L., Editors. (1996) Amsterdam: Elsevier Science B.V., p. 67–118.

[28] Benfer, S., Arki, P. and Tomandl, G., *Ceramic membranes for filtration applications – preparation and characterization*. Advanced Engineering Materials, 6 (7): 495–500 (2004).

[29] Mulder, M., Basic *Principles of Membrane Technology.*2nd ed. (1996) Dordrecht, the Netherlands: Kluwer Academic Publishers

[30] Sing, K. S. W., Everett, D. H., Haul, R. A. W., Moscou, L., Pierotti, R. A., Rouquerol, J. and Siemieniewska, T., *Reporting physisorption data for gas solid systems with special reference to the determination of surface-area and porosity*. Pure and Applied Chemistry, 57 (4): 603–619 (1985).

[31] Fritzsche A, Kurz J The separation of gases by membranes, in: Handbook of industrial membrane technology porter MC, editor. William Andrew Publishing 1990; 559-593.

[32] *The formation of supported membranes*. Journal of Colloid and Interface Science, 105 (1): 27–40 (1985).

[33] Larbot, A., Julbe, A., Guizard, C. and Cot, L., *Silica membranes by the sol-gel process*. Journal of Membrane Science, 44 (2–3): 289–303 (1989).

[34] DeVos, R. M. and Verweij, H., *Improved performance of silica membranes for gas separation*. Journal of Membrane Science, 143 (1–2): 37–51 (1998).

[35] Burggraaf, A. J*., Fundamentals of membrane top layer synthesis and processing, in Fundamentals of Inorganic Membrane Scienc and Technology*, Burggraaf, A. J. and Cot, L. Editors. (1996) Amsterdam, the Netherlands: Elsevier Science B.V., p. 259–329.

[36] Tan, X. Y., Liu, S. M. and Li, K., *Preparation and characterization of inorganic hollow fibre membranes*. Journal of Membrane Science, 188 (1): 87–95 (2001).

[37] Copyright (2003) Elsevier, Ceramics International, 29, Liu, S., Li, K. and Hughes, R*., Preparation of porous aluminium oxide (Al2O3) hollow fibre membranes by a combined phase-inversion and sintering method*, p.875–881

[38] *Preparation and Characterization of dual stimuli-responsive microcapsules with a super paramagnetic porous membrane and thermo-responsive gates*, Yang, Wen-Chuan; Xie, Rui; Xue-Qin; et al., p.324-330

[39] *Effect of surface morphology on membrane fouling by humic acid with the use of cellulose acetate butyrate hollow fibre membranes*, Fu, Xunyao; Maruyama, Tatsuo; Sotani, Tomohiro; Matsuyama, Hideto, p. 483-491

[40] *Inorganic- organic hybrid polymers with pendent suffocated cyclic phosphazene side groups as potential proton conductive materials for direct*

methanol fuel cells, Fei, Shih-To; Wood, Richard M.; Lee, David K.; et al., p. 206-214

[41] Sing, K. S. W., Everett, D. H., Haul, R. A. W., Moscou, L., Pierotti, R. A., Rouquerol, J. and Siemieniewska, T., *Reporting physisorption data for gas solid systems with special reference to the determination of surface-area and porosity*. Pure and Applied Chemistry, 57 (4): 603–619 (1985)

[42] *Low-pressure membrane filtration of secondary effluent in water reuse: Pre-treatment for fouling reduction*, Fan, Linhua; Nguyen, Thang; Roddick, Felicity A.; Harris, John L., p. 135-142

[43] *Morphology changes of polyvinylidene fluoride membrane under different phase separation mechanisms*, Li, Xianfeng; Wang, Yonggang; Xiao, Changfa, p.477-482

[44] Murlidhar Gupta, Irene Coyle and Kelly Thambimuthum. *CO_2 Capture Technologies and Opportunities in Canada, Strawman Document for CO_2 Capture and Storage (CC&S) Technology Roadmap*. CANMET Energy Technology Centre Natural Resources Canada, September 2003.

[45] *Preparation of high-presence MFI membrane with the modified secondary growth method on the macroporous alpha-alumina tubular support*, Zhao, Qingyu; Wang, Jinqu; Chu, Naibo; et al., 303-309

[46] Improving CO_2 selectivity in polymerized room- temperature ionic liquid gas separation membranes through incorporation of polar substituents, Bara, Jason E.; Gabriel, Christopher J.; Hatakeyama, Evan S.; et al.; p.3-7

[47] Baker R. *Future directions of membrane gas separation technology*. Ind Eng. Chem Res 2002; 41:1393.

[48] Powell C, Qias G. *Polymeric CO_2/N_2 gas separation membranes for the capture of carbon dioxide.*

[49] Feron P. CO_2 capture: *The characterisation of gas separation/removal membrane systems applied to the treatment of the flue gases arising from power generation using fossil fuel. Cheltenham*: IEA Greenhouse Gas R & D Programme; 1992.

[50] Mazur W, Chan M. *Membranes for natural gas sweetening and CO_2 enrichment*. Chem Eng Prog 1982; 78: 38-43.

[51] Leenaars, A. F. M. and Burggraaf, A. J., The preparation and characterization of alumina membranes with ultrafine pores.

[52] Abertz V, Brinkmann T, and Dijkstra M, et al. *Developments in membrane research: from material via process design to industrial application*. Adv Eng Mater 2006; 8:328-358.

[53] Coady A, Davis J. *CO_2 recovery by gas permeation*. Chem Eng Prog 1982; 78: 43-49.

[54] Lin, Y. S., *Microporous and dense inorganic membranes: current status and prospective. Separation and Purification Technology*, 25 (1–3): 39–55 (2001).

[55] Wong, W. C., Au, L. T. Y., Lau, P. P. S., Ariso, C. T. and Yeung, K. L*., Effects of synthesis parameters on the zeolite membrane morphology*. Journal of Membrane Science, 193 (2): 141–161 (2001)

[56] Aaron D, Tsouris C. *Separation of CO_2 from flue gas*: *a review*. Separ Sci. Technol 2005; 40: 321-348.

[57] Gielen, D. 2003. *CO_2 Removal in the Iron and Steel Industry*. Energy Convers. Mgmt. Vol. 44, pp. 1027-1037.

[58] Veawab, A., A. Aroonwilas, A. Chakma and P. Tontiwachuthikul. 2001. *Solvent Formulation for CO_2 Separation from Flue Gas Streams.* First National Conference on Carbon Sequestration. May 14-17, 2001, Washington, D.C

[59] IEA GHG R&D Programme. 1993. *Greehouse Gas Emission from Power Station*

[61] Dr.T. J. hovel, Dr. R. Schneider, and Michael Sandell, *Optimal Power Plant Integration of Post-Combustion CO_2 Capture,* Siemens AG, Energy Sector Germany.2009.

[62] J. Gibson, D. Schallehn, Z. Que and C. Jian. *Carbondioxide Capture from Coal-fired Power Plants in China*, Summary Report for NZEC Work Package 3, September, 2009.

[63] *Data Reduction and Error Analysis for Physical Sciences, Second Edition*, by Philip R. Bevington and D. Keith Robinson, McGraw-Hill Inc., 1992.

[64] *Statistical Treatment of Data*, by Hugh D. Young, McGraw-Hill Book Company Inc., New York, 1962.

8 APPENDIX SECTION

8.1 APPENDIX 1: PERMEATION RESULTS

Table 8:1: Cocurrent flow for pure Methane permeation using Support only with retentate valve fully opened

$P_F$eed (Bar) Absolute	$P_{Retentate}$ (Bar) Absolute	$P_{Permeate}$ (Bar) Absolute	ΔP(Bar) Pressure Drop Absolute (P_F - P_P)	Pure Methane Retentate Flow Rate (ml/min)	Pure Methane Permeate Flow Rate (ml/min)
1.05	1.01	1.00	0.05	12	100
1.06	1.02	1.00	0.06	25	210
1.07	1.03	1.00	0.07	90	310
1.08	1.03	1.00	0.08	150	450
1.09	1.04	1.00	0.09	210	550
1.1	1.05	1.00	0.1	250	650

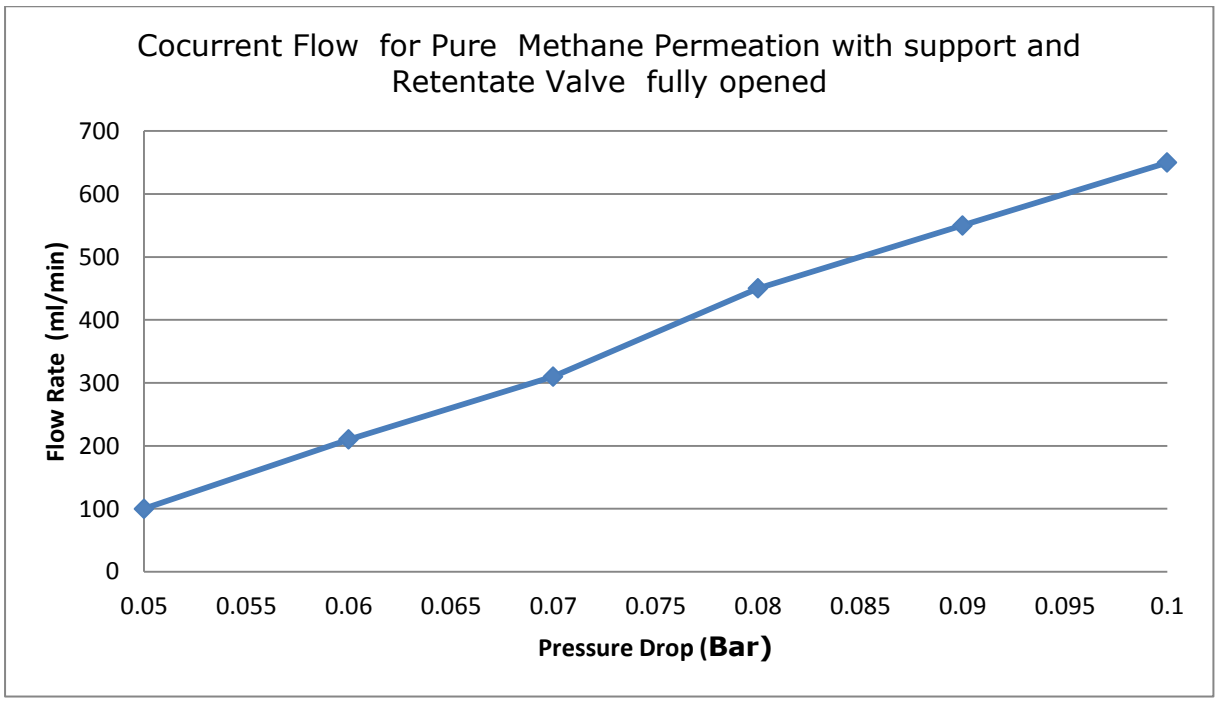

Figure 8:1: Co current flow for pure Methane Permeation using support only with Retentate Valve fully opened

Table 8:2 :Cocurrent flow for pure Methane permeation using support only with retentate valve closed

P_{Feed} (Bar) Absolute	$P_{Retentate}$ (Bar) Absolute	$P_{Permeate}$ (Bar) Absolute	ΔP(Bar) (P_F - P_P) Absolute	Pure Methane Retentate flow Rate (ml/min) Valve closed	Pure Methane Permeate Flow Rate (ml/min)
1.05	1.02	1.00	0.05	0	125
1.06	1.02	1.00	0.06	0	230
1.07	1.03	1.00	0.07	0	410
1.08	1.05	1.00	0.08	0	470
1.09	1.06	1.00	0.09	0	600
1.1	1.08	1.00	0.1	0	660

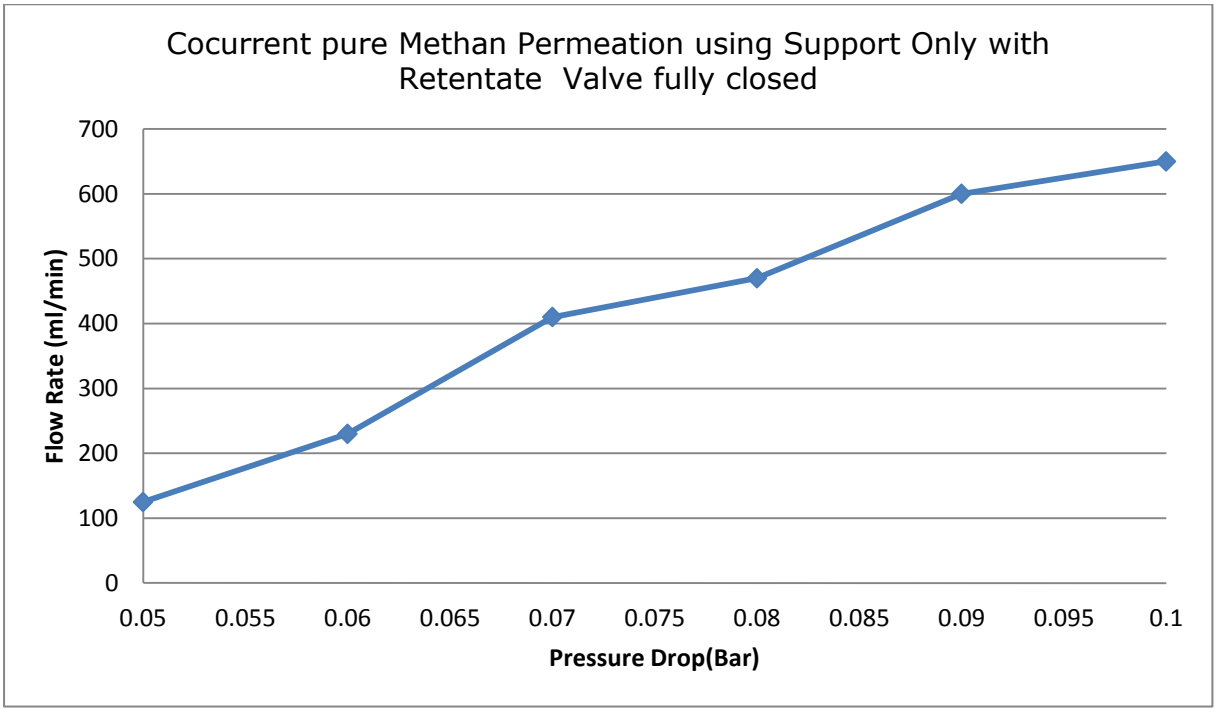

Figure 8:2: Cocurrent Methane Permeation using support only with Retentate valve fully closed

Table 8:3: Counter current flow for pure Methane permeation using support only with retentate valve fully opened.

P_{Feed} (Bar) Absolute	$P_{Retentate}$ (Bar) Absolute	$P_{Permeate}$ (Bar) Absolute	ΔP(Bar) (P_F - P_P) Absolute	Pure Methane Retentate flow Rate (ml/min) Valve opened	Pure Methane Permeate Flow Rate (ml/min)
1.05	1.01	1.00	0.05	11	101
1.06	1.02	1.00	0.06	26	211
1.07	1.03	1.00	0.07	90	310
1.08	1.03	1.00	0.08	150	455
1.09	1.04	1.00	0.09	210	560
1.1	1.05	1.00	0.1	250	655

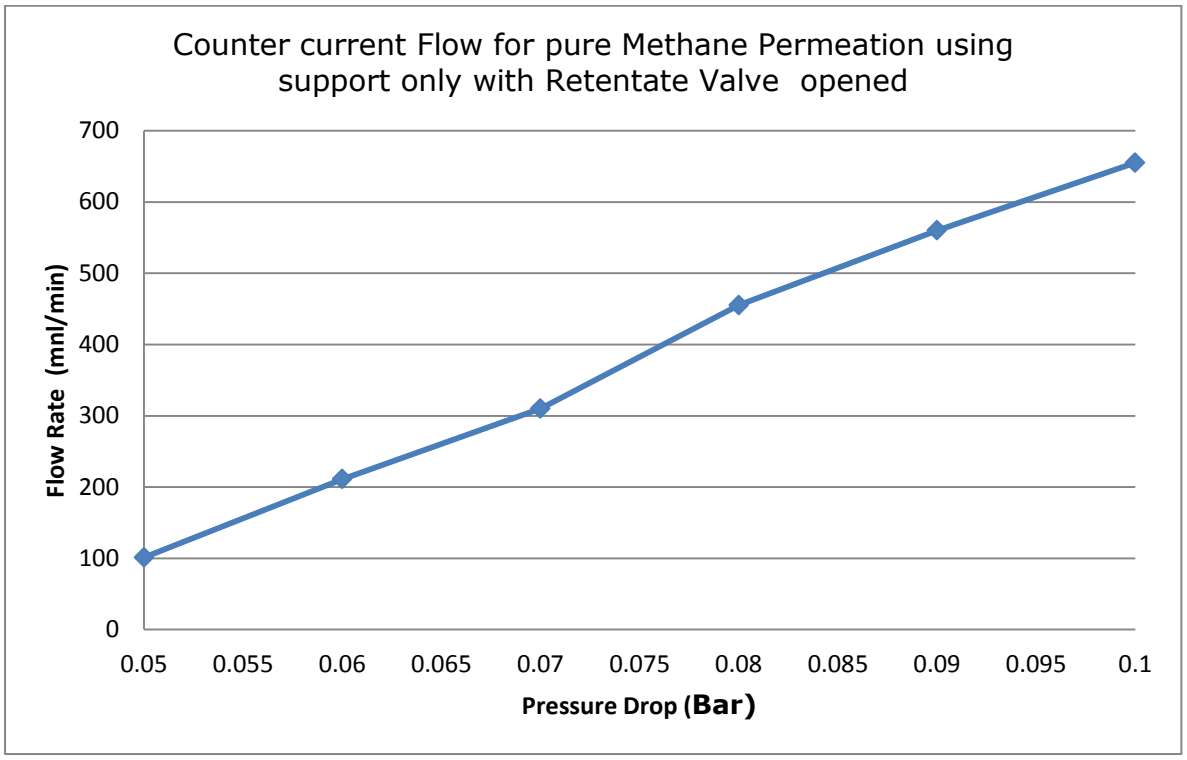

Figure 8:3: Counter current flow for pure Methane Permeation using support only with Retentate Valve opened

Table 8:4 counter current flow for pure Methane permeation using support only with retentate valve Closed.

P_{Feed} (Bar) Absolute	$P_{Retentate}$ (Bar) Absolute	$P_{Permeate}$ (Bar) Absolute	ΔP (Bar) Absolute (P_F - P_P)	Pure Methane Retentate Flow Rate (ml/min) Valve Closed	Pure Methane Permeate Flow Rate (ml/min)
1.05	1.02	1.00	0.05	0	127
1.06	1.02	1.00	0.06	0	232
1.07	1.03	1.00	0.07	0	413
1.08	1.05	1.00	0.08	0	469
1.09	1.06	1.00	0.09	0	602
1.1	1.08	1.00	0.1	0	651

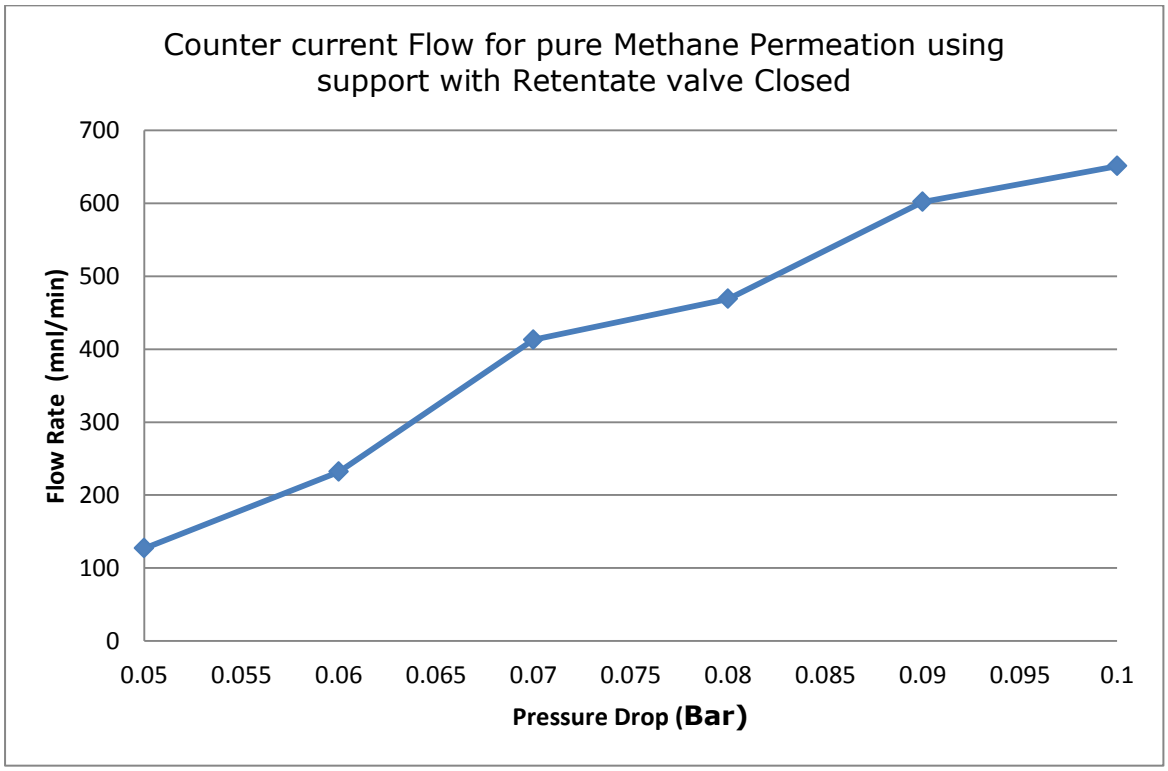

Figure 8:2: Counter current flow for pure Methane Permeation using support only with Retentate Valve closed

Table 8:5: Cocurrent flow for pure Nitrogen permeation using support only with retentate valve fully opened.

P_{Feed} (Bar) Absolute	$P_{Retentate}$ (Bar) Absolute	$P_{Permeate}$ (Bar) Absolute	ΔP(Bar) (P_F - P_P) Absolute	Pure Nitrogen Retentate Flow Rate (ml/min)	Pure Nitrogen Permeate Flow Rate (ml/min)
1.05	1.01	1.00	0.05	12	85
1.06	1.02	1.00	0.06	25	250
1.07	1.03	1.00	0.07	80	310
1.08	1.03	1.00	0.08	90	450
1.09	1.04	1.00	0.09	130	502
1.1	1.05	1.00	0.1	240	600

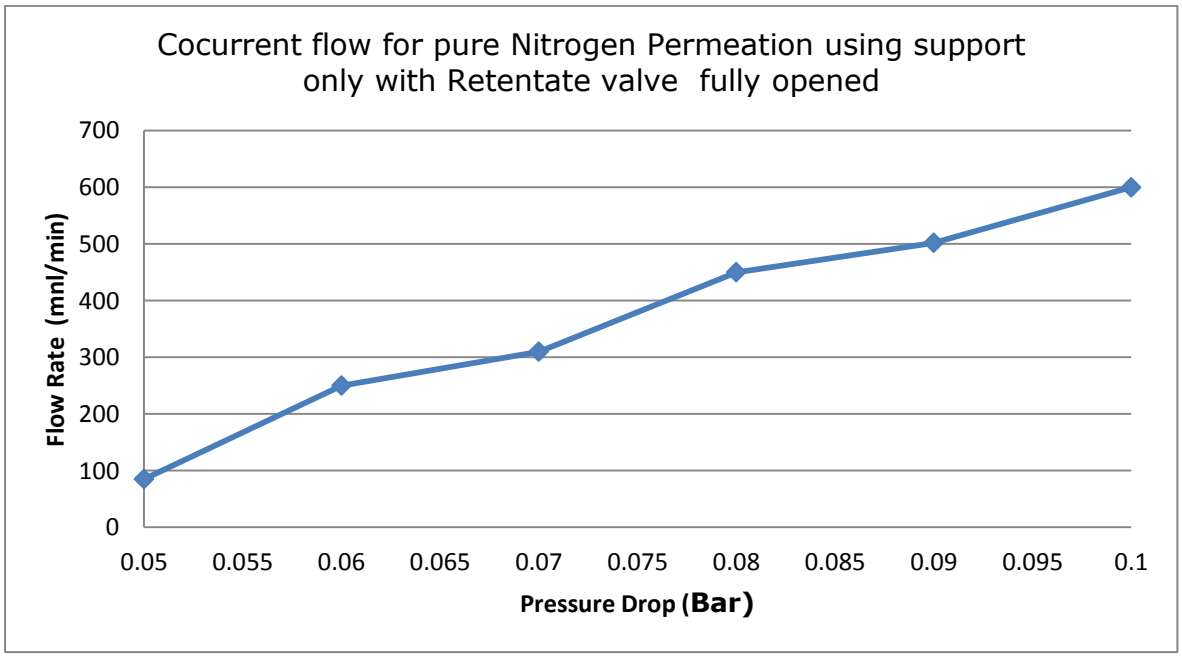

Figure 8:3: Cocurrent Flow for pure Nitrogen permeation using support only with Retentate Valve fully opened

Table 8:6: Cocurrent flow for pure Nitrogen permeation using support only with retentate valve Closed.

P_{Feed} (Bar) Absolute	$P_{Retentate}$ (Bar) Absolute	$P_{Permeate}$ (Bar) Absolute	ΔP (Bar) (P_F - P_P) Absolute	Pure Nitrogen Retentate Flow Rate (ml/min) Valve closed	Pure Nitrogen Permeate Flow Rate (ml/min)
1.05	1.01	1.00	0.05	0	90
1.06	1.03	1.00	0.06	0	198
1.07	1.04	1.00	0.07	0	300
1.08	1.05	1.00	0.08	0	400
1.09	1.06	1.00	0.09	0	450
1.1	1.06	1.00	0.1	0	600

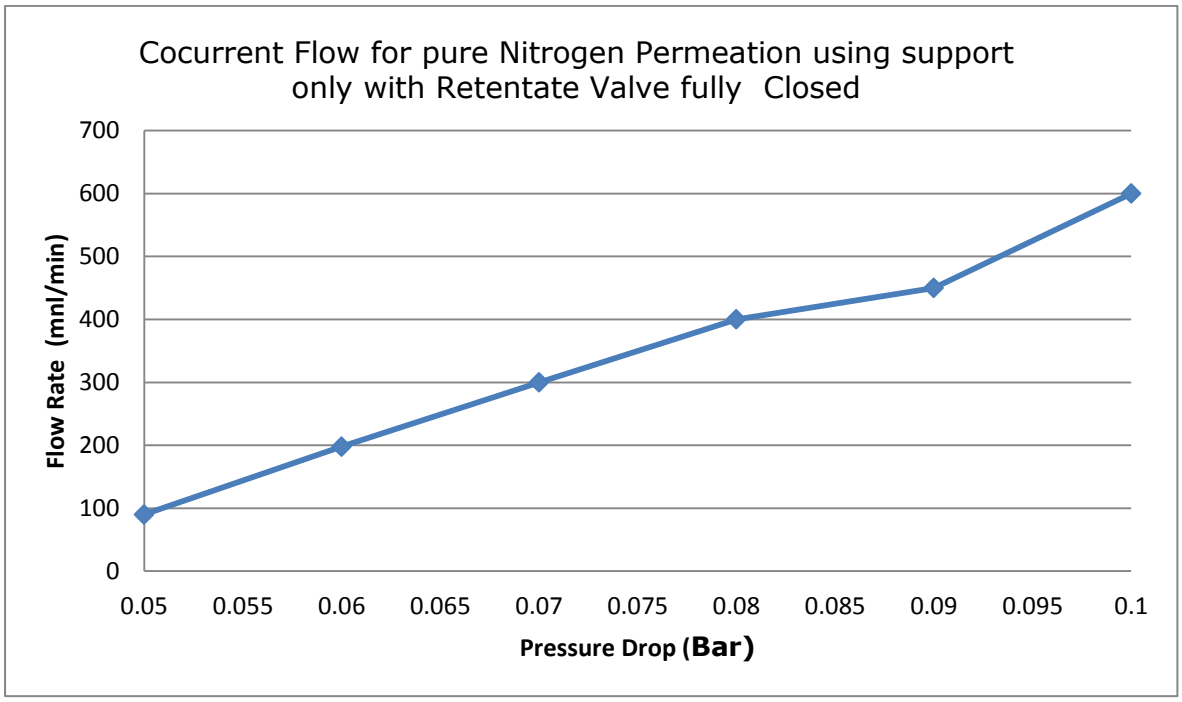

Figure 8:4: Cocurrent flow for pure Nitrogen permeation using support only with retentate valve Closed.

Table 8:7: Counter current flow for pure Nitrogen permeation using support only with retentate opened.

P_{Feed} (Bar)	$P_{Retentate}$ (Bar)	$P_{Permeate}$ (Bar)	ΔP(Bar) (P_F - P_P)	Pure Nitrogen Retentate Flow Rate (ml/min) Valve opened	Pure Nitrogen Permeate Flow Rate (ml/min)
1.05	1.04	1.00	0.05	198	250
1.06	1.04	1.00	0.06	200	320
1.07	1.04	1.00	0.07	221	360
1.08	1.04	1.00	0.08	248	420
1.09	1.04	1.00	0.09	280	480
1.1	1.05	1.00	0.1	300	500

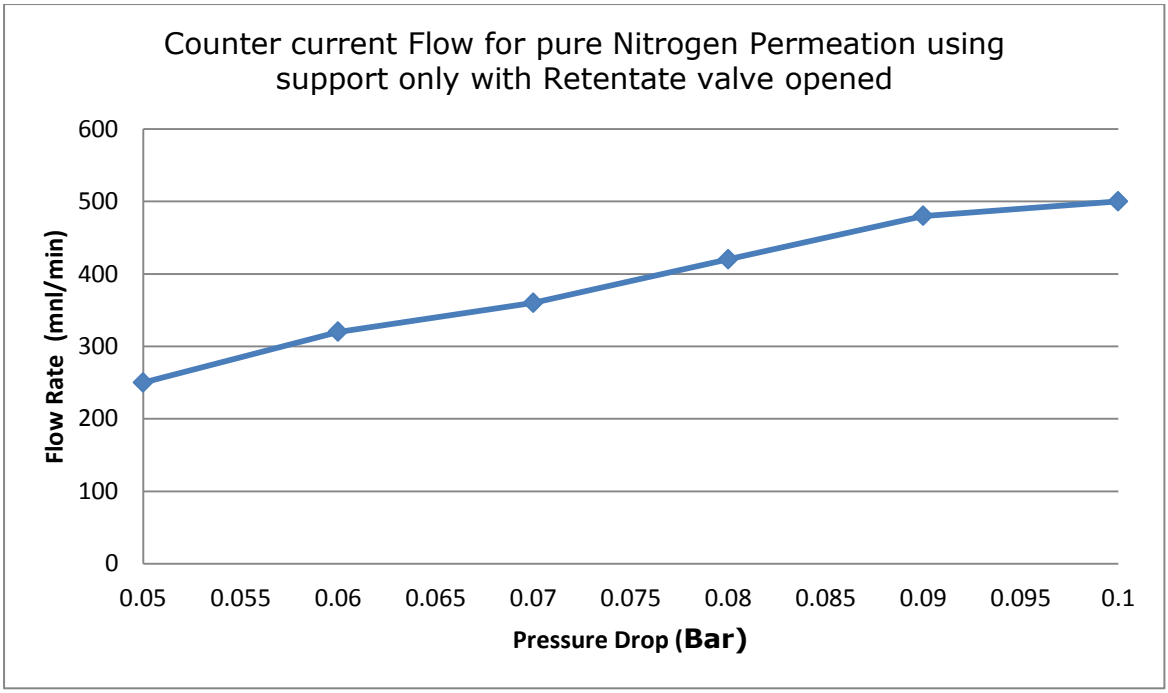

Figure 8:5: Counter current flow arrangement for Nitrogen permeation with Retentate Valve fully opened

Table 8:8: Counter current flow for pure Nitrogen Permeation using support only with retentate valve Closed.

P_{Feed} (Bar) Absolute	$P_{Retentate}$ (Bar) Absolute	$P_{Permeate}$ (Bar) Absolute	ΔP(Bar) (P_F - P_P) Absolute	Pure Nitrogen Retentate Flow Rate (ml/min) Valve closed	Pure Nitrogen Permeate Flow Rate (ml/min)
1.05	1.04	1.00	0.05	0	278
1.06	1.04	1.00	0.06	0	323
1.07	1.04	1.00	0.07	0	344
1.08	1.04	1.00	0.08	0	385
1.09	1.04	1.00	0.09	0	500
1.1	1.05	1.00	0.1	0	600

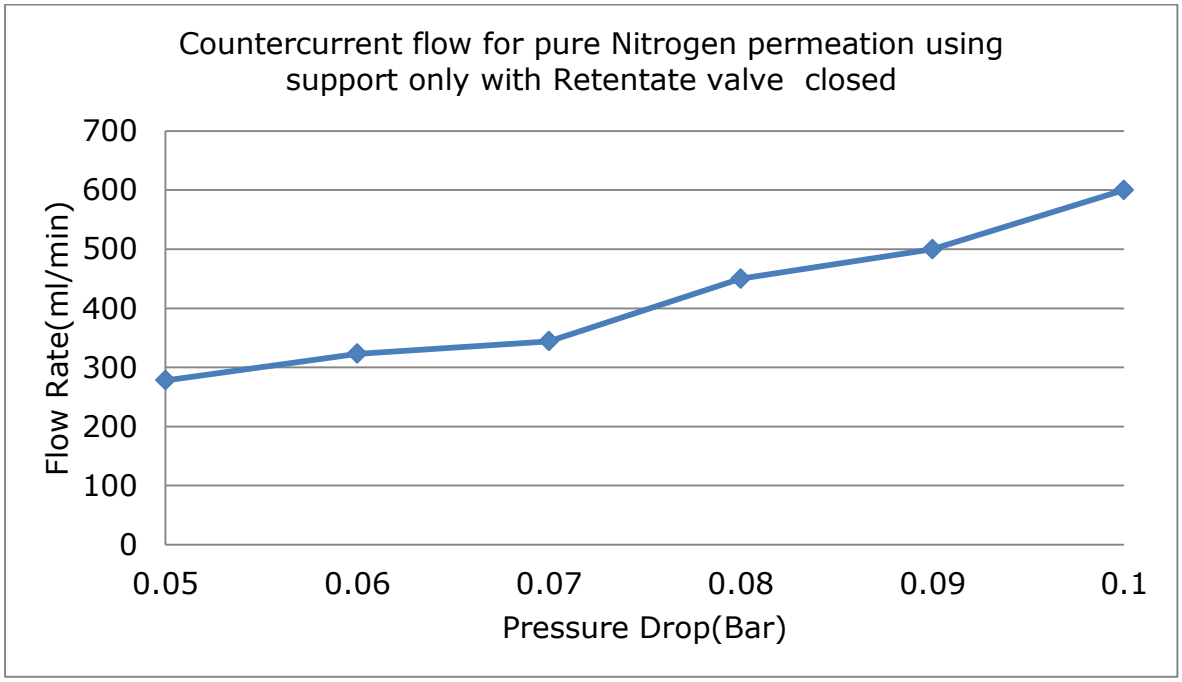

Figure 8:6: Counter current flow for pure Nitrogen Permeation using support only with retentate valve close

Table 8:9: Cocurrent flow for pure CO_2 permeation using membrane support only and retentate valve fully opened.

P_{Feed} (Bar) Absolute	$P_{Retentate}$ (Bar) Absolute	$P_{Permeate}$ (Bar) Absolute	ΔP (Bar) (P_F - P_P) Absolute	Pure CO_2 Retentate Flow Rate (ml/min)	Pure CO_2 Permeate Flow Rate (ml/min)
1.05	1.01	1.00	0.05	16	60
1.06	1.02	1.00	0.06	34	160
1.07	1.03	1.00	0.07	98	200
1.08	1.03	1.00	0.08	109	300
1.09	1.04	1.00	0.09	140	420
1.1	1.05	1.00	0.1	300	490

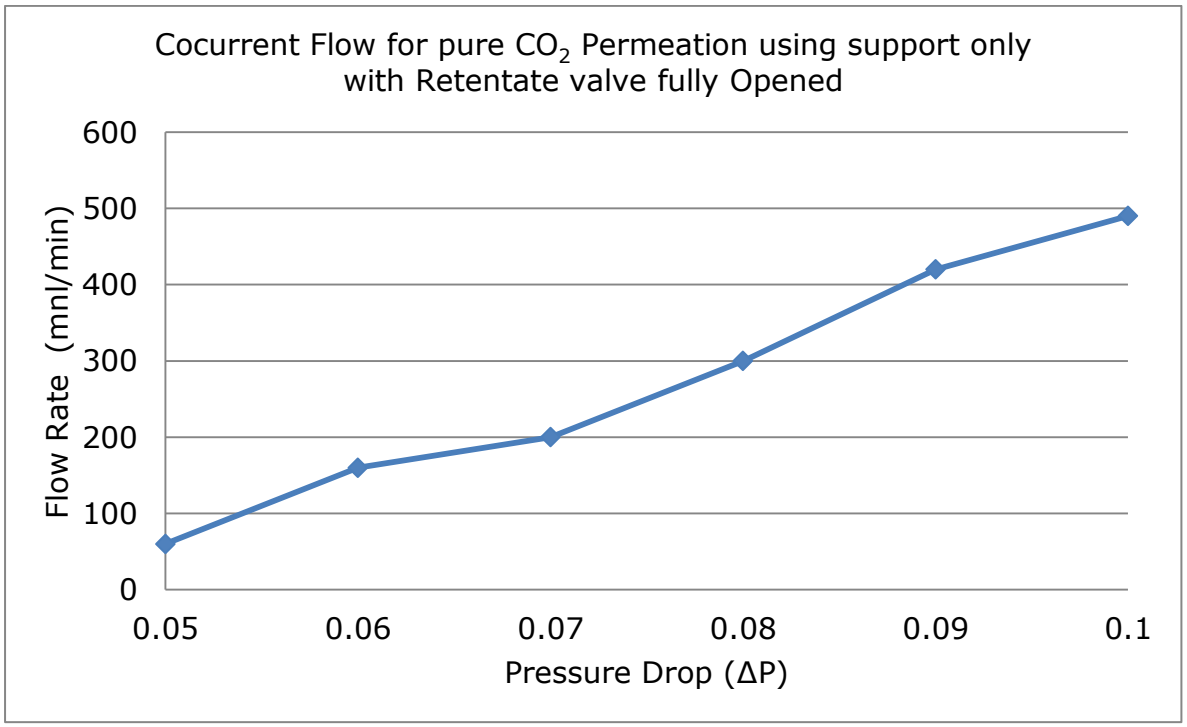

Figure 8:7: Cocurrent flow for pure CO_2 permeation using support only and retentate valve fully opened.

Table 8:10: Cocurrent flow for pure CO_2 permeation using membrane support only with retentate valve Closed.

P_{Feed} (Bar)	$P_{Retentate}$ (Bar)	$P_{Permeate}$ (Bar)	ΔP(Bar) (P_F - P_P)	$C0_2$ Retentate Flow Rate(ml/min) Valve closed	Pure CO_2 Permeate Flow Rate(ml/min)
1.05	1.01	1.00	0.05	0	70
1.06	1.03	1.00	0.06	0	150
1.07	1.04	1.00	0.07	0	250
1.08	1.05	1.00	0.08	0	315
1.09	1.06	1.00	0.09	0	380
0.1	1.06	1.00	0.1	0	550

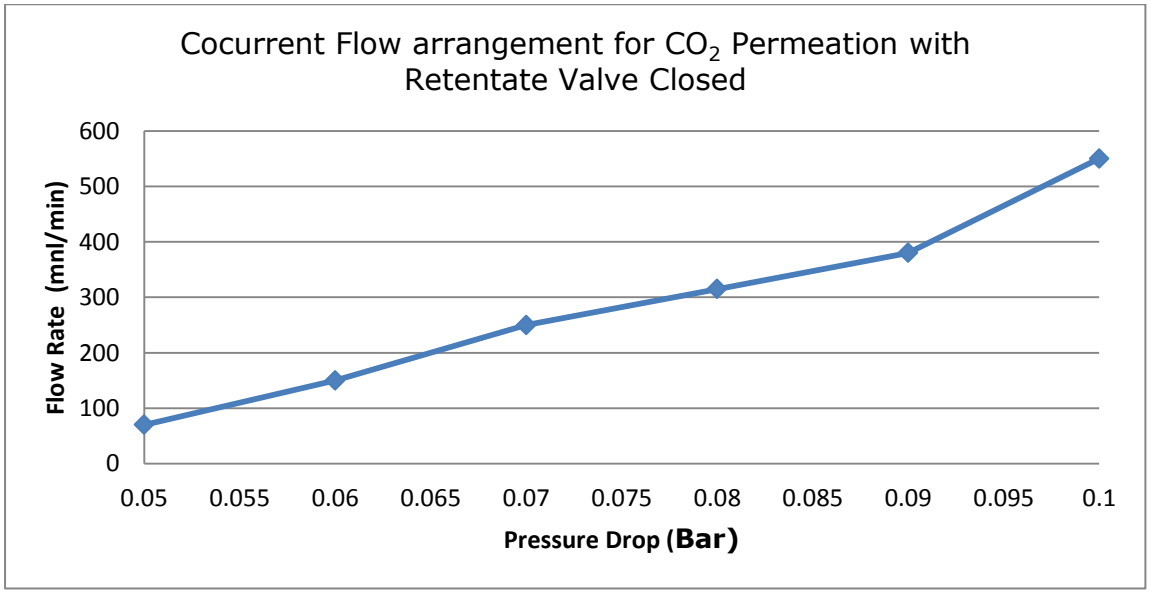

Figure 8:8: Cocurrent flow for pure CO_2 permeation using support only with retentate valve Closed.

Table 8:11: Counter current flow for pure CO_2 permeation using Support only with retentate valve Closed

P_{Feed} (Bar) Absolute	$P_{Retentate}$ (Bar) Absolute	$P_{Permeate}$ (Bar) Absolute	ΔP (Bar) Absolute (P_F - P_P)	CO_2 Retentate Flow Rate (ml/min) Valve Closed	Pure CO_2 Permeate Flow Rate (ml/min)
1.05	1.01	1.00	0.05	0	75
1.06	1.03	1.00	0.06	0	168
1.07	1.04	1.00	0.07	0	200
1.08	1.05	1.00	0.08	0	320
1.09	1.06	1.00	0.09	0	378
1.1	1.06	1.00	0.1	0	480

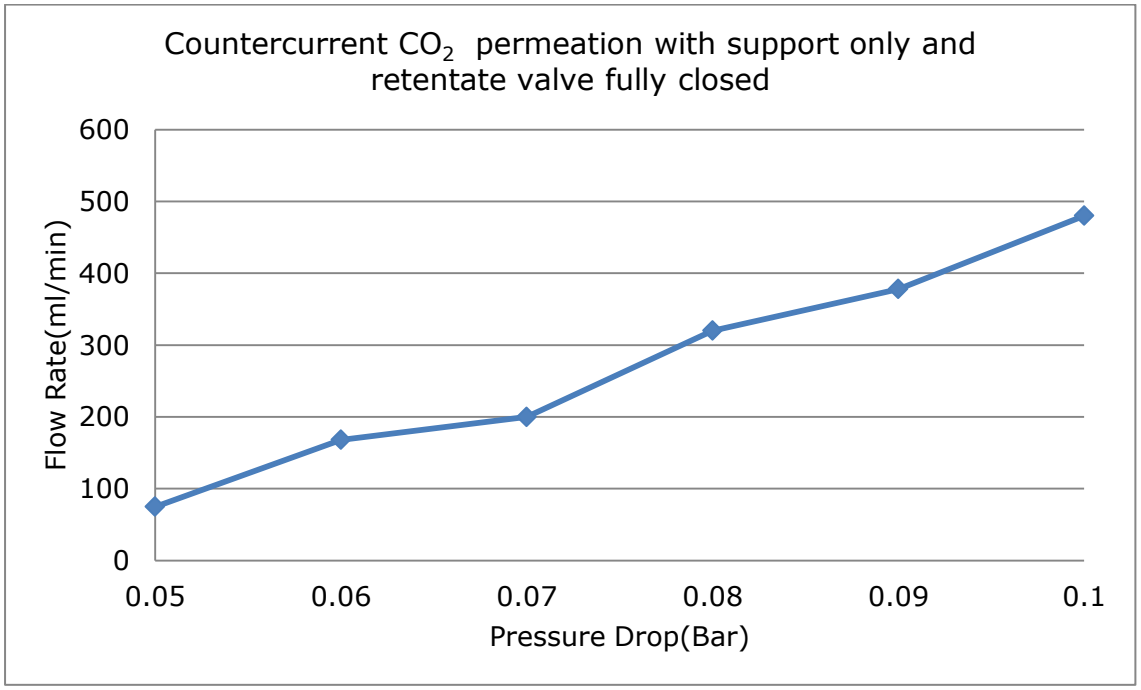

Figure 8:9: Counter current flow for pure CO_2 permeation using support only with Retentate Valve closed

Table 8:12: Counter current flow for pure CO_2 permeation using Support only with retentate valve opened

P_{Feed} (Bar) Absolute	$P_{Retentate}$ (Bar) Absolute	$P_{Permeate}$ (Bar) Absolute	ΔP (Bar) Absolute (P_F - P_P)	CO_2 Retentate Flow Rate (ml/min) Valve Closed	Pure CO_2 Permeate Flow Rate (ml/min)
1.05	1.01	1.00	0.05	20	72
1.06	1.03	1.00	0.06	50	140
1.07	1.04	1.00	0.07	120	160
1.08	1.05	1.00	0.08	140	210
1.09	1.06	1.00	0.09	190	296
1.1	1.06	1.00	0.1	348	320

Table 8:13: Cocurrent flow for pure Helium permeation using support only with Retentate Valve opened

P_{Feed} (Bar)	$P_{Retentate}$ (Bar)	$P_{Permeate}$ (Bar)	ΔP (Bar) (P_F - P_P)	Pure Helium Retentate Flow Rate (ml/min)	Pure Helium Permeate Flow Rate (ml/min)
1.05	1.0	1.00	0.05	120	190
1.06	1.01	1.00	0.06	160	276
1.07	1.01	1.00	0.07	180	352
1.08	1.03	1.00	0.08	210	450
1.09	1.04	1.00	0.09	280	520
1.1	1.05	1.00	0.1	340	610

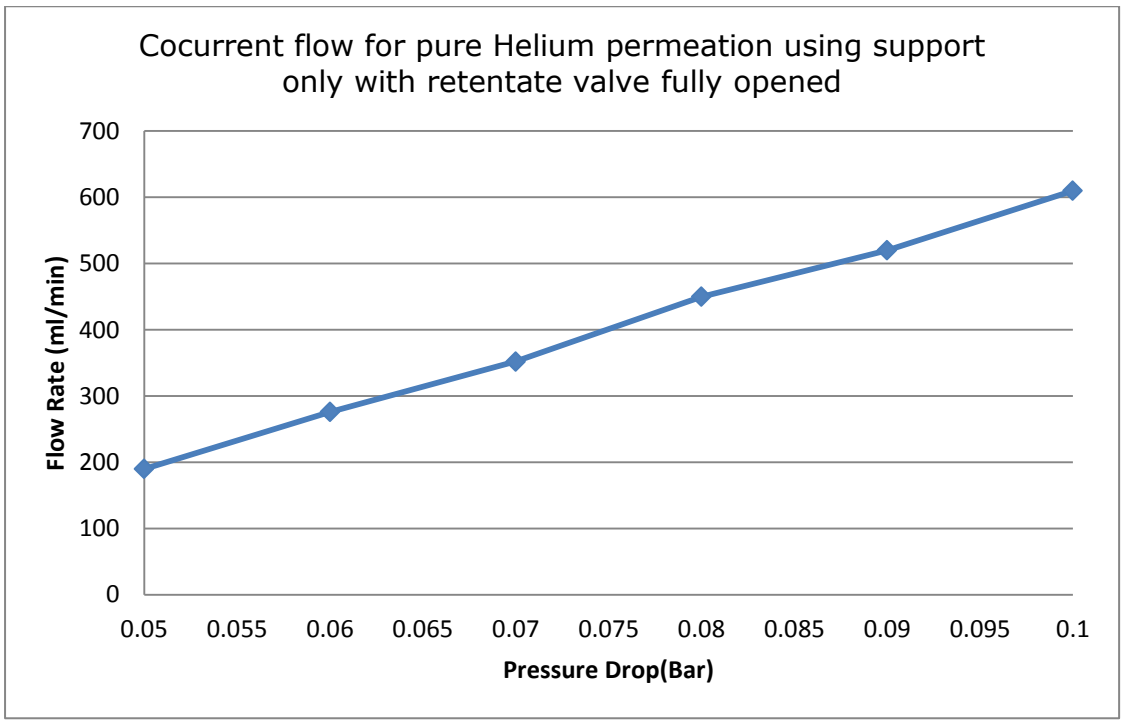

Figure 8:10: Cocurrent flow for pure Helium permeation using support only with Retentate Valve opened

Table 8:14: Values of cocurrent flow for pure Helium permeation.

P_{Feed} (Bar) Absolute	$P_{Retentate}$ (Bar) Absolute	$P_{Permeate}$ (Bar) Absolute	ΔP (Bar) (P_F - P_P) Absolute	Pure Helium Retentate Flow Rate (ml/min)	Pure Helium Permeate Flow Rate (ml/min)
1.05	1.05	1.00	0.05	0	200
1.06	1.03	1.00	0.06	0	300
1.07	1.05	1.00	0.07	0	400
1.08	1.07	1.00	0.08	0	500
1.09	1.07	1.00	0.09	0	560
1.1	1.09	1.00	0.1	0	690

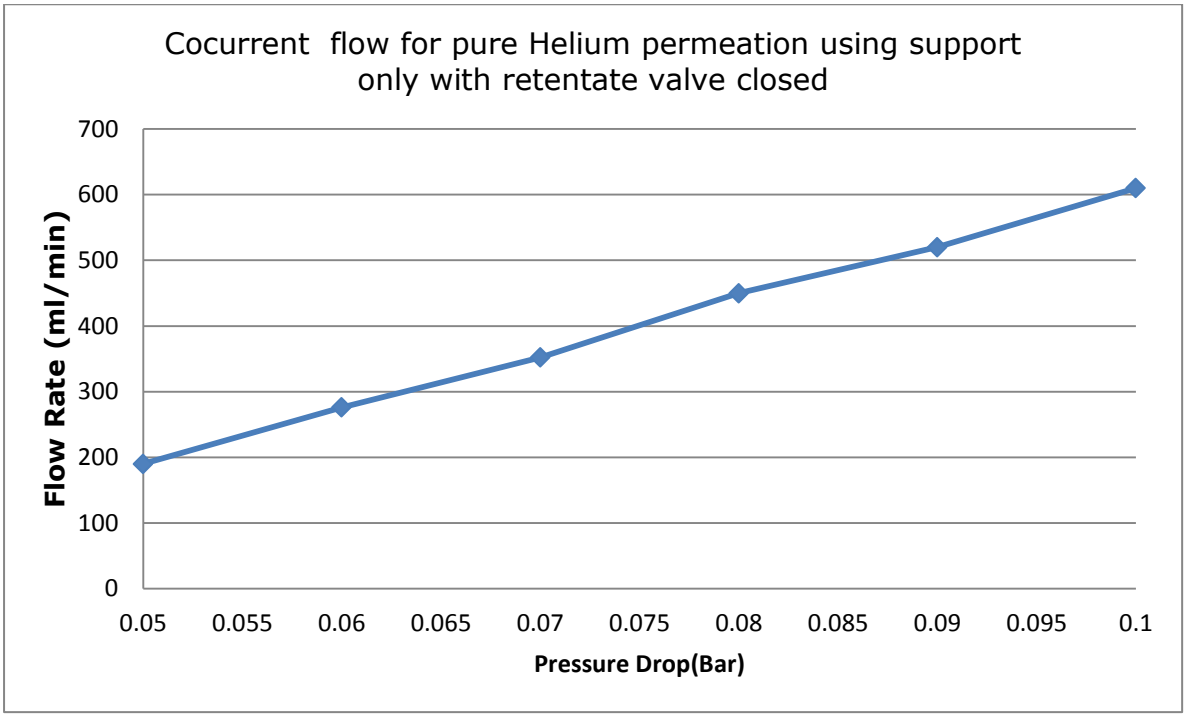

Figure 8:11: Cocurrent flow for pure Helium permeation using support only with Retentate Valve closed

Table 8:15: Counter current flow for pure Helium permeation using support only with retentate valve fully opened

P_{Feed} (Bar) Absolute	$P_{Retentate}$ (Bar) Absolute	P_P (Bar) Absolute	ΔP (Bar) (P_F - P_P)	Pure Helium Retentate Flow Rate (ml/min)	Pure Helium Permeate Flow Rate (ml/min)
1.05	1.0	1.00	0.05	150	175
1.06	1.01	1.00	0.06	200	240
1.07	1.01	1.00	0.07	250	300
1.08	1.03	1.00	0.08	300	451
1.09	1.04	1.00	0.09	360	640
1.1	1.05	1.00	0.1	480	760

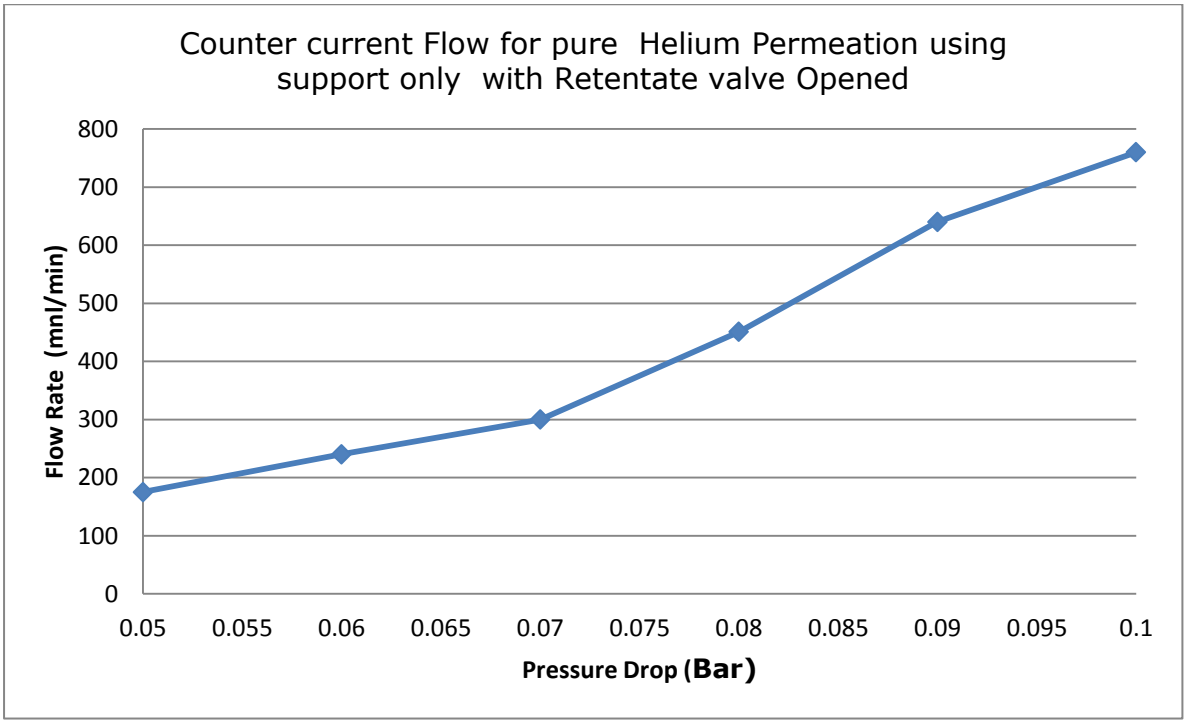

Figure 8:12: Counter current flow for pure Helium permeation using support only with Retentate Valve opened

Table 8:16: Counter current flow arrangement for Helium permeation using membrane A with retentate valve Closed

P_{Feed} (Bar) Absolute	$P_{Retentate}$ (Bar) Absolute	$P_{Permeate}$ (Bar) Absolute	ΔP(Bar) (P_F - P_P)	Pure Helium Retentate Flow Rate (ml/min) Valve Closed	Pure Helium Permeate Flow Rate(ml/min)
1.05	1.0	1.00	0.05	0	250
1.06	1.01	1.00	0.06	0	400
1.07	1.01	1.00	0.07	0	500
1.08	1.03	1.00	0.08	0	650
1.09	1.04	1.00	0.09	0	700
1.1	1.05	1.00	0.1	0	850

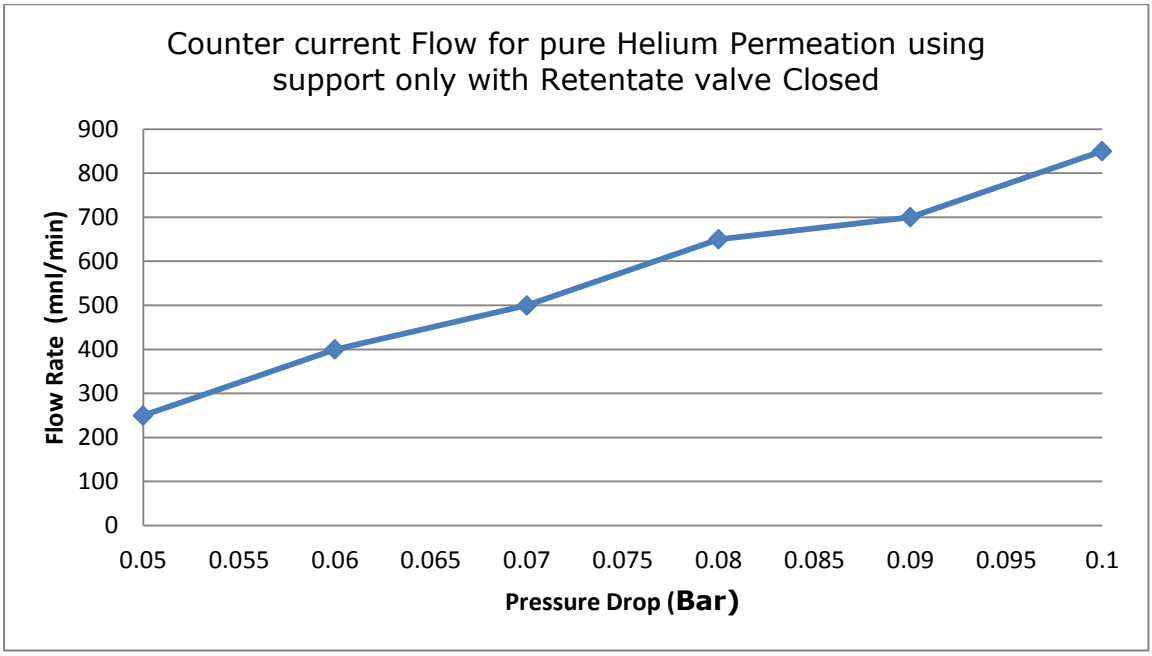

Figure 8:13: Counter current flow for pure Helium permeation using support only with Retentate Valve closed

Table 8:17: Cocurrent flow for feed with mixture A using Support only with retentate valve closed

P_{Feed} (Bar) Absolute	$P_{Retentate}$ (Bar) Absolute	$P_{Permeate}$ (Bar) Absolute	ΔP (Bar) Absolute (P_F - P_P)	Retentate Flow Rate (ml/min) Valve Closed	CO_2/N_2 Permeate Flow Rate (ml/min)	GC values in %	
						CO_2	N_2
1.05	1.05	1.00	0.05	0	138	14	86
1.06	1.06	1.00	0.06	0	190	14	86
1.07	1.07	1.00	0.07	0	238	14	86
1.08	1.08	1.00	0.08	0	320	14	86
1.09	1.09	1.00	0.09	0	400	14	86
1.1	1.1	1.00	0.1	0	520	14	86

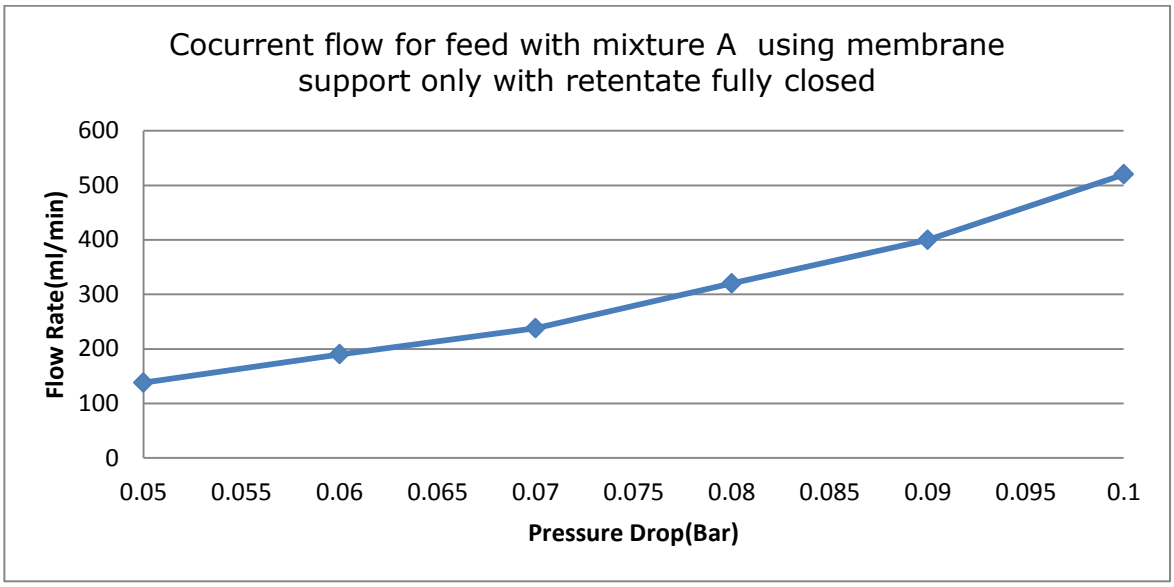

Figure 8:14: Co current flow for feed with mixture A using membrane support only with retentate valve closed

Table 8:18: Values of $C0_2$ permeation for mixture A using Membrane support only

Feed Partial pressure of the CO_2 (Bar)	Permeate partial pressure of the CO_2 (Bar)	(P_{Feed}- $P_{Retentate}$) ΔP(Bar)	CO_2 Permeate Flow Rate(ml/min) membrane using support only
0.147	0.0196	0.1274	19.32
0.148	0.0196	0.1284	26.60
0.150	0.0196	0.1304	33.32
0.151	0.0196	0.1314	44.80
0.153	0.0196	0.1334	56.00
0.154	0.0196	0.1344	72.80

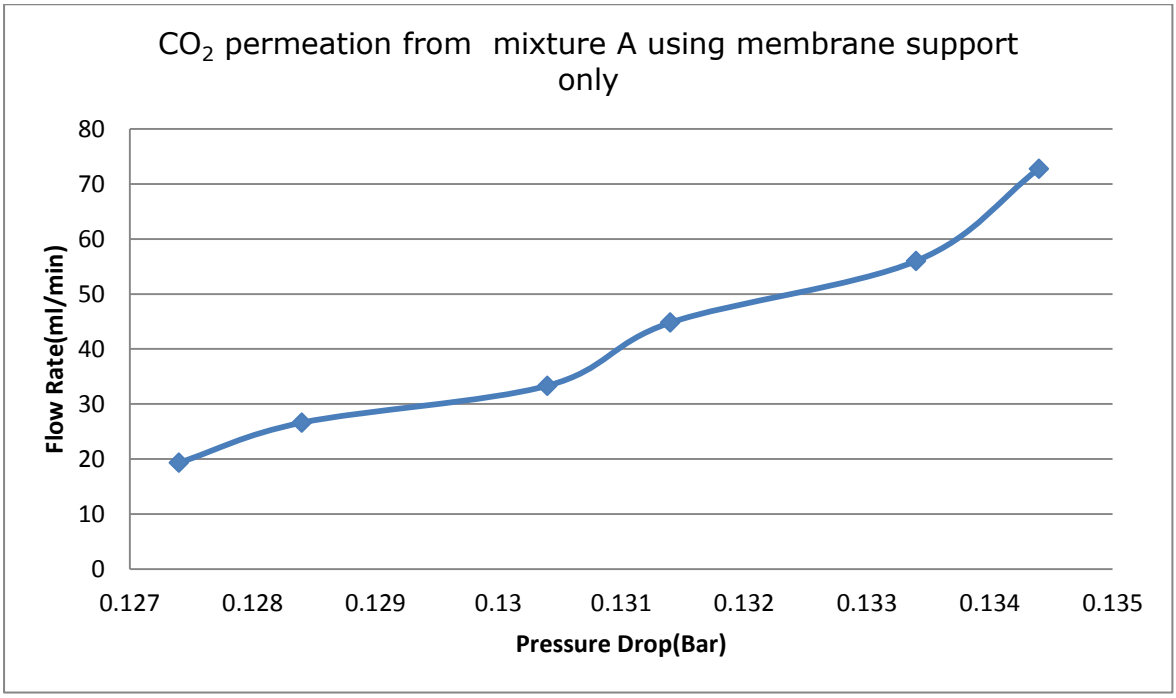

Figure 8:15: CO_2 permeation from mixture A using membrane support only

Table 8:19: Values of N_2 permeation from the mixture A using membrane support only

Feed Partial pressure of the N_2 (Bar)	Permeate partial pressure of the N_2 (Bar)	(P_{Feed}-$P_{Retentate}$) ΔP(Bar)	N_2 Permeate Flow Rate(ml/min) membrane using support only
0.903	0.7396	0.1634	118.68
0.912	0.7396	0.1724	163.40
0.920	0.7396	0.1804	204.68
0.929	0.7396	0.1894	275.20
0.937	0.7396	0.1974	344.00
0.946	0.7396	0.2064	447.20

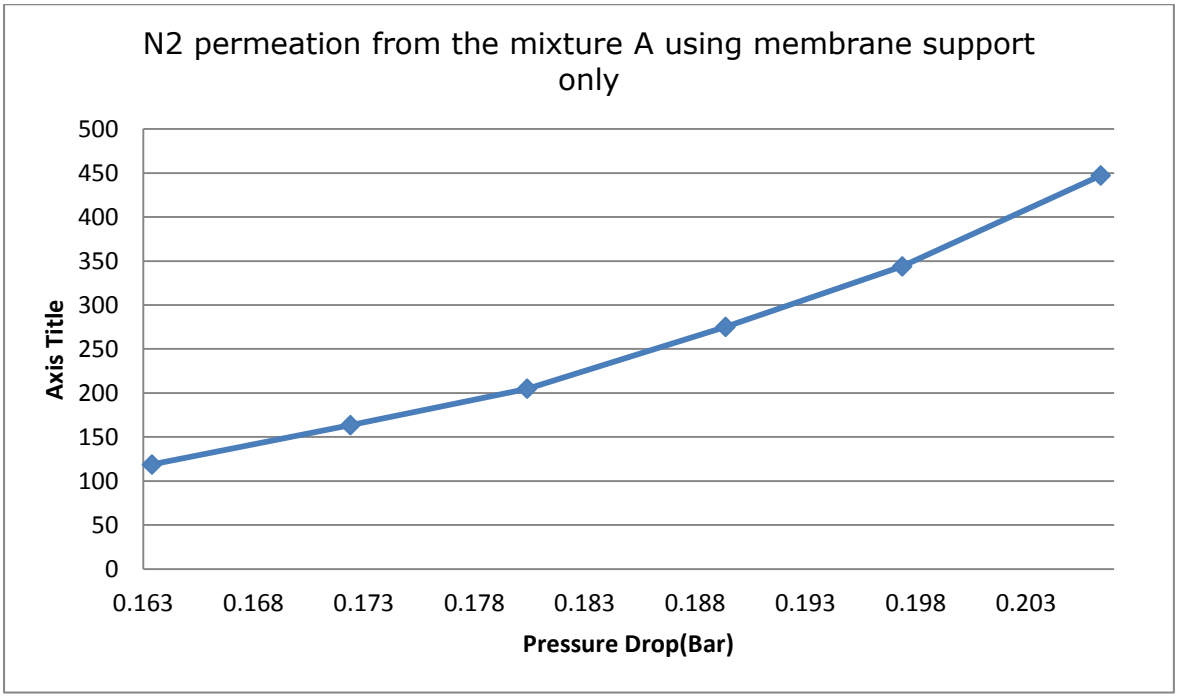

Figure 8:16: N_2 permeation from the mixture A using membrane support only

Table 8:20: Cocurrent flow for pure Argon permeation using membrane support only with retentate valve opened

P_{Feed} (Bar) Absolute	$P_{Retentate}$ (Bar) Absolute	$P_{Permeate}$ (Bar) Absolute	ΔP (Bar) Absolute (P_F - P_P)	Pure Argon Retentate Flow Rate (ml/min)	Pure Argon Permeate Flow Rate (ml/min)
1.05	1.0	1.00	0.05	51.5	161
1.06	1.01	1.00	0.06	80.6	253
1.07	1.01	1.00	0.07	115	348
1.08	1.03	1.00	0.08	121	444
1.09	1.04	1.00	0.09	138	480
1.1	1.05	1.00	0.1	154	537

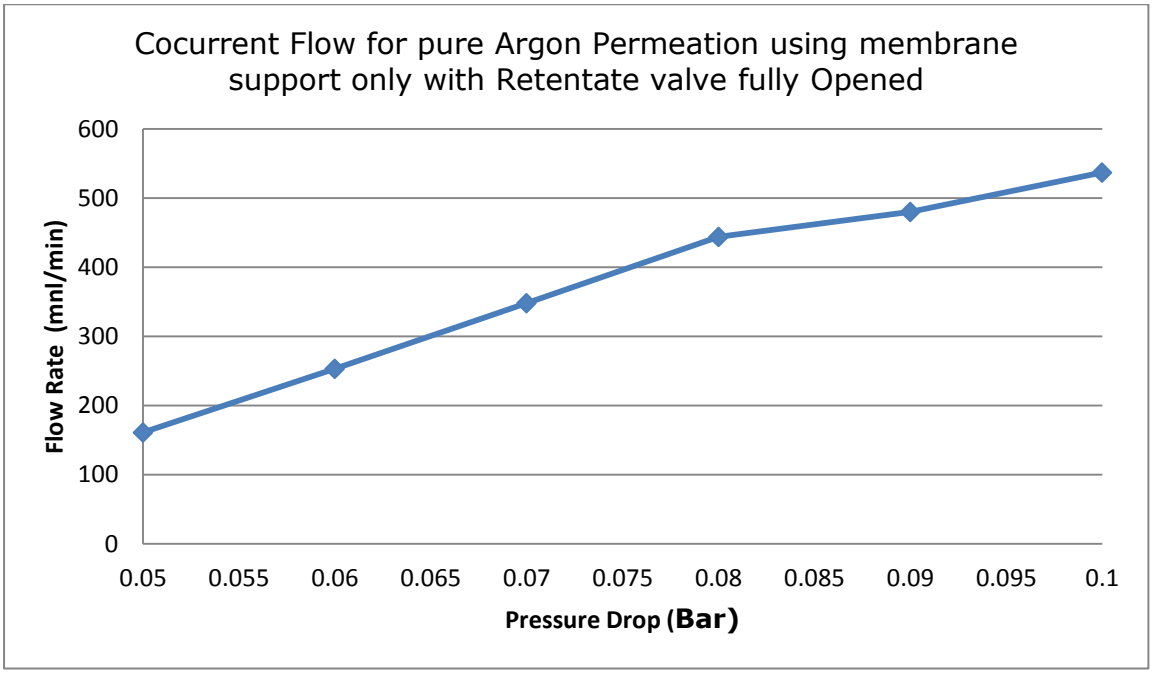

Figure 8:17: Cocurrent flow for pure Argon permeation using membrane support only with Retentate Valve fully opened

Table 8:21: Values of cocurrent flow for pure Argon permeation using membrane support only with retentate valve Closed

P_{Feed} (Bar) Absolute	$P_{Retentate}$ (B Absolute	$P_{Permete}$ (Bar) Absolute	ΔP (Bar) Absolute (P_F - P_P)	Pure Argon Retentate Flow Rate (ml/min) Valve Closed	Pure Argon Permeate Flow Rate (ml/min)
1.05	1.01	1.00	0.05	0	184
1.06	1.02	1.00	0.06	0	257
1.07	1.04	1.00	0.07	0	389
1.08	1.05	1.00	0.08	0	491
1.09	1.06	1.00	0.09	0	572
1.1	1.07	1.00	0.1	0	627

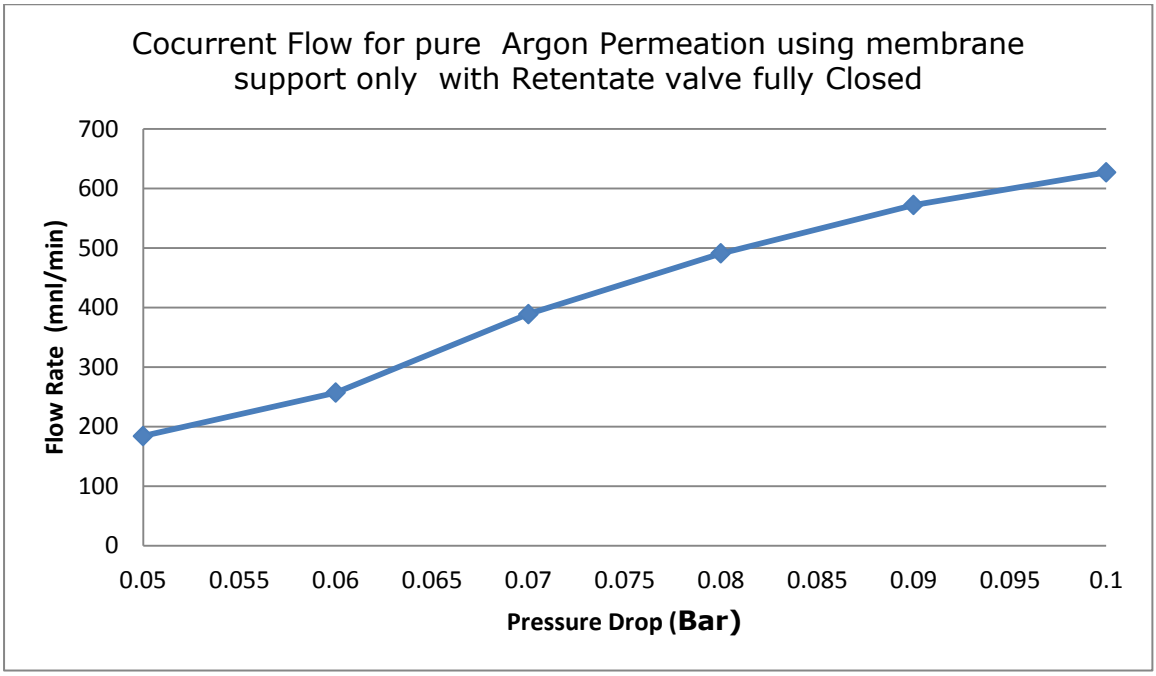

Figure 8:18: Cocurrent flow for pure Argon permeation using membrane support only with Retentate Valve fully closed

Table 8:22: Values of counter current flow for pure Argon permeate flow using membrane A with retentate valve Closed

P_{Feed} (Bar) Absolute	$P_{Retentate}$ (Bar) Absolute	$P_{Permeate}$ (Bar) Absolute	ΔP (Bar) (PF - PP)	Pure Argon Retentate Flow Rate (ml/min) Valve Closed	Pure Argon Permeate Flow Rate (ml/min)
1.05	1.07	1.00	0.05	0	338
1.06	1.07	1.00	0.06	0	422
1.07	1.07	1.00	0.07	0	474
1.08	1.08	1.00	0.08	0	570
1.09	1.09	1.00	0.09	0	650
1.1	1.09	1.00	0.1	0	723

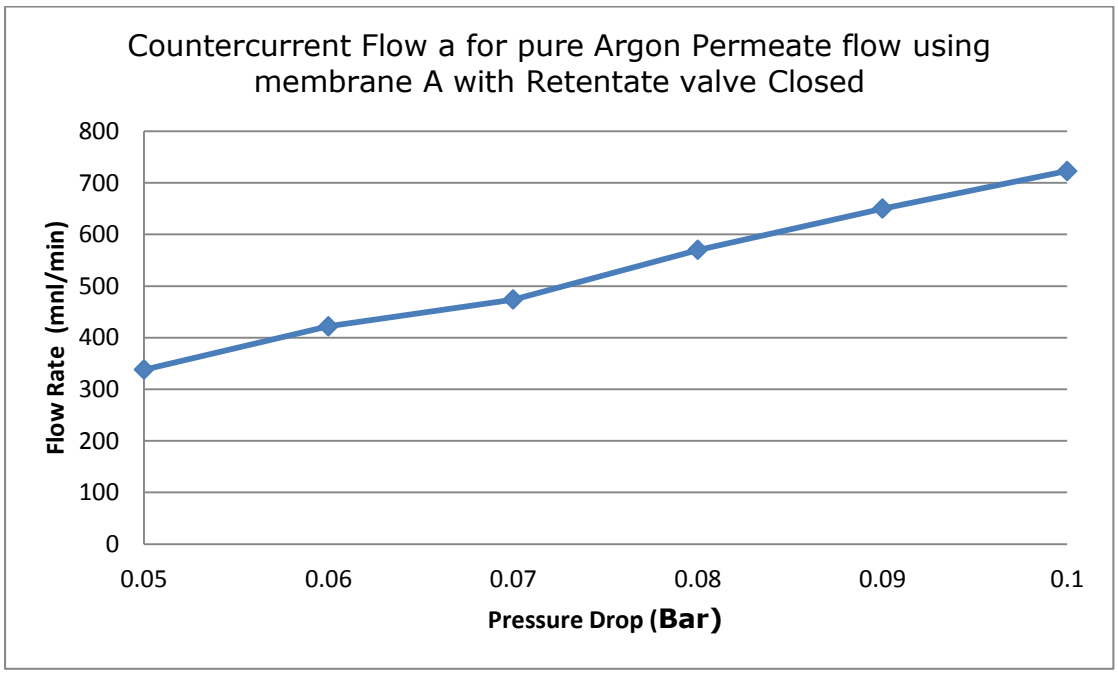

Figure 8:19: Counter current flow for pure Argon permeate flow using membrane A with Retentate Valve fully closed

Table 8:23: Values of counter current flow arrangement for Argon permeate flow using membrane A with retentate valve fully opened

P_{Feed} (Bar) Absolute	$P_{Retentate}$ Bar) Absolute	$P_{Permeate}$ (Bar) Absolute	ΔP (Bar) (P_F - P_P) Absolute	Argon Retentate Flow Rate (ml/min)	Argon Permeate Flow Rate (ml/min)
1.05	1.01	1.00	0.05	174	209
1.06	1.03	1.00	0.06	189	237
1.07	1.04	1.00	0.07	201	256
1.08	1.05	1.00	0.08	238	290
1.09	1.06	1.00	0.09	268	314
1.1	1.06	1.00	0.1	311	350

Table 8:24: Cocurrent flow for CO_2/N_2 permeate flow using Membrane A with retentate Valve fully opened.

P_{Feed} (Bar) Absolute	$P_{Retentate}$ (Bar) Absolute	$P_{Permeate}$ (Bar) Absolute	ΔP (Bar) (P_F - P_P) Absolute	CO_2/N_2 Retentate. Flow Rate (ml/min)	CO_2/N_2 Permeate Flow Rate (ml/min)	GC Values %	
						CO_2	N_2
1.05	1.02	1.00	0.05	122	120	16	84
1.06	1.03	1.00	0.06	138	142	16	84
1.07	1.03	1.00	0.07	152	150	16	84
1.08	1.04	1.00	0.08	161	179	16	84
1.09	1.04	1.00	0.09	166	196	16	84
1.1	1.05	1.00	0.1	172	210	16	84

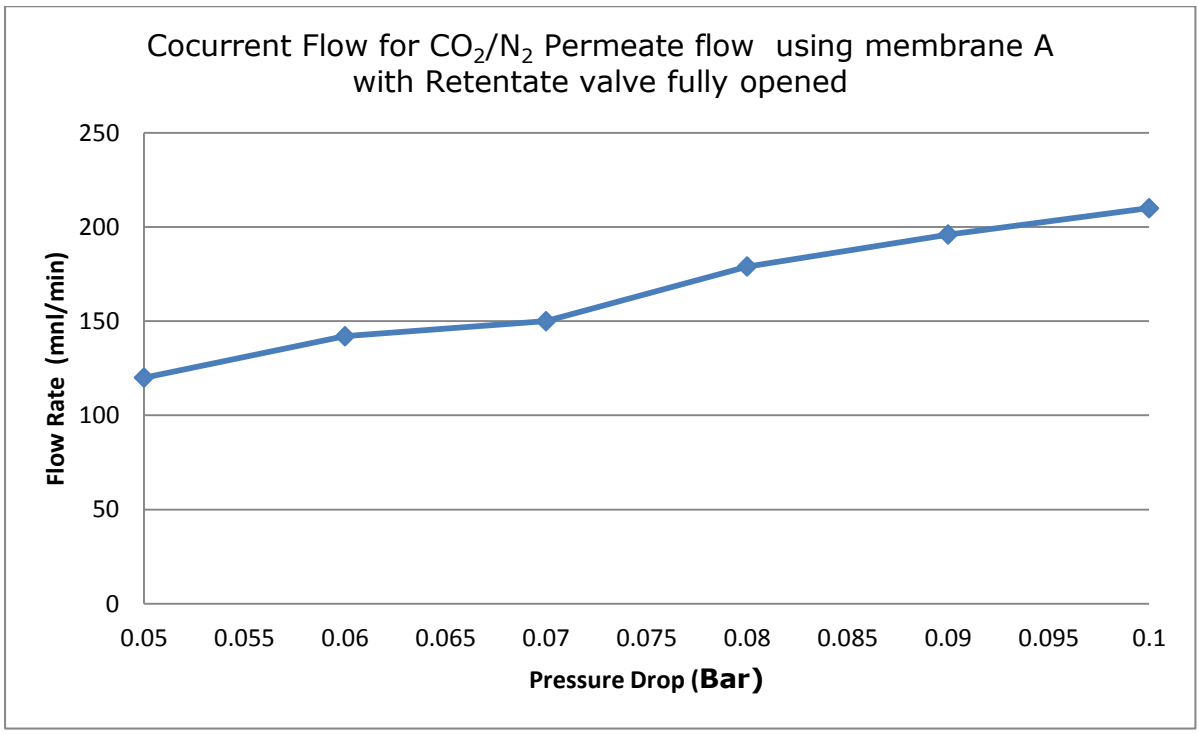

Figure 8:20: Cocurrent flow for CO_2/N_2 permeate flow using membrane A with retentate valve fully opened.

Table 8:25: Cocurrent flow for CO_2/N_2 permeate flow using membrane A with retentate valve fully Closed

P_{Feed} (Bar) Absolute	$P_{Retentate}$ (Bar) Absolute	$P_{Permeate}$ (Bar) Absolute	ΔP(Bar) (P_F-P_P) Absolute)	Retentate Flow Rate (ml/min) Valve Closed	CO_2/N_2 Permeate Flow Rate (ml/min)	GC Values %	
						CO_2	N_2
1.05	1.02	1.00	0.05	0	131	18	82
1.06	1.02	1.00	0.06	0	159	18	82
1.07	1.05	1.00	0.07	0	204	18	82
1.08	1.06	1.00	0.08	0	303	18	82
1.09	1.07	1.00	0.09	0	348	18	82
1.1	1.08	1.00	0.1	0	361	18	82

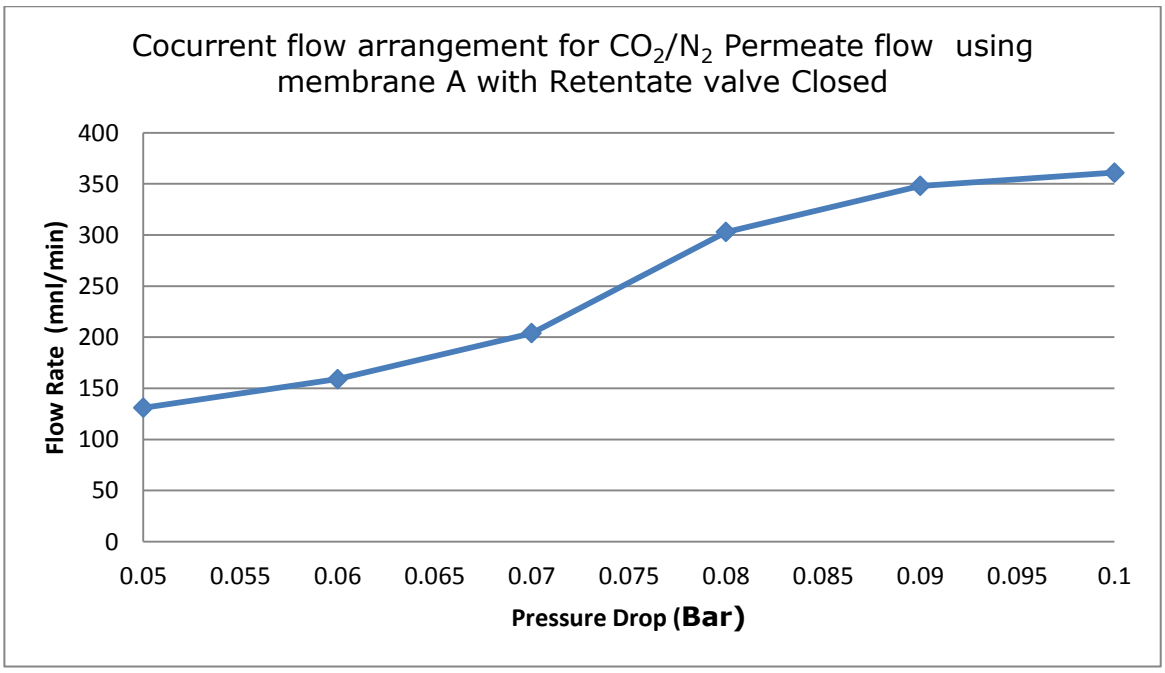

Figure 8:21: Cocurrent flow for CO_2/N_2 permeate flow with retentate valve closed

Table 8:26: CO_2 permeate flow from mixtures A using membrane A with retentate valve fully closed

Feed Partial pressure of the CO_2 (Bar)	Permeate partial pressure of the CO_2 (Bar)	(P_{Feed}-$P_{Retentate}$) ΔP(Bar)	CO_2 Permeate Flow Rate(ml/min)
0.147	0.0252	0.1218	23.58
0.148	0.0252	0.1228	28.62
0.150	0.0252	0.1248	36.72
0.151	0.0252	0.1258	54.54
0.153	0.0252	0.1278	62.64
0.154	0.0252	0.1288	64.98

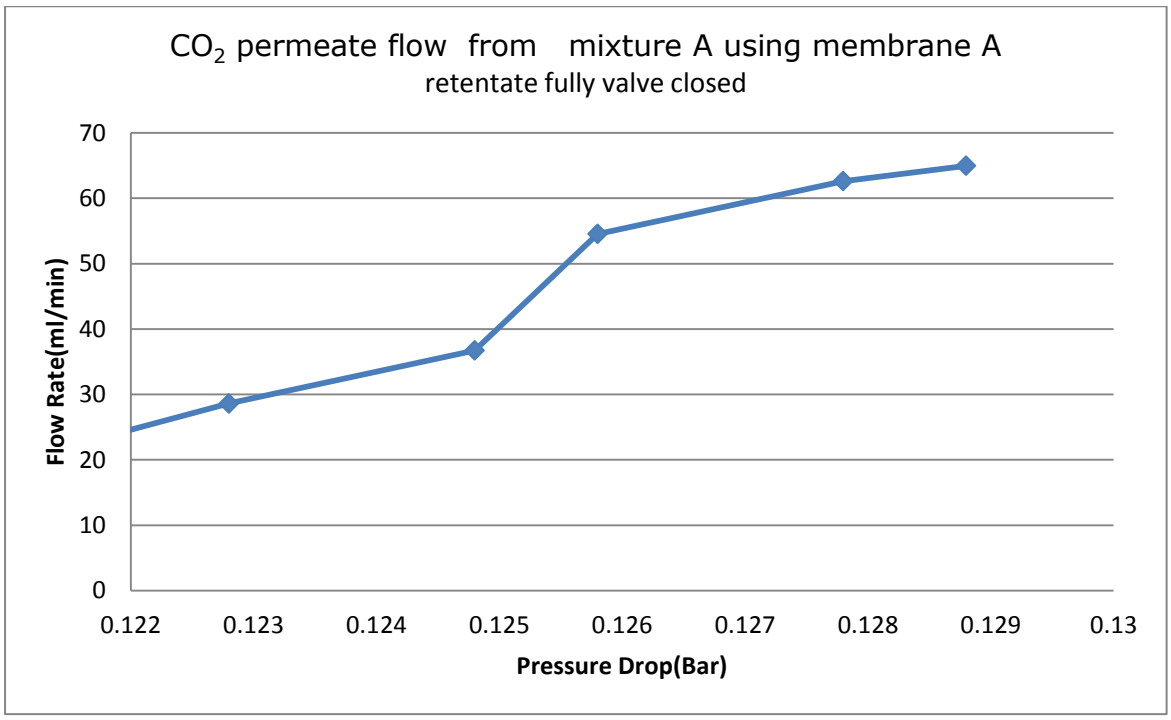

Figure 8:22: CO_2 permeate flow from mixture A using membrane A with retentate valve fully closed

Table 8:27: N_2 permeate flow from mixture A using Membrane A with retentate valve fully closed

Feed Partial pressure of the N_2 (Bar)	Permeate partial pressure of the N_2 (Bar)	(P_{Feed}-$P_{Retentate}$) ΔP(Bar)	N_2 Permeate Flow Rate(ml/min)
0.903	0.7052	0.1978	107.42
0.912	0.7052	0.2068	130.38
0.920	0.7052	0.2148	167.28
0.929	0.7052	0.2238	248.46
0.937	0.7052	0.2318	285.36
0.946	0.7052	0.2408	296.02

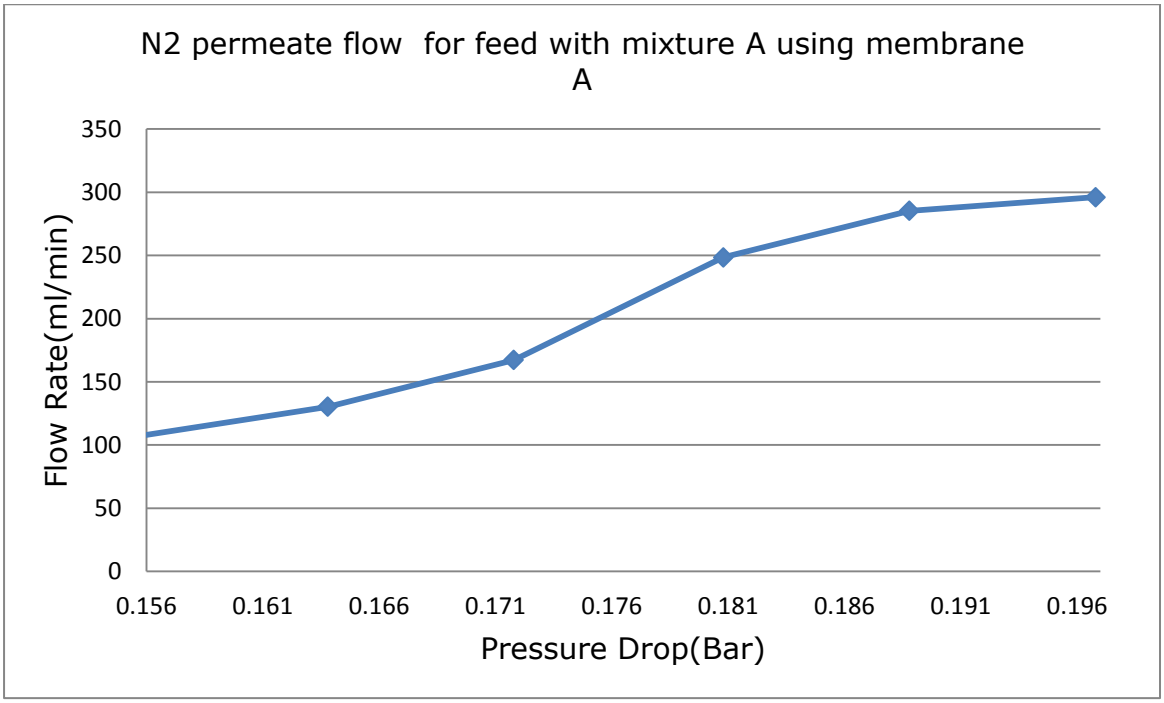

Figure 8:23: N_2 permeate flow from mixture A using membrane A with retentate valve fully closed

Table 8:28: Counter current flow for CO_2/N_2 permeation using membrane A Retentate valve fully opened

P_{Feed} (Bar) Absolute	$P_{Retentate}$ (Bar) Absolute	$P_{Permeate}$ (Bar) Absolute	ΔP (Bar) Absolute (P_F - P_P)	$C0_2/N_2$ Retentate Flow Rate(ml/min)	$C0_2/N_2$ Permeate Flow Rate(ml/min)
1.05	1.03	1.00	0.05	102	116
1.06	1.03	1.00	0.06	138	122
1.07	1.03	1.00	0.07	152	138
1.08	1.03	1.00	0.08	161	149
1.09	1.04	1.00	0.09	146	176
1.1	1.04	1.00	0.1	152	225

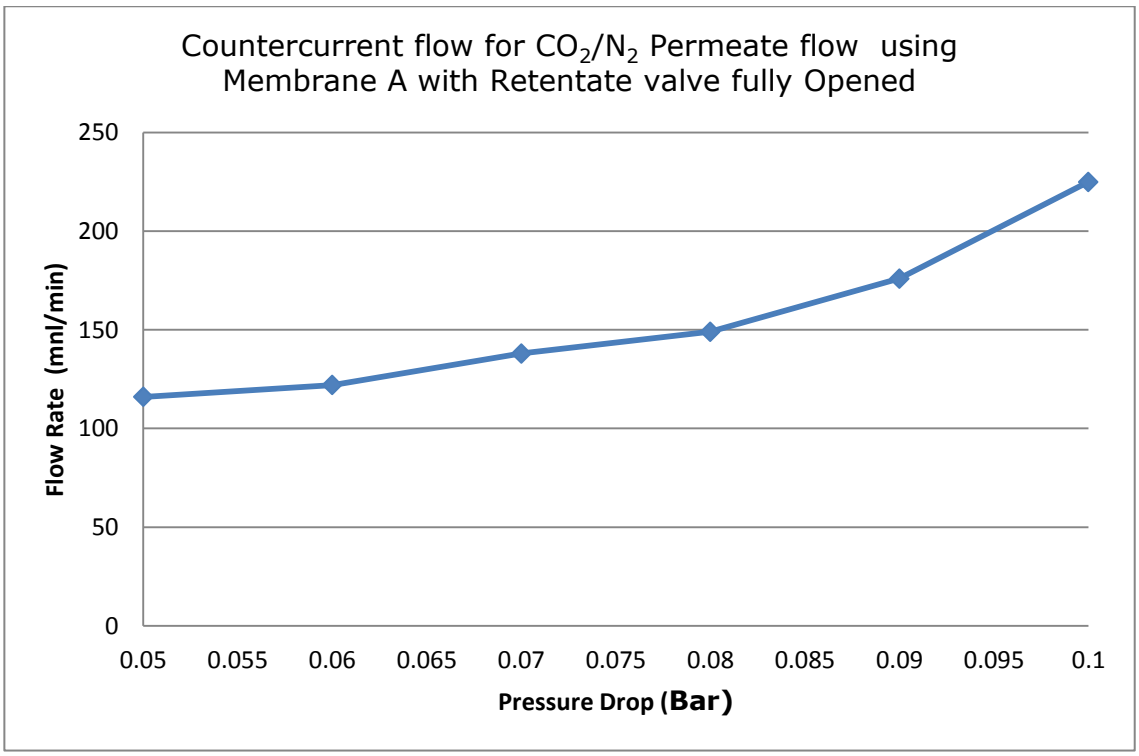

Figure 8:24: Counter current flow for CO_2/N_2 permeate flow using membrane A with Retentate Valve fully opened

Table 8:29: Counter current flow arrangement for CO_2/N_2 permeation using membrane A with retentate valve fully closed

P_{Feed} (Bar) Absolute	$P_{Retentate}$ (Bar) Absolute	$P_{Permeate}$ (Bar) Absolute	ΔP (Bar) Absolute (P_F - P_P)	Retentate Flow Rate (ml/min) Valve Closed	CO_2/N_2 Permeate Flow Rate (ml/min)
1.05	1.07	1.00	0.05	0	121
1.06	1.07	1.00	0.06	0	142
1.07	1.09	1.00	0.07	0	190
1.08	1.09	1.00	0.08	0	296
1.09	1.1	1.00	0.09	0	300
1.1	1.11	1.00	0.1	0	310

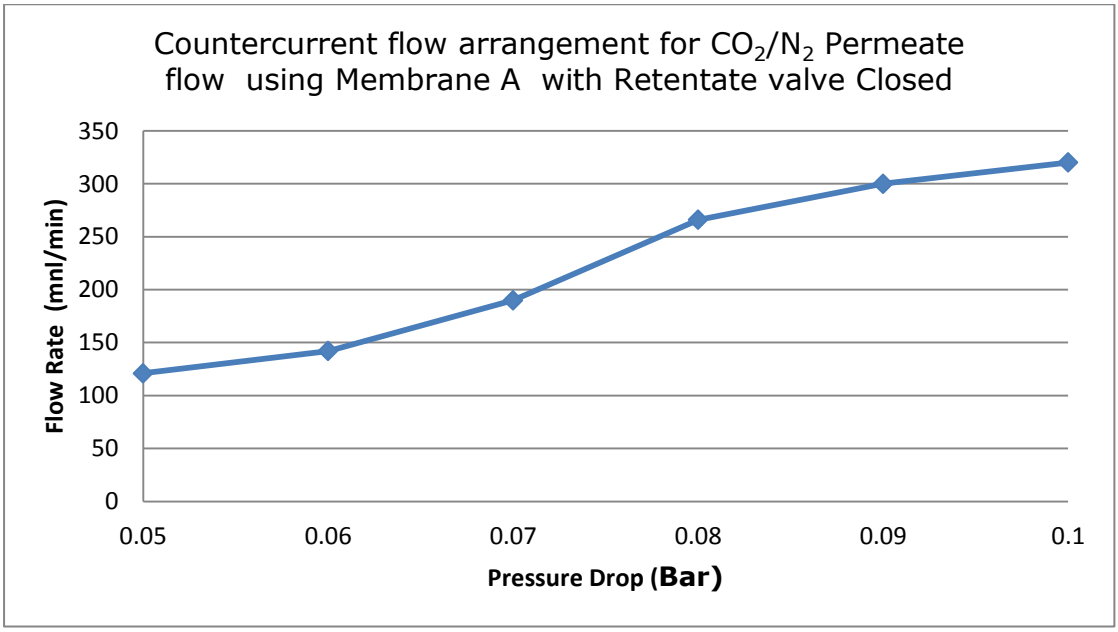

Figure 8:25: Counter current flow for CO_2/N_2 permeate flow using membrane A with Retentate Valve fully closed

Table 8:30: Cocurrent flow for pure CO_2 permeate flow using Membrane A with retentate valve fully closed

P_{Feed} (Bar) Absolute	$P_{Retentate}$ (Bar) Absolute	$P_{Permeate}$ (Bar) Absolute	ΔP (Bar) (P_F - P_P)	$C0_2$ Retentate Flow Rate (ml/min) Valve Closed	Pure CO_2 Permeate Flow Rate (ml/min)
1.05	1.07	1.00	0.05	0	147
1.06	1.07	1.00	0.06	0	200
1.07	1.09	1.00	0.07	0	300
1.08	1.09	1.00	0.08	0	450
1.09	1.1	1.00	0.09	0	550
1.1	1.11	1.00	0.1	0	600

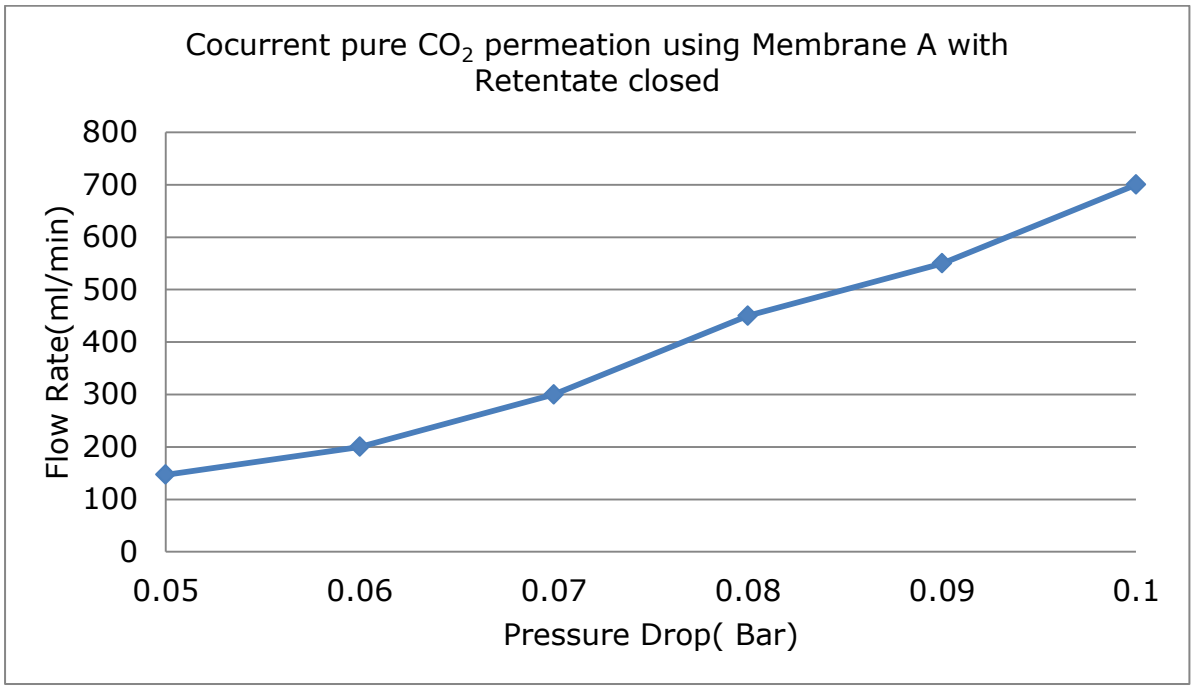

Figure 8:26: Cocurrent CO_2 permeate flow using Membrane A with Retentate Valve closed

Table 8:31: Cocurrent flow for pure N_2 permeate flow using membrane A with retentate Valve closed

P_{Feed} (Bar) Absolute	$P_{Retentate}$ (Bar) Absolute	$P_{Permeate}$ (Bar) Absolute	ΔP(Bar) (P_F - P_P) Absolute	Pure Retentate Flow Rate(ml/min) Valve closed	Pure N_2 Permeate Flow Rate(ml/min)
1.05	1.01	1.00	0.05	0	102
1.06	1.03	1.00	0.06	0	200
1.07	1.04	1.00	0.07	0	385
1.08	1.05	1.00	0.08	0	491
1.09	1.06	1.00	0.09	0	506
1.1	1.06	1.00	0.1	0	590

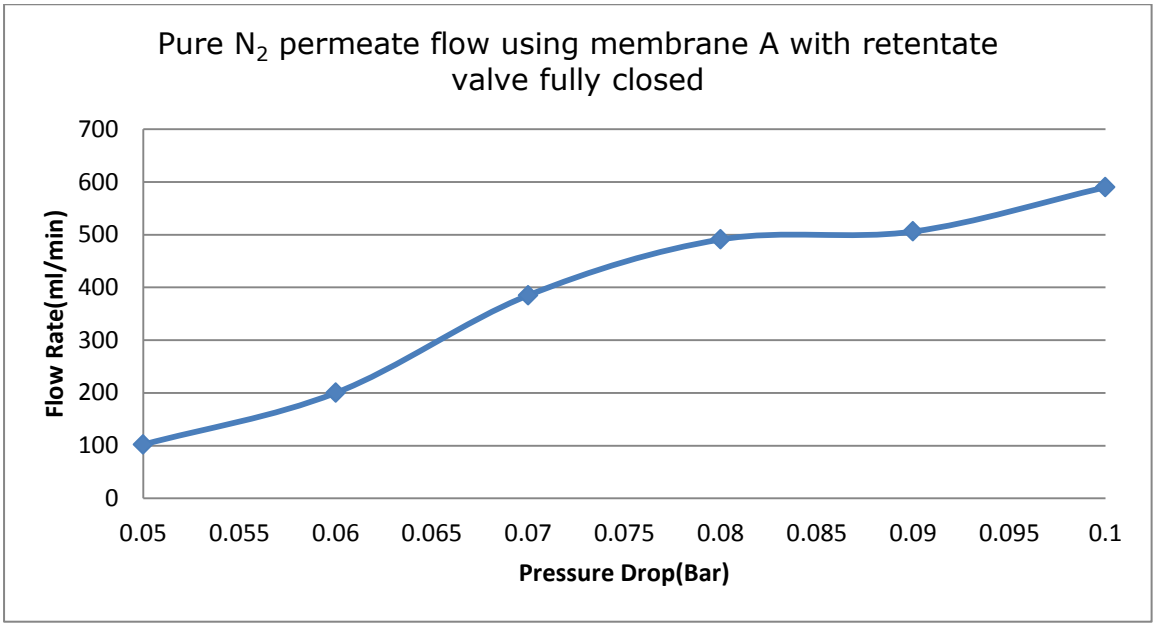

Figure 8:27: Cocurrent pure N_2 permeate flow using Membrane A with Retentate Valve closed

Table 8:32: Cocurrent flow for pure N_2 permeate flow using membrane A at 296 Kelvin with retentate Valve closed

P_{Feed} (Bar) Absolute	$P_{Retentate}$ (Bar) Absolute	$P_{Permeate}$ (Bar) Absolute	ΔP(Bar) (P_F - P_P) Absolute	Pure Retentate Flow Rate(ml/min) Valve closed	Pure N_2 Permeate Flow Rate(ml/min) at 296k
1.05	1.01	1.00	0.05	0	102
1.06	1.03	1.00	0.06	0	200
1.07	1.04	1.00	0.07	0	385
1.08	1.05	1.00	0.08	0	491
1.09	1.06	1.00	0.09	0	506
1.1	1.06	1.00	0.1	0	590

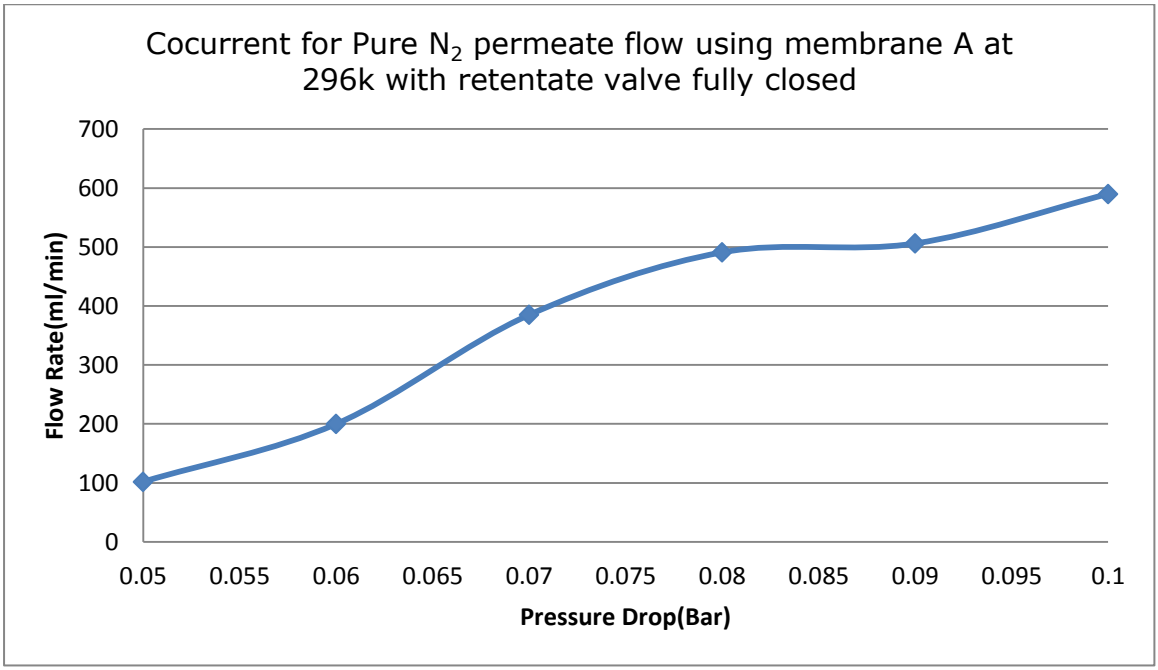

Figure 8:28: Cocurrent flow for pure N_2 permeate flow using membrane A at 296 Kelvin with retentate Valve closed

Table 8:33: Cocurrent flow for pure N_2 permeate flow using membrane A at 338 Kelvin with retentate Valve closed

P_{Feed} (Bar) Absolute	$P_{Retentate}$ (Bar) Absolute	$P_{Permeate}$ (Bar) Absolute	ΔP(Bar) (P_F - P_P) Absolute	Pure Retentate Flow Rate(ml/min) Valve closed	Pure N_2 Permeate Flow Rate(ml/min) at 338k
1.05	1.01	1.00	0.05	0	91
1.06	1.03	1.00	0.06	0	140
1.07	1.04	1.00	0.07	0	265
1.08	1.05	1.00	0.08	0	310
1.09	1.06	1.00	0.09	0	420
1.1	1.06	1.00	0.1	0	510

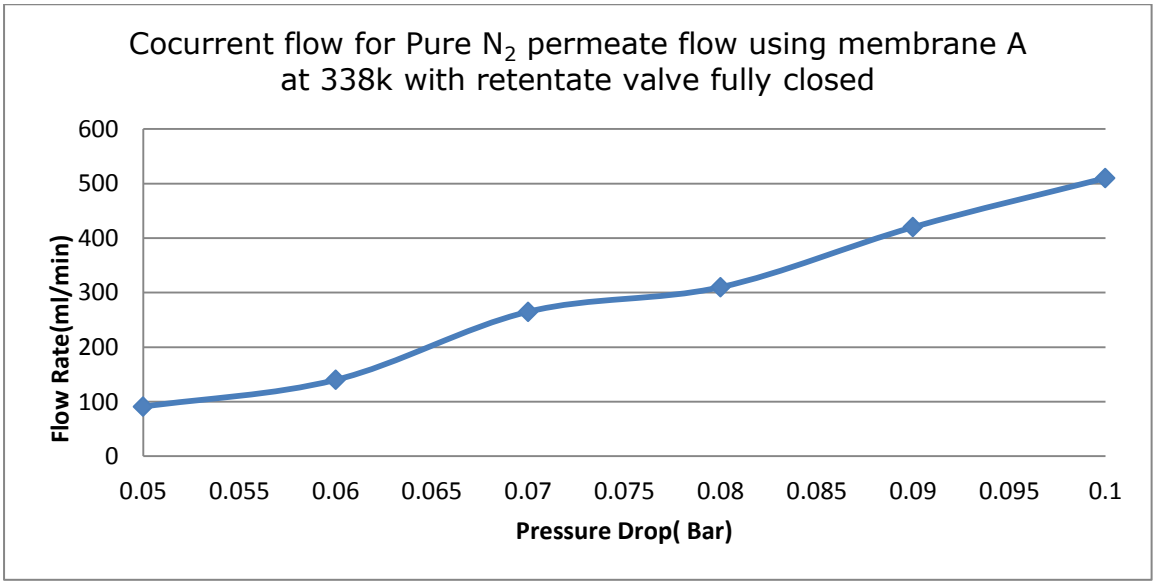

Figure 8:29: Cocurrent flow for pure N_2 permeate flow using membrane A at 338 Kelvin with retentate Valve closed

Table 8:34: Cocurrent flow for pure N_2 permeate flow using membrane A at 423 Kelvin with retentate Valve closed

P_{Feed} (Bar) Absolute	$P_{Retentate}$ (Bar) Absolute	$P_{Permeate}$ (Bar) Absolute	ΔP(Bar) (P_F - P_P) Absolute	Pure Retentate Flow Rate(ml/min) Valve closed	Pure N_2 Permeate Flow Rate(ml/min) at 423k
1.05	1.01	1.00	0.05	0	83
1.06	1.03	1.00	0.06	0	120
1.07	1.04	1.00	0.07	0	189
1.08	1.05	1.00	0.08	0	250
1.09	1.06	1.00	0.09	0	350
1.1	1.06	1.00	0.1	0	425

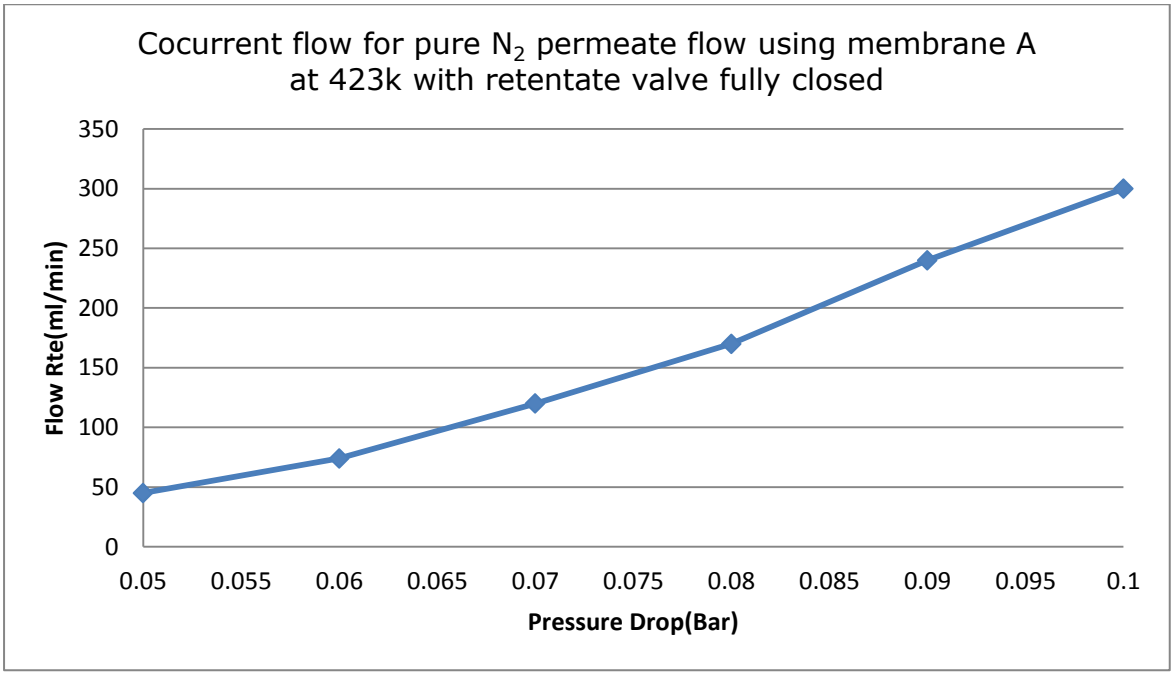

Figure 8:30: Cocurrent flow for pure N_2 permeate flow using membrane A at 423 Kelvin with retentate Valve closed

Table 8:35: Cocurrent flow for pure N_2 permeate flow using membrane A at 523 Kelvin with retentate Valve closed

P_{Feed} (Bar) Absolute	$P_{Retentate}$ (Bar) Absolute	$P_{Permeate}$ (Bar) Absolute	ΔP(Bar) (P_F - P_P) Absolute	Pure Retentate Flow Rate(ml/min) Valve closed	Pure N_2 Permeate Flow Rate(ml/min) at 523k
1.05	1.01	1.00	0.05	0	51
1.06	1.03	1.00	0.06	0	98
1.07	1.04	1.00	0.07	0	150
1.08	1.05	1.00	0.08	0	210
1.09	1.06	1.00	0.09	0	301
1.1	1.06	1.00	0.1	0	389

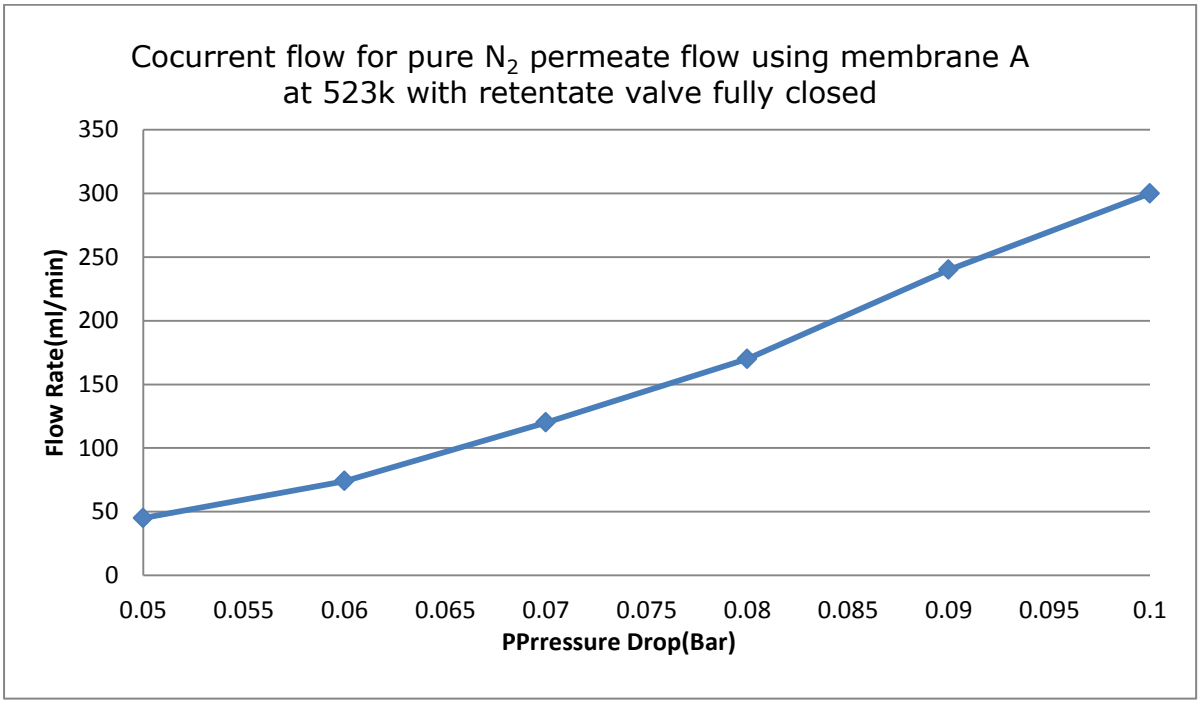

Figure 8:31: Cocurrent flow for pure N_2 permeate flow using membrane A at 523 Kelvin with retentate Valve closed

Table 8:36: Cocurrent flow for pure N_2 permeate flow using membrane A at 723 Kelvin with retentate Valve closed

P_{Feed} (Bar) Absolute	$P_{Retentate}$ (Bar) Absolute	$P_{Permeate}$ (Bar) Absolute	ΔP(Bar) (P_F - P_P) Absolute	Pure Retentate Flow Rate(ml/min) Valve closed	Pure N_2 Permeate Flow Rate(ml/min) at 723k
1.05	1.01	1.00	0.05	0	45
1.06	1.03	1.00	0.06	0	74
1.07	1.04	1.00	0.07	0	120
1.08	1.05	1.00	0.08	0	170
1.09	1.06	1.00	0.09	0	240
1.1	1.06	1.00	0.1	0	300

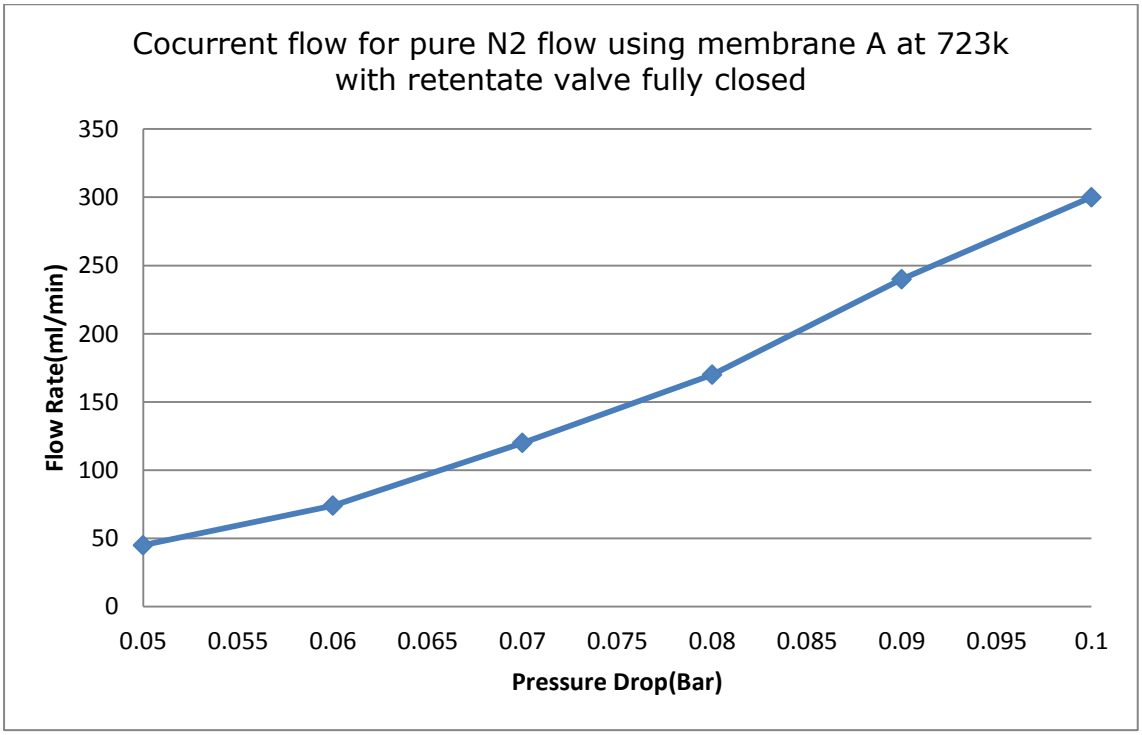

Figure 8:32: Cocurrent flow for pure N_2 permeate flow using membrane A at 723 Kelvin with retentate Valve closed

Table 8:37: Cocurrent flow for pure CO_2 permeate flow using membrane A at 296 Kelvin with retentate valve closed

P_{Feed} (Bar) Absolute	$P_{Retentate}$ (Bar) Absolute	$P_{Permeate}$ (Bar) Absolute	ΔP (Bar) Absolute (P_F - P_P)	Pure CO_2 Retentate Flow Rate (ml/min) Valve Closed	Pure $C0_2$ Permeate Flow Rate at (ml/min) 296K
1.05	1.07	1.00	0.05	0	147
1.06	1.07	1.00	0.06	0	200
1.07	1.09	1.00	0.07	0	300
1.08	1.09	1.00	0.08	0	450
1.09	1.1	1.00	0.09	0	550
1.1	1.11	1.00	0.1	0	600

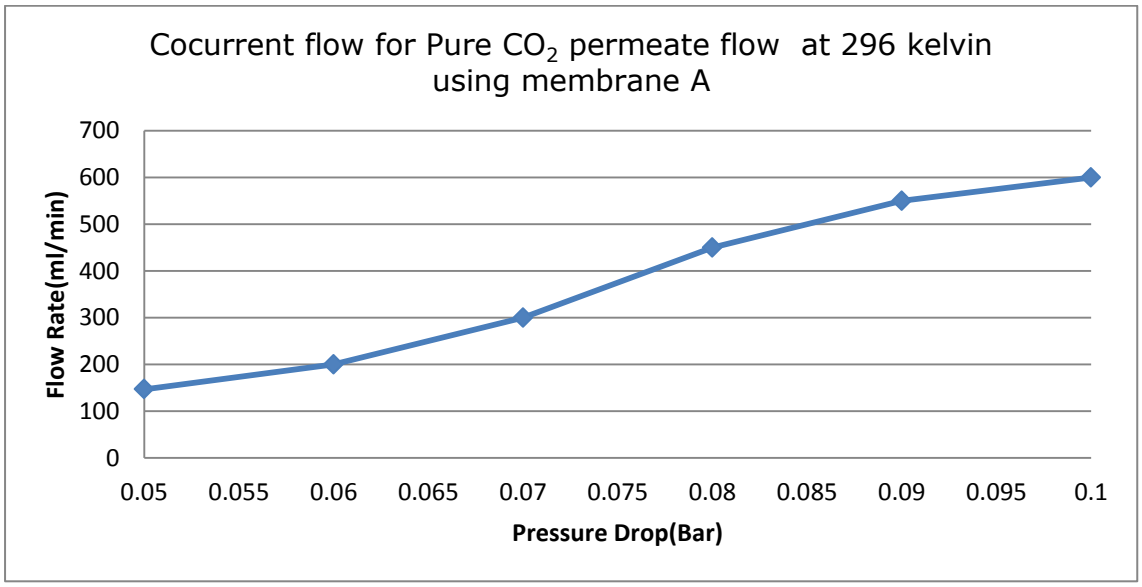

Figure 8:33: Cocurrent flow for pure CO_2 permeate flow using membrane A at 296 Kelvin with retentate valve closed

Table 8:38 Cocurrent flow for pure $C0_2$ permeate flow using membrane A at 338 K with retentate valve closed

P_{Feed} (Bar) Absolute	$P_{Retentate}$ (Bar) Absolute	$P_{Permeate}$ (Bar) Absolute	ΔP (Bar) Absolute (P_F - P_P)	Pure CO_2 Retentate Flow Rate (ml/min) Valve Closed	Pure CO_2 Permeate Flow Rate(ml/min) 338k
1.05	1.06	1.00	0.05	0	120
1.06	1.06	1.00	0.06	0	170
1.07	1.09	1.00	0.07	0	250
1.08	1.09	1.00	0.08	0	330
1.09	1.1	1.00	0.09	0	420
1.1	1.11	1.00	0.1	0	500

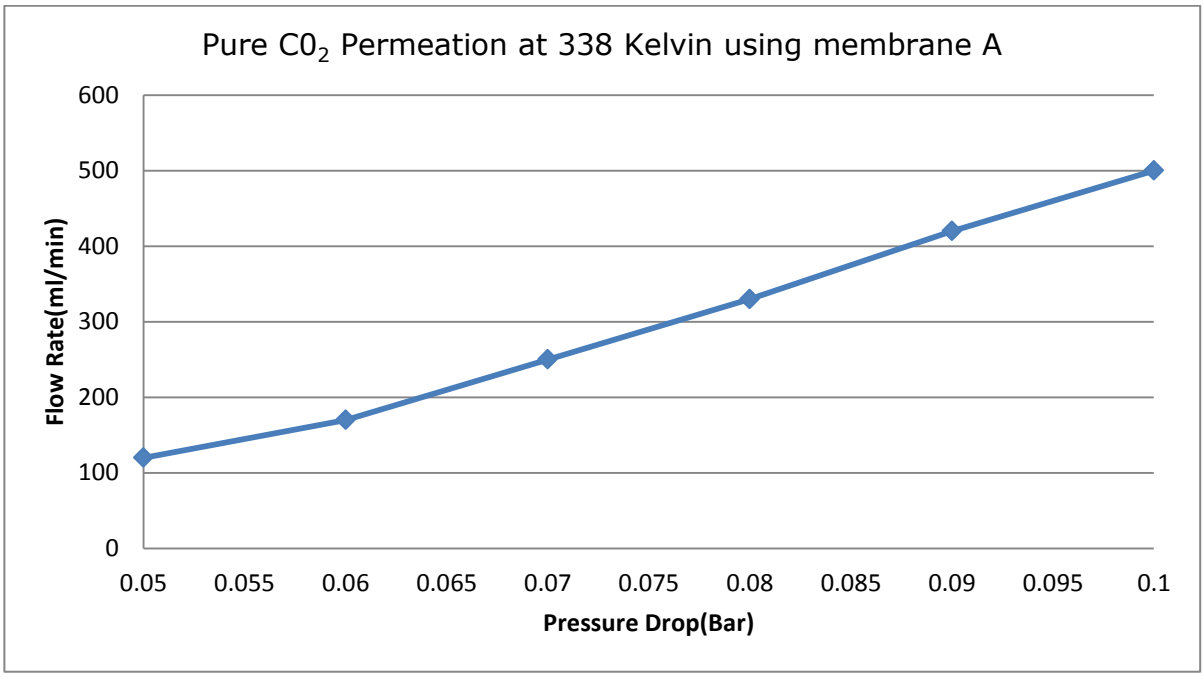

Figure 8:34: Cocurrent flow for pure CO_2 permeate flow using membrane A at 338 Kelvin with retentate valve closed

Table 8:39: Cocurrent flow for pure CO_2 permeate flow using membrane A at 423 Kelvin with retentate valve closed

P_{Feed} (Bar) Absolute	$P_{Retentate}$ (Bar) Absolute	$P_{Permeate}$ (Bar) Absolute	ΔP (Bar) Absolute (P_F - P_P)	Retentate Flow Rate (ml/min) Valve Closed	CO_2 Permeate Flow Rate(ml/min)
1.05	1.06	1.00	0.05	0	90
1.06	1.07	1.00	0.06	0	150
1.07	1.09	1.00	0.07	0	200
1.08	1.09	1.00	0.08	0	270
1.09	1.1	1.00	0.09	0	350
1.1	1.11	1.00	0.1	0	430

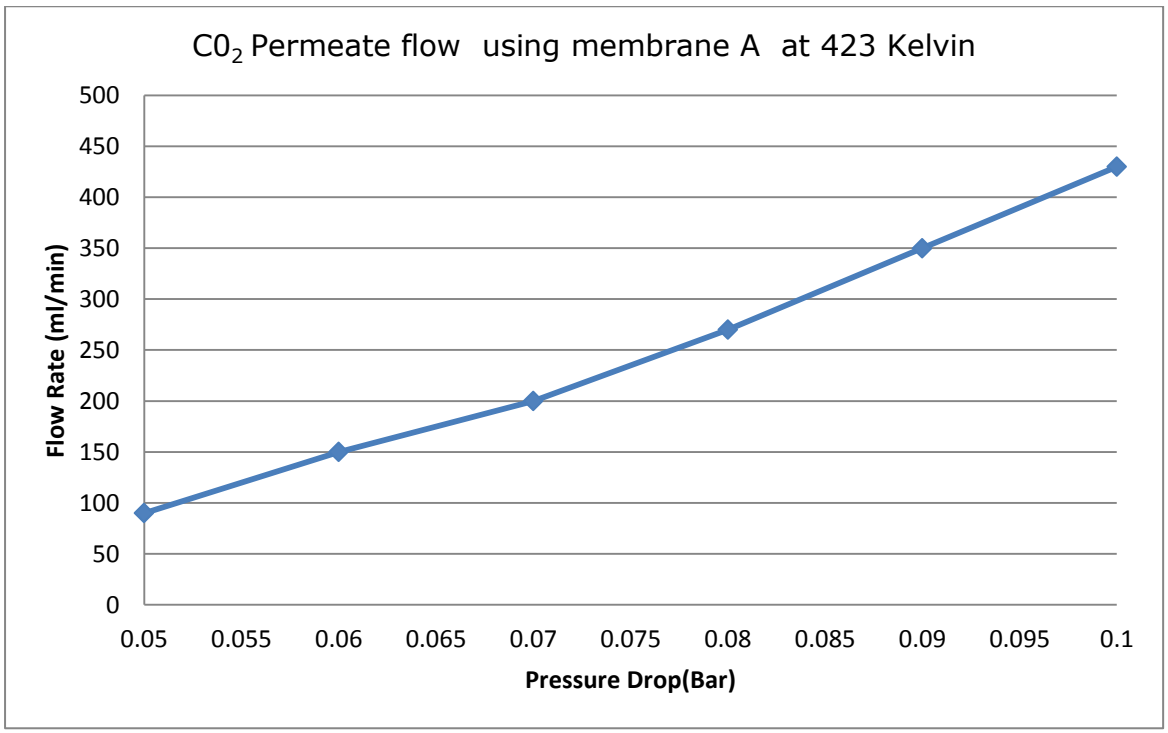

Figure 8:35: Cocurrent flow for pure CO_2 permeate flow using membrane A at 423K with retentate valve closed

Table 8:40: Cocurrent flow for pure CO_2 permeate flow using membrane A at 523 Kelvin with retentate valve closed

P_{Feed} (Bar) Absolute	$P_{Retentate}$ (Bar) Absolute	$P_{Permeate}$ (Bar) Absolute	ΔP (Bar) Absolute (P_F - P_P)	Retentate Flow Rate (ml/min) Valve closed	CO_2 Permeate Flow Rate (ml/min) 523k
1.05	1.05	1.00	0.05	0	50
1.06	1.07	1.00	0.06	0	100
1.07	1.08	1.00	0.07	0	150
1.08	1.09	1.00	0.08	0	200
1.09	1.1	1.00	0.09	0	270
1.1	1.10	1.00	0.1	0	350

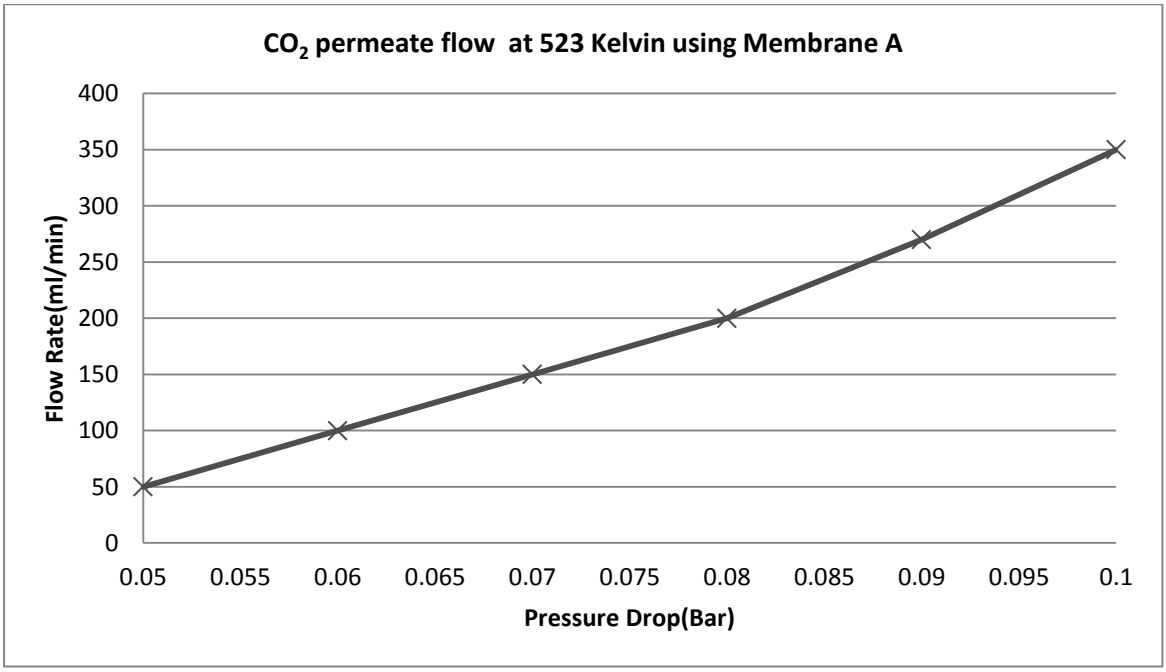

Figure 8:36: Cocurrent flow for pure CO_2 permeate flow using membrane A at 523 Kelvin with retentate valve closed

Table 8:41: Cocurrent flow for pure CO_2 permeate flow using membrane A at 723 Kelvin with retentate valve closed

P_{Feed} (Bar) Absolute	$P_{Retentate}$ (Bar) Absolute	$P_{Permeate}$ (Bar) Absolute	ΔP (Bar) Absolute (P_F - P_P)	Retentate Flow Rate (ml/min) Valve Closed	CO_2 Permeate Flow Rate(ml/min) 723k
1.05	1.06	1.00	0.05	0	35
1.06	1.07	1.00	0.06	0	60
1.07	1.08	1.00	0.07	0	90
1.08	1.09	1.00	0.08	0	120
1.09	1.0	1.00	0.09	0	160
1.1	1.10	1.00	0.1	0	200

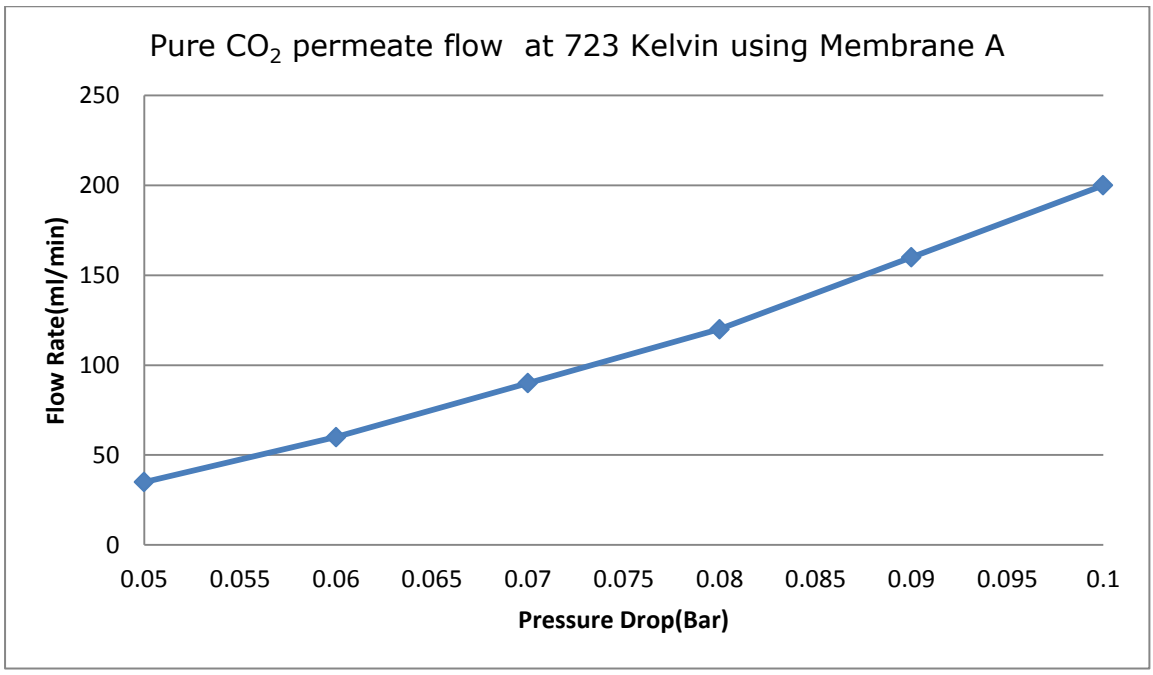

Figure 8:37: Cocurrent flow for pure CO_2 permeate flow using membrane A at 723 Kelvin with retentate valve closed

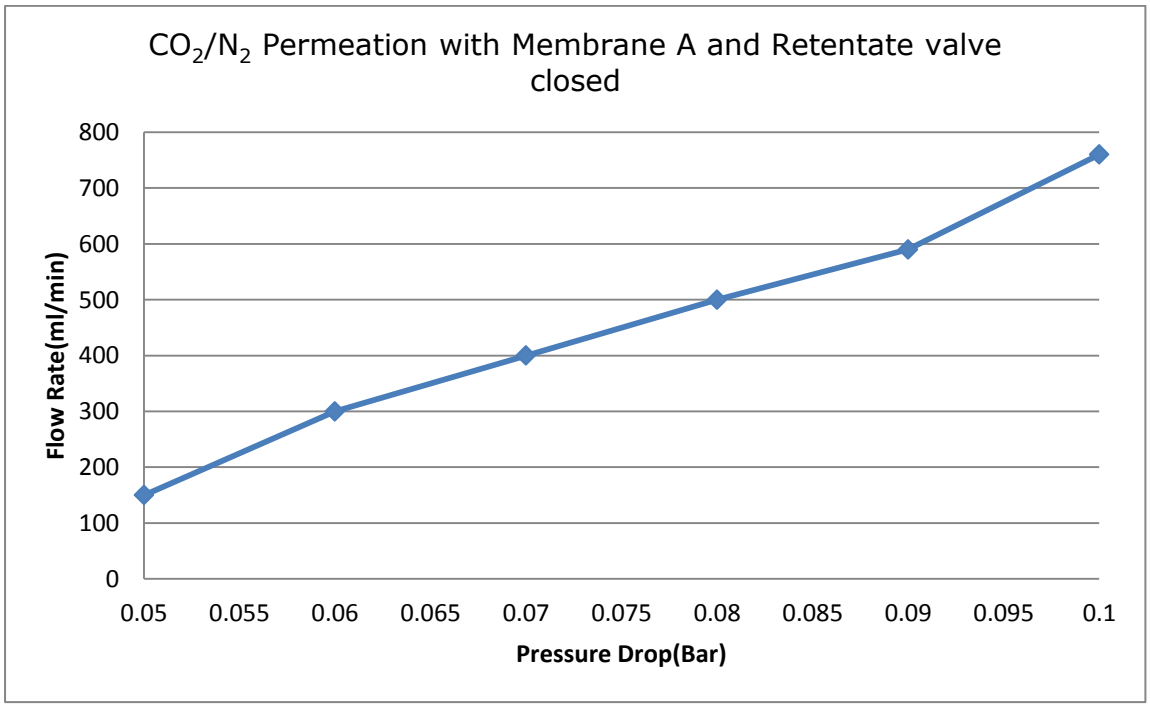

Figure 8:38:CO_2/N_2 Permeate flow with Membrane A and Retentate Valve fully closed

Table 8:42: Cocurrent flows from mixture A permeate using Membrane B with retentate valve fully closed.

P_{Feed} (Bar) Absolute	$P_{Retentate}$ (Bar) Absolute	$P_{Permeate}$ (Bar) Absolute	ΔP (Bar) Absolute	Retentate Flow Rate (ml/min) Valve Closed	Permeate Flow Rate (ml/min) Valve Opened	GC Permeate Result (%)	
						CO_2	N_2
1.05	1.04	1.00	0.05	0	50	25.00	75
1.06	1.05	1.00	0.06	0	80	24.99	75.01
1.07	1.08	1.00	0.07	0	120	25.00	75.00
1.08	1.07	1.00	0.08	0	140	25.00	75.00
1.09	1.90	1.00	0.09	0	165	25.00	75.00
1.1	1.1	1.00	0.1	0	185	25.00	75.00

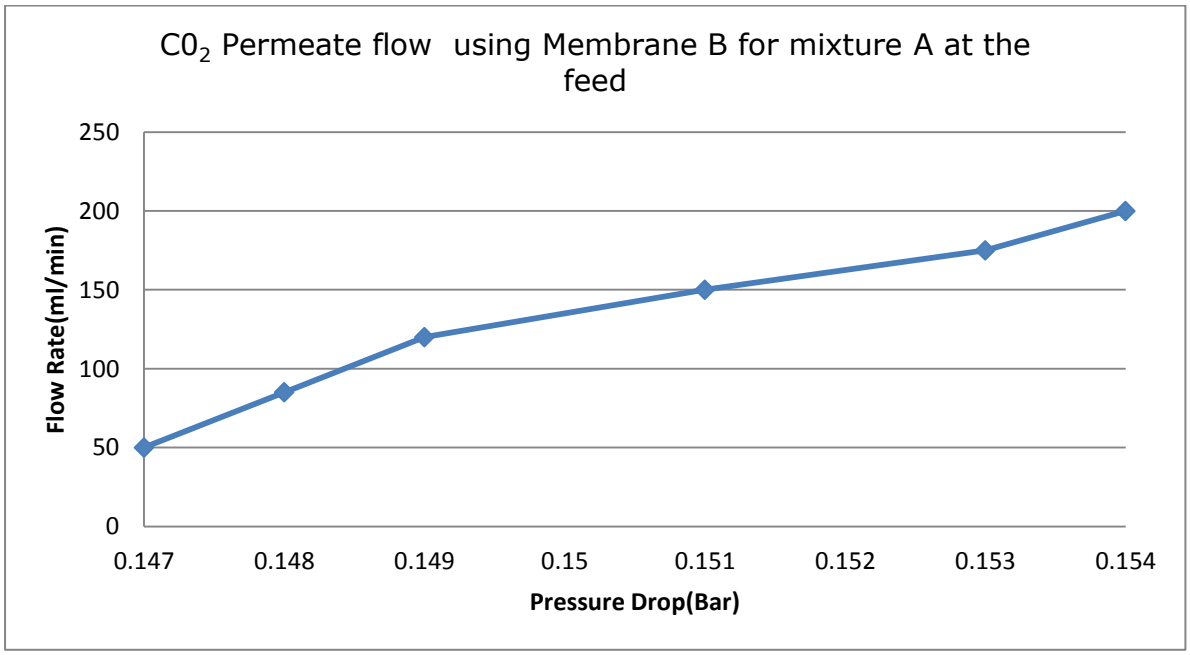

Figure 8:39:CO_2/N_2 Permeate flow using Membrane B for mixture A at the feed

Table 8:43: Values of CO_2 permeate flow for feed condition of mixture A using Membrane B

Feed Partial pressure of the CO_2 (Bar)	Permeate partial pressure of the CO_2 (Bar)	(P_{Feed}-$P_{Retentate}$) ΔP(Bar)	CO_2 Permeate Flow Rate(ml/min)
0.147	0.035	0.112	12.50
0.148	0.035	0.113	19.99
0.150	0.035	0.115	30.00
0.151	0.035	0.116	35.00
0.153	0.035	0.118	41.25
0.154	0.035	0.119	46.25

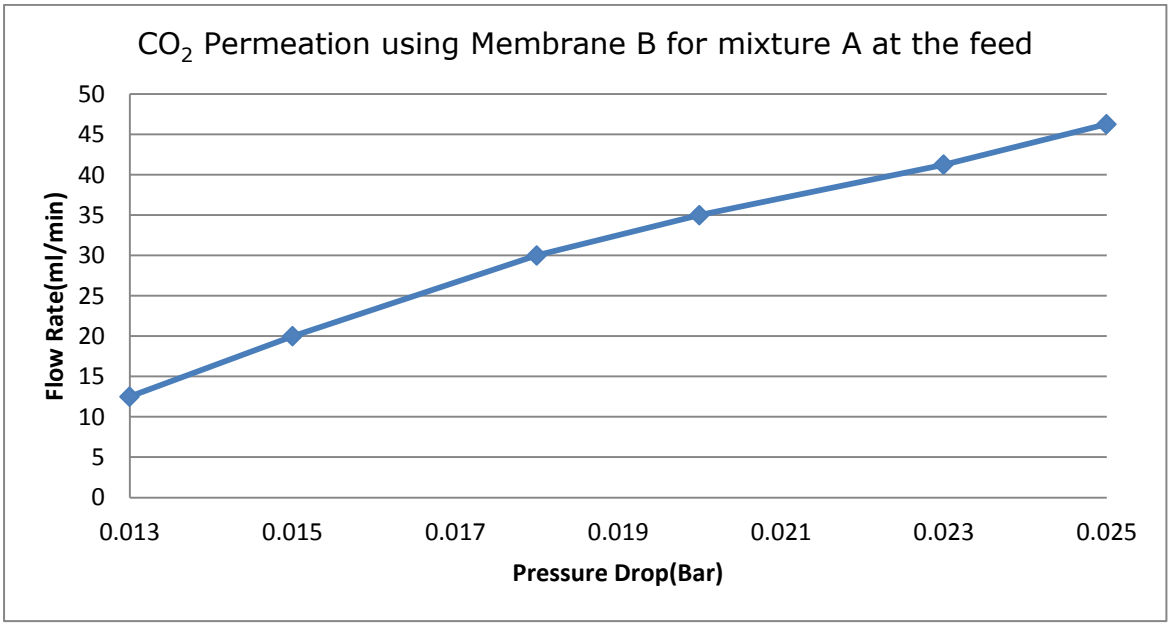

Figure 8:40: CO_2 Permeate flow using Membrane B for mixture A at the feed

Table 8:44: N_2 permeate flow using membrane B for feed condition of mixture A

Feed Partial pressure of the N_2 (Bar)	Permeate partial pressure of the N_2 (Bar)	$(P_{Feed}-P_{Retentate})$ ΔP(Bar)	N_2 Permeate Flow Rate(ml/min)
0.903	0.645	0.258	37.50
0.912	0.645	0.267	60.01
0.920	0.645	0.275	90.00
0.929	0.645	0.284	105.00
0.937	0.645	0.292	123.75
0.946	0.645	0.301	138.75

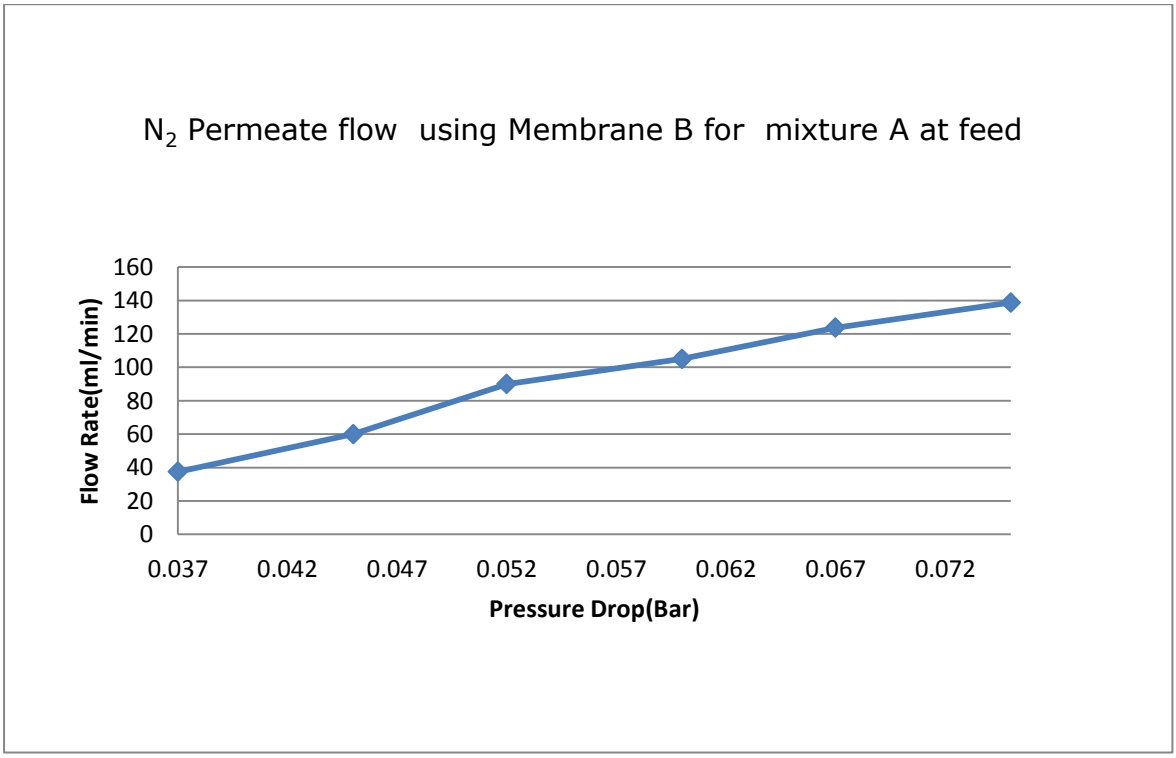

Figure 8:41: N_2 Permeate flow using Membrane B for feed condition of mixture A with retentate valve fully closed

Table 8:45: Values of Cocurrent flow for mixture A permeates flow using Membrane C after first Dip, with retentate valve closed.

P_{Feed} (Bar) Absolute	$P_{Retentate}$ (Bar) Absolute	$P_{Permeate}$ (Bar) Absolute	ΔP(Bar) Absolute	Retentate Flow Rate (ml/min) Valve Closed	CO_2/N_2 Permeate Flow Rate (ml/min)	GC Permeate Result (%)	
						CO_2	N_2
1.05	1.05	1.00	0.05	0	35	30.00	70
1.06	1.06	1.00	0.06	0	55	29.99	70.01
1.07	1.07	1.00	0.07	0	76	29.99	70.00
1.08	1.08	1.00	0.08	0	100	30.00	70.00
1.09	1.09	1.00	0.09	0	120	30.00	70.00
1.1	1.0	1.00	0.1	0	140	30.00	70.00

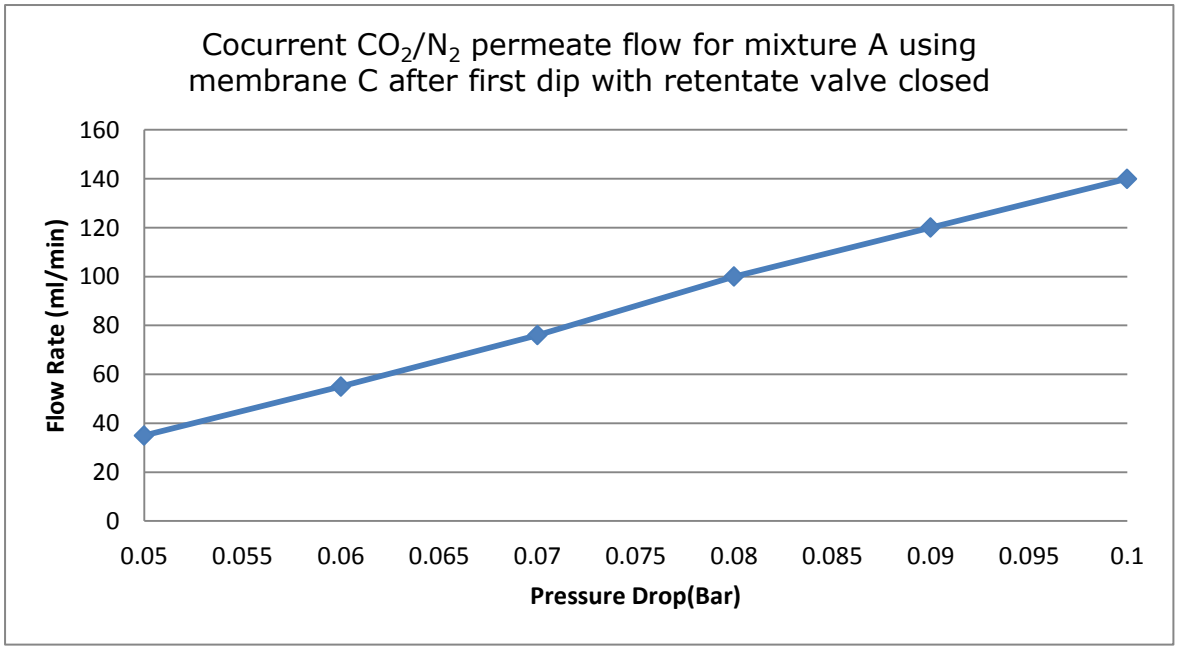

Figure 8:42: Cocurrent CO_2/N_2 permeation for mixture A using membrane C after first Dip, with retentate valve closed.

Table 8:46: Co current CO_2 permeate flow from mixture A using membrane C after first dip with retentate valve fully closed

Feed Partial pressure of the CO_2 (Bar)	Permeate partial pressure of the CO_2 (Bar)	(P_{Feed}-$P_{Retentate}$) ΔP(Bar)	CO_2 Permeate Flow Rate(ml/min) using membrane C
0.147	0.042	0.105	10.50
0.148	0.042	0.106	16.49
0.150	0.042	0.108	22.79
0.151	0.042	0.109	30.00
0.153	0.042	0.111	36.00
0.154	0.042	0.112	42.00

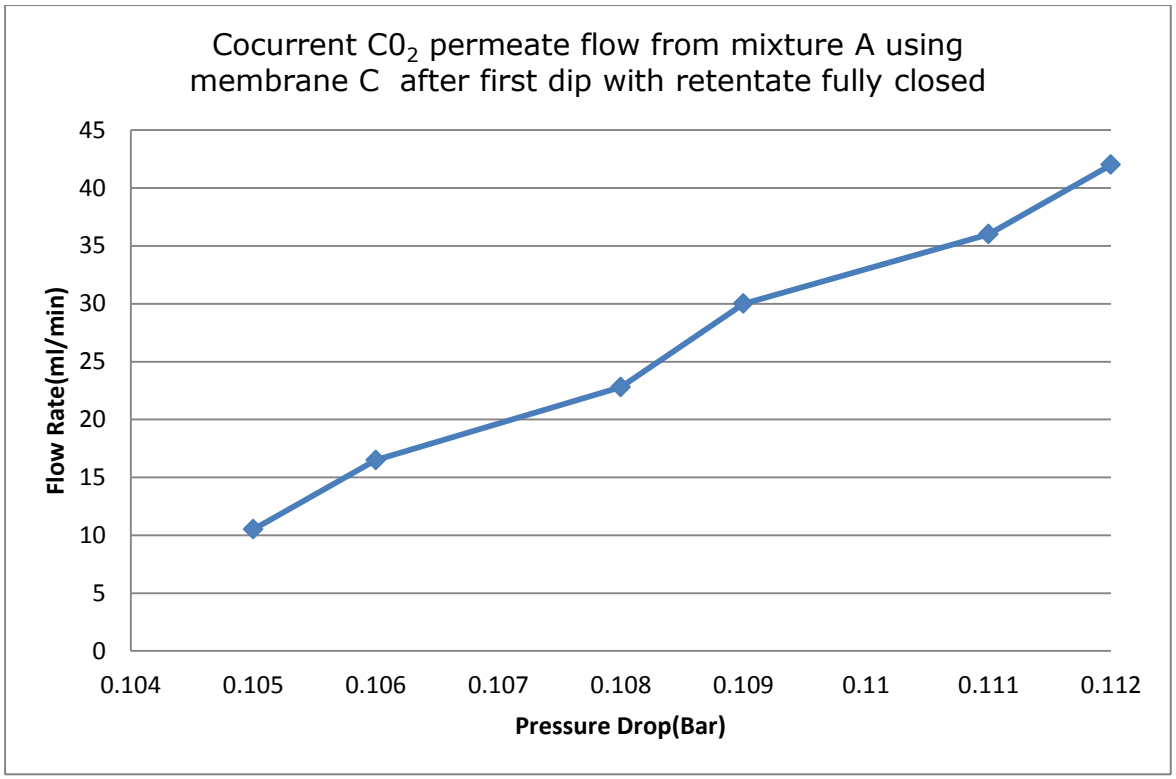

Figure 8:43: CO_2 permeate flow from mixture A using Membrane C after first dip with retentate valve fully closed

Table 8:47: Cocurrent N_2 permeate flow from mixture A using Membrane C after first dip with retentate valve fully closed

Feed Partial pressure of the N_2 (Bar)	Permeate partial pressure of the N_2 (Bar)	$(P_{Feed}-P_{Retentate})$ ΔP(Bar)	N_2 Permeate Flow Rate(ml/min)
0.903	0.602	0.301	24.50
0.912	0.602	0.310	38.51
0.920	0.602	0.318	53.21
0.929	0.602	0.327	70.00
0.937	0.602	0.335	84.00
0.946	0.602	0.344	98.00

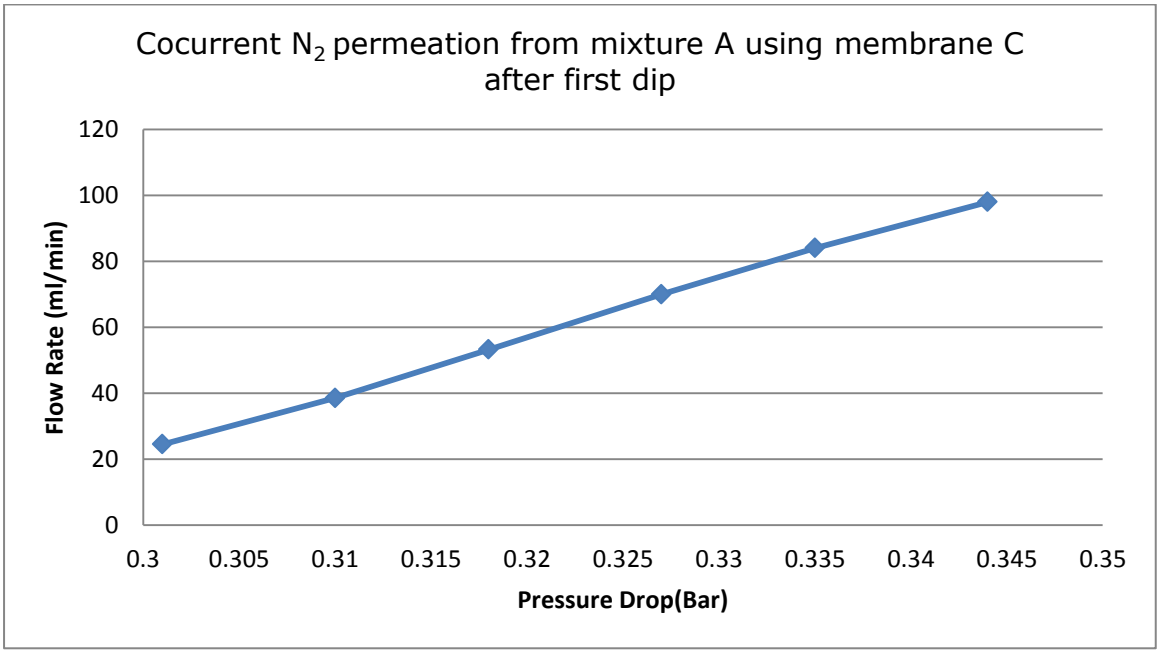

Figure 8:44 : Cocurrent N_2 Permeate flow from mixture A using membrane C after first dip

Table 8:48: Values of Cocurrent flow for mixture A permeation using Membrane C after Second Dip, with retentate valve closed.

P_{Feed} (Bar) Absolute	$P_{Retentate}$ (Bar) Absolute	$P_{permeate}$ (Bar) Absolute	ΔP (Bar) Absolute (P_F - P_P)	Retentate Flow Rate (ml/min) Valve Closed	CO_2 Permeate Flow Rate (ml/min) Using membrane C	GC Permeate Result (%)	
						CO_2	N_2
1.05	1.05	1.00	0.05	0	30	30.00	70.00
1.06	1.06	1.00	0.06	0	40	29.99	69.99
1.07	1.07	1.00	0.07	0	55	29.99	70.00
1.08	1.08	1.00	0.08	0	75	30.00	70.00
1.09	1.09	1.00	0.09	0	85	30.00	70.00
1.1	1.0	1.00	0.1	0	95	30.00	70.00

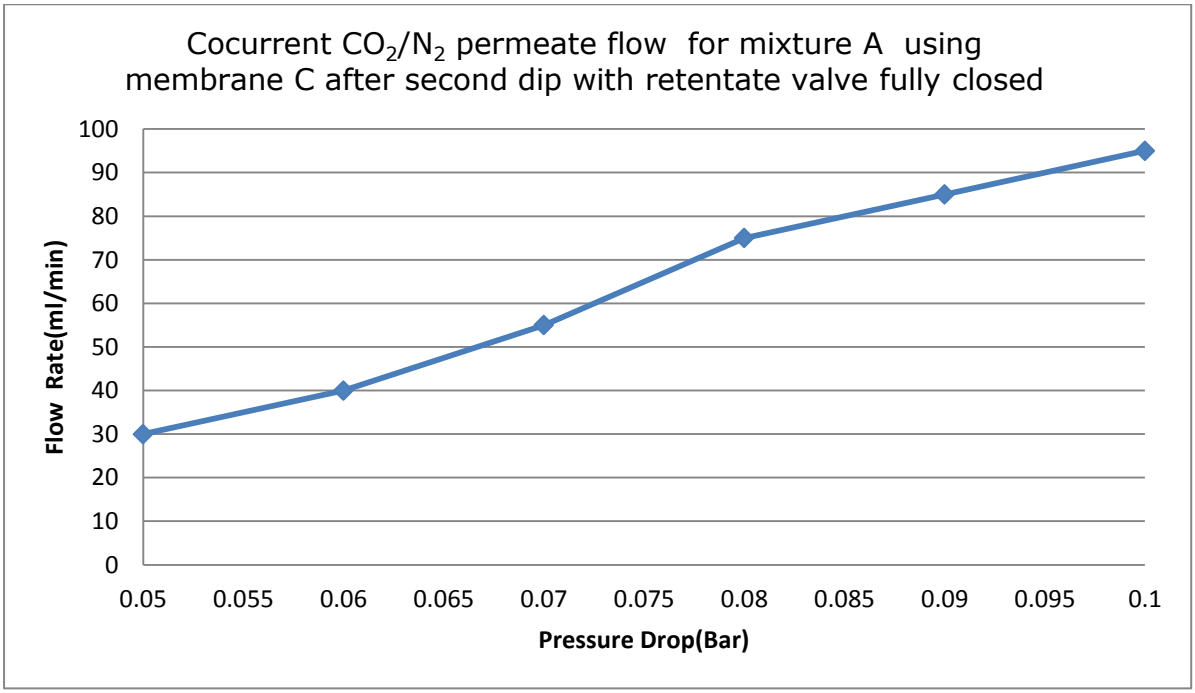

Figure 8:45: Cocurrent CO_2/N_2 permeate flow for mixture A using Membrane C after second dip, with retentate valve closed

Table 8:49 CO_2 permeate flow from mixture A using membrane C after second dip with retentate valve fully closed

Partial pressure of the CO_2 in Feed (Bar)	Partial pressure of the CO_2 in the Permeate (Bar)	Pressure Drop(ΔP) (Bar)	CO_2 Permeate Flow Rate(ml/min) Using Membrane C after second dip
0.147	0.042	0.105	9.00
0.148	0.042	0.106	12.00
0.150	0.042	0.108	16.49
0.151	0.042	0.109	22.50
0.153	0.042	0.111	25.50
0.154	0.042	0.112	28.50

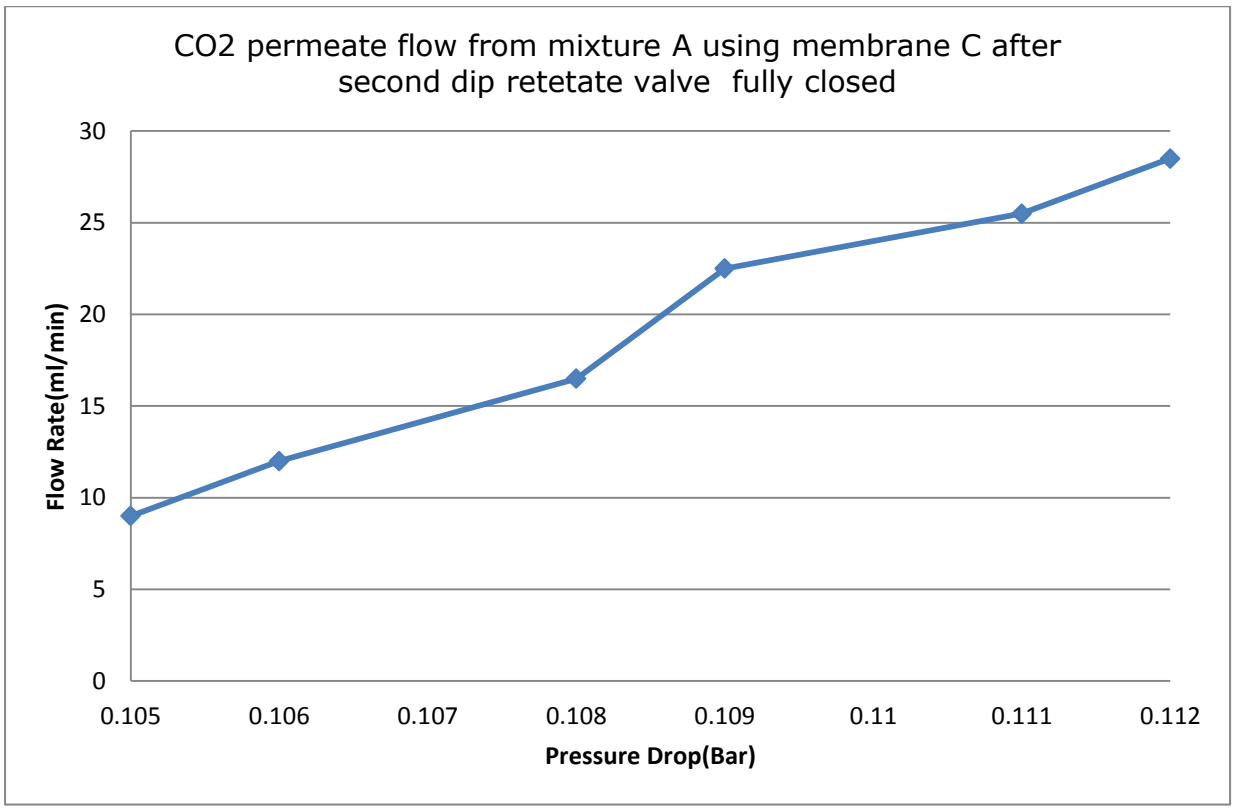

Figure 8:46: CO_2 permeate flow from mixture A using Membrane C after second dip with retentate valve fully closed

Table 8:50: N_2 permeate flow from mixture A using Membrane C after second dip with retentate valve fully closed

Feed Partial pressure of the N_2 (Bar)	Permeate partial pressure of the N_2 (Bar)	(P_{Feed}-$P_{Retentate}$) ΔP(Bar)	N_2 Permeate Flow Rate(ml/min)
0.903	0.602	0.301	21.00
0.912	0.602	0.310	28.00
0.920	0.602	0.318	38.51
0.929	0.602	0.327	52.50
0.937	0.602	0.335	56.00
0.946	0.602	0.344	66.50

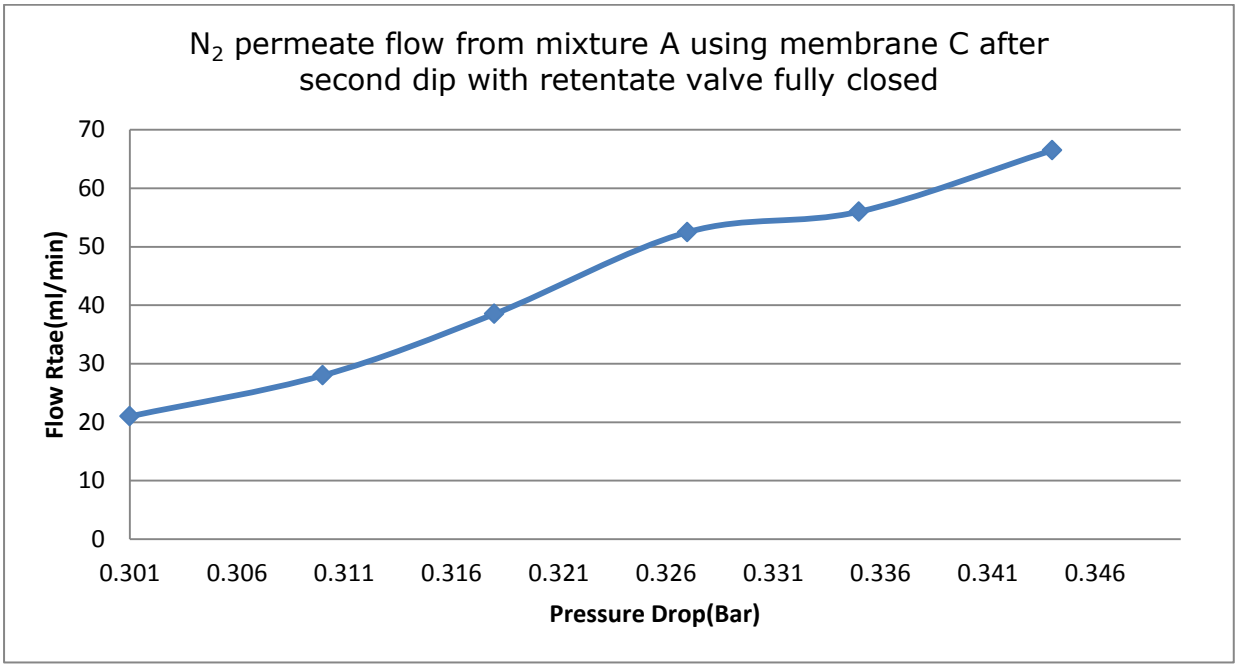

Figure 8:47: N_2 permeate flow from mixture A using membrane C after second dip with retentate valve fully closed

Table 8:51: Cocurrent flow for mixture A permeation using Membrane C after third dip, with retentate valve closed.

P_{Feed} (Bar) Absolute	$P_{Retentate}$ (Bar) Absolute	$P_{Permeate}$ (Bar) Absolute	ΔP (Bar) Absolute (P_F - P_P)	Retentate Flow Rate (ml/min) Valve closed	CO_2/N_2 Permeate Flow Rate (ml/min)	GC Permeate Result (%)	
						CO_2	N_2
1.05	1.06	1.00	0.05	0	15	30.00	70
1.06	1.05	1.00	0.06	0	25	29.99	69.01
1.07	1.07	1.00	0.07	0	35	29.99	70.00
1.08	1.08	1.00	0.08	0	50	30.00	70.00
1.09	1.09	1.00	0.09	0	65	30.00	70.00
1.1	1.0	1.00	0.1	0	75	30.00	70.00

Table 8:52:CO_2 permeate flow from mixture A using membrane C after third dip with retentate valve fully closed

Feed Partial pressure of the CO_2 (Bar)	Permeate partial pressure of the CO_2 (Bar)	Pressure Drop(ΔP) (Bar)	CO_2 Permeate Flow Rate(ml/min)
0.147	0.042	0.105	4.50
0.148	0.042	0.106	7.50
0.150	0.042	0.108	10.50
0.151	0.042	0.109	15.00
0.153	0.042	0.111	19.50
0.154	0.042	0.112	22.50

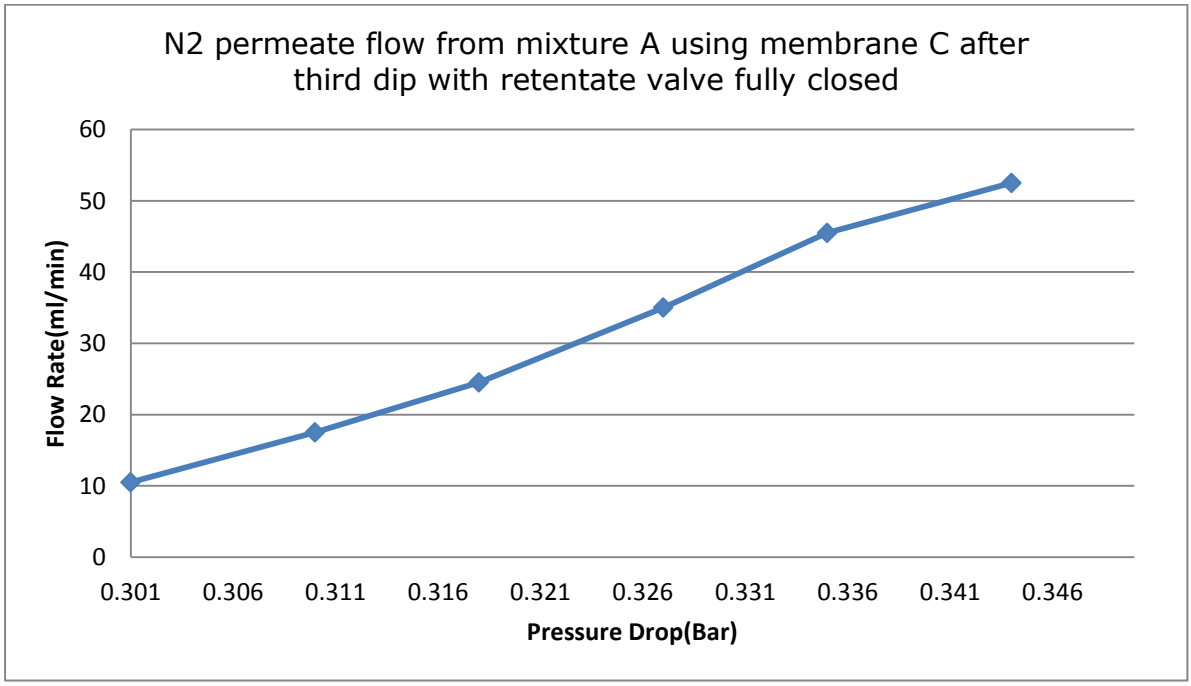

Figure 8:48: CO_2 permeate flow from mixture A using membrane C after third dip with retentate valve fully closed

Table 8:53: N_2 permeate flow from mixture A using Membrane C after third dip with retentate valve fully closed

Feed Partial pressure of the N_2 (Bar)	Permeate partial pressure of the N_2 (Bar)	$(P_{Feed}-P_{Retentate})$ ΔP(Bar)	N_2 Permeate Flow Rate(ml/min)
0.903	0.602	0.301	10.50
0.912	0.602	0.310	17.50
0.920	0.602	0.318	24.50
0.929	0.602	0.327	35.00
0.937	0.602	0.335	45.50
0.946	0.602	0.344	52.50

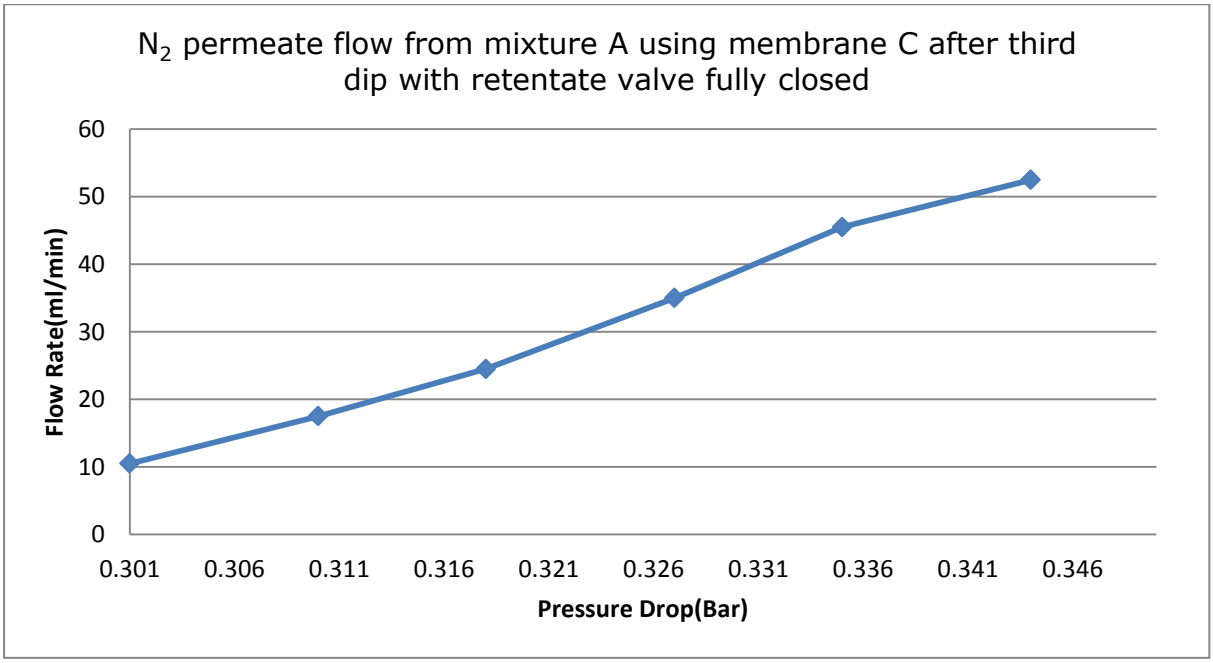

Figure 8:49: N_2 permeate flow from mixture A using Membrane C after third dip with retentate valve fully closed

Table 8:54: Cocurrent flow for mixture A permeation using Membrane C after fourth dip.

P_{Feed} (Bar) Absolute	$P_{Retentate}$ (Bar) Absolute	$P_{Permeate}$ (Bar) Absolute	ΔP (Bar) Absolute (P_F - P_P)	Retentate Flow Rate (ml/min) Valve Closed	CO_2/N_2 Flow Rate (ml/min)	GC Permeate Result (%)	
						CO_2	N_2
1.05	1.06	1.00	0.05	0	3	30.00	70
1.06	1.05	1.00	0.06	0	8	29.99	69.01
1.07	1.07	1.00	0.07	0	12	29.99	70.00
1.08	1.08	1.00	0.08	0	19	30.00	70.00
1.09	1.09	1.00	0.09	0	25	30.00	70.00
1.1	1.0	1.00	0.1	0	35	30.00	70.00

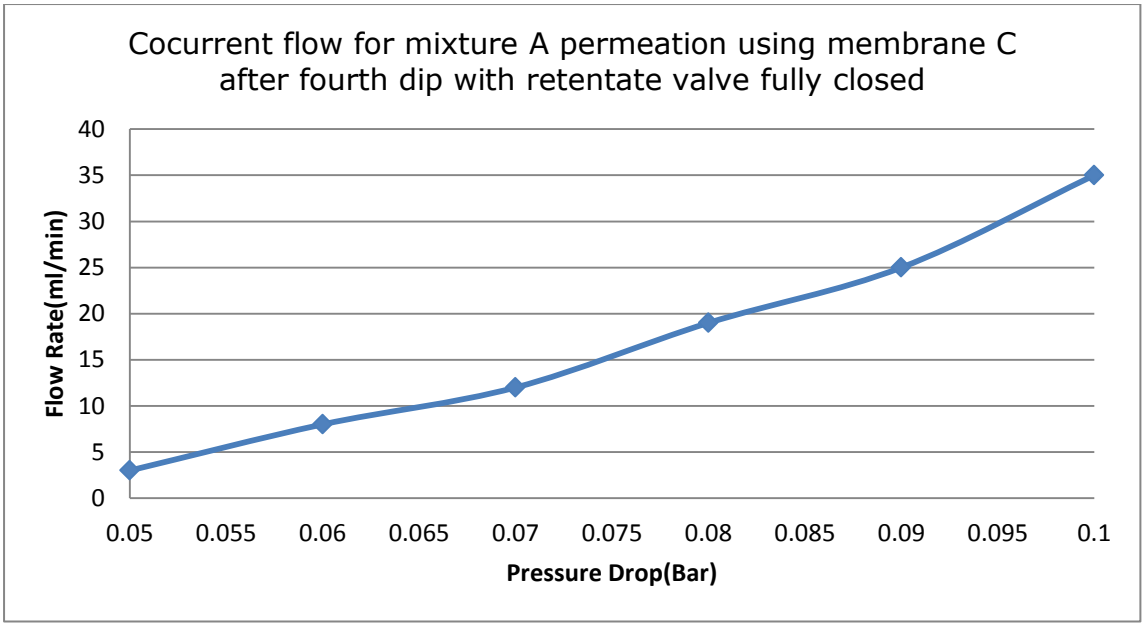

Figure 8:50: Cocurrent flow for mixture A permeation using membrane C after fourth dip with retentate valve fully closed

Table 8:55: CO_2 permeate flow from mixture A using Membrane C after fourth dip with retentate valve fully closed

Feed Partial pressure of the CO_2 (Bar)	Permeate partial pressure of the CO_2 (Bar)	Pressure Drop(ΔP) (Bar)	CO_2 Permeate Flow Rate(ml/min)
0.147	0.042	0.105	0.90
0.148	0.042	0.106	2.40
0.150	0.042	0.108	3.60
0.151	0.042	0.109	5.70
0.153	0.042	0.111	7.50
0.154	0.042	0.112	10.50

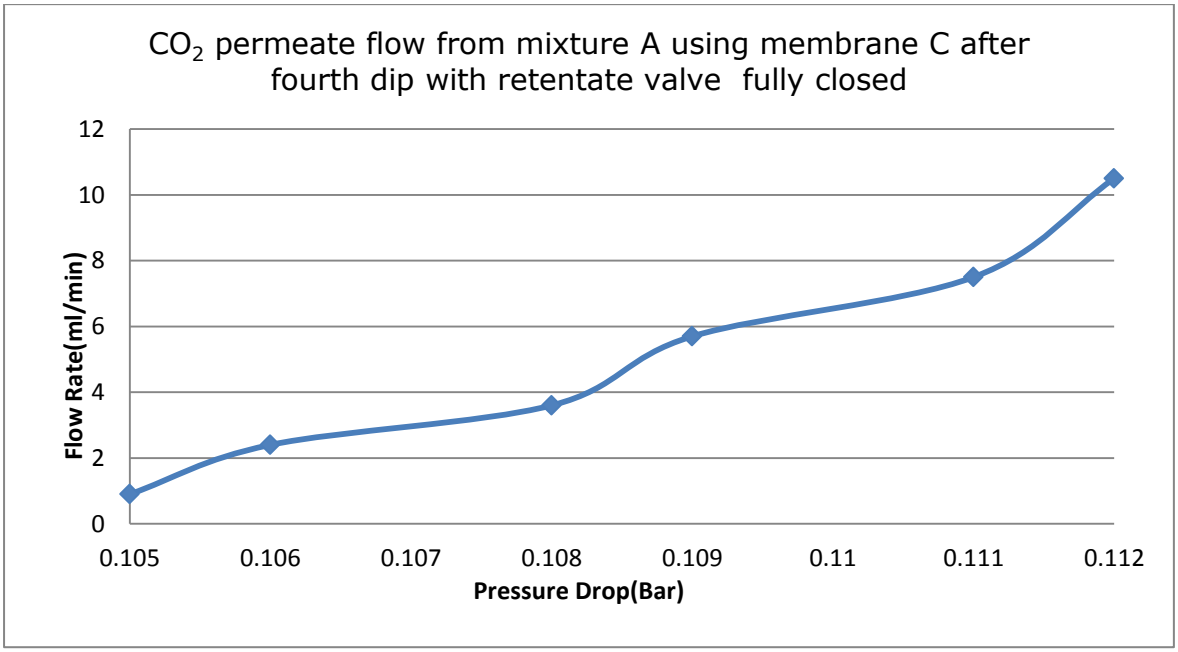

Figure 8:51: CO_2 permeate flow from mixture A using membrane C after fourth dip with retentate valve fully closed

Table 8:56: N_2 permeate flow from mixture A using Membrane C after fourth dip with retentate valve fully closed

Feed Partial pressure of the N_2 (Bar)	Permeate partial pressure of the N_2 (Bar)	$(P_{Feed}-P_{Retentate})$ ΔP(Bar)	N_2 Permeate Flow Rate(ml/min)
0.903	0.602	0.301	2.10
0.912	0.602	0.310	5.60
0.920	0.602	0.318	8.40
0.929	0.602	0.327	13.30
0.937	0.602	0.335	17.50
0.946	0.602	0.344	24.50

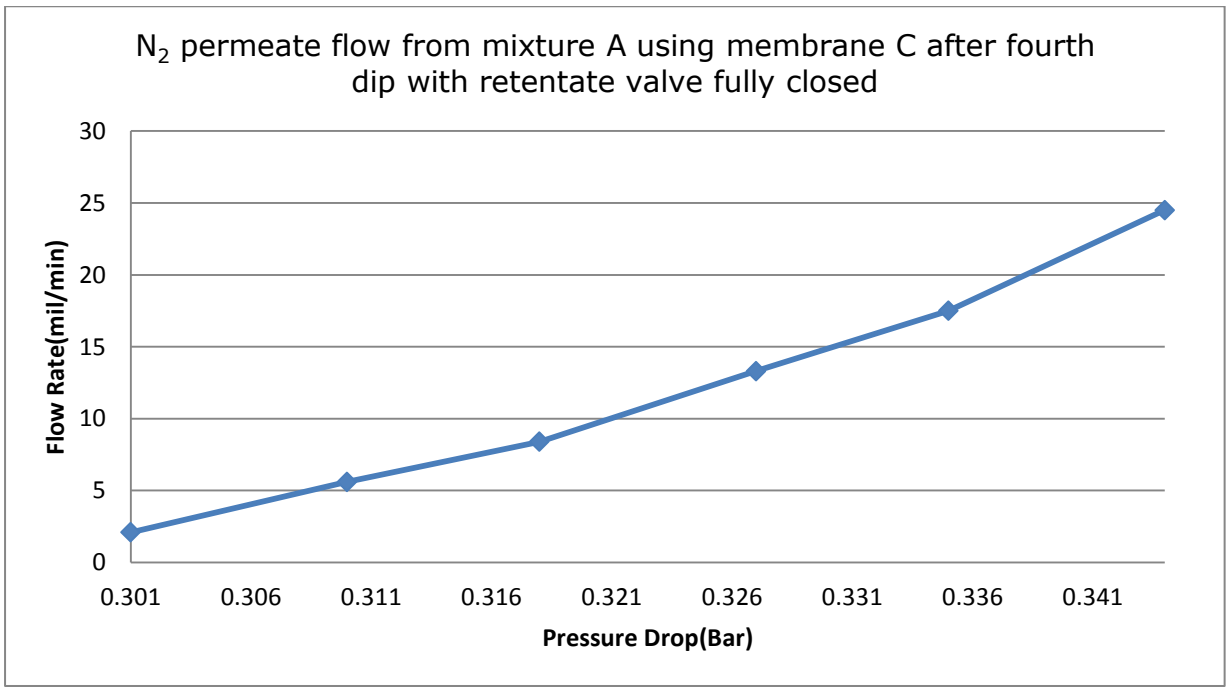

Figure 8:52: N_2 permeate flow from mixture A using Membrane C after fourth Dip with retentate valve fully closed

Table 8:57: Pure Methane permeate flow using Membrane C after fourth dip with retentate valve fully closed.

P_{Feed} Absolute (Bar)	$P_{Retentate}$ Absolute (Bar)	$P_{Permeate}$ Absolute (Bar)	ΔP(Bar) Pressure Drop (P_{F-} P_P)	Retentate Flow Rate (ml/min) Valve Closed	Pure Methane Permeate Flow Rate(ml/min)
1.05	1.04	1.00	0.05	0	0
1.06	1.05	1.00	0.06	0	0
1.07	1.07	1.00	0.07	0	0.01
1.08	1.07	1.00	0.08	0	0.1
1.09	1.08	1.00	0.09	0	0.5
1.1	1.08	1.00	0.1	0	1.0

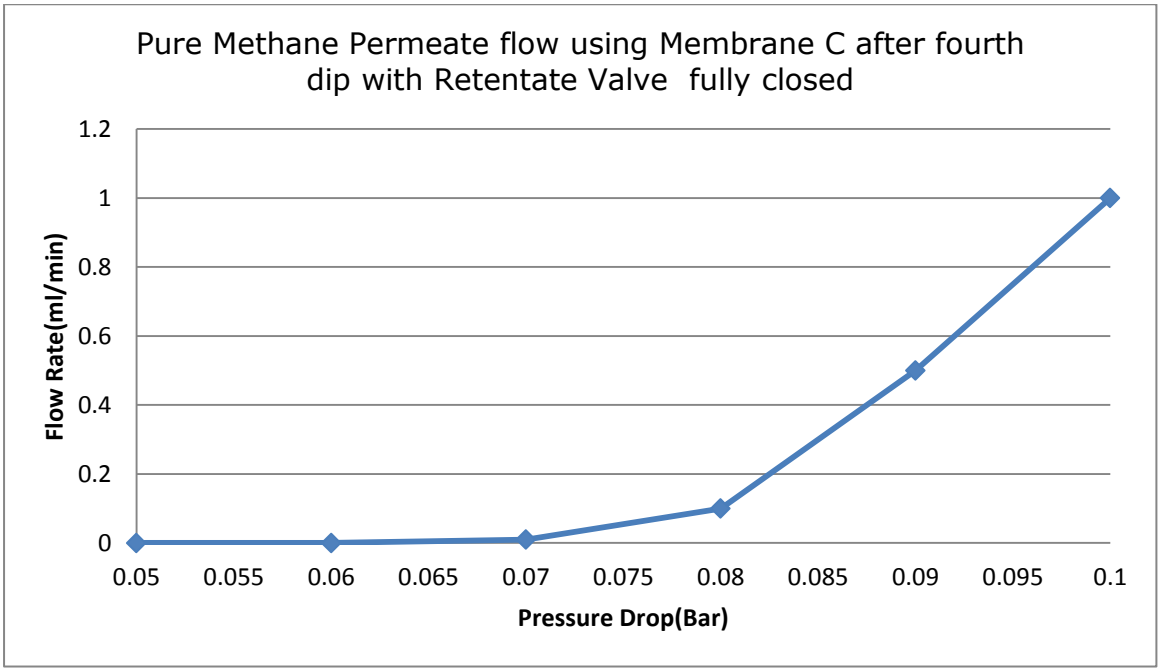

Figure 8:53: Pure Methane Permeation using Membrane C after fourth dip with retentate valve fully closed

Table 8:58: Pure Helium permeates flow using Membrane C after fourth dip with retentate valve fully closed.

P_{Feed} (Bar) Absolute	$P_{Retentate}$ (Bar) Absolute	$P_{Permeate}$ (Bar) Absolute	ΔP (Bar) Absolute (P_F - P_P)	Pure Helium Retentate Flow Rate (ml/min) Valve Closed	Pure Helium Permeate Flow Rate (ml/min)
1.05	1.05	1.00	0.05	0	0.20
1.06	1.06	1.00	0.06	0	0.35
1.07	1.06	1.00	0.07	0	1.5
1.08	1.07	1.00	0.08	0	2.5
1.09	1.08	1.00	0.09	0	4
1.1	1.09	1.00	0.1	0	6

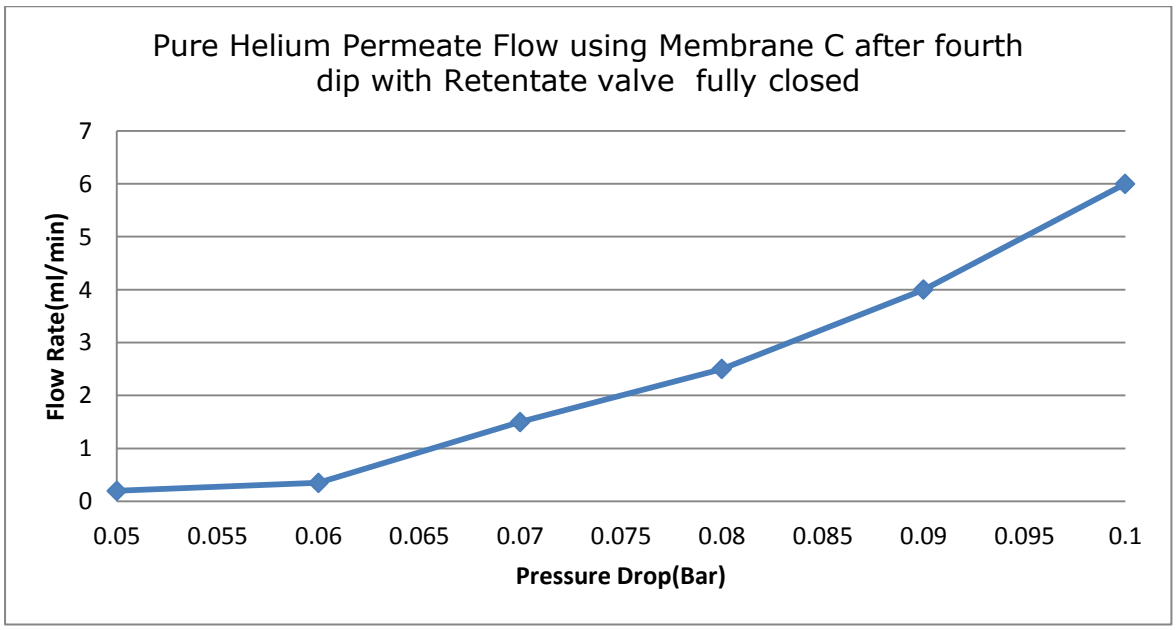

Figure 8:54: Pure Helium permeate flow using Membrane C after fourth dip with retentate valve fully closed

Table 8:59: Pure Argon permeate flow using Membrane C after fourth dip with retentate valve fully closed.

P_{Feed} (Bar) Absolute	$P_{Retentate}$ (Bar) Absolute	$P_{Permeate}$ (Bar) Absolute	ΔP (Bar) Absolute (P_F - P_P)	Pure Argon Retentate Flow Rate (ml/min) Valve Closed	Pure Argon Permeate Flow Rate(ml/min)
1.05	1.05	1.00	0.05	0	0.00
1.06	1.07	1.00	0.06	0	0.00
1.07	1.07	1.00	0.07	0	0.00
1.08	1.08	1.00	0.08	0	0.00
1.09	1.09	1.00	0.09	0	0.02
1.1	1.1	1.00	0.1	0	0.1

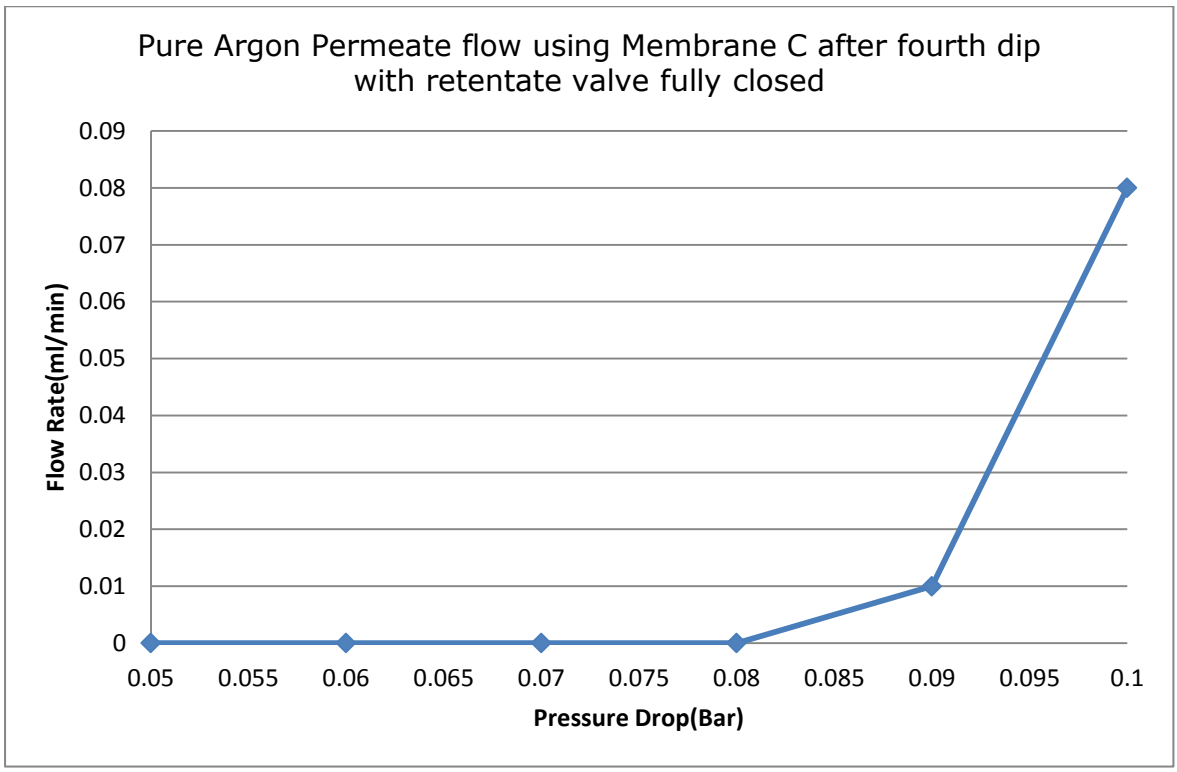

Figure 8:55: Pure Argon permeate flow using Membrane C after fourth dip with retentate Valve fully closed

Table 8:60: Pure $C0_2$ permeate flow using Membrane C after fourth dip with retentate valve fully closed

P_{Feed} (Bar) Absolute	$P_{Retentate}$ (Bar) Absolute	$P_{Permeate}$ (Bar) Absolute	ΔP (Bar) Absolute (P_F - P_P)	Pure CO_2 Retentate Flow Rate (ml/min) Valve Closed	Pure $C0_2$ Permeate Flow Rate (ml/min)
1.05	1.05	1.00	0.05	0	5.12
1.06	1.07	1.00	0.06	0	15.20
1.07	1.07	1.00	0.07	0	25.0
1.08	1.08	1.00	0.08	0	40.56
1.09	1.09	1.00	0.09	0	59.01
1.1	1.1	1.00	0.1	0	70.40

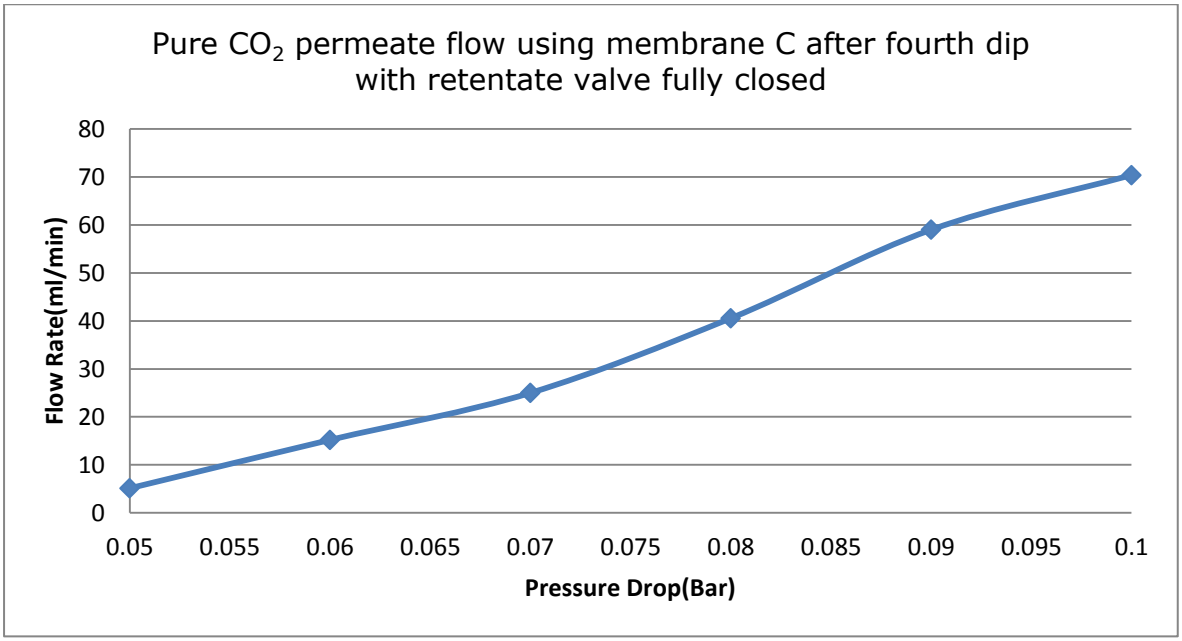

Figure 8:56: Pure $C0_2$ permeate flow using Membrane C after fourth dip with retentate valve fully closed.

Table 8:61: Pure Nitrogen permeate flow using Membrane C after fourth dip with retentate valve fully closed.

P_{Feed} Absolute (Bar)	$P_{Retentate}$ Absolute (Bar)	P_P(Bar)	ΔP(Bar) (P_{F-} P_P)	Pure Retentate Flow Rate(ml/min) Valve closed	Pure Nitrogen Permeate Flow Rate(ml/min)
1.05	1.05	1.00	0.05	0	0.00
1.06	1.06	1.00	0.06	0	0.00
1.07	1.06	1.00	0.07	0	0.50
1.08	1.08	1.00	0.08	0	1.10
1.09	1.09	1.00	0.09	0	2.12
1.1	1.1	1.00	0.1	0	3.01

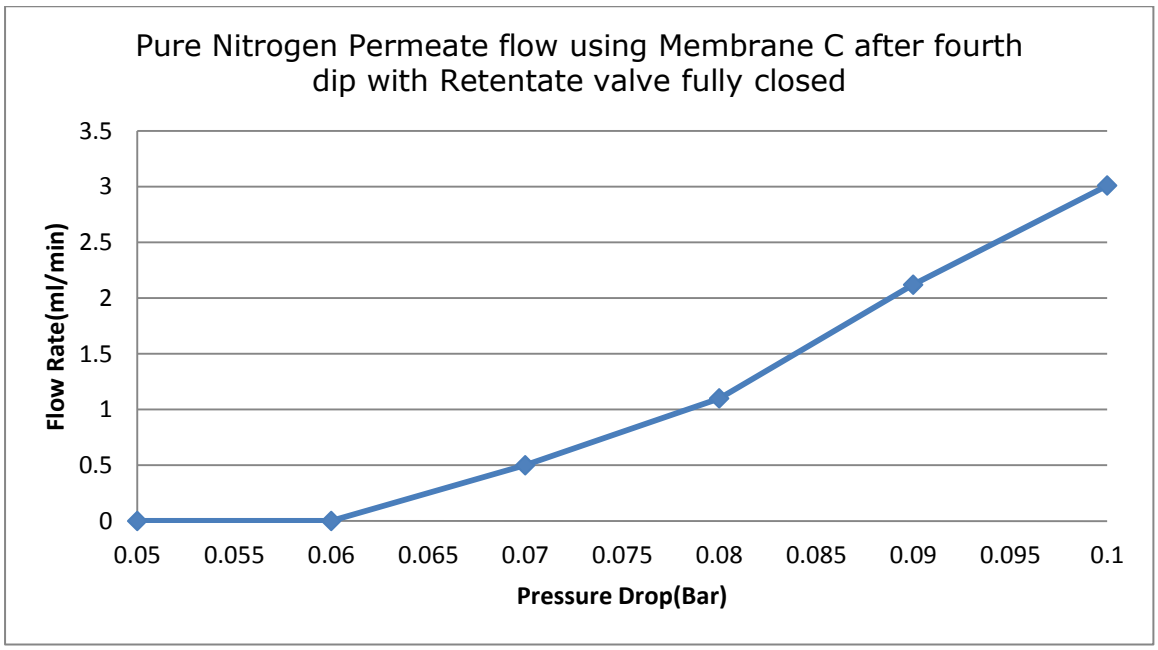

Figure 8:57: Pure Nitrogen permeate flow using membrane C after fourth dip with retentate valve fully closed

8.2 APPENDIX 2: CALCULATION OF MEMBRANE THICKNESS FOR EACH DIP

From the figure 1.85 shown in the previous chapter, the membrane has the profile below:

Outer Diameter (OD): 25.81mm (0.02581m)

Internal Diameter (ID):20.5mm (0.0205m)

Total Length of the support: 360.5mm (0.3605m)

Effective Length of the support: 310.5mm (0.3105m)

Thickness of the support: 5mm (0.005m)

Mass of the support before dipping: 274.6g (0.2746kg) before Calcination

Mass of the support after calcination: 274.7g (0.2747kg)

Mass of the support after being dipped in solution 1: 274.91g (0.27491kg).

Gain after dipped in solution 1 is (274.91-274.7) g=0.21g (2.1E-04kg).

Mass of the support after first dipped in solution 2 = 283.1g (0.2831kg)

Gain in mass after first dip in solution 2= (0.2831-0.27491) kg; 8.19E-03kg. This represents the mass of the Membrane C after the first dip.

Mass of the support after second dipped in solution 2=288.1g (0.2881kg).

Gain in mass after second dip = (0.2881-0.2831) kg; 5.0E-03kg. This represents the mass of the Membrane C after the second dip.

Mass of the support after third dipped in solution 2 =293.2g (0.2932kg).

Gain in mass after third dip = (0.2932-0.2881) kg; 5.1E-03kg. This represents the mass of the Membrane C after the third dip.

Mass of the support after fourth dipped in solution 2 = 298.4g (0.2984kg).

Gain in mass after fourth dip = (0.2984-0.2932) kg; 5.2E-03kg.This represents the mass of the Membrane C after the fourth dip

8.3 APPENDIX 3: FOR THICKNESS OF MEMBRANE

Membrane thickness after the First Dip in Solution 2

Mass of the coating after the first dip= 8.19E-03kg

Effective Length of the membrane;L_0= 0.3105m

Outer Diameter; D_0=0.02581m

Radius of the Outer Diameter, r_2= 0.012905m

Internal Diameter=0.0205m,

Radius of the Internal Diameter, r_1 = 0.01025m

Surface Area of the Membrane = $\pi D_0 L_0$

= 3.142 x 0.02581x0.3105= 0.0252m^2

Volume of the Coating= $\pi D_0 L_0 \delta$ (where δ is the thickness of the membrane)

Then, the Volume =0.0252 x δ

Density of Silicon Elastomer= 1030kg/m^3

$$\text{But} \quad \text{Density} = \frac{M}{V}$$

thickness = (Mass/ Area x Density)

where m is the mass gained after the membrane C was first dipped in the Solution 2

$$\text{thickness} = \frac{8.19E-03}{(0.0252)(1030)} = (8.19E\text{-}03/25.956)$$

$\delta =$ 3.155E-04m

thickness of the Membrane C after first dipped in solution 2 is then 3.155E-04m.

Then, the Volume of the membrane C after first dipped in solution 2 is 0.0252 x 3.155E-04 = 7.95E-6m^3

<u>Membrane thickness after the Second Dip in Solution 2</u>

For the Membrane C thickness after Second Dip in Solution 2,

$\delta =$ (Gain in mass after second Dip in solution 2)/ (Area x Density)

(5.0E-03)/ (0.0252 X1030) = (5.0E-03/25.956)

= 1.926E-04m

Volume of the Membrane C after Second Dipped in Solution 2 is (0.0252 x 1.926E-04) = 4.853E-06m^3

Membrane thickness after the Third Dip in Solution 2

For the Membrane C thickness after Third Dip in Solution 2,

δ = (Gain in mass after Third Dip in solution 2)/ (Area x Density)

(5.1E-03)/ (0.0252 X1030) = (5.1E-03/25.956)

= 1.965E-04m

Volume of the Membrane C after Third Dipped in Solution 2 is (0.0252 x 1.965E-04) = 4.952E-06m^3

Membrane thickness after the Fourth Dip in Solution 2

For the Membrane C thickness after Fourth Dip in Solution 2,

δ = (Gain in mass after Fourth Dip in solution 2)/ (Area x Density)

(5.2E-03)/ (0.0252 X1030) = (5.2E-03/25.956)

= 2.00E-04m

Volume of the Membrane C after Fourth Dipped in Solution 2 is (0.0252 x 2.00E-04) = 5.04E-6m^3

8.4 APPENDIX 4: PERMEANCE, FLUX, PERMEABILITY AND SELECTIVITY OF THE FABRICATED MEMBRANES, ALL UNITS IN S.I. UNIT.

The permeance of each gas was evaluated using the following corrections:

1 Litre=1E-03m

1min= 60 Sec

Molar Volume of gases at S.T.P =22.4L= 22400ml

1kmol of gas will occupy $22.4m^{3,}$ hence $22.4m^3$/sec=1kmol/sec

$$\frac{1mol}{\frac{\min)}{60}} = mol/\sec$$

Area= $2\pi L_0 \frac{r_2 - r_1}{\ln \frac{r_2}{r_1}}$ this area is referred as log mean area. This is used for the membrane flux, permeance and permeability.

To calculate the Log Mean Area, I referred to the support profile listed above.

However, Area = 2 x 3.142 x 0.3105 $\frac{(0.012905 - 0.01025)}{\ln(\frac{0.012905}{0.01025})}$

Area = $0.0245m^2$

Table 8:62: Second Stage CO_2/N_2 permeate flow using Membrane C with retentate valve fully closed

P_{Feed} (Bar) Absolute	$P_{Retentate}$ (Bar) Absolute	$P_{Permeate}$ (Bar) Absolute	ΔP (Bar) Absolute (P_F - P_P)	Retentate Flow Rate (ml/min) Valve Closed	CO_2/N_2 Permeate Flow Rate (ml/min)	GC Permeate Result (%)	
						CO_2	N_2
1.05	1.06	1.00	0.05	0	2.00	60.00	40.00
1.06	1.05	1.00	0.06	0	4.50	59.99	40.01
1.07	1.07	1.00	0.07	0	6.80	60.00	40.00
1.08	1.08	1.00	0.08	0	8.00	60.00	40.00
1.09	1.09	1.00	0.09	0	10	60.01	39.99
1.1	1.0	1.00	0.1	0	13.50	60.00	40.00

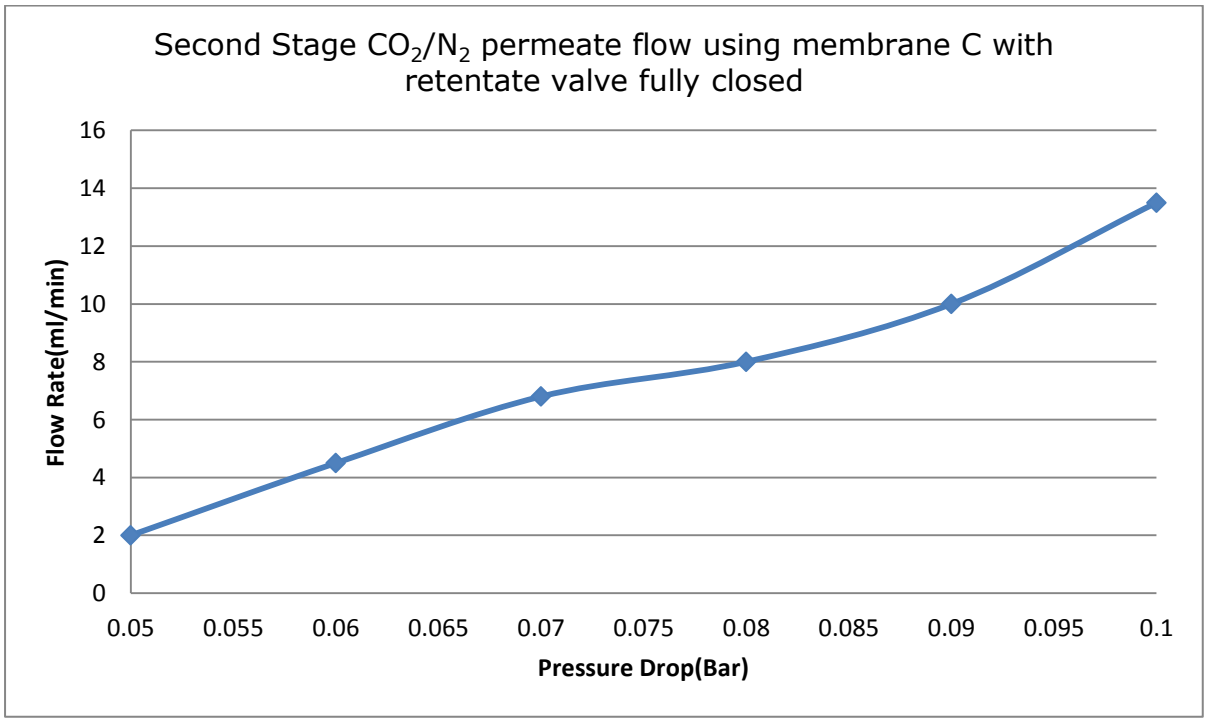

Figure 8:58: Second Stage CO_2/N_2 permeate flow using Membrane C with retentate valve fully closed

Table 8:63: Second Stage CO_2 permeate flow from mixture B using Membrane C after fourth dip with retentate valve fully closed

Feed Partial pressure of the CO_2 (Bar)	Permeate partial pressure of the CO_2 (Bar)	(P_{Feed}-$P_{Retentate}$) ΔP(Bar)	CO_2 Permeate Flow Rate(ml/min)
0.315	0.18	0.135	1.20
0.318	0.18	0.138	2.70
0.321	0.18	0.141	4.08
0.324	0.18	0.144	4.80
0.327	0.18	0.147	6.00
0.33	0.18	0.15	8.10

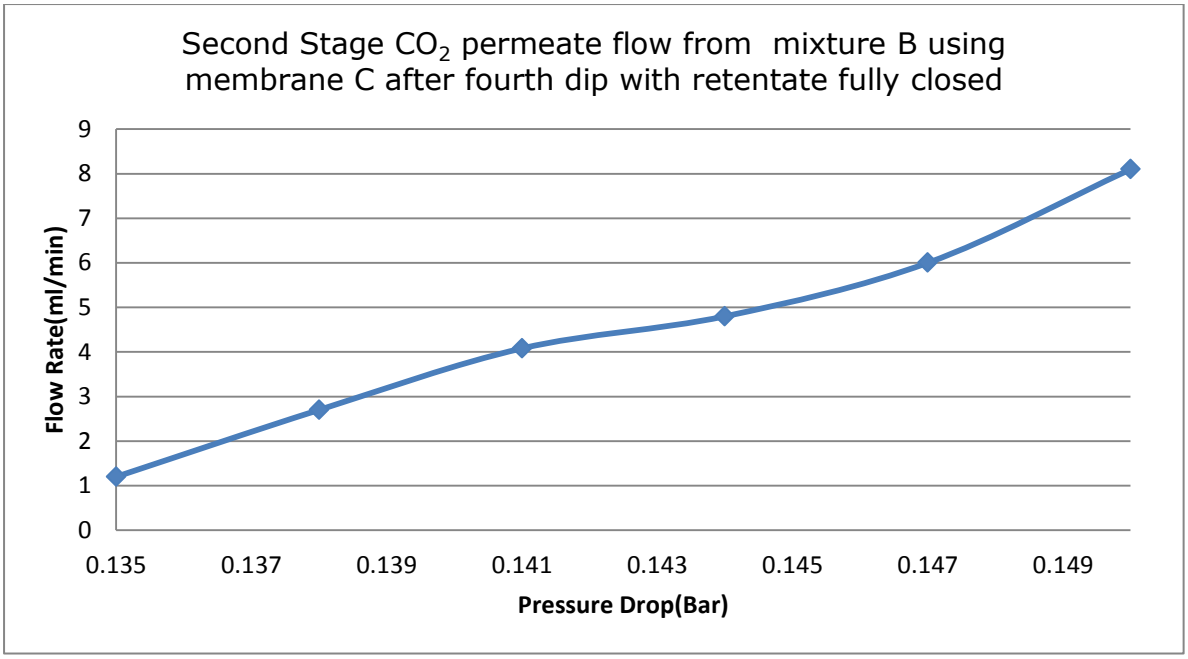

Figure 8:59: Second Stage CO_2 permeate flow from mixture B using membrane C after fourth dip with retentate valve fully closed

Table 8:64: Second Stage N_2 permeate flow from mixtures B using Membrane C after fourth dip with retentate valve fully closed

Feed Partial pressure of the N_2 (Bar)	Permeate partial pressure of the N_2 (Bar)	$(P_{Feed}-P_{Retentate})$ ΔP(Bar)	N_2 Permeate Flow Rate(ml/min)
0.735	0.28	0.455	0.80
0.742	0.28	0.462	1.85
0.749	0.28	0.469	2.72
0.756	0.28	0.476	3.20
0.763	0.28	0.483	4.00
0.77	0.28	0.49	5.40

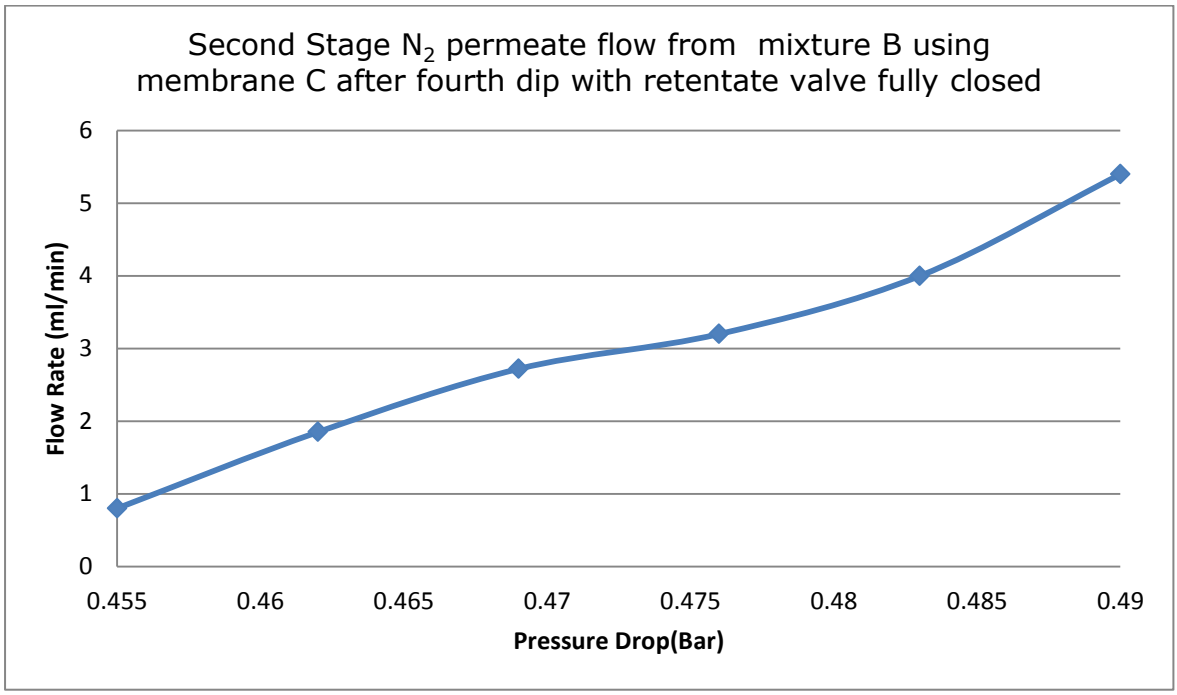

Figure 8:60: Second Stage N_2 permeate flow from mixture B using Membrane C after fourth dip with retentate valve fully closed

Table 8:65: Third Stage CO_2/N_2 permeate flow using Membrane C with retentate valve fully closed

P_{Feed} (Bar) Absolute	$P_{Retentate}$ (Bar) Absolute	$P_{Permeate}$ (Bar) Absolute	ΔP (Bar) Absolute (P_F - P_P)	Flow Rate (ml/min) Valve closed	CO_2/N_2 Flow Rate (ml/min)	GC Permeate Result (%)	
						CO_2	N_2
1.05	1.06	1.00	0.05	0	1.60	90.00	9.99
1.06	1.05	1.00	0.06	0	2.70	90.00	9.99
1.07	1.07	1.00	0.07	0	3.80	90.00	9.99
1.08	1.08	1.00	0.08	0	5.00	90.00	10.00
1.09	1.09	1.00	0.09	0	6.00	90.01	9.99
1.1	1.0	1.00	0.1	0	7.50	90.00	10.00

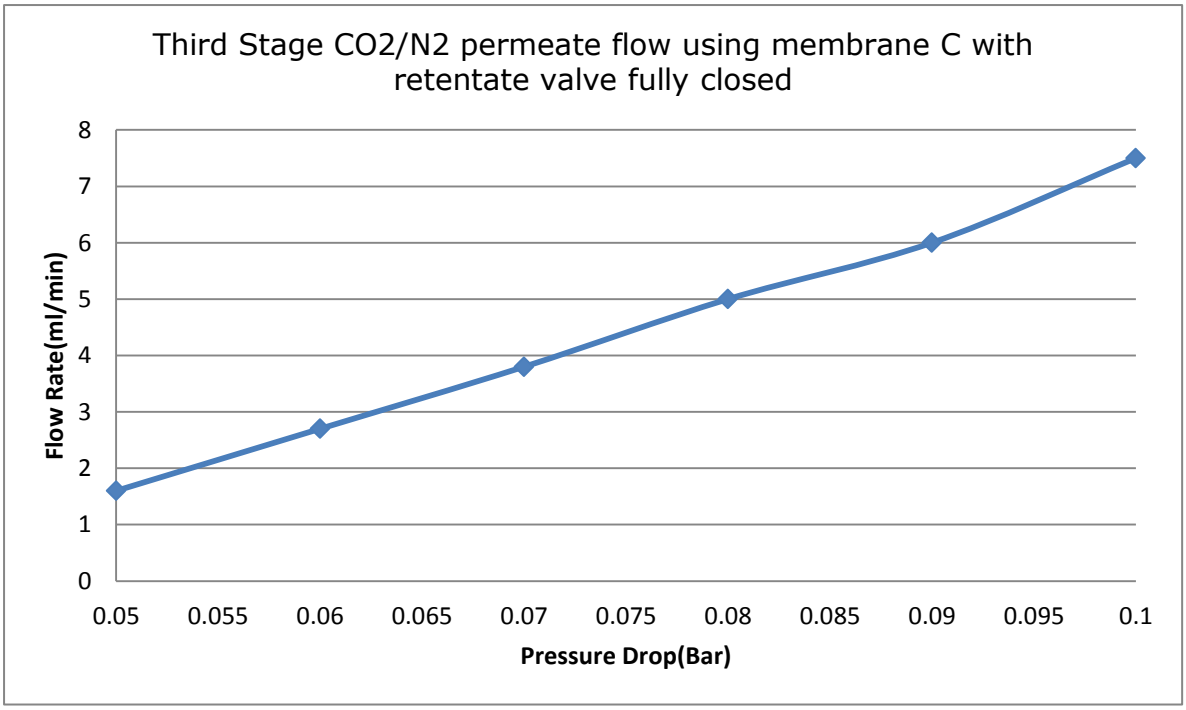

Figure 8:61: Third Stage CO_2/N_2 permeate flow using membrane C with retentate valve fully closed

Table 8:66: Third Stage CO_2 permeate flow from mixture C using membrane C after fourth dip with retentate valve fully closed

Feed Partial pressure of the CO_2 (Bar)	Permeate partial pressure of the CO_2 (Bar)	(P_{Feed}-$P_{Retentate}$) ΔP(Bar)	CO_2 Permeate Flow Rate (ml/min)
0.63	0.54	0.09	1.44
0.64	0.54	0.10	2.43
0.642	0.54	0.102	3.42
0.65	0.54	0.11	4.50
0.654	0.54	0.114	5.40
0.66	0.54	0.12	6.75

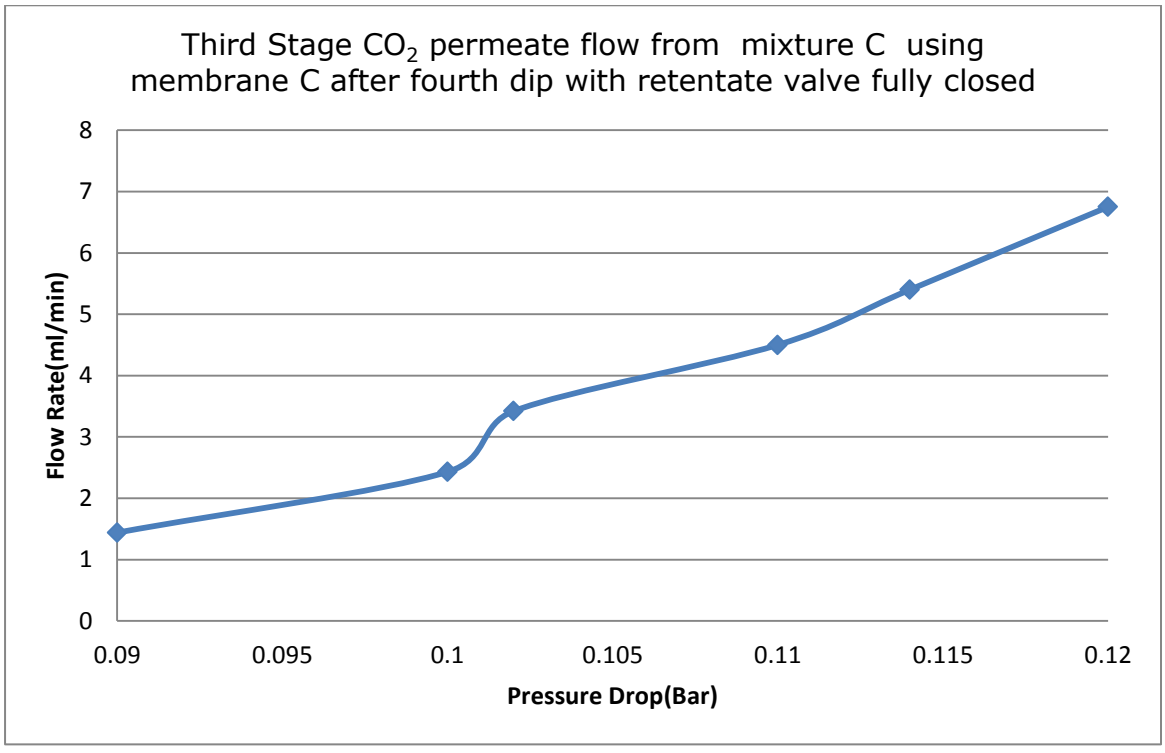

Figure 8:62: Third Stage CO_2 permeate flow from mixtures C using Membrane C after fourth dip with retentate valve fully closed

Table 8:67: Third Stage N_2 permeate flow from mixture C using Membrane C after fourth dip with retentate valve fully closed

Feed Partial pressure of the N_2 (Bar)	Permeate partial pressure of the N_2 (Bar)	$(P_{Feed}-P_{Retentate})$ ΔP(Bar)	N_2 Permeate Flow Rate(ml/min)
0.420	0.04	0.380	0.16
0.424	0.04	0.384	0.27
0.428	0.04	0.388	0.38
0.432	0.04	0.392	0.50
0.436	0.04	0.396	0.60
0.44	0.04	0.400	0.75

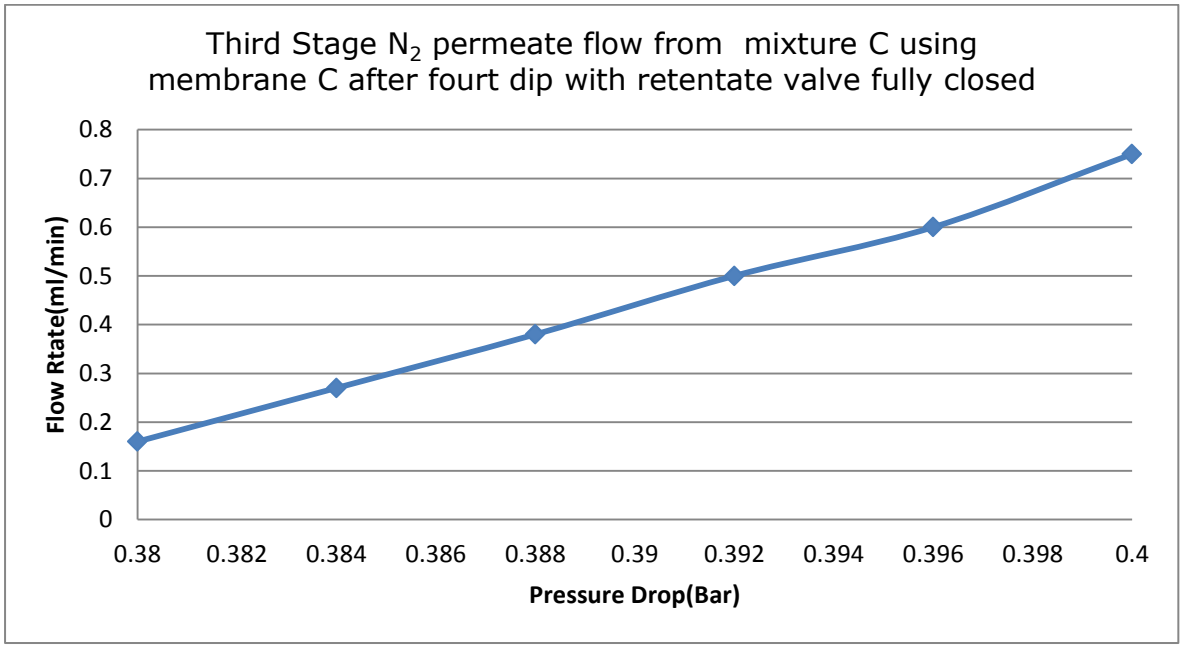

Figure 8:63: Third Stage N_2 permeate flow from mixture C using Membrane C after fourth dip with retentate valve fully closed

Table 8:68: Pure Methane permeance using membrane support only

ΔP(Bar) (P_F - P_P) Absolute	Pressure Drop ΔP (Pascal)	Average Pressure (Pascal)	Pure Methane Permeate Flow Rate (ml/min)	Pure Methane Permeate Flow Rate(mol/s)	pure methane Permeance through Support Only
0.05	5000	102500	125	9.30E-05	7.59E-07
0.06	6000	103000	230	1.71E-04	1.16E-06
0.07	7000	103500	410	3.05E-04	1.78E-06
0.08	8000	104000	470	3.50E-04	1.79E-06
0.09	9000	104500	600	4.46E-04	2.02E-06
0.1	10000	105000	660	4.91E-04	2.00E-06

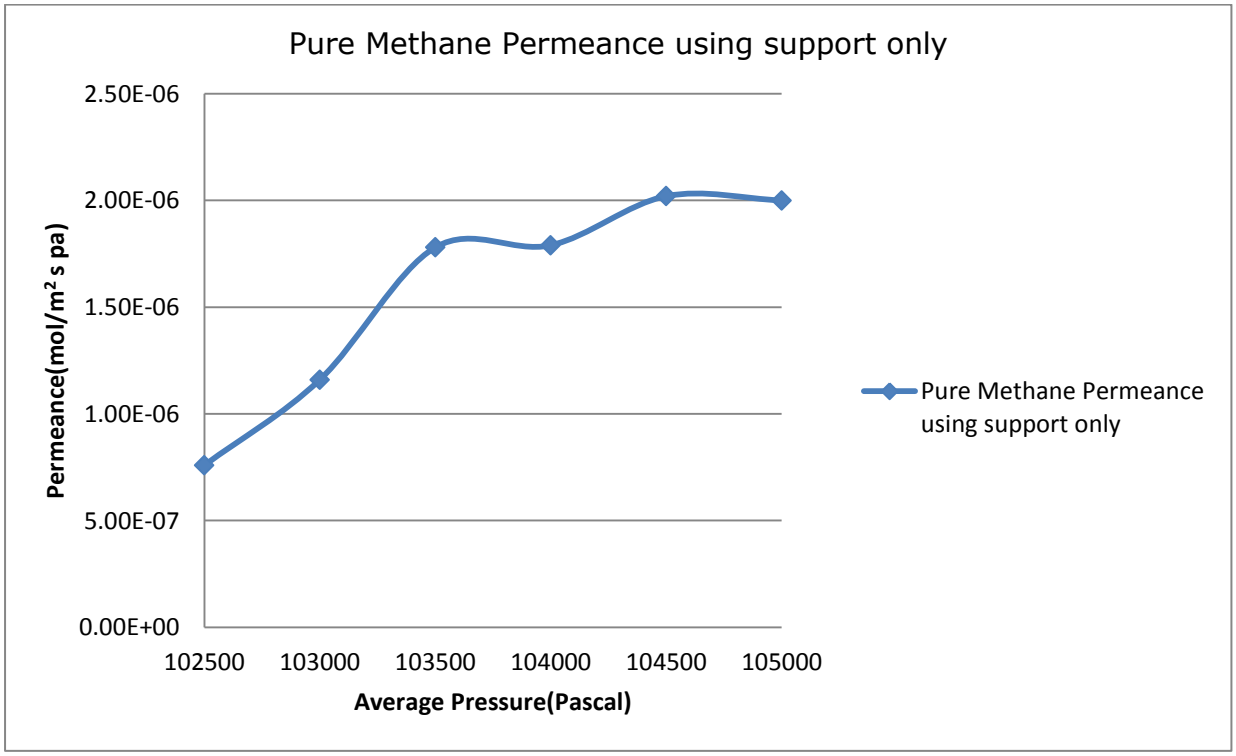

Figure 8:64: Pure Methane permeance using support only

Table 8:69: Pure Nitrogen permeance using membrane support only

ΔP(Bar) (P_F - P_P) Absolute	Pressure Drop (Pascal)	Average Pressure (Pascal)	Pure Nitrogen Permeate Flow Rate (ml/min)	Pure Nitrogen Permeate Flow Rate(mol/s)	pure Nitrogen Permeance through Support Only
0.05	5000	102500	90	6.70E-05	5.47E-07
0.06	6000	103000	198	1.47E-04	1.00E-06
0.07	7000	103500	300	2.23E-04	1.30E-06
0.08	8000	104000	400	2.98E-04	1.52E-06
0.09	9000	104500	450	3.35E-04	1.52E-06
0.1	10000	105000	600	4.46E-04	1.82E-06

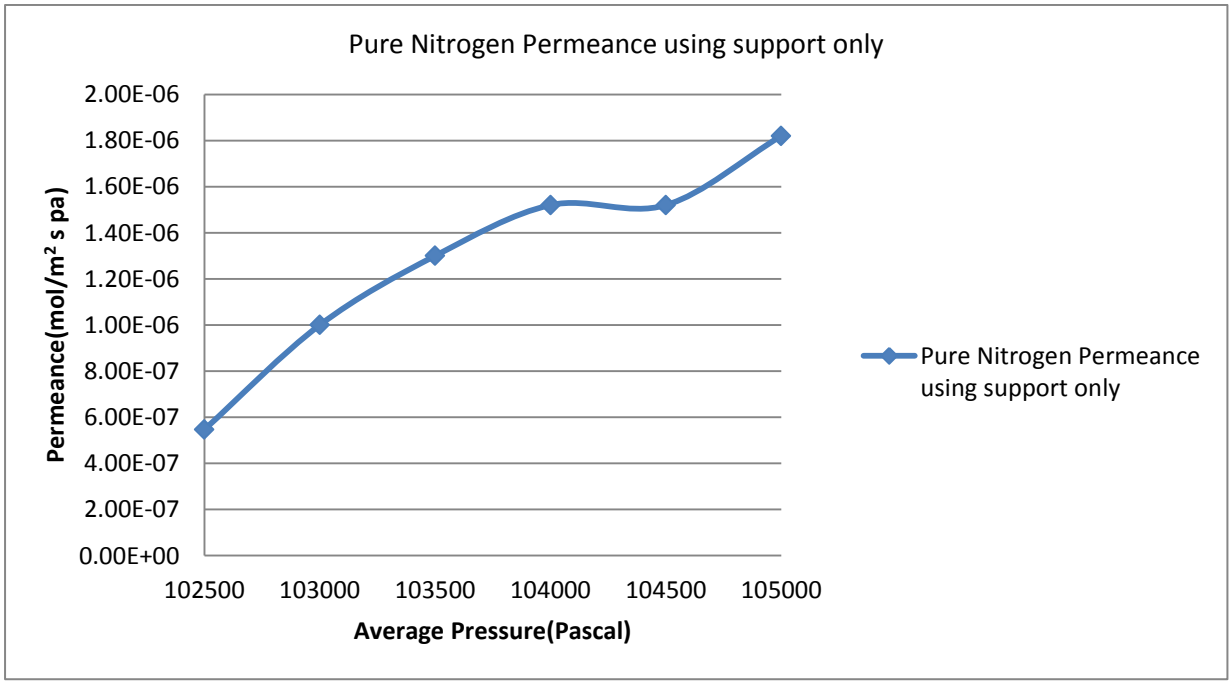

Figure 8:65: Pure Nitrogen Permeance using membrane support only

Table 8:70: Pure CO_2 permeance using membrane support only

ΔP(Bar) (P_F - P_P) Absolute	Pressure Drop (Pascal)	Average Pressure (Pascal)	Pure CO_2 Permeate Flow Rate (ml/min)	Pure CO_2 Permeate Flow Rate(mol/s)	pure CO_2 Permeance through Support Only
0.05	5000	102500	70	5.21E-05	4.25E-07
0.06	6000	103000	150	1.12E-04	7.60E-07
0.07	7000	103500	250	1.86E-04	1.08E-06
0.08	8000	104000	315	2.34E-04	1.20E-06
0.09	9000	104500	380	2.83E-04	1.28E-06
0.1	10000	105000	550	4.09E-04	1.67E-06

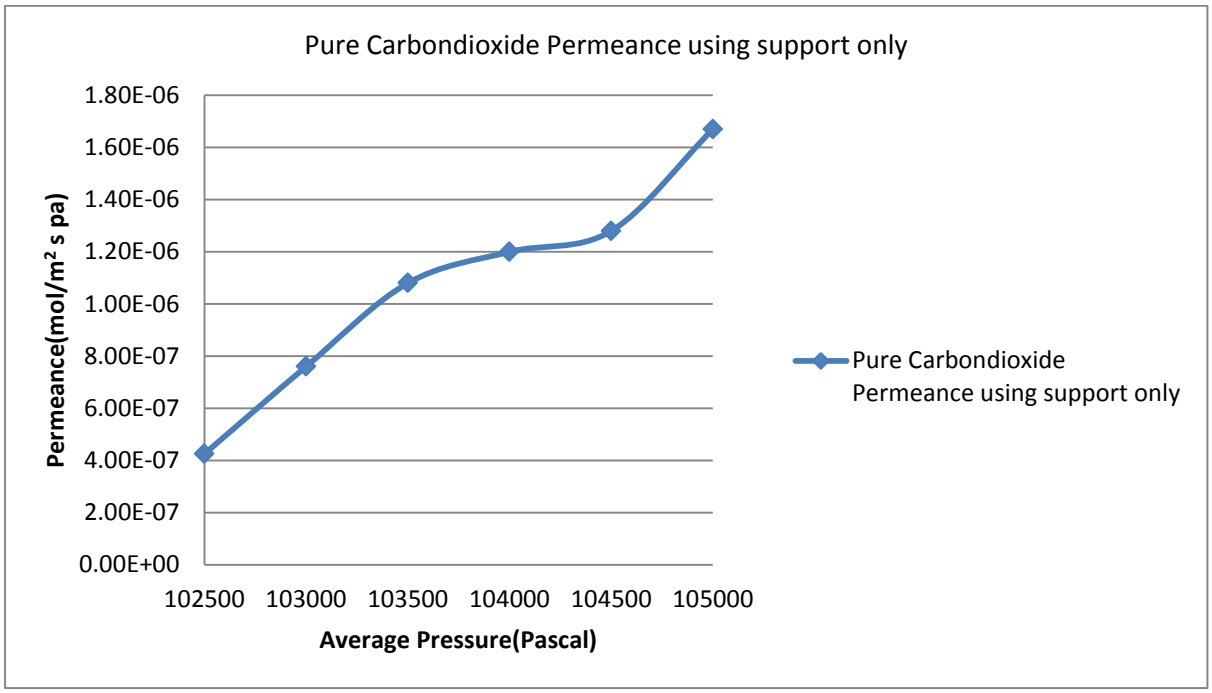

Figure 8:66: Pure CO_2 Permeance using membrane support only

Table 8:71: Pure Helium permeance using membrane support only

ΔP(Bar) (P_F - P_P) Absolute	Pressure Drop (Pascal)	Average Pressure (Pascal)	Pure Helium Permeate Flow Rate (ml/min)	Pure Helium Permeate Flow Rate(mol/s)	pure Helium Permeance through Membrane Support Only
0.05	5000	102500	200	1.49E-04	1.21E-06
0.06	6000	103000	300	2.23E-04	1.52E-06
0.07	7000	103500	400	2.98E-04	1.74E-06
0.08	8000	104000	500	3.72E-04	1.90E-06
0.09	9000	104500	560	4.17E-04	1.89E-06
0.1	10000	105000	690	5.13E-04	2.10E-06

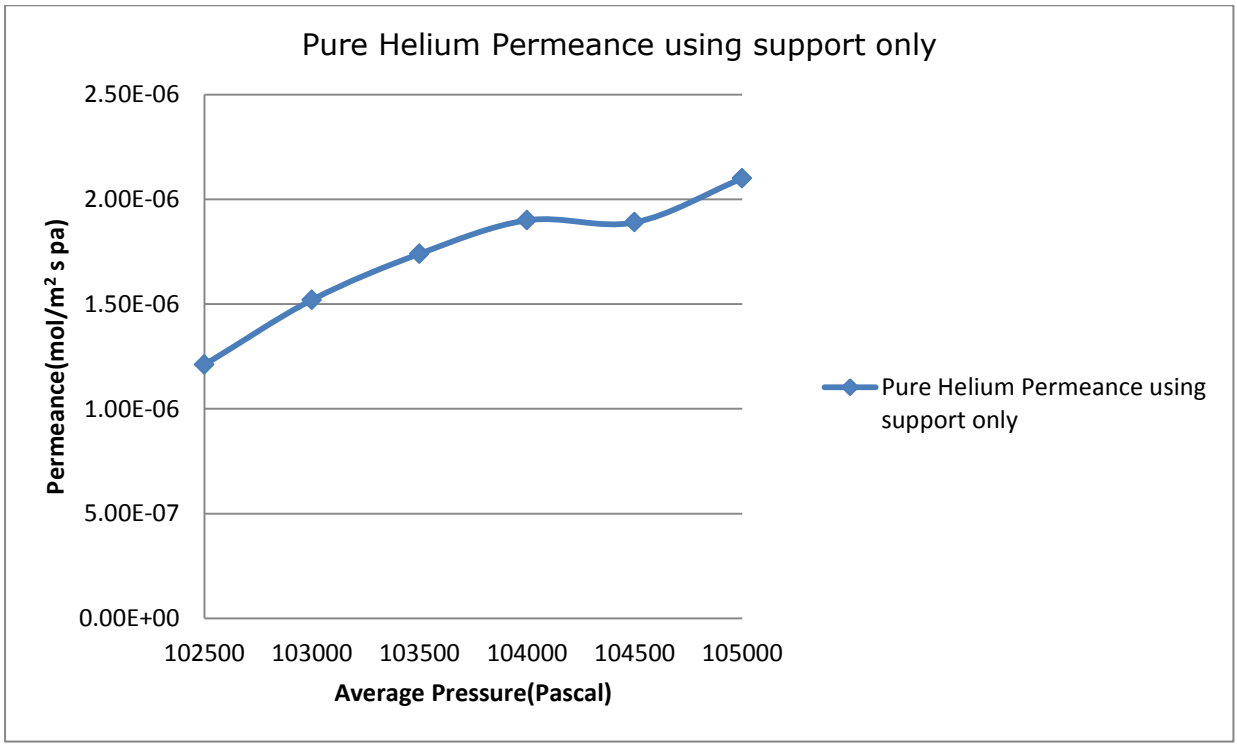

Figure 8:67: Pure Helium Permeance using support only

Table 8:72: Pure Argon permeance using membrane support only

ΔP(Bar) (P_F - P_P) Absolute	Pressure Drop (Pascal)	Average Pressure (Pascal)	Pure Argon Permeate Flow Rate (ml/min)	Pure Argon Permeate Flow Rate(mol/s)	pure Argon Permeance through Membrane Support Only
0.05	5000	102500	184	1.37E-04	1.12E-06
0.06	6000	103000	257	1.91E-04	1.30E-06
0.07	7000	103500	389	2.89E-04	1.69E-06
0.08	8000	104000	491	3.65E-04	1.86E-06
0.09	9000	104500	572	4.26E-04	1.93E-06
0.1	10000	105000	627	4.67E-04	1.90E-06

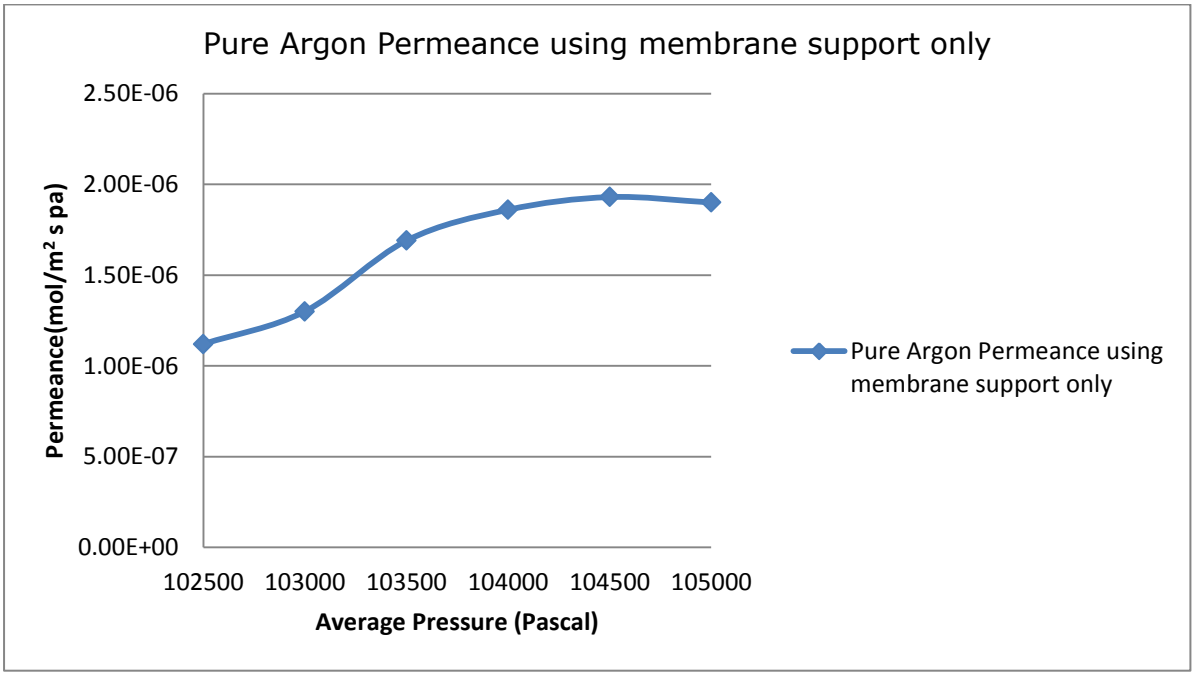

Figure 8:68: Pure Argon Permeance using membrane support only

Table 8:73: CO_2/N_2 permeance using membrane support only retentate valve fully closed

ΔP(Bar) (P_F - P_P) Absolute	Pressure Drop(Pascal)	CO_2/N_2 Permeate Flow Rate (ml/min)	CO_2/N_2 Permeate Flow Rate(mol/s)	CO_2/N_2 Permeance through Membrane Support Only without G.C
0.05	5000	138	1.03E-04	8.38E-07
0.06	6000	190	1.41E-04	9.62E-07
0.07	7000	238	1.77E-04	1.03E-06
0.08	8000	320	2.38E-04	1.21E-06
0.09	9000	400	4.98E-04	1.35E-06
0.1	10000	520	3.87E-04	1.58E-06

Table 8:74: CO_2 permeance from mixture A using membrane support only retentate valve fully closed

ΔP(Bar) (P_F - P_P) Absolute	Pressure Drop(Pascal)	Average Pressure (Pascal)	CO_2 Permeate Flow Rate (ml/min)	CO_2 Permeate Flow Rate(mol/s)	CO_2 Permeance through Membrane Support Only with G.C
0.1274	12740	8330	19.32	1.44E-05	4.61E-08
0.1284	12840	8380	26.60	1.98E-05	6.29E-08
0.1304	13040	8480	33.32	2.48E-05	7.76E-08
0.1314	13140	8530	44.80	3.33E-05	1.03E-07
0.1334	13340	8630	56.00	4.17E-05	1.28E-07
0.1344	13440	8680	72.80	5.42E-05	1.65E-07

Table 8:75: N_2 permeance from mixture A using membrane support only retentate valve fully closed

ΔP(Bar) (P_F - P_P) Absolute	Pressure Drop(Pascal)	Average Pressure (Pascal)	N_2 Permeate Flow Rate (ml/min)	N_2 Permeate Flow Rate(mol/s)	N_2 Permeance through Membrane Support Only with G.C
0.1634	16340	82130	118.68	8.83E-05	2.21E-07
0.1724	17240	82580	163.40	1.22E-04	2.89E-07
0.1804	18040	82980	204.68	1.52E-04	3.44E-07
0.1894	18940	83430	275.20	2.05E-04	4.41E-07
0.1974	19740	83830	344.00	2.56E-04	5.29E-07
0.2064	20640	84280	447.20	3.33E-04	6.58E-07

Table 8:76: CO_2 permeance from mixture A using membrane A with retentate valve fully closed

ΔP(Bar) (P_F - P_P) Absolute	Pressure Drop(Pascal)	Average Pressure (Pascal)	CO_2 Permeate Flow Rate (ml/min)	CO_2 Permeate Flow Rate(mol/s)	CO_2 Permeance through Membrane A with G.C
0.1218	12180	8610	23.58	1.75E-05	5.88E-08
0.1228	12280	8660	28.62	2.13E-05	7.08E-08
0.1248	12480	8760	36.72	2.73E-05	8.94E-08
0.1258	12580	8810	54.54	4.06E-05	1.32E-07
0.1278	12780	8910	62.64	4.67E-05	1.49E-07
0.1288	12880	8960	64.98	4.83E-05	1.53E-07

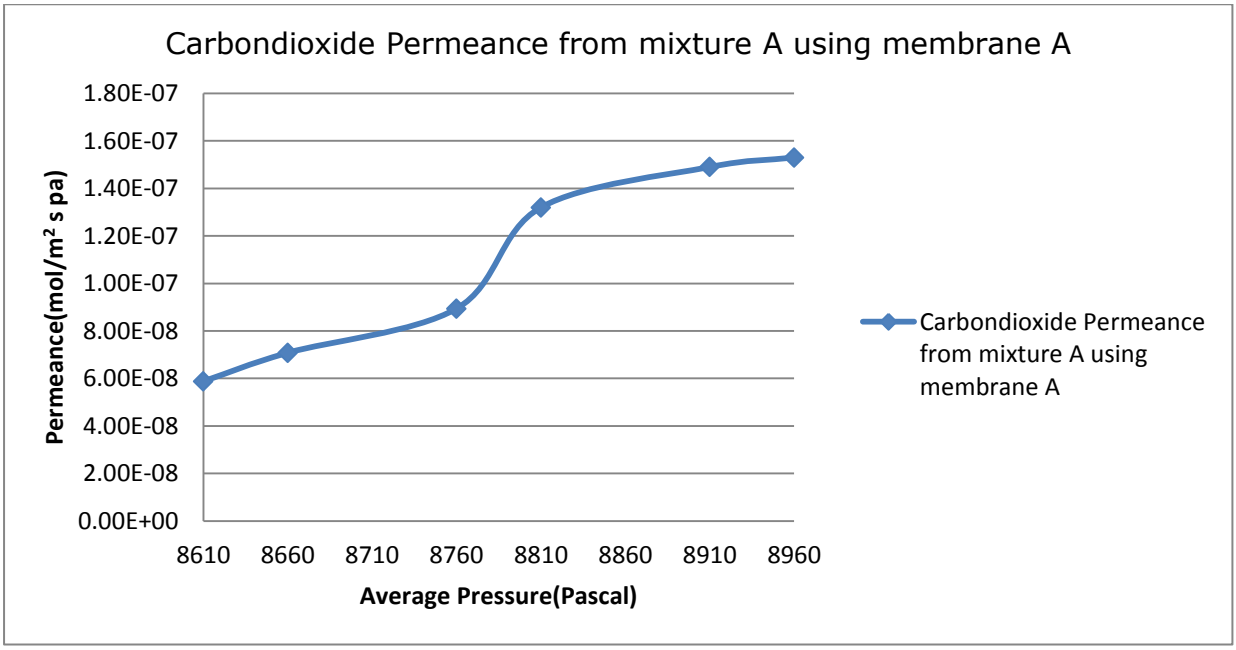

Figure 8:69: Carbondioxide Permeance from mixture A using Membrane A

Table 8:77: N_2 permeance from mixture A using membrane A with retentate valve fully closed

ΔP(Bar) (P_F - P_P) Absolute	Pressure Drop(Pascal)	Average Pressure (Pascal)	N_2 Permeate Flow Rate (ml/min)	N_2 Permeate Flow Rate(mol/s)	N_2 Permeance through Membrane A with G.C
0.1978	19780	80410	107.42	7.99E-05	1.65E-07
0.2068	20680	80860	130.38	9.70E-05	1.91E-07
0.2148	21480	81260	167.28	1.24E-04	2.36E-07
0.2238	22380	81710	248.46	1.85E-04	3.37E-07
0.2318	23180	82110	285.36	2.12E-04	3.73E-07
0.2408	24080	82560	296.02	2.20E-04	3.73E-07

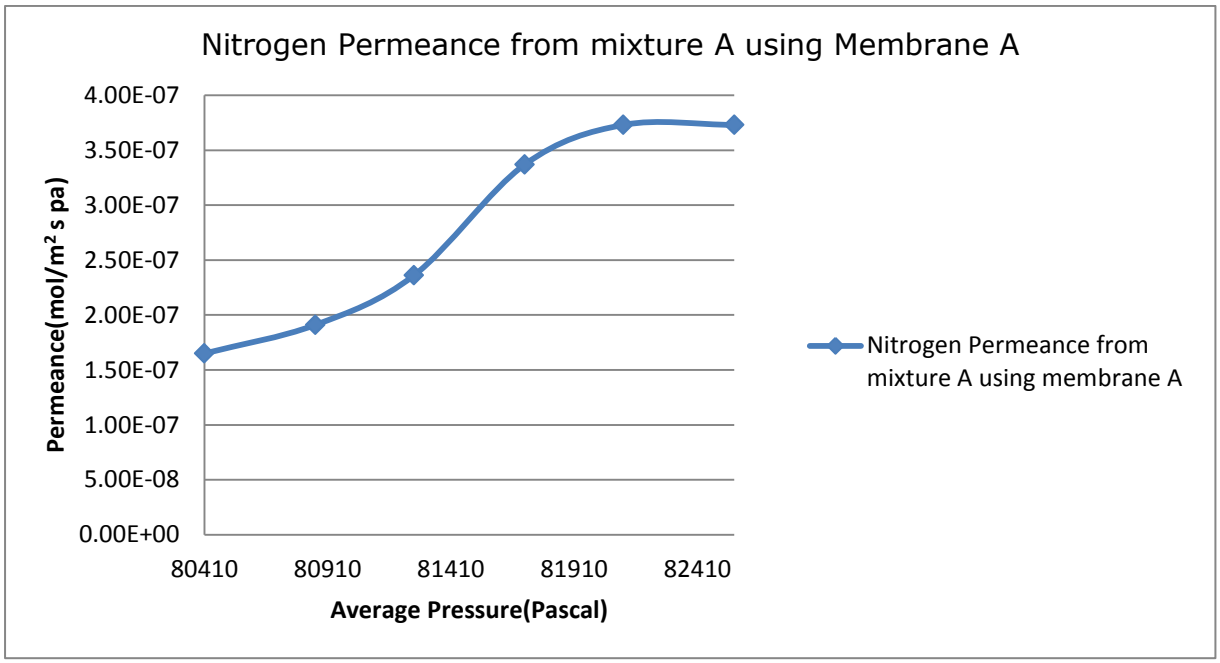

Figure 8:70: Nitrogen Permeance from mixture A using Membrane A

Table 8:78: Pure CO_2 permeance using Membrane A using retentate valve fully closed

ΔP(Bar) (P_F - P_P) Absolute	Pressure Drop(Pascal)	Average Pressure (Pascal)	Pure CO_2 Permeate Flow Rate (ml/min)	Pure CO_2 Permeate Flow Rate(mol/s)	Pure CO_2 Permeance through membrane A
0.05	5000	102500	147	1.09E-04	8.93E-07
0.06	6000	103000	200	1.49E-04	1.01E-06
0.07	7000	103500	300	2.23E-04	1.30E-06
0.08	8000	104000	450	3.35E-04	1.71E-06
0.09	9000	104500	550	4.09E-04	1.86E-06
0.1	10000	105000	600	4.46E-04	1.82E-06

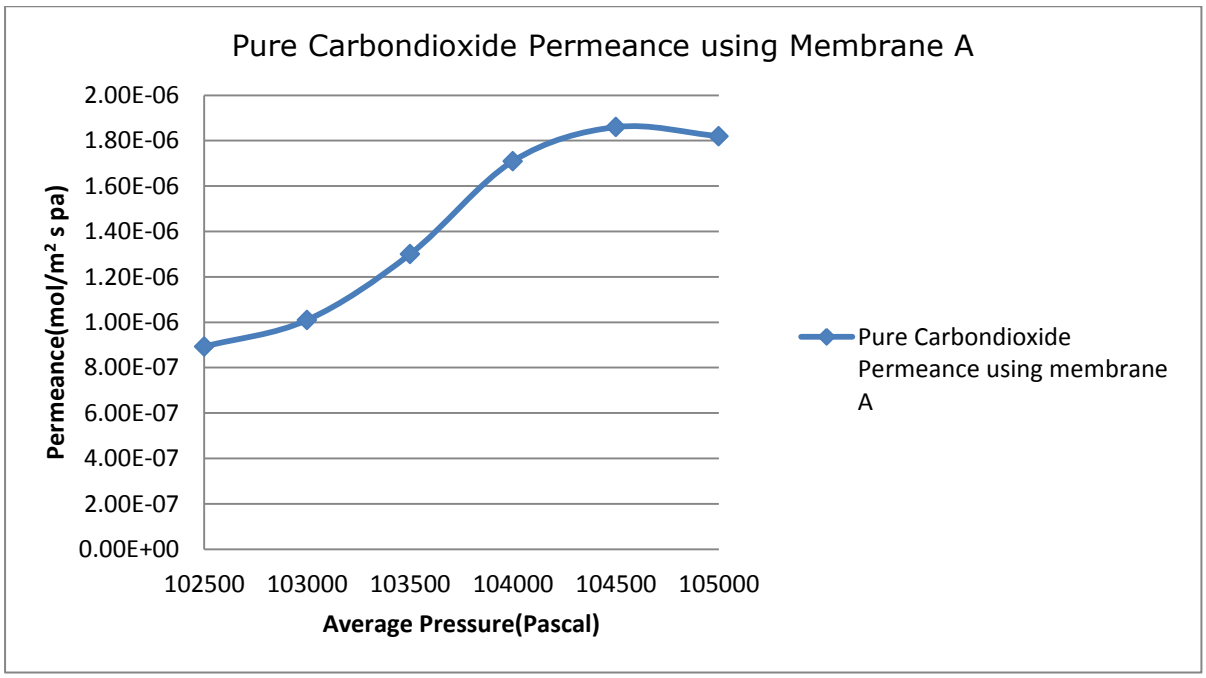

Figure 8:71: Pure Carbondioxide Permeance using Membrane A

Table 8:79: Pure CO_2 Permeance at 5000 (Pascal) Pressure Drop using membrane A

	CO_2 Permeance at 5000 (Pascal) Pressure Drop using Membrane A		
CO_2 Permeance (mol/m^2.s.pa)	In(Permeance) (mol/m^2.s.pa)	Temperature in (Kelvin)	1/Temperature $(Kelvin)^{-1}$
8.93E-07	-4.72	296	3.38E-03
7.29E-07	-14.13	338	2.96E-03
5.47E-07	-14.42	423	2.36E-03
3.04E-07	-15.00	523	1.91E-03
2.13E-07	-15.36	723	1.38E-03

Table 8:80: Pure CO_2 Permeance at 6000 (Pascal) Pressure Drop using membrane A

	CO_2 Permeance at 6000 (Pascal) Pressure Drop using Membrane A		
CO_2 Permeance (mol/m^2.s.pa)	In(Permeance) (mol/m^2.s.pa)	Temperature in (Kelvin)	1/Temperature $(Kelvin)^{-1}$
1.01E-06	-13.81	296	3.38E-03
8.60E-07	-13.97	338	2.96E-03
7.59E-07	-14.09	423	2.36E-03
5.06E-07	-14.50	523	1.91E-03
3.04E-07	-15.01	723	1.38E-03

Table 8:81: Pure CO_2 Permeance at 7000 (Pascal) Pressure Drop using membrane A

	CO_2 Permeance at 7000 (Pascal) Pressure Drop using Membrane A		
CO_2 Permeance (mol/m^2.s.pa)	In(Permeance) (mol/m^2.s.pa)	Temperature in (Kelvin)	1/Temperature $(Kelvin)^{-1}$
1.30E-06	-13.55	296	3.38E-03
1.08E-06	-13.74	338	2.96E-03
8.68E-07	-13.96	423	2.36E-03
6.51E-07	-14.24	523	1.91E-03
5.47E-07	-14.42	723	1.38E-03

Table 8:82: Pure CO_2 Permeance at 8000 (Pascal) Pressure Drop using membrane A

CO_2 Permeance at 8000 (Pascal) Pressure Drop using Membrane A			
CO_2 Permeance (mol/m^2.s.pa)	In(Permeance) (mol/m^2.s.pa)	Temperature in (Kelvin)	1/Temperature $(Kelvin)^{-1}$
1.71E-06	-13.28	296	3.38E-03
1.25E-06	-13.59	338	2.96E-03
1.02E-06	-13.80	423	2.36E-03
7.59E-07	-14.09	523	1.91E-03
7.29E-07	-14.13	723	1.38E-03

Table 8:83: Pure CO_2 Permeance at 9000 (Pascal) Pressure Drop using membrane A

CO_2 Permeance at 9000 (Pascal) Pressure Drop using Membrane A			
CO_2 Permeance (mol/m^2.s.pa)	In(Permeance) (mol/m^2.s.pa)	Temperature in (Kelvin)	1/Temperature $(Kelvin)^{-1}$
1.86E-06	-13.94	296	3.38E-03
1.42E-06	-13.46	338	2.96E-03
1.18E-06	-13.65	423	2.36E-03
9.11E-07	-13.91	523	1.91E-03
5.40E-07	-14.43	723	1.38E-03

Table 8:84 : Pure CO_2 Permeance at 10000 (Pascal) Pressure Drop using membrane A

	CO_2 Permeance at 10000 (Pascal) Pressure Drop using Membrane A		
CO_2 Permeance ($mol/m^2.s.pa$)	In(Permeance) ($mol/m^2.s.pa$)	Temperature in (Kelvin)	1/Temperature $(Kelvin)^{-1}$
1.82E-06	-13.22	296	3.38E-03
1.52E-06	-13.40	338	2.96E-03
1.31E-06	-13.55	423	2.36E-03
1.06E-06	-13.76	523	1.91E-03
6.07E-06	-12.01	723	1.38E-03

Table 8:85: Pure N_2 permeance using Membrane A with retentate valve fully closed

ΔP(Bar) (P_F - P_P) Absolute	Pressure Drop(Pascal)	Average Pressure (Pascal)	Pure N_2 Permeate Flow Rate (ml/min)	Pure N_2 Permeate Flow Rate(mol/s)	Pure N_2 Permeance through Membrane A
0.05	5000	102500	102	7.59E-05	6.20E-07
0.06	6000	103000	200	1.49E-04	1.01E-06
0.07	7000	103500	385	2.86E-04	1.67E-06
0.08	8000	104000	491	3.65E-04	1.86E-06
0.09	9000	104500	506	3.76E-04	1.71E-06
0.1	10000	105000	590	4.39E-04	1.79E-06

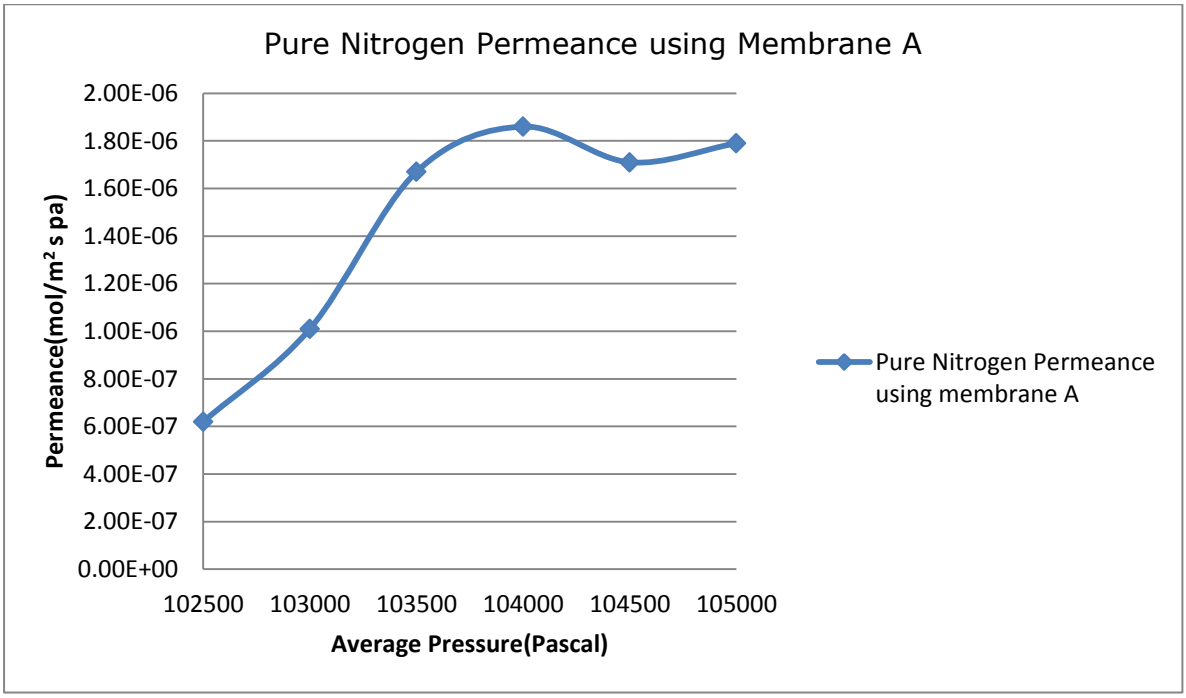

Figure 8:72: Pure Nitrogen Permeance using Membrane A

Table 8:86: Pure N_2 permeance using Membrane A at 296K with retentate valve fully closed

ΔP(Bar) (P_F - P_P) Absolute	Pressure Drop(Pascal)	Pure N_2 Permeate Flow Rate (ml/min)	Pure N_2 Permeate Flow Rate(mol/s)	Pure N_2 Permeance through Membrane A at 296K
0.05	5000	102	7.59E-05	6.20E-07
0.06	6000	200	1.49E-04	1.01E-06
0.07	7000	385	2.86E-04	1.67E-06
0.08	8000	491	3.65E-04	1.86E-06
0.09	9000	506	3.76E-04	1.71E-06
0.1	10000	590	4.39E-04	1.79E-06

Table 8:87: Pure N_2 permeance using Membrane A at 338K with retentate valve fully closed

ΔP(Bar) (P_F - P_P) Absolute	Pressure Drop(Pascal)	Pure N_2 Permeate Flow Rate (ml/min)	Pure N_2 Permeate Flow Rate(mol/s)	Pure N_2 Permeance through Membrane A at 338k
0.05	5000	91	6.77E-05	5.52E-07
0.06	6000	140	1.04E-04	7.09E-07
0.07	7000	265	1.97E-04	1.15E-06
0.08	8000	310	2.31E-04	1.18E-06
0.09	9000	420	3.13E-04	1.42E-06
0.1	10000	510	3.79E-04	1.55E-06

Table 8:88: Pure N_2 permeance using Membrane A at 423K with retentate valve fully closed

ΔP(Bar) (P_F - P_P) Absolute	Pressure Drop(Pascal)	Pure N_2 Permeate Flow Rate (ml/min)	Pure N_2 Permeate Flow Rate(mol/s)	Pure N_2 Permeance through Membrane A at 423k
0.05	5000	83	6.18E-05	5.04E-07
0.06	6000	120	8.93E-05	6.07E-07
0.07	7000	189	1.41E-04	8.20E-07
0.08	8000	250	1.86E-04	9.49E-07
0.09	9000	350	2.60E-04	1.18E-06
0.1	10000	425	3.16E-04	1.29E-06

Table 8:89: Pure N_2 permeance using Membrane A at 523K with retentate valve fully closed

ΔP(Bar)	Pressure	Pure N_2	Pure N_2	Pure N_2 Permeance

(P_F - P_P) Absolute	Drop(Pascal)	Permeate Flow Rate (ml/min)	Permeate Flow Rate(mol/s)	through Membrane A at 523k
0.05	5000	51	3.79E-05	3.10E-07
0.06	6000	98	7.29E-05	4.96E-07
0.07	7000	150	1.12E-04	6.51E-07
0.08	8000	210	1.56E-04	7.97E-07
0.09	9000	301	2.24E-04	1.02E-06
0.1	10000	389	2.89E-04	1.18E-06

Table 8:90: Pure N_2 permeance using Membrane A at 723K with retentate valve fully closed

ΔP(Bar) (P_F - P_P) Absolute	Pressure Drop(Pascal)	Pure N_2 Permeate Flow Rate (ml/min)	Pure N_2 Permeate Flow Rate(mol/s)	Pure N_2 Permeance through Membrane A at 723k
0.05	5000	45	3.35E-05	2.73E-07
0.06	6000	74	5.51E-05	3.75E-07
0.07	7000	120	8.93E-05	5.21E-07
0.08	8000	170	1.26E-04	6.45E-07
0.09	9000	240	1.79E-04	8.10E-07
0.1	10000	300	2.23E-04	9.11E-07

Table 8:91: Pure CO_2 permeance using Membrane A at 296K with retentate valve fully closed

ΔP(Bar) (P_F - P_P) Absolute	Pressure Drop(Pascal)	Pure CO_2 Permeate Flow Rate (ml/min)	Pure CO_2 Permeate Flow Rate(mol/s)	pure CO_2 Permeance through Membrane A at 296K
0.05	5000	147	1.09E-04	8.93E-07
0.06	6000	200	1.49E-04	1.01E-06
0.07	7000	300	2.23E-04	1.30E-06
0.08	8000	450	3.35E-04	1.71E-06
0.09	9000	550	4.09E-04	1.86E-06
0.1	10000	600	4.46E-04	1.82E-06

Table 8:92: Pure CO_2 permeance using Membrane A at 338K with retentate valve fully closed

ΔP(Bar) (P_F - P_P) Absolute	Pressure Drop(Pascal)	Pure CO_2 Permeate Flow Rate (ml/min)	Pure CO_2 Permeate Flow Rate(mol/s)	pure CO_2 Permeance through Membrane A at 338K
0.05	5000	120	8.93E-05	7.29E-07
0.06	6000	170	1.26E-04	8.60E-07
0.07	7000	250	1.86E-04	1.08E-06
0.08	8000	330	2.46E-04	1.25E-06
0.09	9000	420	3.13E-04	1.42E-06
0.1	10000	500	3.72E-04	1.52E-06

Table 8:93: Pure CO_2 permeance using Membrane A at 423K with retentate valve fully closed

ΔP(Bar) (P_F - P_P) Absolute	Pressure Drop(Pascal)	Pure CO_2 Permeate Flow Rate (ml/min)	Pure CO_2 Permeate Flow Rate(mol/s)	pure CO_2 Permeance through Membrane A at 423K
0.05	5000	90	6.70E-05	5.47E-07
0.06	6000	150	1.12E-04	7.59E-07
0.07	7000	200	1.49E-04	8.68E-07
0.08	8000	270	2.00E-04	1.02E-06
0.09	9000	350	2.60E-04	1.18E-06
0.1	10000	430	3.20E-04	1.31E-06

Table 8:94: Pure CO_2 permeance using Membrane A at 523K with retentate valve fully closed

ΔP(Bar) (P_F - P_P) Absolute	Pressure Drop(Pascal)	Pure CO_2 Permeate Flow Rate (ml/min)	Pure CO_2 Permeate Flow Rate(mol/s)	pure CO_2 Permeance through Membrane A at 523K
0.05	5000	50	3.72E-05	3.04E-07
0.06	6000	100	7.44E-05	5.06E-07
0.07	7000	150	1.12E-04	6.51E-07
0.08	8000	200	21.49E-04	7.59E-07
0.09	9000	270	2.00E-04	9.11E-07
0.1	10000	350	2.60E-04	1.06E-06

Table 8:95: Pure CO_2 permeance using Membrane A at 723K with retentate valve fully closed

ΔP(Bar) (P_F - P_P) Absolute	Pressure Drop(Pascal)	Pure CO_2 Permeate Flow Rate (ml/min)	Pure CO_2 Permeate Flow Rate(mol/s)	pure CO_2 Permeance through Membrane A at 723K
0.05	5000	35	2.60E-05	2.13E-07
0.06	6000	60	4.46E-05	3.04E-07
0.07	7000	90	6.70E-05	5.47E-07
0.08	8000	120	8.93E-05	7.29E-07
0.09	9000	160	1.19E-04	5.40E-07
0.1	10000	200	1.49E-04	6.07E-06

Table 8:96: Pure CO_2 permeance using Membrane B with retentate valve fully closed

ΔP(Bar) (P_F - P_P) Absolute	Pressure Drop(Pascal)	Pure CO_2 Permeate Flow Rate (ml/min)	Pure CO_2 Permeate Flow Rate(mol/s)	Pure CO_2 Permeance through membrane B
0.05	5000	200	1.49E-04	1.22E-06
0.06	6000	250	1.86E-04	1.27E-06
0.07	7000	370	2.75E-04	1.60E-06
0.08	8000	540	4.02E-04	2.05E-06
0.09	9000	660	4.91E-04	2.23E-06
0.1	10000	750	5.58E-04	2.28E-06

Table 8:97: CO_2 permeance from mixture A using Membrane B with retentate valve fully closed

ΔP(Bar) (P_F - P_P) Absolute	Pressure Drop(Pascal)	CO_2 Permeate Flow Rate (ml/min)	CO_2 Permeate Flow Rate(mol/s)	CO_2 Permeance through Membrane B with G.C
0.112	11200	12.50	9.30E-06	3.39E-08
0.113	11300	19.99	1.49E-05	5.37E-08
0.115	11500	23.00	1.71E-05	6.07E-08
0.116	11600	35.00	2.60E-05	9.16E-08
0.118	11800	41.25	3.07E-05	1.06E-07
0.119	11900	46.25	3.44E-05	1.18E-07

Table 8:98: N_2 permeance from mixture A using Membrane B with retentate valve fully closed

ΔP(Bar) (P_F - P_P) Absolute	Pressure Drop(Pascal)	N_2 Permeate Flow Rate (ml/min)	N_2 Permeate Flow Rate(mol/s)	N_2 Permeance through Membrane B
0.258	25800	37.50	2.79E-05	4.41E-08
0.267	26700	60.01	4.47E-05	6.83E-08
0.275	27500	90.00	6.70E-05	9.94E-08
0.284	28400	105.00	7.81E-05	1.12E-07
0.292	29200	123.75	9.21E-05	1.29E-07
0.301	30100	138.75	1.03E-04	1.40E-06

Table 8:99:CO_2 permeance from mixture A using Membrane C after first dip with retentate valve fully closed

ΔP(Bar) (P_F - P_P) Absolute	Pressure Drop(Pascal)	CO_2 Permeate Flow Rate (ml/min)	CO_2 Permeate Flow Rate(mol/s)	CO_2 Permeance through Membrane C
0.105	10500	10.50	7.81E-06	3.04E-08
0.106	10600	16.49	1.23E-05	4.72E-08
0.108	10800	22.79	1.70E-05	6.41E-08
0.109	10900	30.00	2.23E-05	8.36E-08
0.111	11100	36.00	2.68E-05	9.85E-08
0.112	11200	42.00	3.13E-05	1.14E-07

Table 8:100: CO_2 permeability from mixture A using Membrane C after first dip with retentate valve fully close

Feed Partial pressure of the CO_2 (Pascal)	Permeate partial pressure of the $C0_2$ (Pascal)	Average Pressure (Pascal)	CO_2 Permeate Flow Rate (ml/min)	CO_2 Permeance through Membrane C	CO_2 Permeability through Membrane C after first dip
14700	4200	9450	10.50	3.04E-08	9.59E-12
14800	4200	9500	16.49	4.72E-08	1.49E-11
15000	4200	9600	22.79	6.41E-08	2.02E-11
15100	4200	9650	30.00	8.36E-08	2.64E-11
15300	4200	9750	36.00	9.85E-08	3.11E-11
15400	4200	9800	42.00	1.14E-07	3.60E-11

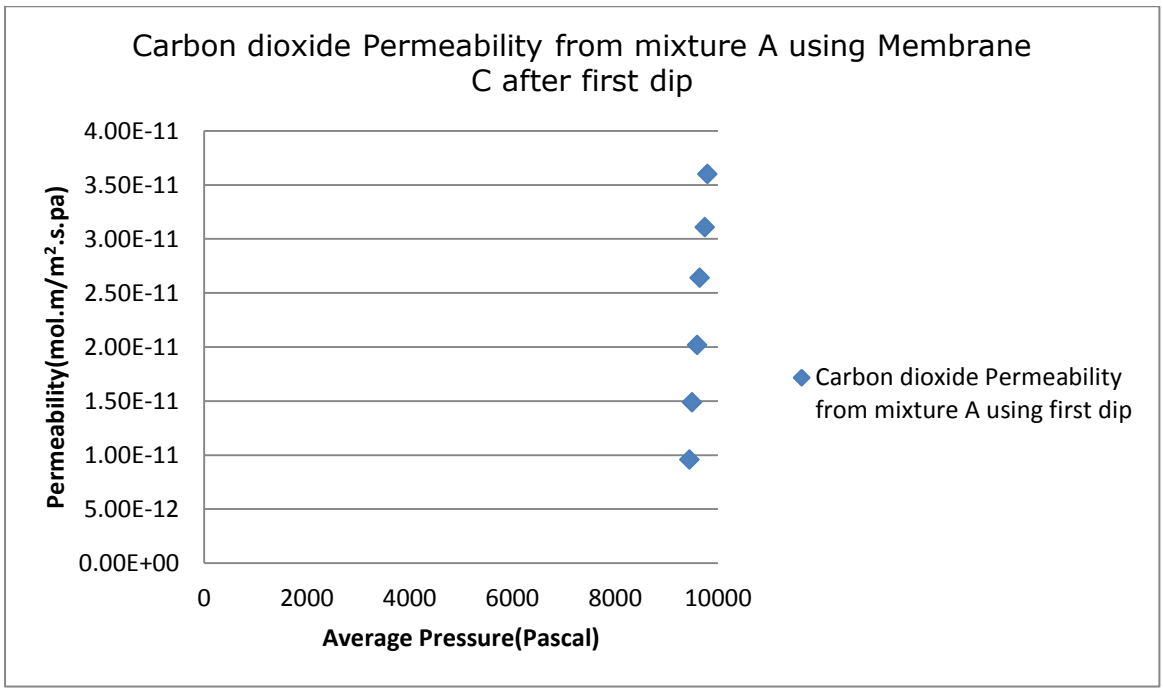

Figure 8:73: CO_2 Permeability from mixture A using Membrane C with retentate valve fully closed

Table 8:101: N_2 permeance from mixture A using Membrane C after first dip with retentate valve fully closed

ΔP(Bar) (P_F - P_P) Absolute	Pressure Drop(Pascal)	N_2 Permeate Flow Rate (ml/min)	N_2 Permeate Flow Rate (mol/s)	N_2 Permeance through Membrane C after first dip
0.301	30100	24.50	1.82E-05	2.47E-08
0.310	31000	38.51	2.87E-05	3.78E-08
0.318	31800	53.21	3.96E-05	5.08E-08
0.327	32700	70.00	5.21E-05	6.50E-08
0.335	33500	84.00	6.25E-05	7.61E-08
0.344	34400	98.00	7.29E-05	8.65E-08

Table 8:102: N_2 permeability from mixture A using Membrane C after first dip with retentate valve fully closed

Feed Partial pressure of the N_2 (Pascal)	Permeate partial pressure of the N_2 (Pascal)	Average Pressure (Pascal)	N_2 Permeate Flow Rate (ml/min)	N_2 Permeance through Membrane C	N_2 Permeability through Membrane C after first dip
90300	60200	75250	24.50	2.47E-08	7.79E-12
91200	60200	75700	38.51	3.78E-08	1.19E-11
92000	60200	76100	53.21	5.08E-08	1.60E-11
92900	60200	76550	70.00	6.50E-08	2.05E-11
93700	60200	76950	84.00	7.61E-08	2.40E-11
94600	60200	77400	98.00	8.65E-08	2.73E-11

Table 8:103: CO_2 permeance from mixture A using Membrane C after second dip with retentate valve fully closed

ΔP(Bar) (P_F - P_P) Absolute	Pressure Drop(Pascal)	CO_2 Permeate Flow Rate (ml/min)	CO_2 Permeate Flow Rate(mol/s)	CO_2 Permeance through Membrane C after second dip
0.105	10500	9.00	6.70E-06	2.60E-08
0.106	10600	12.00	8.93E-06	3.44E-08
0.108	10800	16.49	1.23E-05	4.64E-08
0.109	10900	22.50	1.67E-05	6.27E-08
0.111	11100	25.50	1.90E-05	6.98E-08
0.112	11200	28.50	2.12E-05	7.73E-08

Table 8:104: CO_2 permeability from mixture A using Membrane C after second dip with retentate valve fully closed

Feed Partial pressure of the CO_2 (Pascal)	Permeate partial pressure of the $C0_2$ (Pascal)	Average Pressure (Pascal)	CO_2 Permeate Flow Rate (ml/min)	CO_2 Permeance through Membrane C	CO_2 Permeability through Membrane C after second dip
14700	4200	9450	9.00	2.60E-08	5.00E-12
14800	4200	9500	12.00	3.44E-08	6.63E-12
15000	4200	9600	16.49	4.64E-08	8.94E-12
15100	4200	9650	22.50	6.27E-08	1.21E-11
15300	4200	9750	25.50	6.98E-08	1.34E-11
15400	4200	9800	28.50	7.73E-08	1.49E-11

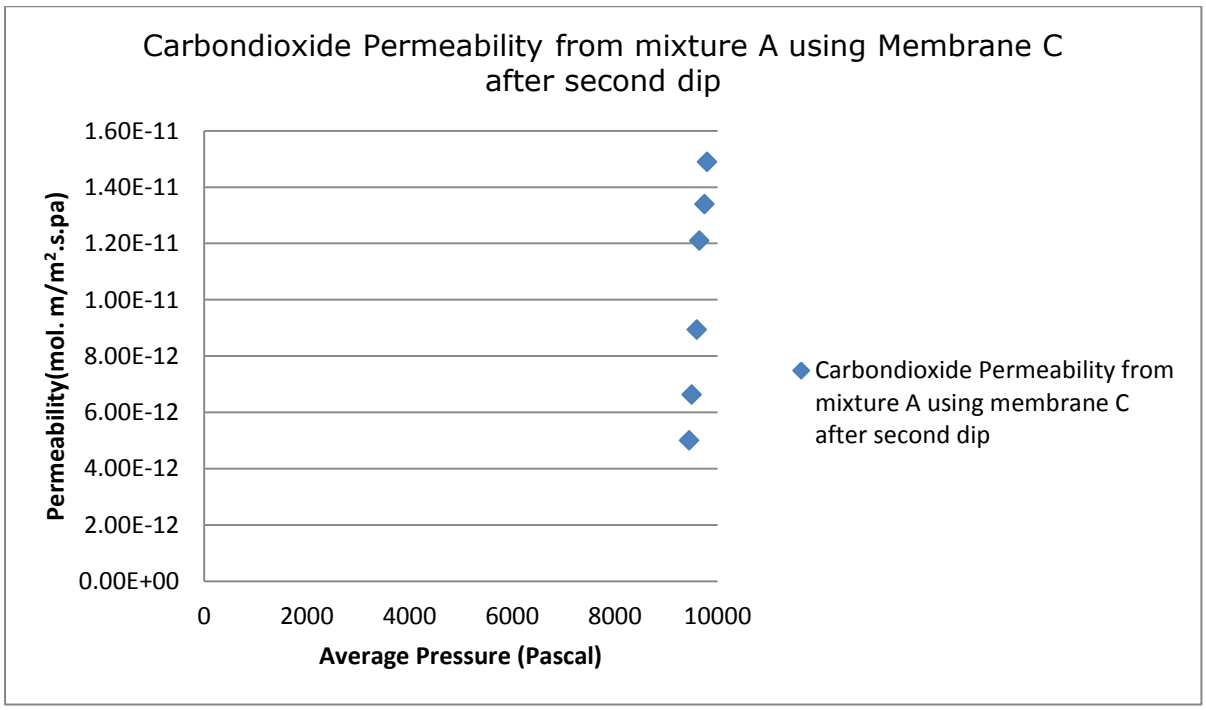

Figure 8:74: CO_2 permeability from mixture A using Membrane C after second dip with retentate valve fully closed

Table 8:105: N_2 permeance from mixture A using Membrane C after second dip with retentate valve fully closed

ΔP(Bar) (P_F - P_P) Absolute	Pressure Drop(Pascal)	N_2 Permeate Flow Rate (ml/min)	N_2 Permeate Flow Rate (mol/s)	N_2 Permeance through Membrane C after second dip
0.301	30100	21.00	1.56E-05	2.12E-08
0.310	31000	28.00	2.08E-05	2.74E-08
0.318	31800	38.51	2.86E-05	3.68E-08
0.327	32700	52.50	3.91E-05	4.88E-08
0.335	33500	56.00	4.17E-05	5.08E-08
0.344	34400	66.50	4.95E-05	5.87E-08

Table 8:106: N_2 permeability from mixture A using Membrane C after second dip with retentate valve fully closed.

Feed Partial pressure of the N_2 (Pascal)	Permeate partial pressure of the N_2 (Pascal)	Average Pressure (Pascal)	N_2 Permeate Flow Rate (ml/min)	N_2 Permeance through Membrane C	N_2 Permeability through Membrane C after second dip
90300	60200	75250	21.00	1.56E-05	3.00E-09
91200	60200	75700	28.00	2.08E-05	4.01E-09
92000	60200	76100	38.51	2.86E-05	5.51E-09
92900	60200	76550	52.50	3.91E-05	7.53E-09
93700	60200	76950	56.00	4.17E-05	8.03E-09
94600	60200	77400	66.50	4.95E-05	9.53E-09

Table 8:107: CO_2 permeance from mixture A using Membrane C after third dip with retentate valve fully closed

ΔP(Bar) (P_F - P_P) Absolute	Pressure Drop(Pascal)	CO_2 Permeate Flow Rate (ml/min)	CO_2 Permeate Flow Rate(mol/s)	CO_2 Permeance through Membrane C after third dip
0.105	10500	4.50	3.35E-06	1.30E-08
0.106	10600	7.50	5.58E-06	2.15E-08
0.108	10800	10.50	7.81E-06	2.95E-08
0.109	10900	15.00	1.12E-05	4.18E-08
0.111	11100	19.50	1.45E-05	5.34E-08
0.112	11200	22.50	1.67E-05	6.10E-08

Table 8:108 CO_2 permeability from mixture A using Membrane C after third dip with retentate valve fully closed

Feed Partial pressure of the CO_2 (Pascal)	Permeate partial pressure of the $C0_2$ (Pascal)	Average Pressure (Pascal)	CO_2 Permeate Flow Rate (ml/min)	CO_2 Permeance through Membrane C	CO_2 Permeability through Membrane C after third dip
14700	4200	9450	4.50	1.30E-08	2.55E-12
14800	4200	9500	7.50	2.15E-08	4.22E-12
15000	4200	9600	10.50	2.95E-08	5.80E-12
15100	4200	9650	15.00	4.18E-08	8.21E-12
15300	4200	9750	19.50	5.34E-08	1.05E-11
15400	4200	9800	22.50	6.10E-08	1.20E-11

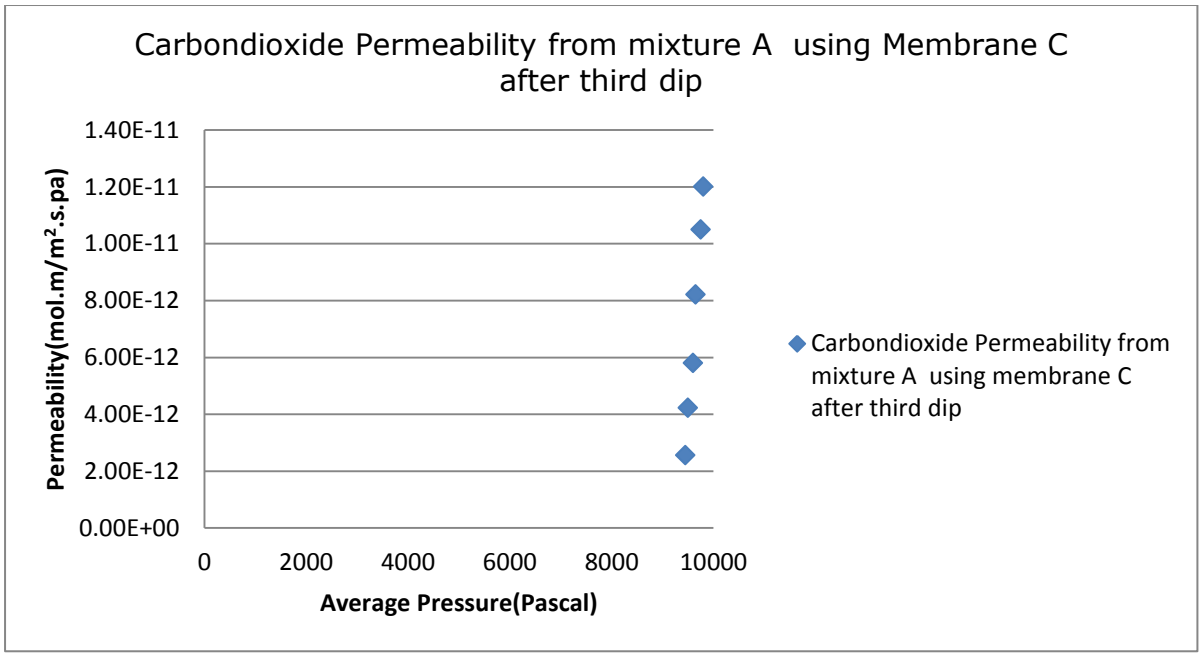

Figure 8:75: CO_2 permeability from mixture A using Membrane C after third dip with retentate valve fully closed.

Table 8:109: N_2 permeance from mixtures A using Membrane C after third dip with retentate valve fully closed

ΔP(Bar) (P_F - P_P) Absolute	Pressure Drop(Pascal)	N_2 Permeate Flow Rate (ml/min)	N_2 Permeate Flow Rate (mol/s)	N_2 Permeance through Membrane C after third dip
0.301	30100	10.50	7.81E-06	1.06E-08
0.310	31000	17.50	1.30E-05	1.71E-08
0.318	31800	24.50	1.82E-05	2.34E-08
0.327	32700	35.00	2.60E-05	3.25E-08
0.335	33500	45.50	3.39E-05	4.12E-08
0.344	34400	52.50	3.91E-05	4.63E-08

Table 8:110: N_2 permeability from mixture A using Membrane C after third dip with retentate valve fully closed.

Feed Partial pressure of the N_2 (Pascal)	Permeate partial pressure of the N_2 (Pascal)	Average Pressure (Pascal)	N_2 Permeate Flow Rate (ml/min)	N_2 Permeance through Membrane C	N_2 Permeability through Membrane C after second dip
90300	60200	75250	10.50	1.06E-08	2.08E-12
91200	60200	75700	17.50	1.71E-08	3.36E-12
92000	60200	76100	24.50	2.34E-08	4.60E-12
92900	60200	76550	35.00	3.25E-08	6.39E-12
93700	60200	76950	45.50	4.12E-08	8.10E-12
94600	60200	77400	52.50	4.63E-08	9.10E-12

Table 8:111:CO_2 permeance from mixture A using Membrane C after fourth dip with retentate valve fully closed

ΔP(Bar) (P_F - P_P) Absolute	Pressure Drop(Pascal)	CO_2 Permeate Flow Rate (ml/min)	CO_2 Permeate Flow Rate(mol/s)	CO_2 Permeance through Membrane C after fourth dip
0.105	10500	0.90	6.70E-07	2.60E-09
0.106	10600	2.40	1.79E-06	6.88E-09
0.108	10800	3.60	2.68E-06	1.01E-08
0.109	10900	5.70	4.24E-06	1.59E-08
0.111	11100	7.50	5.58E-06	2.05E-08
0.112	11200	10.50	7.81E-06	2.85E-08

Table 8:112:CO_2 permeability from mixture A using Membrane C after fourth dip with retentate valve fully closed

Feed Partial pressure of the CO_2 (Pascal)	Permeate partial pressure of the $C0_2$ (Pascal)	Average Pressure (Pascal)	CO_2 Permeate Flow Rate (ml/min)	CO_2 Permeance through Membrane C	CO_2 Permeability through Membrane C after fourth dip
14700	4200	9450	0.90	2.60E-09	5.20E-13
14800	4200	9500	2.40	6.88E-09	1.38E-12
15000	4200	9600	3.60	1.01E-08	2.02E-12
15100	4200	9650	5.70	1.59E-08	3.18E-12
15300	4200	9750	7.50	2.05E-08	4.10E-12
15400	4200	9800	10.50	2.85E-08	5.70E-12

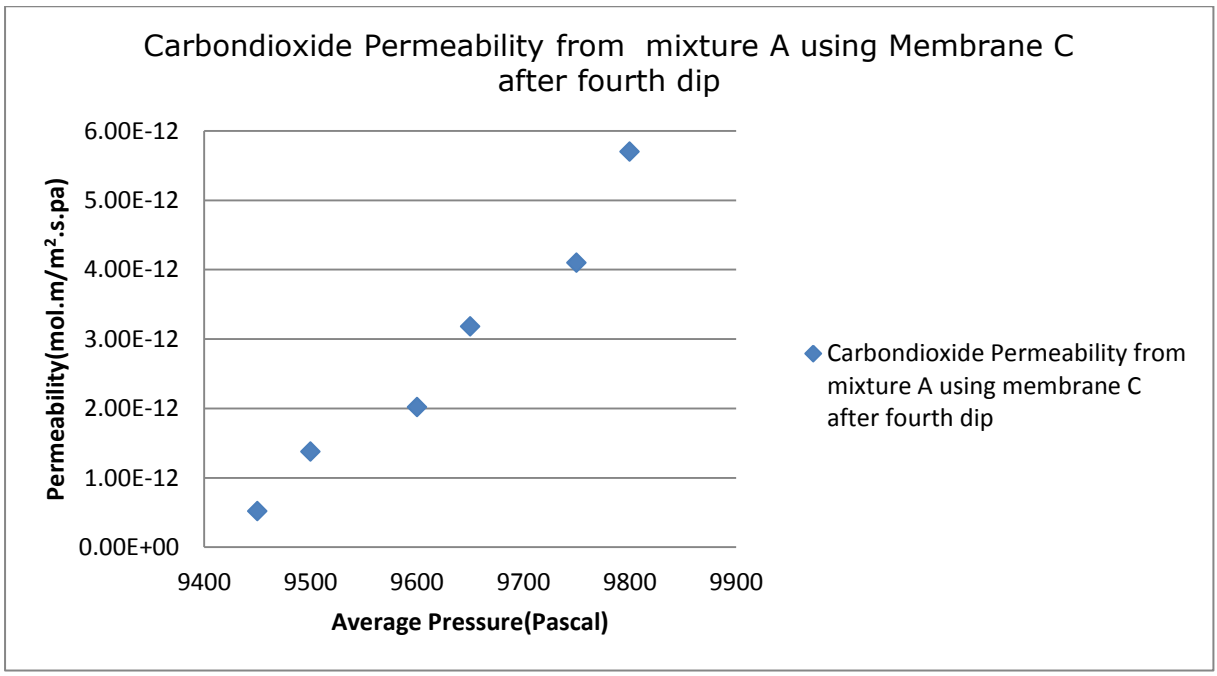

Figure 8:76: CO_2 permeability from mixture A using Membrane C after fourth dip with retentate valve fully closed

Table 8:113: N_2 permeance from mixture A using Membrane C after fourth dip with retentate valve fully closed

ΔP(Bar) (P_F - P_P) Absolute	Pressure Drop(Pascal)	N_2 Permeate Flow Rate (ml/min)	N_2 Permeate Flow Rate (mol/s)	N_2 Permeance through Membrane C after fourth dip
0.301	30100	2.10	1.56E-06	2.12E-09
0.310	31000	5.60	4.17E-06	5.49E-09
0.318	31800	8.40	6.25E-06	8.02E-09
0.327	32700	13.30	9.90E-06	1.24E-08
0.335	33500	17.50	1.30E-05	1.59E-08
0.344	34400	24.50	1.82E-05	2.16E-08

Table 8:114: N_2 permeability from mixture A using Membrane C after fourth dip with retentate valve fully closed

Feed Partial pressure of the N_2 (Pascal)	Permeate partial pressure of the N_2 (Pascal)	Average Pressure (Pascal)	N_2 Permeate Flow Rate (ml/min)	N_2 Permeance through Membrane C	N_2 Permeability through Membrane C after second dip
90300	60200	75250	2.10	2.12E-09	4.24E-13
91200	60200	75700	5.60	5.49E-09	1.10E-12
92000	60200	76100	8.40	8.02E-09	1.60E-12
92900	60200	76550	13.30	1.24E-08	2.48E-12
93700	60200	76950	17.50	1.59E-08	3.18E-12
94600	60200	77400	24.50	2.16E-08	4.32E-12

Table 8:115: Pure Methane permeance using Membrane C after fourth dip

ΔP(Bar) (P_F - P_P) Absolute	Pressure Drop(Pascal)	Pure Methane Permeate Flow Rate (ml/min)	Pure Methane Permeate Flow Rate(mol/s)	Pure methane Permeance membrane C after fourth dip
0.05	5000	0	0.00	0.00
0.06	6000	0	0.00	0.00
0.07	7000	0.01	7.44E-09	4.34E-11
0.08	8000	0.1	7.44E-08	3.80E-10
0.09	9000	0.5	3.72E-07	1.69E-09
0.1	10000	1.0	7.44E-07	3.04E-09

Table 8:116: Pure Methane permeability using Membrane C after fourth dip

Feed Pressure (Pascal)	Permeate Pressure (Pascal)	Average Pressure (Pascal)	Pure Methane Permeate Flow Rate (ml/min)	Pure methane Permeance membrane C after fourth dip	Pure methane Permeability through Membrane C after fourth dip
105000	100000	102500	0	0.00	0.00
106000	100000	103000	0	0.00	0.00
107000	100000	103500	0.01	4.34E-11	8.68E-15
108000	100000	104000	0.1	3.80E-10	7.60E-14
109000	100000	104500	0.5	1.69E-09	3.38E-13
110000	100000	105000	1.0	3.04E-09	6.08E-13

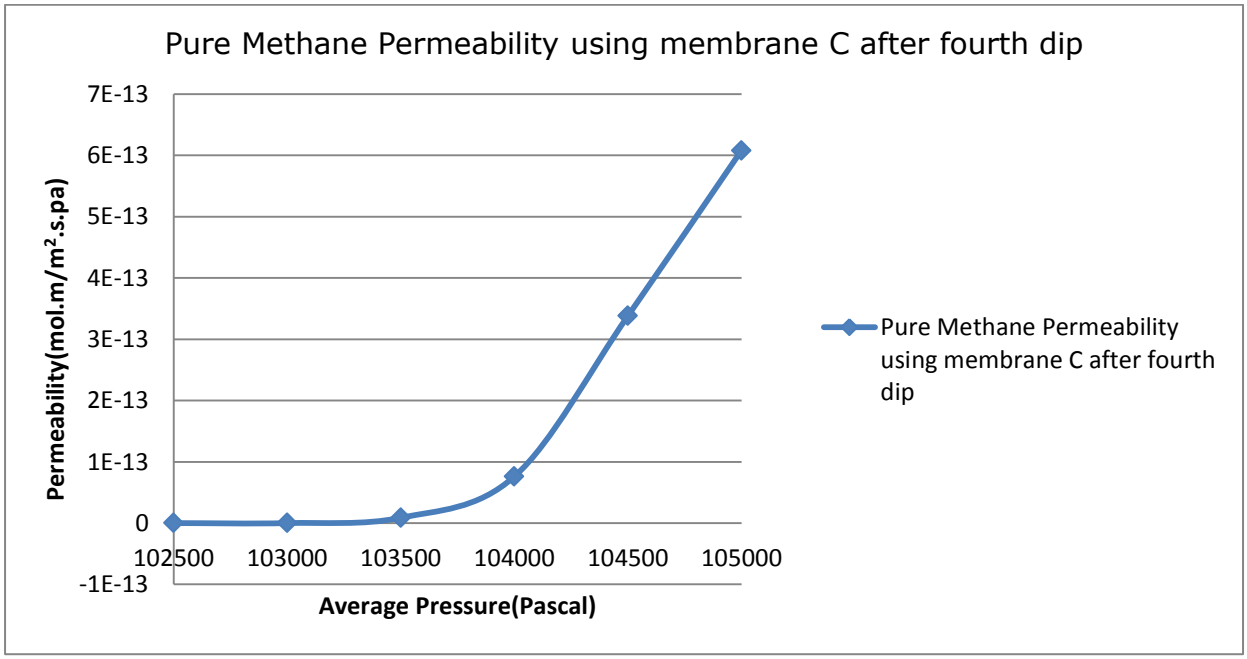

Figure 8:77 : Pure Methane permeability using membrane C after fourth dip

Table 8:117: Pure Helium permeance using membrane C after fourth dip

ΔP(Bar) (P_F - P_P) Absolute	Pressure Drop(Pascal)	Pure Helium Permeate Flow Rate (ml/min)	Pure Helium Permeate Flow Rate(mol/s)	Pure Helium Permeance Membrane C after fourth dip
0.05	5000	0.20	1.49E-07	1.22E-09
0.06	6000	0.35	2.60E-07	1.77E-09
0.07	7000	1.5	1.12E-06	6.51E-09
0.08	8000	2.5	1.86E-06	9.49E-09
0.09	9000	4	2.98E-06	1.35E-08
0.1	10000	6	4.46E-06	1.82E-08

Table 8:118: Pure Helium permeability using Membrane C after fourth dip

Feed Pressure (Pascal)	Permeate Pressure (Pascal)	Average Pressure (Pascal)	Pure Helium Permeate Flow Rate (ml/min)	Pure Helium Permeance membrane C after fourth dip	Pure Helium Permeability through Membrane C after fourth dip
105000	100000	102500	0.20	1.22E-09	2.44E-13
106000	100000	103000	0.35	1.77E-09	3.54E-13
107000	100000	103500	1.5	6.51E-09	1.30E-12
108000	100000	104000	2.5	9.49E-09	1.90E-12
109000	100000	104500	4	1.35E-08	2.70E-12
110000	100000	105000	6	1.82E-08	3.64E-12

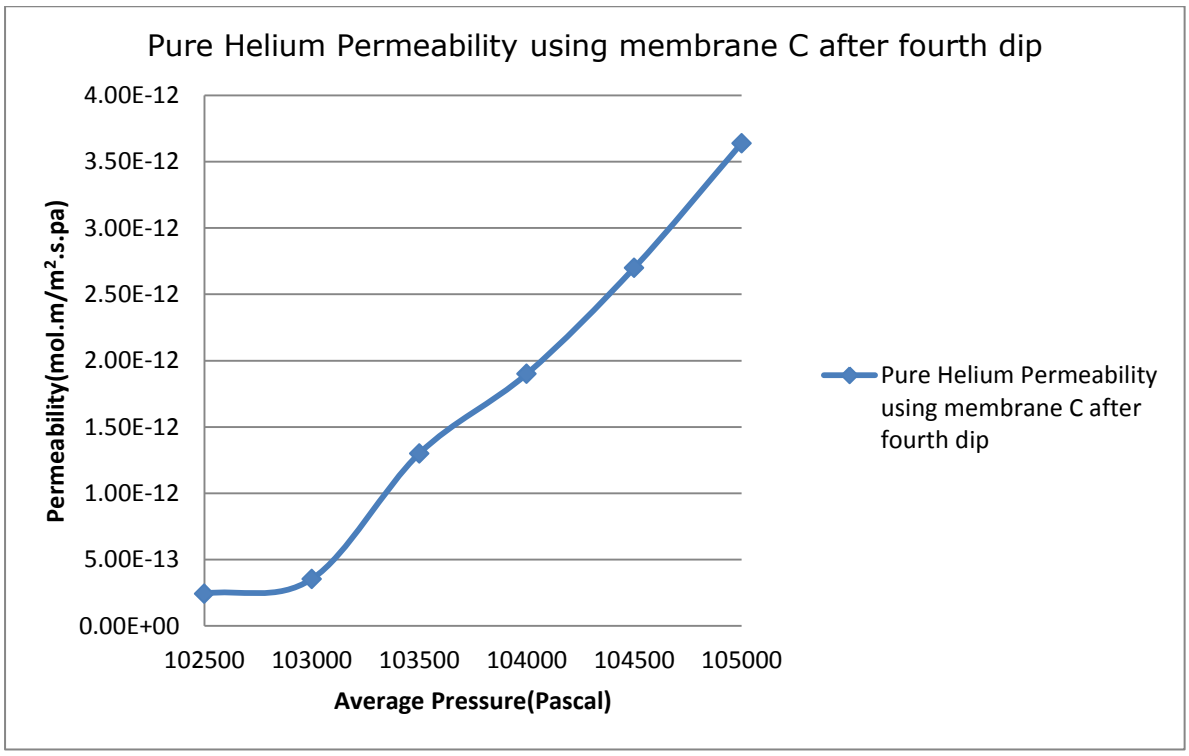

Figure 8:78: Pure Helium permeability using Membrane C after fourth dip

Table 8:119: Pure Argon permeance using Membrane C after fourth dip with retentate valve fully closed

ΔP(Bar) (P_F - P_P) Absolute	Pressure Drop(Pascal)	Pure Argon Permeate Flow Rate (ml/min)	Pure Argon Permeate Flow Rate(mol/s)	Pure Argon Permeance Membrane C after fourth dip
0.05	5000	0.00	0.00	0.00
0.06	6000	0.00	0.00	0.00
0.07	7000	0.00	0.00	0.00
0.08	8000	0.00	0.00	0.00
0.09	9000	0.02	1.49E-08	6.75E-11
0.1	10000	0.1	7.44E-08	3.04E-10

Table 8:120: Argon permeability using Membrane C after fourth dip

Feed Pressure (Pascal)	Permeate Pressure (Pascal)	Average Pressure (Pascal)	Pure Argon Permeate Flow Rate (ml/min)	Pure Argon Permeance membrane C after fourth dip	Pure Argon Permeability through Membrane C after fourth dip
105000	100000	102500	0.00	0.00	0
106000	100000	103000	0.00	0.00	0
107000	100000	103500	0.00	0.00	0
108000	100000	104000	0.00	0.00	0
109000	100000	104500	0.02	6.75E-11	1.35E-14
110000	100000	105000	0.1	3.04E-10	6.08E-14

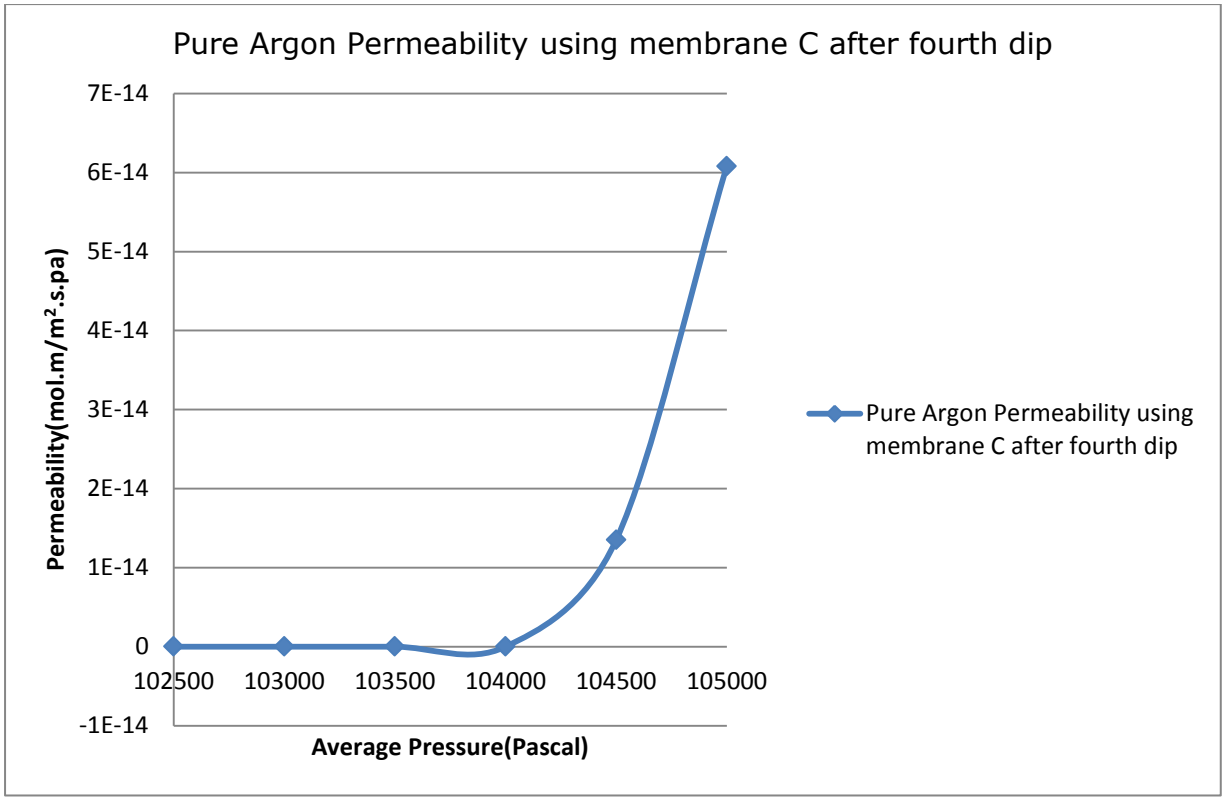

Figure 8:79: Pure Argon permeability using Membrane C after fourth dip

Table 8:121: Pure CO_2 permeance at 296k using Membrane C with retentate valve fully closed

ΔP(Bar) (P_F - P_P) Absolute	Pressure Drop(Pascal)	Pure CO_2 Permeate Flow Rate (ml/min)	Pure CO_2 Permeate Flow Rate(mol/s)	pure CO_2 Permeance through Membrane C 296K
0.05	5000	5.12	3.81E-06	3.11E-08
0.06	6000	15.20	1.13E-05	7.69E-08
0.07	7000	25.0	1.86E-05	1.08E-07
0.08	8000	40.56	3.02E-05	1.54E-07
0.09	9000	59.01	4.39E-05	1.99E-07
0.1	10000	70.40	5.24E-05	2.14E-07

Table 8:122: Pure $C0_2$ permeability using Membrane C after fourth dip

Feed Pressure (Pascal)	Permeate Pressure (Pascal)	Average Pressure (Pascal)	Pure $C0_2$ Permeate Flow Rate (ml/min)	Pure $C0_2$ Permeance membrane C after fourth dip	Pure $C0_2$ Permeability through Membrane C after fourth dip
105000	100000	102500	5.12	3.11E-08	6.22E-12
106000	100000	103000	15.20	7.69E-08	1.54E-11
107000	100000	103500	25.0	1.08E-07	2.16E-11
108000	100000	104000	40.56	1.54E-07	3.08E-11
109000	100000	104500	59.01	1.99E-07	3.98E-11
110000	100000	105000	70.40	2.14E-07	4.28E-11

Table 8:123: Pure CO_2 permeance at 338k using Membrane C with retentate valve fully closed

ΔP(Bar) (P_F - P_P) Absolute	Pressure Drop(Pascal)	Pure CO_2 Permeate Flow Rate (ml/min)	Pure CO_2 Permeate Flow Rate(mol/s)	pure CO_2 Permeance through Membrane C 338K
0.05	5000	4.00	2.60E-06	2.43E-08
0.06	6000	7.20	5.36E-06	3.64E-08
0.07	7000	16.00	1.19E-05	6.94E-08
0.08	8000	25.00	1.86E-05	9.49E-08
0.09	9000	35.00	2.60E-05	1.18E-07
0.1	10000	40.00	2.98E-05	1.21E-07

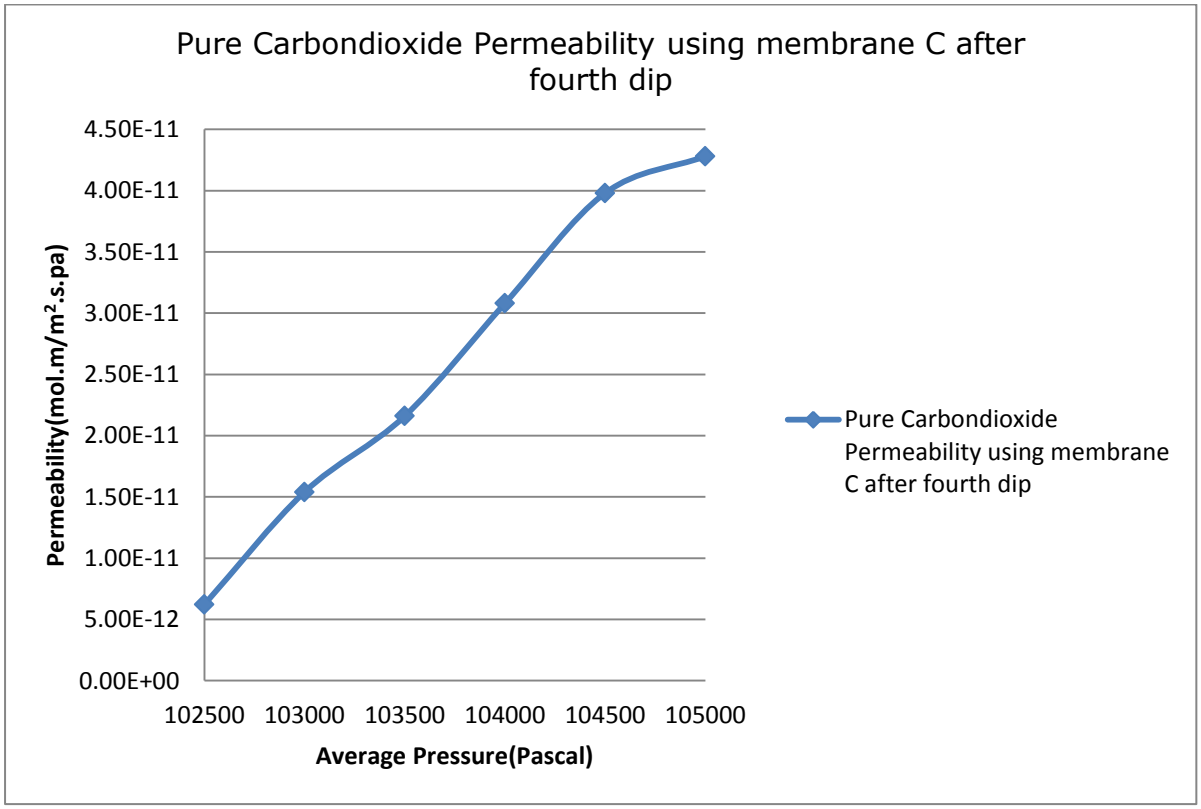

Figure 8:80: Pure $C0_2$ permeability using Membrane C after fourth dip

Table 8:124: Pure CO_2 permeance at 423k using Membrane C with retentate valve fully

ΔP(Bar) (P_F - P_P) Absolute	Pressure Drop(Pascal)	Pure CO_2 Permeate Flow Rate (ml/min)	Pure CO_2 Permeate Flow Rate(mol/s)	pure CO_2 Permeance through Membrane C 423K
0.05	5000	3.20	2.38E-06	1.94E-08
0.06	6000	6.00	4.46E-06	3.04E-08
0.07	7000	11.00	8.18E-06	4.77E-08
0.08	8000	16.00	1.19E-05	6.07E-08
0.09	9000	21.00	1.56E-05	7.09E-08
0.1	10000	29.00	2.16E-05	8.81E-08

Table 8:125: Pure CO_2 permeance at 523k using Membrane C with retentate valve fully

ΔP(Bar) (P_F - P_P) Absolute	Pressure Drop(Pascal)	Pure CO_2 Permeate Flow Rate (ml/min)	Pure CO_2 Permeate Flow Rate(mol/s)	pure CO_2 Permeance through Membrane C 523K
0.05	5000	2.9	2.16E-06	1.76E-08
0.06	6000	4.23	3.15E-06	2.14E-08
0.07	7000	8	5.95E-06	3.47E-08
0.08	8000	12	8.93E-06	4.56E-08
0.09	9000	16	1.19E-05	5.40E-08
0.1	10000	20	1.49E-05	6.07E-08

Table 8:126: Pure CO_2 permeance at 723k using embrane C with retentate valve fully

ΔP(Bar) (P_F - P_P) Absolute	Pressure Drop(Pascal)	Pure CO_2 Permeate Flow Rate (ml/min)	Pure CO_2 Permeate Flow Rate(mol/s)	pure CO_2 Permeance through Membrane C 723K
0.05	5000	1.4	1.04E-06	8.50E-09
0.06	6000	3.3	2.46E-06	1.67E-08
0.07	7000	6	4.46E-06	2.60E-08
0.08	8000	8	5.95E-06	3.04E-08
0.09	9000	10	7.44E-06	3.37E-08
0.1	10000	13.5	1.00E-05	4.10E-08

Table 8:127: Pure N_2 permeance using membrane C with retentate valve fully closed

ΔP(Bar) (P_F - P_P) Absolute	Pressure Drop(Pascal)	Pure N_2 Permeate Flow Rate (ml/min)	Pure N_2 Permeate Flow Rate(mol/s)	Pure N_2 Permeance through Membrane C at 296k
0.05	5000	0.00	0.00	0.00
0.06	6000	0.00	0.00	0.00
0.07	7000	0.50	3.72E-07	2.17E-09
0.08	8000	1.10	8.18E-07	4.18E-09
0.09	9000	2.12	1.58E-06	7.15E-09
0.1	10000	3.01	2.24E-06	9.14E-09

Table 8:128: Pure N_2 permeability using Membrane C after fourth dip

Feed Pressure (Pascal)	Permeate Pressure (Pascal)	Average Pressure (Pascal)	Pure N_2 Permeate Flow Rate (ml/min)	Pure N_2 Permeance membrane C after fourth dip	Pure N_2 Permeability through Membrane C after fourth dip
105000	100000	102500	0.00	0.00	0
106000	100000	103000	0.00	0.00	0
107000	100000	103500	0.50	2.17E-09	4.34E-13
108000	100000	104000	1.10	4.18E-09	8.36E-13
109000	100000	104500	2.12	7.15E-09	1.43E-12
110000	100000	105000	3.01	9.14E-09	1.83E-12

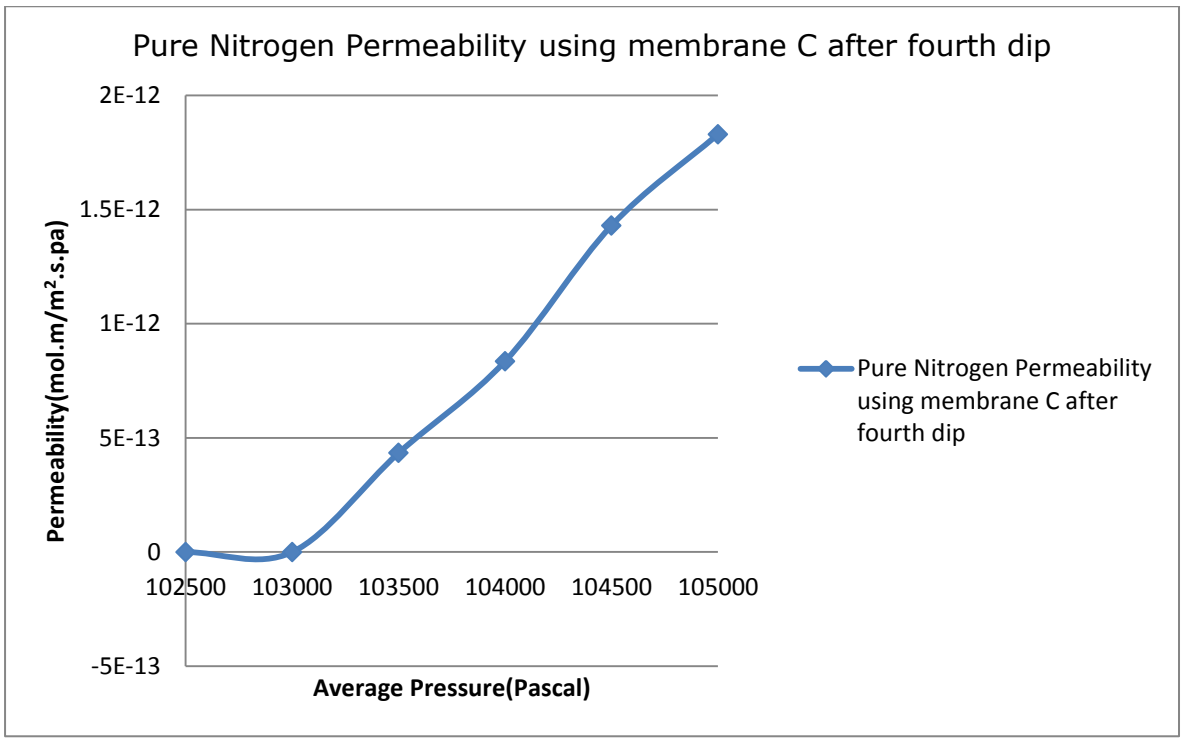

Figure 8:81: Pure N_2 permeability using Membrane C after fourth dip

Table 8:129: Pure N_2 permeance at 338k using Membrane C with retentate valve fully closed

ΔP(Bar) (P_F - P_P) Absolute	Pressure Drop(Pascal)	Pure N_2 Permeate Flow Rate (ml/min)	Pure N_2 Permeate Flow Rate(mol/s)	Pure N_2 Permeance through Membrane C at 338k
0.05	5000	0	0.00	0.00
0.06	6000	0	0.00	0.00
0.07	7000	0.4	2.98E-07	1.74E-09
0.08	8000	0.95	7.07E-07	3.61E-09
0.09	9000	1.34	9.97E-07	4.52E-09
0.1	10000	2.00	1.49E-06	6.07E-09

Table 8:130: Pure N_2 permeance at 423k using Membrane C with retentate valve fully closed

ΔP(Bar) (P_F - P_P) Absolute	Pressure Drop(Pascal)	Pure N_2 Permeate Flow Rate (ml/min)	Pure N_2 Permeate Flow Rate(mol/s)	Pure N_2 Permeance through Membrane C at 423k
0.05	5000	0	0.00	0.00
0.06	6000	0	0.00	0.00
0.07	7000	0.28	2.08E-07	1.21E-09
0.08	8000	0.7	5.21E-07	2.66E-09
0.09	9000	1.1	8.18E-07	3.71E-09
0.1	10000	1.4	1.04E-06	4.25E-09

Table 8:131: Pure N_2 permeance at 523k using Membrane C with retentate valve fully closed

ΔP(Bar) (P_F - P_P) Absolute	Pressure Drop(Pascal)	Pure N_2 Permeate Flow Rate (ml/min)	Pure N_2 Permeate Flow Rate(mol/s)	Pure N_2 Permeance through Membrane C at 523k
0.05	5000	0	0.00	0.00
0.06	6000	0	0.00	0.00
0.07	7000	0	0.00	0.00
0.08	8000	0	0.00	0.00
0.09	9000	0.2	1.49E-07	6.75E-10
0.1	10000	0.5	3.72E-06	1.52E-09

Table 8:132: Pure N_2 permeance at 723k using Membrane C with retentate valve fully close

ΔP(Bar) (P_F - P_P) Absolute	Pressure Drop(Pascal)	Pure N_2 Permeate Flow Rate (ml/min)	Pure N_2 Permeate Flow Rate(mol/s)	Pure N_2 Permeance through Membrane C at 723k
0.05	5000	0	0.00	0.00
0.06	6000	0	0.00	0.00
0.07	7000	0	0.00	0.00
0.08	8000	0	0.00	0.00
0.09	9000	0.01	7.44E-09	3.37E-11
0.1	10000	0.03	2.23E-08	9.11E-11

Table 8:133: Second Stage CO_2/N_2 permeance using Membrane C with retentate valve fully closed

ΔP(Bar) (P_F - P_P) Absolute	Pressure Drop(Pascal)	CO_2/N_2 Permeate Flow Rate (ml/min)	CO_2/N_2 Permeate Flow Rate(mol/s)	Second Stage CO_2/N_2 Permeance through Membrane C after fourth dip
0.05	5000	2.00	1.49E-06	1.21E-08
0.06	6000	4.50	3.35E-06	2.28E-08
0.07	7000	6.80	5.06E-06	2.95E-08
0.08	8000	8.00	5.95E-06	3.04E-08
0.09	9000	10	7.44E-06	3.37E-08
0.1	10000	13.50	1.00E-05	4.10E-08

Table 8:134: Second Stage CO_2/N_2 permeability using Membrane C after fourth dip

Feed Pressure (Pascal)	Permeate Pressure (Pascal)	Average Pressure (Pascal)	$C0_2/N_2$ Permeate Flow Rate (ml/min)	CO_2/N_2 Permeance membrane C after fourth dip	Second Stage CO_2/N_2 Permeability through Membrane C after fourth dip
105000	100000	102500	2.00	1.21E-08	2.42E-12
106000	100000	103000	4.50	2.28E-08	4.56E-12
107000	100000	103500	6.80	2.95E-08	5.90E-12
108000	100000	104000	8.00	3.04E-08	6.08E-12
109000	100000	104500	10	3.37E-08	6.74E-12
110000	100000	105000	13.50	4.10E-08	8.20E-12

Table 8:135: Second Stage CO_2 permeance from mixture B using Membrane C after fourth dip with retentate valve fully closed

ΔP(Bar) (P_F - P_P) Absolute	Pressure Drop(Pascal)	CO_2 Permeate Flow Rate (ml/min)	CO_2 Permeate Flow Rate(mol/s)	Second Stage CO_2 Permeance through Membrane C after fourth dip
0.135	13500	1.20	8.93E-07	2.70E-09
0.138	13800	2.70	2.01E-06	5.94E-09
0.141	14100	4.08	3.04E-06	8.79E-09
0.144	14400	4.80	3.57E-06	1.01E-08
0.147	14700	6.00	4.46E-06	1.24E-08
0.15	15000	8.10	6.03E-06	1.64E-08

Table 8:136: Second Stage CO_2 permeability from mixture B using Membrane C after fourth dip with retentate valve fully closed

Feed Pressure (Pascal)	Permeate Pressure (Pascal)	Average Pressure (Pascal)	Second Stage $C0_2$ Permeate Flow Rate (ml/min)	Second Stage $C0_2$ Permeance membrane C after fourth dip	Second Stage $C0_2$ Permeability through Membrane C after fourth dip
31500	18000	24750	1.20	2.70E-09	5.40E-13
31800	18000	24900	2.70	5.94E-09	1.19E-12
32100	18000	25050	4.08	8.79E-09	1.76E-12
32400	18000	25200	4.80	1.01E-08	2.02E-12
32700	18000	25350	6.00	1.24E-08	2.48E-12
33000	18000	25500	8.10	1.64E-08	3.28E-12

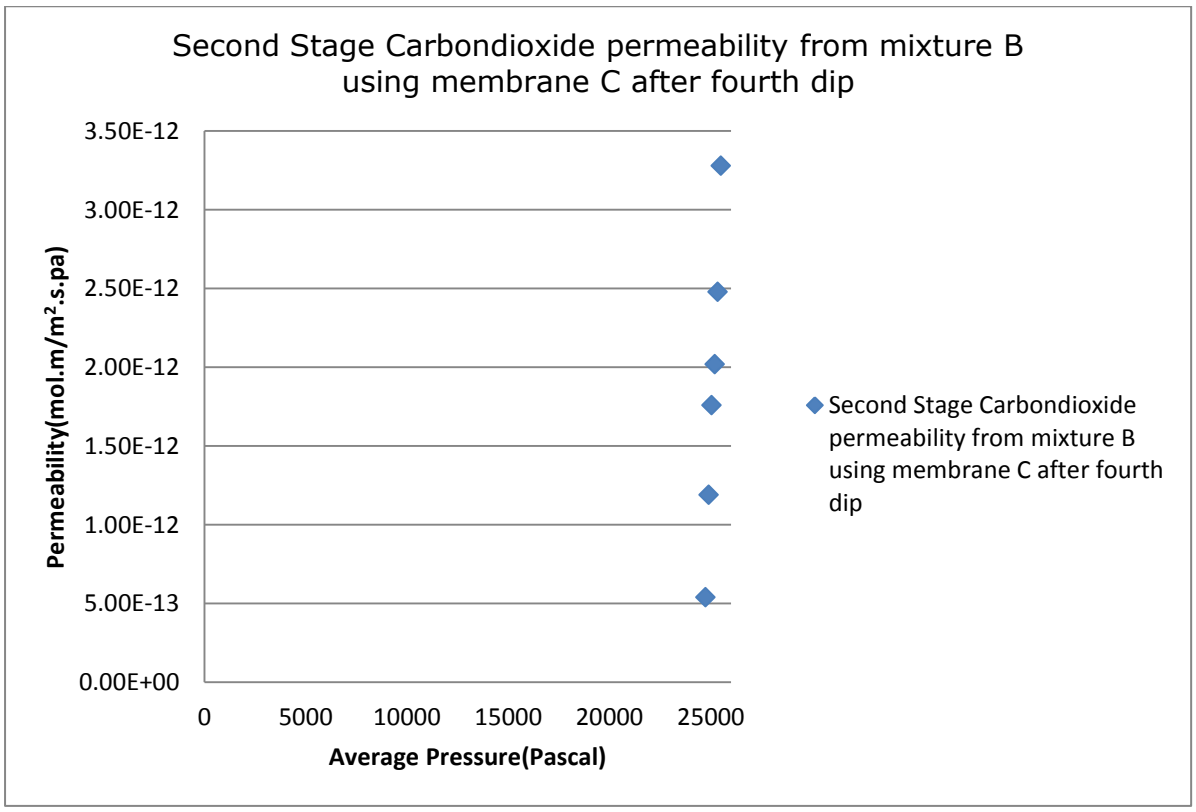

Figure 8:82: Second Stage CO_2 permeability from mixture B using Membrane C after fourth dip with retentate valve fully closed

Table 8:137: Second Stage N_2 permeance from B mixture using Membrane C after fourth dip with retentate valve fully closed

ΔP(Bar) (P_F - P_P) Absolute	Pressure Drop (Pascal)	N_2 Permeate Flow Rate (ml/min)	N_2 Permeate Flow Rate(mol/s)	Second Stage N_2 Permeance through Membrane C after fourth dip
0.455	45500	0.80	5.95E-07	5.34E-10
0.462	46200	1.85	1.38E-06	1.22E-09
0.469	46900	2.72	2.02E-06	1.76E-09
0.476	47600	3.20	3.38E-06	2.04E-09
0.483	48300	4.00	2.98E-06	2.52E-09
0.49	49000	5.40	4.02E-06	3.34E-09

Table 8:138: Second Stage N_2 permeability from mixture B using Membrane C after fourth dip with retentate valve fully closed

Feed Pressure (Pascal)	Permeate Pressure (Pascal)	Average Pressure (Pascal)	Second Stage N_2 Permeate Flow Rate (ml/min)	Second Stage N_2 Permeance membrane C after fourth dip	Second Stage N_2 Permeability through Membrane C after fourth dip
73500	28000	50750	0.80	5.34E-10	1.07E-13
74200	28000	51100	1.85	1.22E-09	2.44E-13
74900	28000	51450	2.72	1.76E-09	3.52E-13
75600	28000	51800	3.20	2.04E-09	4.08E-13
76300	28000	52150	4.00	2.52E-09	5.04E-13
77000	28000	52500	5.40	3.34E-09	6.68E-13

Table 8:139: Third Stage CO_2/N_2 permeance using Membrane C with retentate valve fully closed

ΔP(Bar) (P_F - P_P) Absolute	Pressure Drop(Pascal)	CO_2/N_2 Permeate Flow Rate (ml/min)	CO_2/N_2 Permeate Flow Rate(mol/s)	Third Stage CO_2/N_2 Permeance through Membrane C after fourth dip
0.05	5000	1.60	1.19E-06	9.72E-09
0.06	6000	2.70	2.01E-06	1.37E-08
0.07	7000	3.80	2.83E-06	1.65E-08
0.08	8000	5.00	3.72E-06	1.90E-08
0.09	9000	6.00	4.46E-06	2.02E-08
0.1	10000	7.50	5.58E-06	2.28E-08

Table 8:140: Third Stage CO_2/N_2 permeability using Membrane C after fourth dip

Feed Pressure (Pascal)	Permeate Pressure (Pascal)	Average Pressure (Pascal)	Third $C0_2/N_2$ Permeate Flow Rate (ml/min)	Third CO_2/N_2 Permeance membrane C after fourth dip	Third Stage CO_2/N_2 Permeability through Membrane C after fourth dip
105000	100000	102500	1.60	9.72E-09	1.94E-12
106000	100000	103000	2.70	1.37E-08	2.74E-12
107000	100000	103500	3.80	1.65E-08	3.30E-12
108000	100000	104000	5.00	1.90E-08	3.80E-12
109000	100000	104500	6.00	2.02E-08	4.04E-12
110000	100000	105000	7.50	2.28E-08	4.56E-12

Table 8:141: Third Stage CO_2 permeance from mixture C using Membrane C after fourth dip with retentate valve fully closed

ΔP(Bar) (P_F - P_P) Absolute	Pressure Drop (Pascal)	Third CO_2 Permeate Flow Rate (ml/min)	Third Stage CO_2 Permeate Flow Rate(mol/s)	Third Stage CO_2 Permeance through Membrane C after fourth dip
0.09	9000	1.44	1.07E-06	4.86E-09
0.10	10000	2.43	1.81E-06	7.38E-09
0.102	10200	3.42	2.54E-06	1.02E-08
0.11	11000	4.50	3.45E-06	1.24E-08
0.114	11400	5.40	4.02E-06	1.44E-08
0.12	12000	6.75	5.02E-06	1.71E-08

Table 8:142: Third Stage CO_2 permeability from mixture C using Membrane C after fourth dip with retentate valve fully closed

Feed Pressure (Pascal)	Permeate Pressure (Pascal)	Average Pressure (Pascal)	Third Stage $C0_2$ Permeate Flow Rate (ml/min)	Third Stage $C0_2$ Permeance membrane C after fourth dip	Third Stage $C0_2$ Permeability through Membrane C after fourth dip
63000	54000	58500	1.44	4.86E-09	9.72E-13
64000	54000	59000	2.43	7.38E-09	1.48E-12
64200	54000	59100	3.42	1.02E-08	2.04E-12
65000	54000	59500	4.50	1.24E-08	2.48E-12
65400	54000	59700	5.40	1.44E-08	2.88E-12
66000	54000	60000	6.75	1.71E-08	3.42E-12

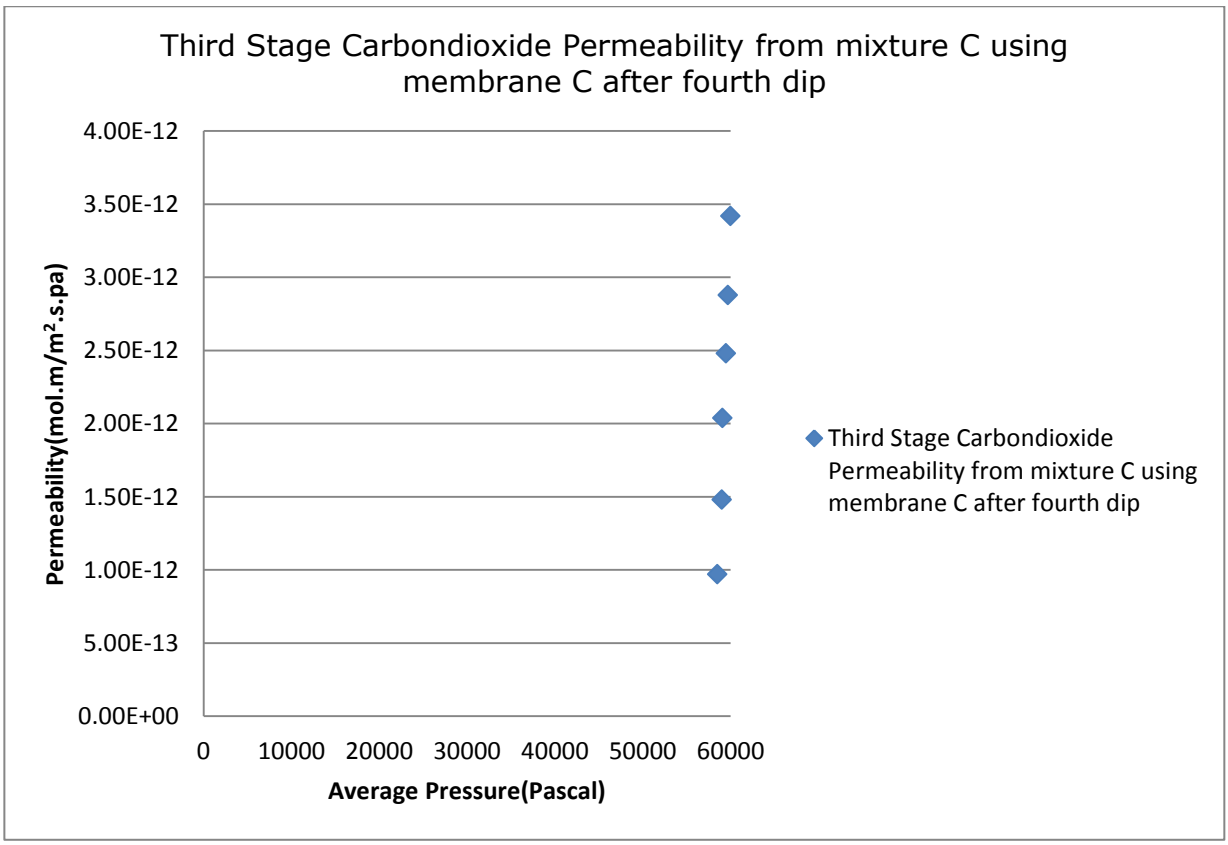

Figure 8:83: Third Stage CO_2 permeability from mixture C using Membrane C after fourth dip with retentate valve fully closed

Table 8:143: Third Stage N_2 permeance from mixture C using Membrane C after fourth dip with retentate valve fully closed

ΔP(Bar) (P_F - P_P) Absolute	Pressure Drop(Pascal)	N_2 Permeate Flow Rate (ml/min)	N_2 Permeate Flow Rate(mol/s)	Third Stage N_2 Permeance through Membrane C after fourth dip
0.38	38000	0.16	1.19E-07	1.28E-10
0.384	38400	0.27	2.01E-07	2.14E-10
0.388	38800	0.38	2.83E-07	2.97E-10
0.392	39200	0.50	3.72E-07	3.87E-10
0.396	39600	0.60	4.46E-07	4.60E-10
0.400	40000	0.75	5.58E-07	5.69E-10

Table 8:144: Third Stage N_2 permeability from mixture C using Membrane C after fourth dip with retentate valve fully closed

Feed Pressure (Pascal)	Permeate Pressure (Pascal)	Average Pressure (Pascal)	Third Stage N_2 Permeate Flow Rate (ml/min)	Third Stage N_2 Permeance membrane C after fourth dip	Third Stage N_2 Permeability through Membrane C after fourth dip
42000	4000	23000	0.16	1.28E-10	2.56E-14
42400	4000	23200	0.27	2.14E-10	4.28E-14
42800	4000	23400	0.38	2.97E-10	5.94E-14
43200	4000	23600	0.50	3.87E-10	7.74E-14
43600	4000	23800	0.60	4.60E-10	9.20E-14
44000	4000	24000	0.75	5.69E-10	1.14E-13

8.5 APPENDIX 5: CALCULATION OF MEMBRANE PORE SIZES

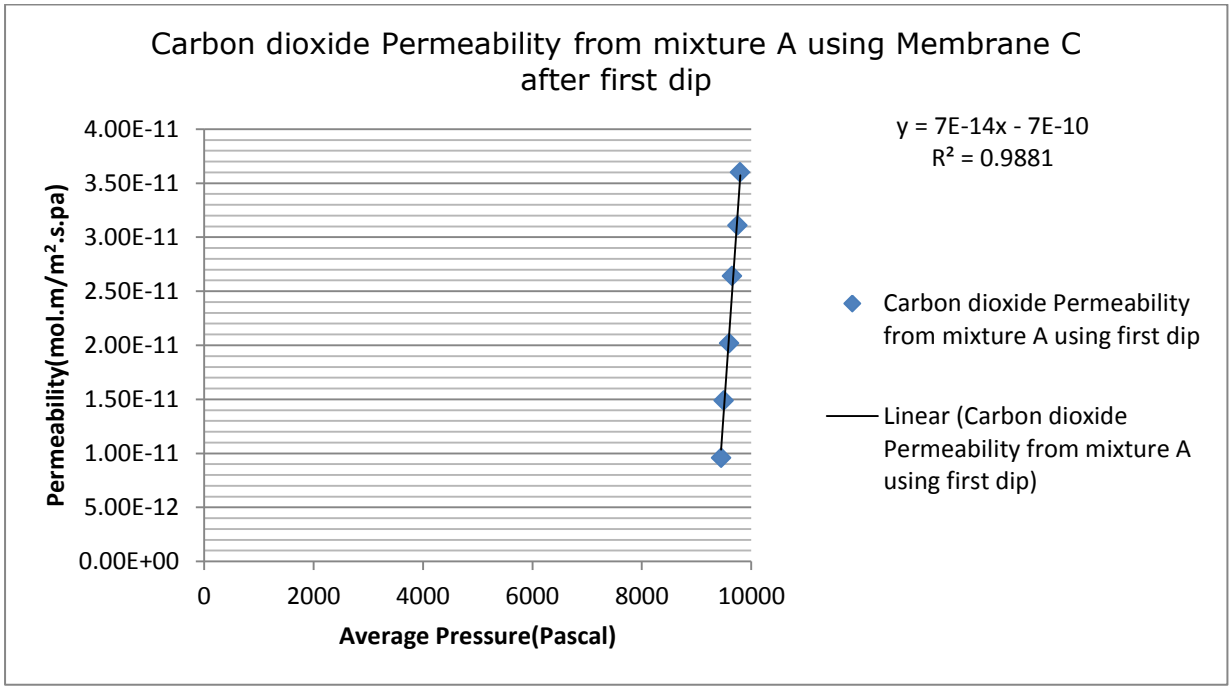

Figure 8:84: Carbondioxide Permeability from mixture A using mixture C after first dip

From the figure 8:84 above, Slope= 7.0E-14 $\frac{mol.m}{m^2.s.Pa^2}$

Then, the intercept =-7.00E-10(mol.m/m^2.s.Pa).

Recalling equation 1.9, Bo= Slope= $\frac{r_p^{\ 2}}{8\mu RT}$ = 7.0E-14, when the flow is Viscous flow $r_p = \sqrt{(8)(1.372E-5)(8.3145)(296)(7.0E-14)}$ = 1.38E-07 metres

Where T is the absolute temperature in Kelvin

μ = $C0_2$ gas viscosity; 1.372E-5 Pa.s

T= 296 Kelvin

R= 8.3145J/mol.K

r_p= 1.38E-07 metres= 138 nm and also equals to 1380Å

For the Knudsen contribution, from the graph figure above, the intercept was recorded to be -7.0E-10(mol.m/m^2.s.Pa). This makes the Knudsen mechanism not applicable to the Carbondioxide flow through the membrane C after first dip since Knudsen does not have a negative contribution to the gas flow.

The pore size of Membrane C after First Dip was 138nm or 1380 Å which was found to be a meso porous ceramic membrane based on the IUPACK pore size classification discussed in chapter 2. From the results above, the Viscous mechanism has a positive valve, but because the viscous flow does not bring about separation of the gas and the membrane C recovering of the Carbondioxide from the mixture A after first dip was 30%. This confirmed that another mechanism was responsible for the flow of the Carbondioxide through membrane C after first dip.

For the membrane pore size after the Second Dip, the plot of permeability against average pressure is shown in table below and from the slope, the pore size was estimated.

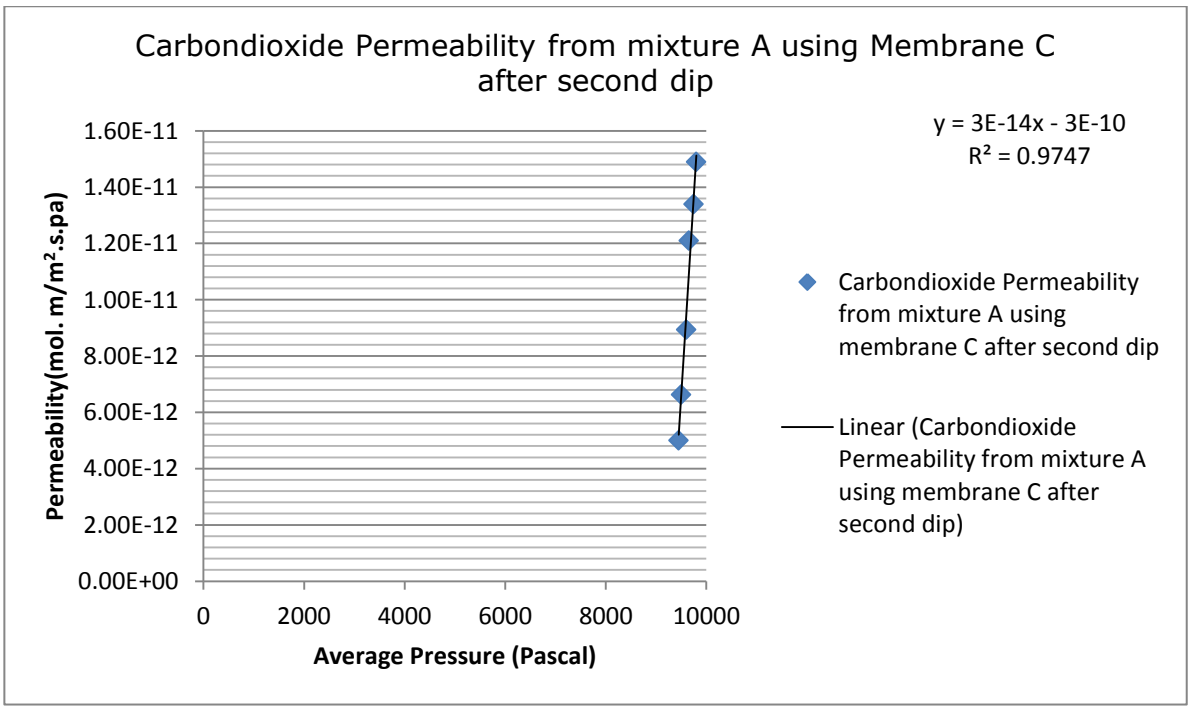

Figure 8:85: Carbondioxide Permeability from mixture A using Membrane C after second dip

From the figure 8:85 above, Slope= 3.0E-14 $\frac{mol.m}{m^2.s.Pa^2}$

Then, the intercept =3.0E-10(mol.m/m^2.s.Pa).

Recalling equation 1.9, Bo= Slope= $\frac{r_p^{\ 2}}{8\mu RT}$ = 3.0E-14, when the flow is Viscous flow

r_p = $\sqrt{(8)(1.372E-5)(8.3145)(296)(3.0E-14)}$ = 9.00E-08 metres

Where T is the absolute temperature in Kelvin

μ = $C0_2$ gas viscosity; 1.372E-5 Pa.s

T= 296 Kelvin

R= 8.3145J/mol.K

r_p= 9.00E-08 metres= 90 nm and also equals to 900Å

From the graph figure above, the intercept was recorded to be to be -3.0E-10(mol.m/m^2.s.Pa). This makes the Knudsen mechanism not applicable to the

Carbondioxide flow through the membrane C after first dip since Knudsen does not have a negative contribution to the gas flow.

The pore size of Membrane C after First Dip was 90nm or 90 Å which was found to be a meso porous ceramic membrane based on the IUPACK pore size classification discussed in chapter 2. From the results above, the Viscous mechanism has a positive valve, but because the viscous flow does not bring about separation of the gas and the Membrane C recovering of the Carbondioxide from the mixture A, after first dip was 30%. This confirmed that another mechanism was responsible for the flow of the Carbondioxide through Membrane C after second dip.

The pore size of Membrane C after Second Dip was 90nm or 900Å which was found to be a macro porous ceramic membrane based on IUPACK pore size classification discussed in chapter 2.

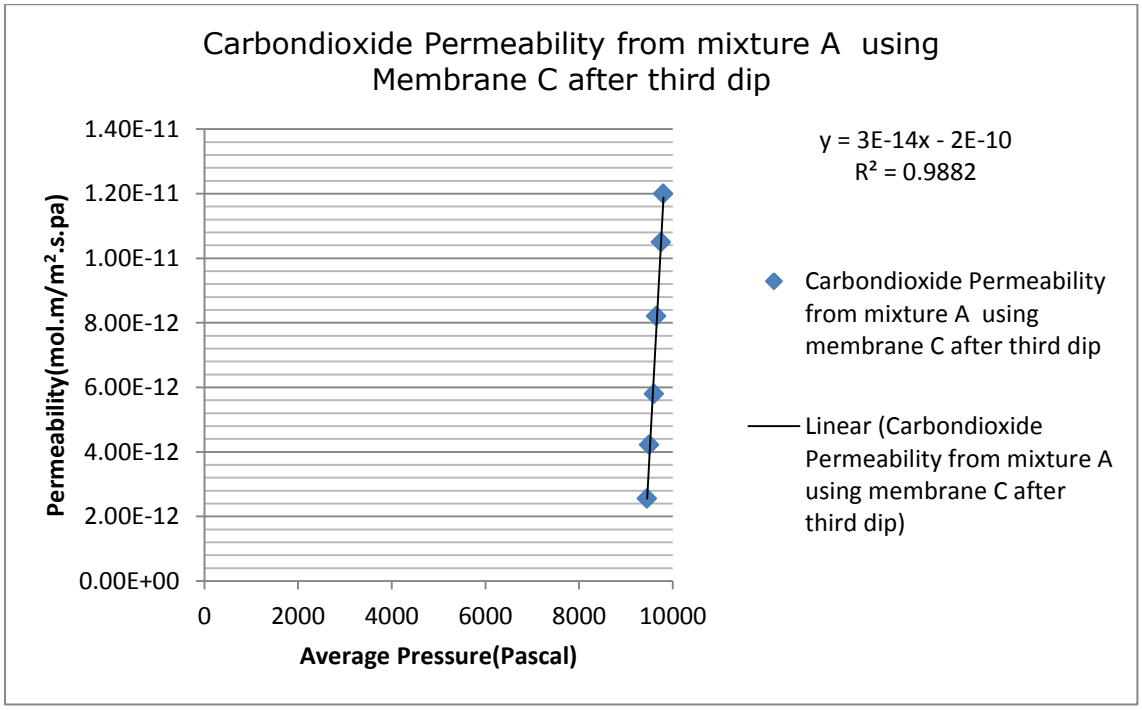

Figure 8:86: Carbon dioxide Permeability from mixture A using Membrane C after third dip

From the figure 8:86 above, Slope= 3. 0E-14 $\frac{mol.m}{m^2.s.Pa^2}$

Then, the intercept =-2.0E-10(mol.m/m^2.s.Pa).

Recalling equation 1.9, Bo= Slope= $\frac{r_p^{\,2}}{8\mu RT}$ = 3.0E-14,

When the flow is viscous flow

r_p = $\sqrt{(8)(1.372E-5)(8.3145)(296)(3.0E-14)}$ = 9.0E-08 metres

Where T is the absolute temperature in Kelvin

μ = $C0_2$ gas viscosity; 1.372E-5 Pa.s

T= 296 Kelvin

R= 8.3145J/mol.K

r_p= 9.0E-08 metres= 90.0 nm and also equals to 900Å

Similarly to the membrane C after the first and second dips, the intercept was recorded to be to be -2.0E-10(mol.m/m^2.s.Pa). This makes the Knudsen mechanism not applicable to the Carbondioxide flow through the membrane C after first dip since Knudsen does not have a negative contribution to the gas flow.

The pore size of membrane C after First Dip was 90nm or 900 Å which was found to be a meso porous ceramic membrane based on the IUPACK pore size classification discussed in chapter 2.

From the results above, the Viscous mechanism has a positive valve, but because the viscous flow does not bring about separation of the gas and the membrane C recovering of the Carbondioxide from the mixture A after first dip was 30%. This confirmed that another mechanism was responsible for the flow of the Carbondioxide through membrane C after third dip.

The pore size of membrane C after third dip was 90nm or 900Å which was found to be a macro porous ceramic membrane based on IUPACK pore size classification discussed in chapter 2.

To estimate the pore size after the fourth Dip, the plot of permeability against average pressure is shown in the figure below and from the slope, the pore size was estimated.

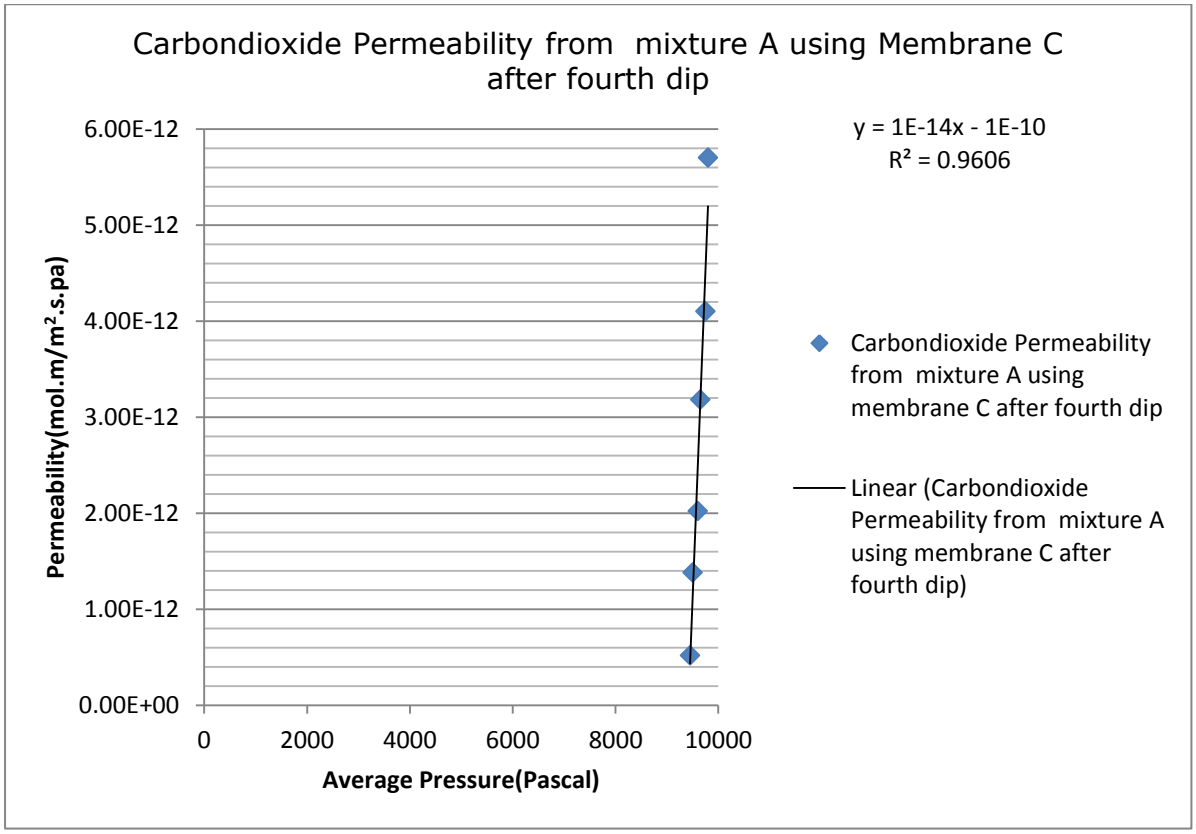

Figure 8:87: Carbon dioxide permeability from mixture A using Membrane C after fourth dip

From the figure 8:87 above, Slope= 1.0E-14 $\frac{mol.m}{m^2.s.Pa^2}$

Then, the intercept =-1.0E-10(mol.m/m^2.s.Pa).

Recalling equation 1.9, Bo= Slope= $\frac{r_p^{\ 2}}{8\mu RT}$ = 1.0E-14, when the flow is Viscous flow

$r_p = \sqrt{(8)(1.372E-5)(8.3145)(296)(1.0E-14)}$ = 5.20E-08 metres

Where T is the absolute temperature in Kelvin

μ = $C0_2$ gas viscosity; 1.372E-5 Pa.s

T= 296K

R= 8.3145J/mol.K

r_p= 5.20E-08 metres= 52 nm and also equals to 520Å

From the graph figure above, the intercept was recorded to be to be -1.0E-10(mol.m/m^2.S.Pa). This makes the Knudsen mechanism not applicable to the Carbondioxide flow through the Membrane C after first dip since Knudsen does not have a negative contribution to the gas flow.

The pore size of membrane C after First Dip was 52nm or 520 Å which was found to be a Meso porous Ceramic membrane based on the IUPACK pore size classification discussed in chapter 2.

Similarly to the earlier results, although Viscous mechanism has a positive valve, because the viscous flow does not bring about separation of the gas mixtures and the Membrane C recovering of the Carbon dioxide from the mixture A after first dip was 30% of the feed concentration as indicated earlier. This confirmed that another mechanism other than pore flow mechanism was responsible for the flow of the Carbondioxide through Membrane C after fourth dip.

For the membrane pore size after second stage, the plot of permeability against average pressure is shown in the figure below and from the slope, the pore size was estimated.

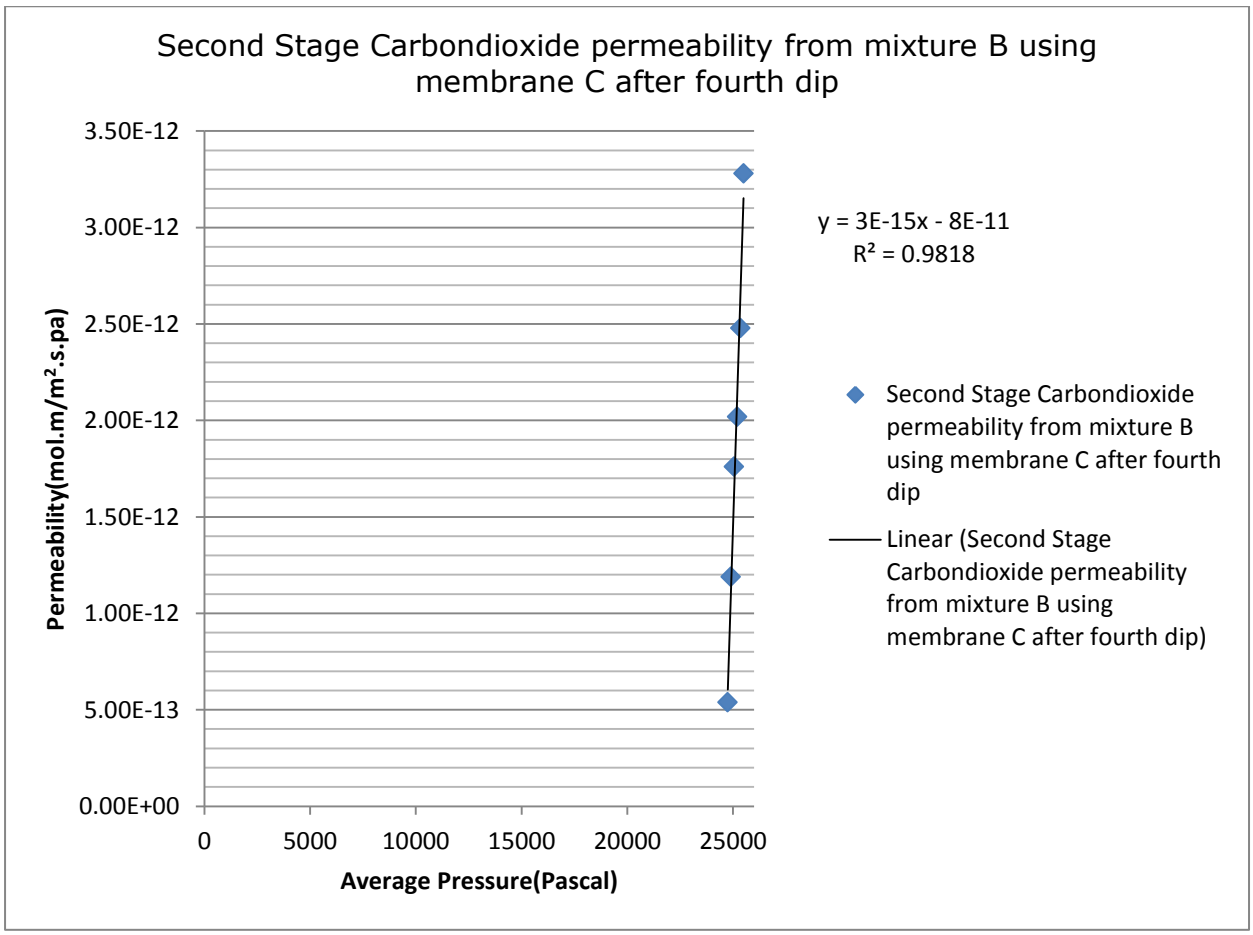

Figure 8:88: Second Stage Carbon dioxide permeability from mixture B using Membrane C after fourth dip

From figure 8:88 above, Slope= 3.0E-15 $\frac{mol.m}{m^2.s.Pa^2}$

Then, the intercept = -8.0E-11(mol.m/m^2.s.Pa).

Recalling equation 1.9, Bo= Slope= $\frac{r_p^{\ 2}}{8\mu RT}$ = 3.0E-15, when the flow is Viscous flow

r_p = $\sqrt{(8)(1.372E-5)(8.3145)(296)(3.0E-15)}$ = 2.85E-08 metres

Where T is the absolute temperature in Kelvin

μ = $C0_2$ gas viscosity; 1.372E-5 Pa.s

T= 296 Kelvin

R= 8.3145J/mol.K

r_p= 2.85E-08 metres= 28.5 nm and also equals to 285Å

From the graph figure above, the intercept was recorded to be to be -8.0x10^{-10} (mol.m/m^2.S.Pa). This makes the Knudsen mechanism not applicable to the Carbon dioxide flow through the Membrane C at Second Stage permeation. However, Knudsen mechanism does not have a negative contribution to the gas mixture through a membrane.

The pore size of membrane C at second stage permeation was estimated to be 28.5 nm or 285 Å which was found to be a Macro porous Ceramic membrane based on the IUPACK pore size classification discussed in chapter 2.

Similarly to the earlier results, seemly, the viscous mechanism has a positive value, but, because the it does not bring about separation of the gas mixtures, however, the flow through the membrane C was aided by another mechanism other than a pore flow mechanism since the recovering of the Carbondioxide from the mixture B after at second stage was 60% of the feed concentration as indicated earlier.

The pore size of membrane C after second stage was 28.5nm or 285Å which was found to be a micro porous ceramic membrane based on IUPAC pore size classification discussed in chapter 2.
For the membrane pore size after third stage, the plot of permeability against average pressure is shown in the figure below and from the slope, the pore size was estimated.

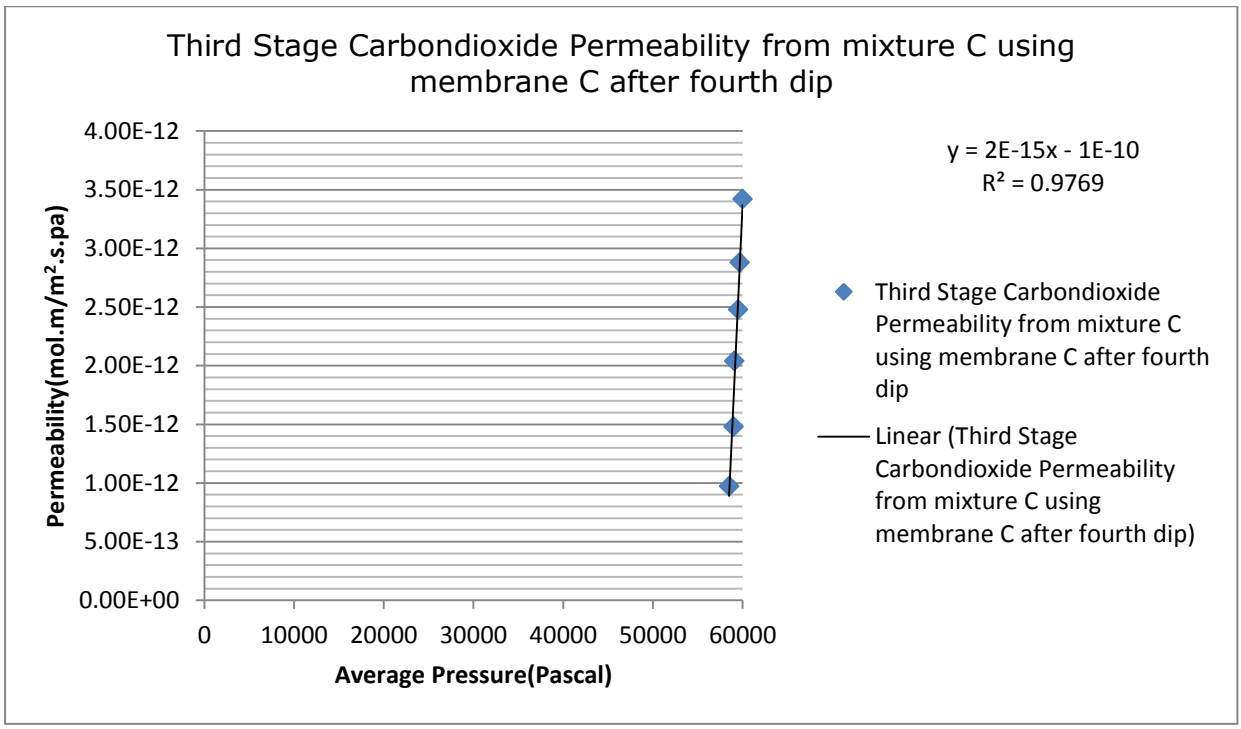

Figure 8:89: Third Stage Carbondioxide Permeability from mixture C using Membrane C after fourth dip

From figure 8:89 above, Slope= 2.0E-15 $\frac{mol.m}{m^2.s.Pa^2}$

Then, the intercept =-1.0E-10(mol.m/m^2.s.Pa).

Recalling equation 1.9, Bo= Slope= $\frac{r_p^{\ 2}}{8\mu RT}$ = 2.0E-15, when the flow is Viscous flow

r_p = $\sqrt{(8)(1.372E-5)(8.3145)(296)(2.0E-15)}$ = 2.32E-08 metres

Where T is the absolute temperature in Kelvin

μ = $C0_2$ gas viscosity; 1.372E-5 Pa.s

T= 296 Kelvin

R= 8.3145J/mol.K

r_p= 2.32E-08 metres= 23.2 nm and also equals to 232Å

Apparently, the Knudsen contribution from the graph above indicated a negative valve which clearly shows that it does not apply at this gas flow through the membrane C. Also, for the viscous flow which is showing a positive valve, does not apply in this flow either, because, viscous does not contribute in gas mixture separation and here there was up to 90 percent recovery of the feed concentration of the Carbon dioxide by the Membrane C at third stage permeation. This confirmed the presence of another flow mechanism other than pore flow mechanism.

The pore size of Membrane C after third stage was 23.2nm or 232Å which was found to be a macro porous ceramic membrane based on IUPAC pore size classification discussed in chapter 2.

8.6 APPENDIX 6: EFFECT OF GAS KINETIC DIAMETER, MOLECULAR WEIGHT TO MEMBRANE PERMEATION

Table 8:145: Effect of Kinetic Diameter of gases to the Gas Permeation at 0.05 Bar after fourth Dip

Kinetic Diameter(Å)	Flow Rate(ml/min)
2.60	0.20
3.30	5.12
3.46	0.00
3.64	0.00
3.80	0.00

Table 8:146: Effect of Kinetic Diameter of gases to the Gas Permeation at 0.06 Bar after fourth Dip

Kinetic Diameter(Å)	Flow Rate(ml/min)
2.60	0.35
3.30	15.20
3.46	0.00
3.64	0.00
3.80	0.00

Table 8:147: Effect of Kinetic Diameter of gases to the Gas Permeation at 0.07 Bar after fourth Dip

Kinetic Diameter(Å)	Flow Rate(ml/min)
2.60	1.50
3.30	25.00
3.46	0.00
3.64	0.50
3.80	0.01

Table 8:148: Effect of Kinetic Diameter of gases to the Gas Permeation at 0.08 Bar after fourth Dip

Kinetic Diameter(Å)	Flow Rate(ml/min)
2.60	2.50
3.30	40.56
3.46	0.00
3.64	1.10
3.80	0.10

Table 8:149: Effect of Kinetic Diameter of gases to the Gas Permeation at 0.09 Bar after fourth Dip

Kinetic Diameter(Å)	Flow Rate(ml/min)
2.6	4.00
3.3	59.01
3.46	0.02
3.64	2.12
3.8	0.50

Table 8:150: Effect of Kinetic Diameter of gases to the Gas Permeation at 0.1 Bar after fourth Dip

Kinetic Diameter(Å)	Flow Rate(ml/min)
2.6	6.00
3.3	70.40
3.46	0.10
3.64	3.01
3.8	1.00

Table 8:151: Effect of Kinetic Diameter of gases to the Gas Permeation at 296 K after fourth Dip

Molecular Weight (g/mol)	Flow Rate(ml/min)
4	0.20
16	0.00
28	0.00
40	0.00
44	4.98

Table 8:152: Effect of Molecular Weight of gases to the Gas Permeation at 338K after fourth Dip

Molecular Weight(g/mol)	Flow Rate(ml/min)
4	0.34
16	0.00
28	0.00
40	0.00
44	14.30

Table 8:153: Effect of Molecular Weight of gases to the Gas Permeation at 363 K after fourth Dip

Molecular Weight(g/mol)	Flow Rate(ml/min)
4	1.34
16	0.01
28	0.40
40	0.00
44	24.50

Table 8:154: Effect of Molecular Weight of gases to the Gas Permeation at 393 K after fourth Dip

Molecular Weight(g/mol)	Flow Rate(ml/min)
4	2.50
16	0.09
28	0.10
40	0.00
44	37.56

Table 8:155: Effect of Molecular Weight of gases to the Gas Permeation at 423K after fourth Dip

Molecular Weight(g/mol)	Flow Rate(ml/min)
4	2.70
16	0.35
28	1.66
40	0.02
44	54.01

Table 8:156: Effect of Molecular Weight of gases to the Gas Permeation at 473K after fourth Dip

Molecular Weight(g/mol)	Flow Rate(ml/min)
4	4.60
16	0.99
28	3.00
40	0.09
44	60.40

8.7 APPENDIX 7: SELECTIVITY CALCULATIONS

The Selectivity worked out here in this project was categorised into pure gas and mixed gas selectivities.

Membrane Support Only

For Co current Flow with Retentate Valve fully opened at 0.05Bar Pressure Drop Absolute Value

Selectivity; $\alpha_{CO_2/N_2} = \frac{CO_2 Permeation}{N_2 Permeation} = \frac{PCO_2}{PN_2} = \frac{60ml}{85ml} = 0.71$

For Co current Flow with Retentate Valve fully closed at 0.05Bar Pressure Drop Absolute Value

Selectivity; $\alpha_{CO_2/N_2} = \frac{CO_2 Permeation}{N_2 Permeation} = \frac{PCO_2}{PN_2} = \frac{70ml}{90ml} = 0.78$

For Counter current Flow with Retentate Valve fully closed at 0.05Bar Pressure Drop Absolute Value

Selectivity; $\alpha_{CO_2/N_2} = \frac{CO_2 Permeation}{N_2 Permeation} = \frac{PCO_2}{PN_2} = \frac{75ml}{278ml} = 0.27$

For Counter current Flow with Retentate Valve fully closed at 0.05Bar Pressure Drop Absolute Value

Selectivity; $\alpha_{CO_2/N_2} = \frac{CO_2 Permeation}{N_2 Permeation} = \frac{PCO_2}{PN_2} = \frac{72ml}{323ml} = 0.22$

For Membrane Support only with mixture A for feed

Selectivity; $\alpha_{C0_2/N_2} = \frac{\%C0_{2P}/\%N_{2P}}{\%C0_{2F}/\%N_{2F}}$

Then,

$$\frac{14\%/86\%}{14\%/86\%} = 1$$

$\alpha_{C02/N2}$ = 1

For Membrane A

For Co current Flow with Retentate Valve fully opened with mixture A as feed

Selectivity; $\alpha_{C0_2/N_2} = \frac{\%C0_{2P}/\%N_{2P}}{\%C0_{2F}/\%N_{2F}}$

$\frac{16\%/84\%}{14\%/86\%}$ = 1.17

For Co current Flow with Retentate Valve fully closed with mixture A as feed

Selectivity; $\alpha_{C0_2/N_2} = \frac{\%C0_{2P}/\%N_{2P}}{\%C0_{2F}/\%N_{2F}}$

$\frac{18\%/82\%}{14\%/86\%}$ = 1.3

For Co current Flow with Retentate Valve fully closed at 0.05Bar Pressure Drop Absolute Value

Selectivity; $\alpha_{CO_2/N_2} = \frac{CO_2 Permeation}{N_2 Permeation} = \frac{PCO_2}{PN_2} = \frac{147ml}{102ml}$ = 1.44

For Membrane B

For Co current Flow with Retentate Valve fully closed with mixture A as feed

Selectivity; $\alpha_{C0_2/N_2} = \frac{\%C0_{2P}/\%N_{2P}}{\%C0_{2F}/\%N_{2F}}$

$$\frac{25\%/75\%}{14\%/86\%} = \quad 2.04$$

For Membrane C after first Dip using mixture A as feed

Selectivity; $\alpha_{C0_2/N_2} = \quad \frac{\%C0_{2P}/\%N_{2P}}{\%C0_{2F}/\%N_{2F}}$

$$\frac{30\%/70\%}{14\%/86\%} = \quad 2.63 \approx 3$$

For Membrane C after second Dip using mixture A as feed

Selectivity; $\alpha_{C0_2/N_2} = \quad \frac{\%C0_{2P}/\%N_{2P}}{\%C0_{2F}/\%N_{2F}}$

$$\frac{30\%/70\%}{14\%/86\%} = \quad 2.63 \approx 3$$

For Membrane C after third Dip using mixture A as feed

Selectivity; $\alpha_{C0_2/N_2} = \quad \frac{\%C0_{2P}/\%N_{2P}}{\%C0_{2F}/\%N_{2F}}$

$$\frac{30\%/70\%}{14\%/86\%} = \quad 2.63 \approx 3$$

For Membrane C after fourth Dip using mixture A as feed

Selectivity; $\alpha_{C0_2/N_2} = \dfrac{\%C0_{2P}/\%N_{2P}}{\%C0_{2F}/\%N_{2F}}$

$\dfrac{30\%/70\%}{14\%/86\%} = 2.63 \approx 3$

For Membrane C after fourth Dip for pure gases as feed

For Methane (CH4) at 0.05 Bar Pressure Drop Absolute value

Selectivity; $\alpha_{CO_2/CH4} = \dfrac{CO_2 Permeation}{CH4 Permeation} = \dfrac{PCO_2}{PCH4} = \dfrac{5.12ml}{0ml} = \infty$ (Infinity)

For Helium (He) at 0.05 Bar Pressure Drop Absolute value

Selectivity; $\alpha_{CO_2/He} = \dfrac{CO_2 Permeation}{He Permeation} = \dfrac{PCO_2}{PHe} = \dfrac{5.12ml}{0.2ml} = 25.6 \approx 26$

For Argon (Arg) at 0.05 Bar Pressure Drop Absolute value

Selectivity; $\alpha_{CO_2/Arg} = \dfrac{CO_2 Permeation}{Argon Permeation} = \dfrac{PCO_2}{PArg} = \dfrac{5.12ml}{0.0ml} = \infty$ (Infinity)

For Nitrogen (N_2) at 0.05 and 0.06 Bar Pressure Drop Absolute value

Selectivity; $\alpha_{CO_2/N_2} = \dfrac{CO_2 Permeation}{N_2 Permeation} = \dfrac{PCO_2}{PN_2} = \dfrac{5.12ml}{0.0ml} = \infty$ (Infinity)

For Nitrogen (N_2) at 0.07 Bar Pressure Drop Absolute value

Selectivity; $\alpha_{CO_2/N_2} = \frac{CO_2 Permeation}{N_2 Permeation} = \frac{PCO_2}{PN_2} = \frac{5.12ml}{0.5ml} = 10.24$

For Second Stage System with Membrane C with mixture B as feed and Permeate Condition of $C0_2$-60%, N_2-40% after Fourth Dip

Selectivity; $\alpha_{C0_2/N_2} = \frac{\%C0_{2P}/\%N_{2P}}{\%C0_{2F}/\%N_{2F}}$

$\frac{60\%/40\%}{30\%/70\%} = 3.5 \approx 4$

For third Stage System with Membrane C with feed: mixture C and Permeate Condition of $C0_2$-90%, N_2-10% after Fourth Dip

Selectivity; $\alpha_{C0_2/N_2} = \frac{\%C0_{2P}/\%N_{2P}}{\%C0_{2F}/\%N_{2F}}$

$\frac{90\%/10\%}{60\%/40\%} = 6$

Table 8:157: Selectivity of $C0_2$ to different gases using different Membranes

Selectivity	Membrane Type
0.71 α_{C0_2/N_2}	Membrane Support Only For Co current Flow with Retentate Valve fully opened at 0.05 Bar Pressure Drop Absolute Value
0.78 α_{C0_2/N_2}	Membrane Support Only For Co current Flow with Retentate Valve fully closed at 0.05 Bar Pressure Drop Absolute Value
0.27 α_{C0_2/N_2}	Membrane Support Only For Counter current Flow with Retentate Valve fully closed at 0.05 Bar Pressure Drop Absolute Value
0.22 α_{C0_2/N_2}	Membrane Support Only For Counter current Flow with Retentate Valve fully closed at 0.05 Bar Pressure Drop Absolute Value
1.44 α_{C0_2/N_2}	For Membrane A For Co current Flow with Retentate Valve fully closed at 0.05Bar Pressure Drop Absolute Value
∞ (Infinity) α_{C0_2/CH_4}	For Membrane C after fourth Dip for pure gases as feed

	For Methane (CH_4) at 0.05 Bar Pressure Drop Absolute value
26 α_{C0_2/H_E}	For Membrane C after fourth Dip for pure gases as feed For Helium (He) at 0.05 Bar Pressure Drop Absolute value
∞ (Infinity) α_{C0_2/ARG_E}	For Membrane C after fourth Dip for pure gases as feed For Argon (Arg) at 0.05 Bar Pressure Drop Absolute value
∞ (Infinity) α_{C0_2/N_2}	For Membrane C after fourth Dip for pure gases as feed For Nitrogen (N_2) at 0.05 and 0.06 Bar Pressure Drop Absolute value
10.24 α_{C0_2/N_2}	For Membrane C after fourth Dip for pure gases as feed For Nitrogen (N_2) at 0.07 Bar Pressure Drop Absolute value

8.7.1 Membranes and their Selectivity and Permeance

Table 8:158: Selectivity and Permeance of different membranes from different mixtures

Selectivity	Membrane Support Only Permeance (mol/m^2.s.Pa)	Membrane A Permeance (mol/m^2.s.Pa)	Membrane B Permeance (mol/m^2.s.Pa)
1	4.61E-08	5.88E-08	3.39E-08
1.3	6.29E-08	7.08E-08	5.37E-08
2.04	7.76E-08	8.94E-08	6.07E-08
3.0	1.03E-07	1.32E-07	9.16E-08
4	1.28E-07	1.49E-07	1.06E-07
6	1.65E-07	1.53E-07	1.18E-07

Table 8:159: Selectivity and Permeance of different membranes from different mixtures

Membrane C at first Stage Permeance (mol/m^2.s.Pa)	Selectivity	Membrane C at second Stage Permeance (mol/m^2.s.Pa)	Membrane C at third Stage Permeance (mol/m^2.s.Pa)
2.60E-09	1	2.70E-09	4.86E-09
6.88E-09	1.3	5.94E-09	7.38E-09
1.01E-08	2.04	8.79E-09	1.02E-08
1.59E-08	3.0	1.01E-08	1.24E-08
2.05E-08	4	1.24E-08	1.44E-08
2.85E-08	6	1.64E-08	1.71E-08

Table 8:160: Selectivity and Permeance of membrane support only from mixture A

Selectivity	Membrane Support Only Permeance ($mol/m^2.s.Pa$)
1.0	4.61E-08
1.0	6.29E-08
1.0	7.76E-08
1.0	1.03E-07
1.0	1.28E-07
1.0	1.65E-07

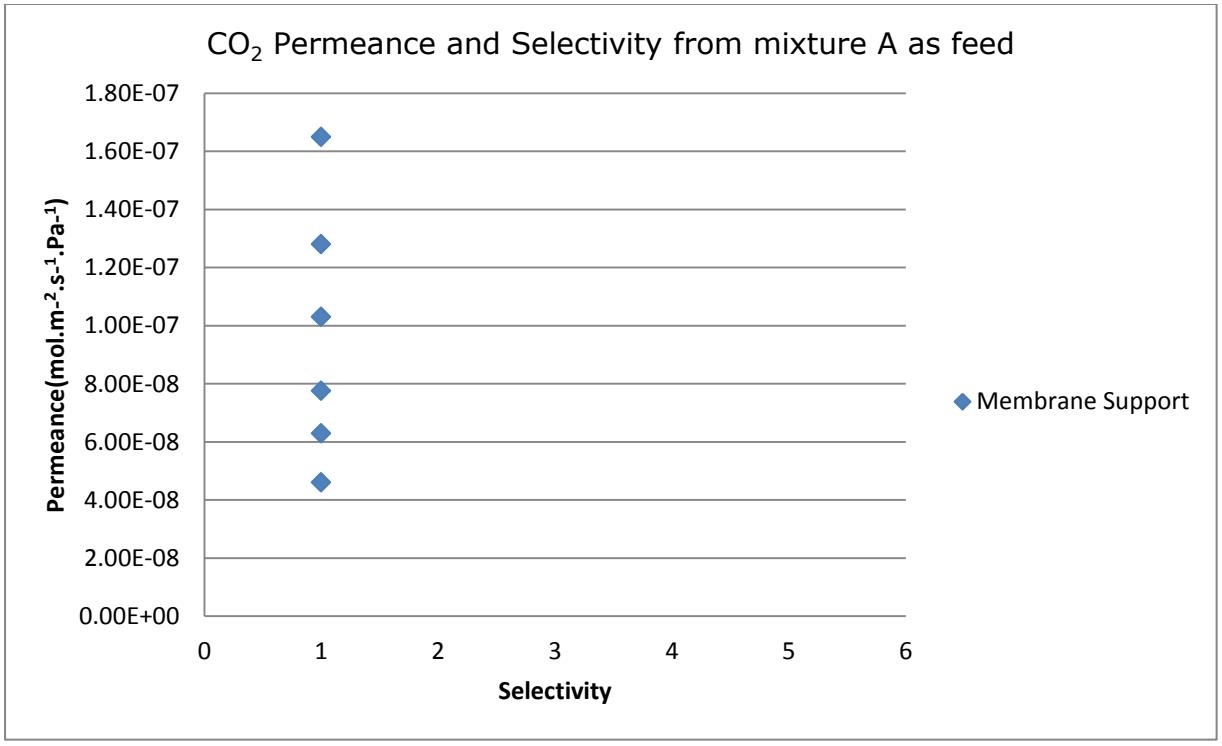

Figure 8:90: Selectivity and Permeance of membrane support only from mixture A

Table 8:161: Selectivity and Permeance of Membrane A from a mixture

Selectivity	Membrane A Permeance ($mol/m^2.s.Pa$)
1.3	5.88E-08
1.3	7.08E-08
1.3	8.94E-08
1.3	1.32E-07
1.3	1.49E-07
1.3	1.53E-07

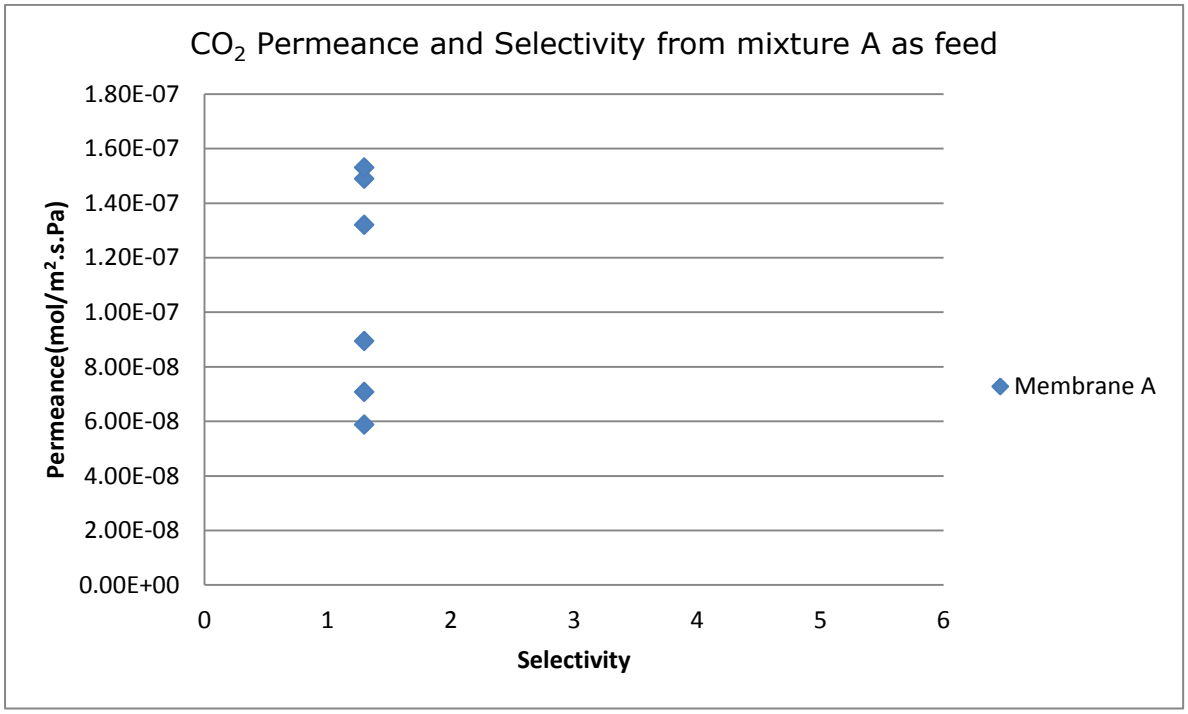

Figure 8:91: Selectivity and Permeance of Membrane A from a mixture

Table 8:162: Selectivity and Permeance of Membrane B from a mixture

Selectivity	Membrane B Permeance ($mol/m^2.s.Pa$)
2.04	3.39E-08
2.04	5.37E-08
2.04	6.07E-08
2.04	9.16E-08
2.04	1.06E-07
2.04	1.18E-07

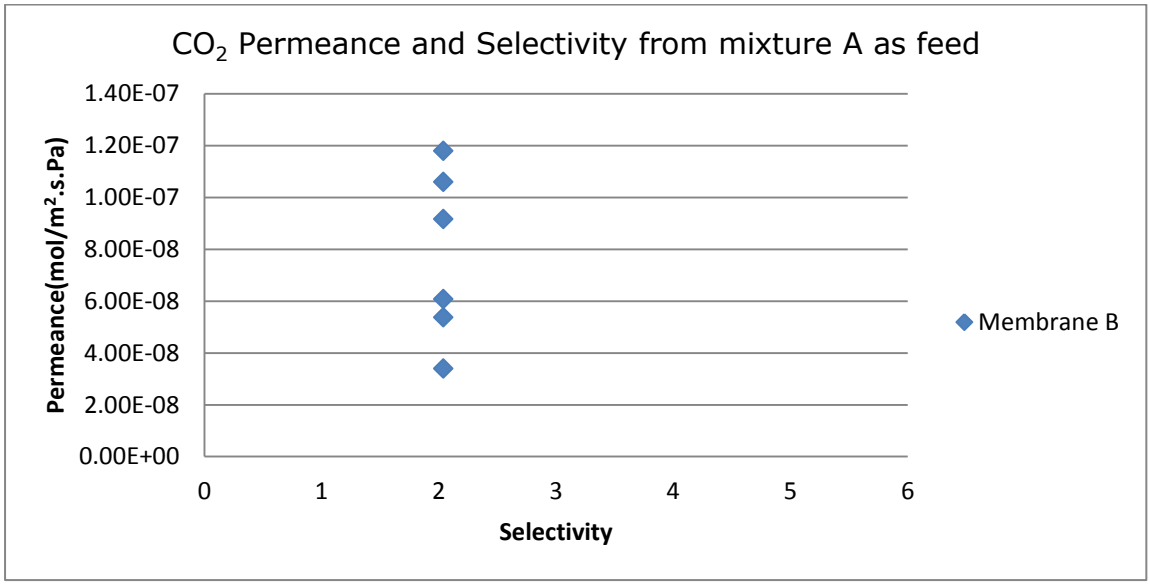

Figure 8:92: Selectivity and Permeance of Membrane B from mixture A

Table 8:163: Selectivity and Permeance of Membrane C at first stage

Selectivity	Membrane C at first Stage Permeance (mol/m^2.s.Pa)
3	2.60E-09
3	6.88E-09
3	1.01E-08
3	1.59E-08
3	2.05E-08
3	2.85E-08

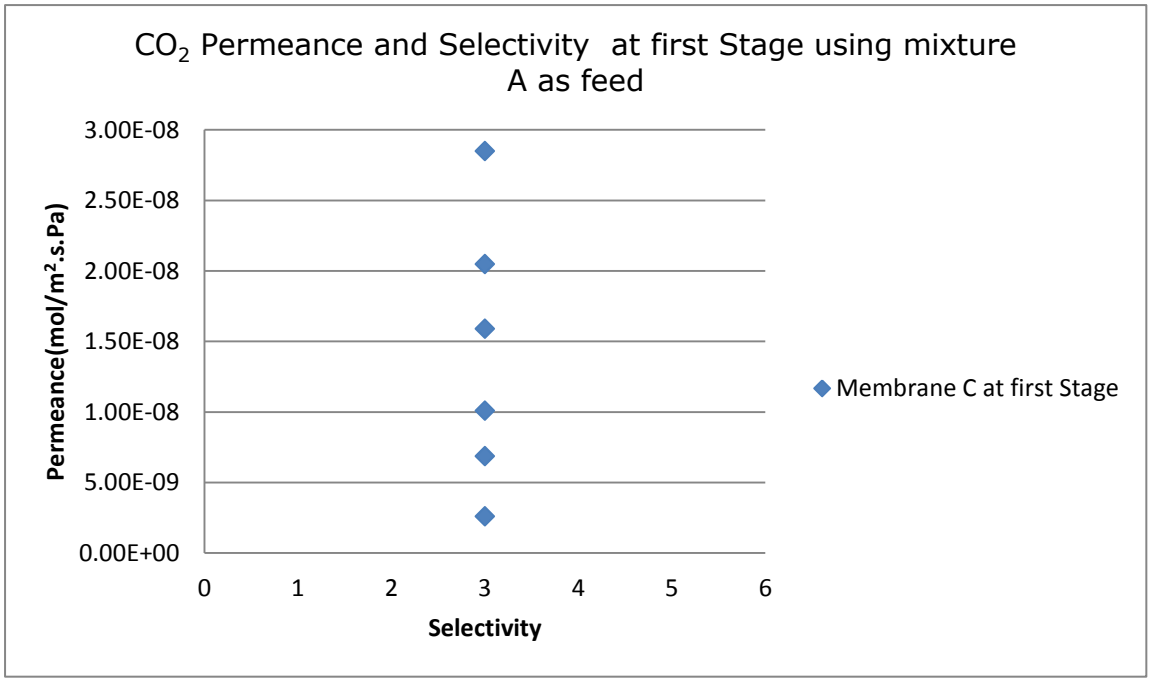

Figure 8:93: Selectivity and Permeance of Membrane C at first stage

Table 8:164: Selectivity and Permeance of Membrane C at second stage

Selectivity	Membrane C at second Stage Permeance ($mol/m^2.s.Pa$)
4	2.70E-09
4	5.94E-09
4	8.79E-09
4	1.01E-08
4	1.24E-08
4	1.64E-08

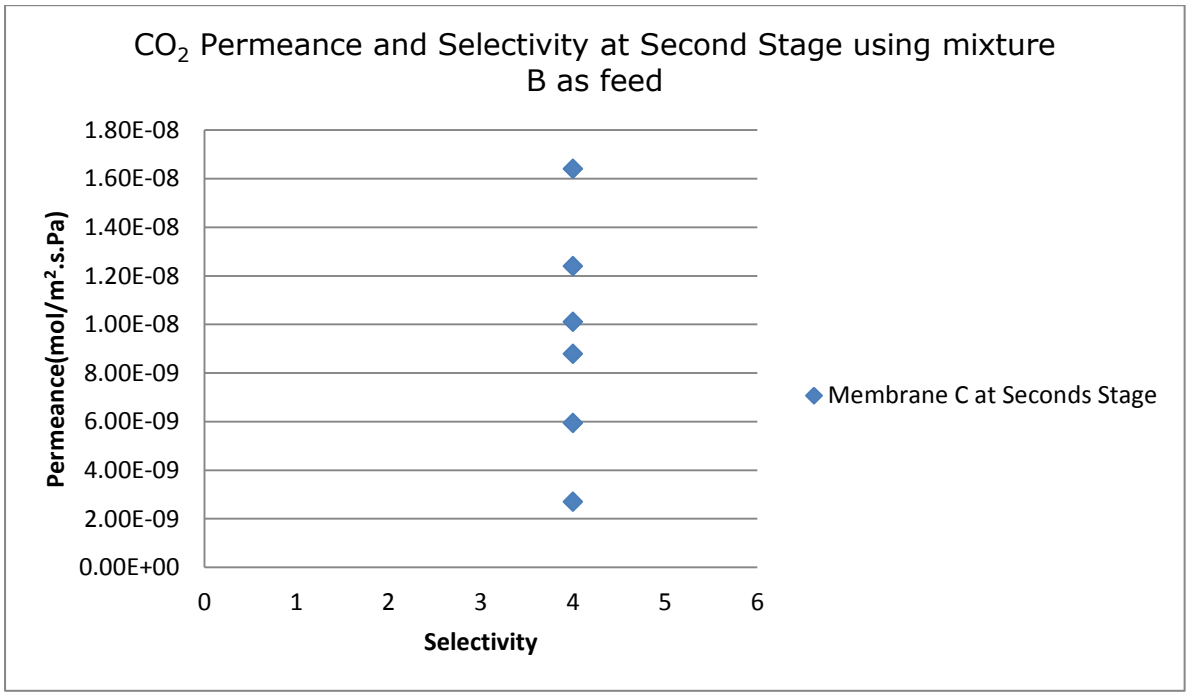

Figure 8:94: Selectivity and Permeance of Membrane C at second stage

Table 8:165: Selectivity and Permeance of Membrane C at third stage

Selectivity	Membrane C at third Stage Permeance ($mol/m^2.s.Pa$)
6	4.86E-09
6	7.38E-09
6	1.02E-08
6	1.24E-08
6	1.44E-08
6	1.71E-08

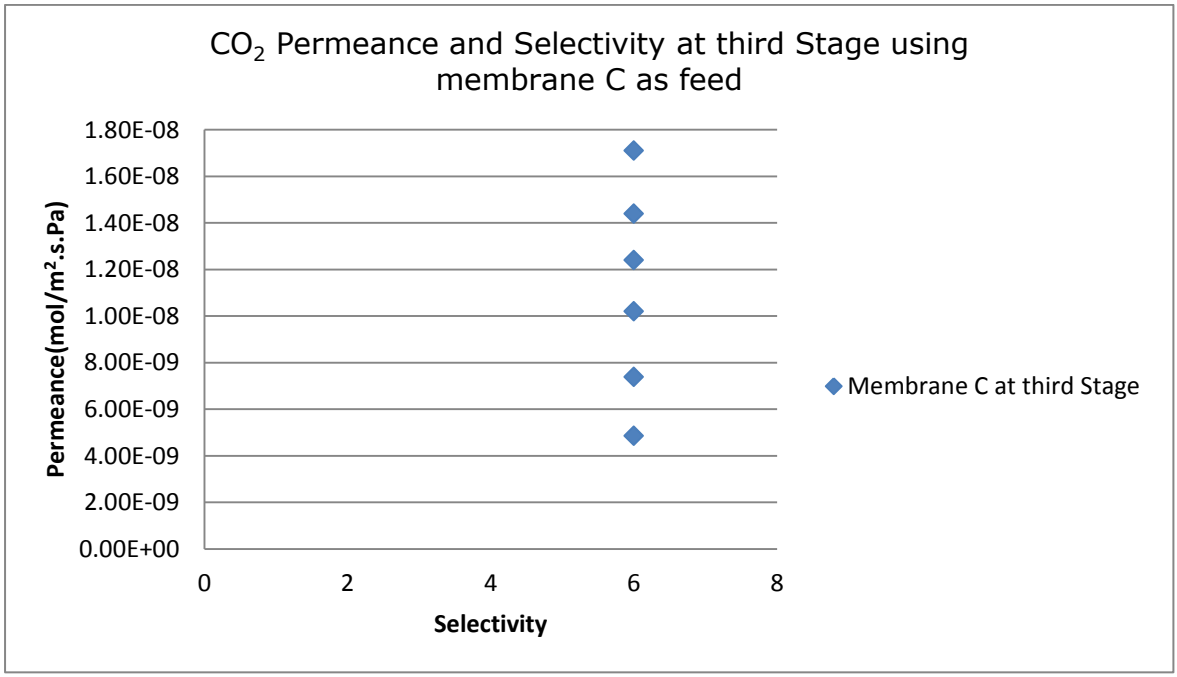

Figure 8:95: CO_2 Permeance and Selectivity at third Stage using Membrane C as feed

8.8 APPENDIX 8: MEMBRANE PERMEABILITY CALCULATION

For Membrane C $C0_2$ permeability after First Dip

Table 8:166: Values of C02 for mixture A as using Membrane C after First Dip.

P_{Feed} (Pascal)	$P_{Permeate}$ (Pascal)	Permeate Flow Rate (ml/min)	Permeation Rate (mol/sec)	Average Pressure (Pascal)	Permeability (mol.m)/ (m^2.m.Pa)
14700	30000	10.50	7.81E-06	22000	6.72E-11
14800	30000	16.49	1.22E-05	22400	8.74E-11
15000	30000	22.79	1.70E-05	22500	1.04E-10
15100	30000	30.00	2.23E-05	22600	1.20E-10
15300	30000	36.00	2.68E-05	22700	1.28E-10
15400	30000	42.00	3.13E-05	22700	1.34E-10

For Membrane C $C0_2$ permeability after Second Dip

Table 8:167: Values of $C0_2$ for mixture A as feed using Membrane C after Second Dip.

P_{Feed} (Pascal)	$P_{Permeate}$ (Pascal)	Permeate Flow Rate (ml/min)	Permeation Rate (mol/sec)	Average Pressure (Pascal)	Permeability (mol.m)/ (m^2.m.Pa)
14700	30000	9.00	1.82E-07	22000	3.51E-11
14800	30000	12.00	2.02E-07	22400	3.89E-11
15000	30000	16.49	2.39E-07	22500	4.60E-11
15100	30000	22.50	2.85E-07	22600	5.48E-11
15300	30000	25.50	2.87E-07	22650	5.53E-11
15400	30000	28.5	2.89E-07	22700	5.56E-11

For Membrane C $C0_2$ permeability after Third Dip

Table 8:168: Values of $C0_2$ for mixture A as feed using Membrane C after Third Dip.

P_{Feed} (Pascal)	$P_{Permeate}$ (Pascal)	Permeate Flow Rate (ml/min)	Permeation Rate (mol/sec)	Average Pressure (Pascal)	Permeability (mol.m)/ (m^2.m.Pa)
14700	30000	4.50	3.35E-06	22000	1.79E-11
14800	30000	7.50	5.58E-06	22400	2.48E-11
15000	30000	10.50	7.81E-06	22500	2.99E-11
15100	30000	15.00	1.12E-05	22600	3.73E-11
15300	30000	19.50	1.45E-05	22700	4.30E-11
15400	30000	22.50	1.67E-05	22700	4.46E-11

For Membrane C $C0_2$ permeability after Fourth Dip

Table 8:169 : Values of $C0_2$ for mixture A as feed using Membrane C after Fourth Dip.

P_{Feed} (Pascal)	$P_{Permeate}$ (Pascal)	Permeate Flow Rate (ml/min)	Permeation Rate (mol/sec)	Average Pressure (Pa)	Permeability (mol.m)/ (m^2.m.Pa)
14700	30000	0.90	6.70E-07	22000	3.64E-12
14800	30000	2.40	1.79E-06	22400	8.12E-12
15000	30000	3.60	2.68E-06	22500	1.04E-11
15100	30000	5.70	4.24E-06	22600	1.44E-11
15300	30000	7.50	5.58E-06	22650	1.69E-11
15400	30000	10.50	7.81E-06	22700	2.12E-11

8.9 APPENDIX 9: ESTIMATION OF THE HEAT OF ADSORPTION

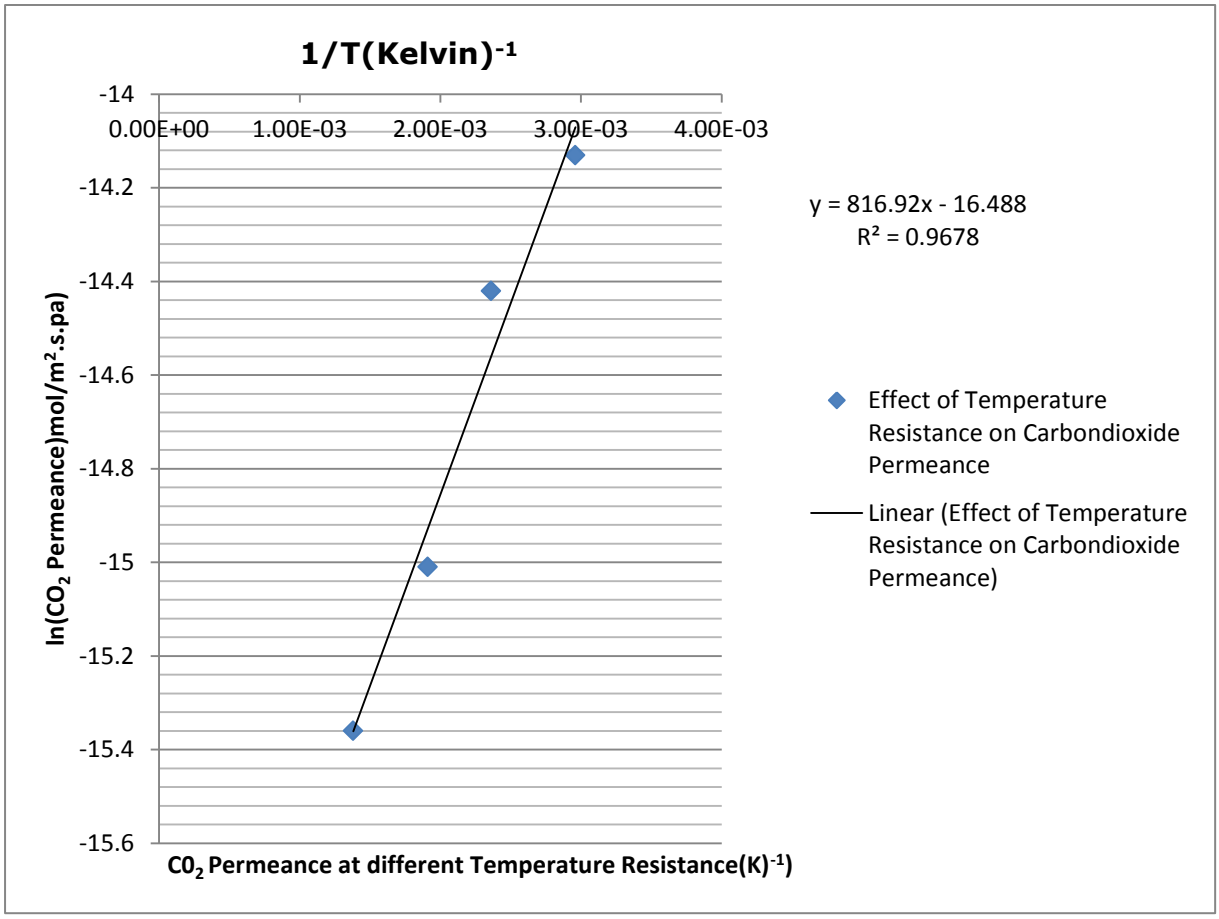

Figure 8:96: Effect of Temperature Resistance on CO_2 Permeance using membrane A

From the temperature dependence on the gas permeance is shown by the Arrhenius equation in equation 2.5 in the previous chapter. Also, in a linear form, we have ln P = $\ln P_0$ + $\frac{\Delta H_a}{RT}$ .Then, plotting ln (permeance) and Temperature Resistance (1/T) has $\frac{\Delta H_a}{R}$ as the slope and $\ln P_0$ as the intercept. Where ΔH_a is the heat of adsorption and R is the universal gas constant (8.3145J/mol.K).

Then, $\frac{\Delta H_a}{R}$ = slope

ΔHa = 816.92x8.3145 = 6.792KJ/mol

The intercept from the Carbondioxide graph above is -16.49 mol/m^2 .s. Pa

For Nitrogen

Table 8:170: Pure N_2 Permeance at 5000 (Pascal) Pressure Drop and different temperatures using Membrane A

N_2 Permeance (mol/m^2.s.pa)	In(Permeance) (mol/m^2.s.pa)	Temperature in (Kelvin)	1/Temperature (Kelvin)$^{-1}$
6.20E-07	-14.29	296	3.38E-03
5.52E-07	-14.41	338	2.96E-03
5.04E-07	-14.50	423	2.36E-03
3.10E-07	-14.99	523	1.91E-03
2.73E-07	-15.11	723	1.38E-03

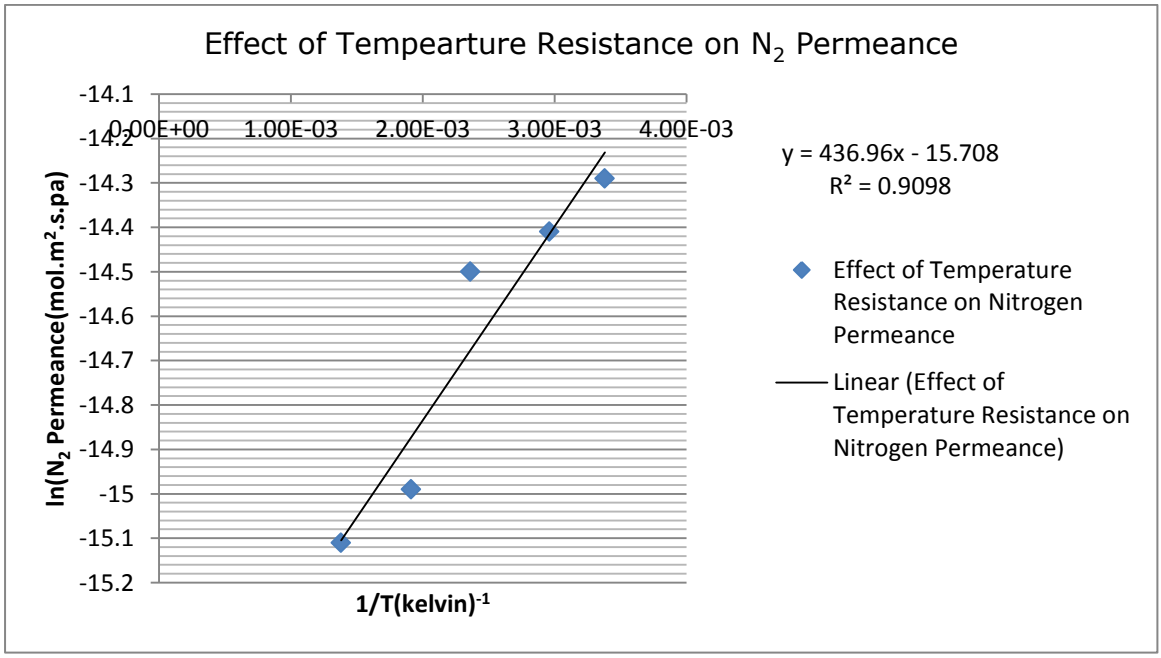

Figure 8:97: Effect of Temperature Resistance on Nitrogen Permeance using Membrane A

Table 8:171: Pure CO_2 Permeance at 5000 (Pascal) Pressure Drop and different temperatures using membrane C

CO_2 Permeance (mol/m^2.s.pa)	In(Permeance) (mol/m^2.s.pa)	Temperature in (Kelvin)	1/Temperature $(Kelvin)^{-1}$
3.11E-08	-17.29	296	3.38E-03
2.43E-08	-17.53	338	2.96E-03
1.94E-08	-17.76	423	2.36E-03
1.76E-08	-17.86	523	1.91E-03
8.50E-09	-18.58	723	1.38E-03

Table 8:172: Pure CO_2 Permeance at 10000 (Pascal) Pressure Drop and different temperatures using Membrane C

CO_2 Permeance (mol/m^2.s.pa)	In(Permeance) (mol/m^2.s.pa)	Temperature in (Kelvin)	1/Temperature $(Kelvin)^{-1}$
2.14E-07	-15.36	296	3.38E-03
1.21E-07	-15.93	338	2.96E-03
8.81E-08	-16.24	423	2.36E-03
6.07E-08	-16.62	523	1.91E-03
4.10E-08	-17.01	723	1.38E-03

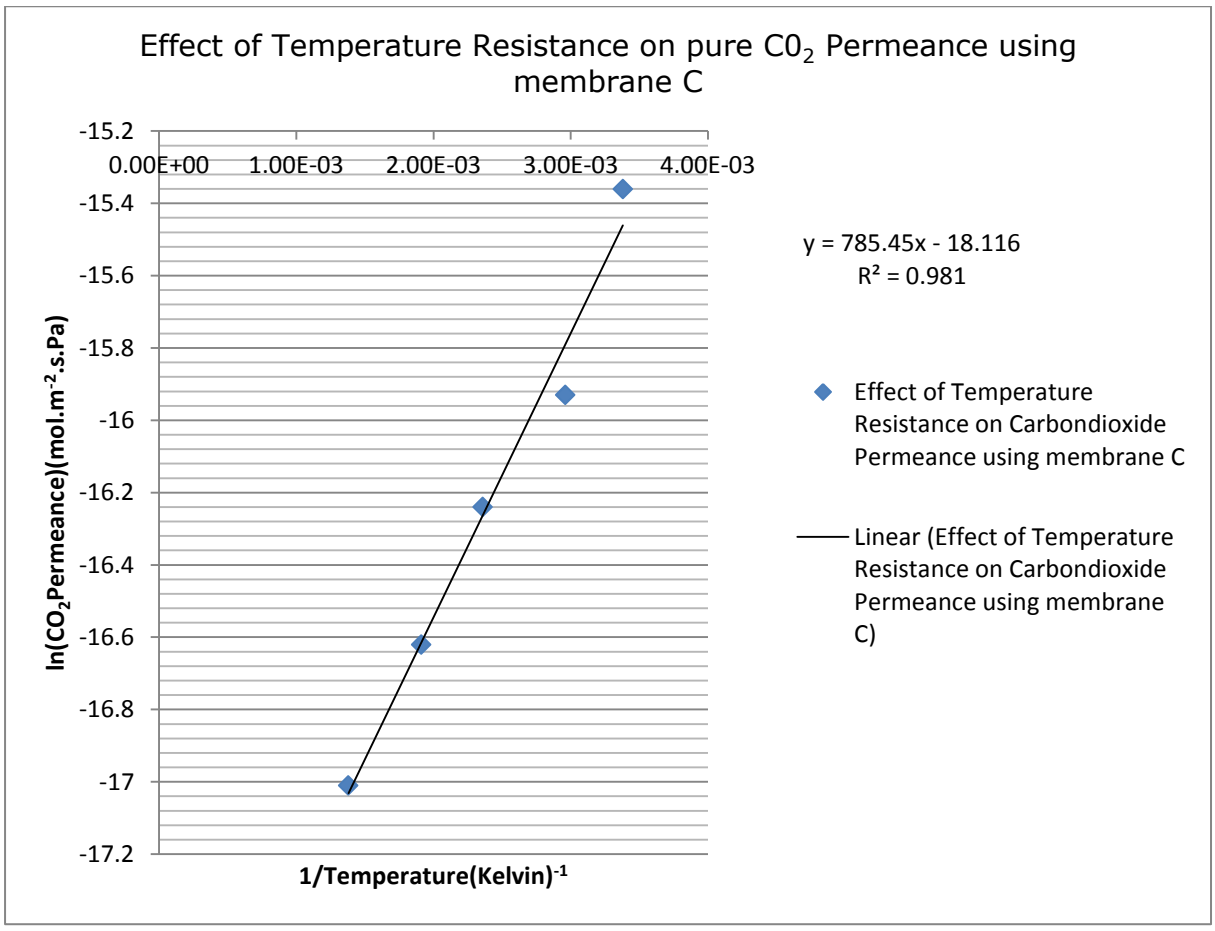

Figure 8:98: Pure CO_2 Permeance at 10000 (Pascal) Pressure Drop and different temperatures using membrane C

Table 8:173: Pure N_2 Permeance at 10000 (Pascal) Pressure Drop and different temperatures using Membrane C

N_2 Permeance (mol/m^2.s.pa)	In(Permeance) (mol/m^2.s.pa)	Temperature in (Kelvin)	1/Temperature (Kelvin)$^{-1}$
9.14E-09	-18.51	296	3.38E-03
6.07E-09	-18.92	338	2.96E-03
4.25E-09	-19.28	423	2.36E-03
1.52E-09	-20.30	523	1.91E-03
9.11E-09	-23.12	723	1.38E-03

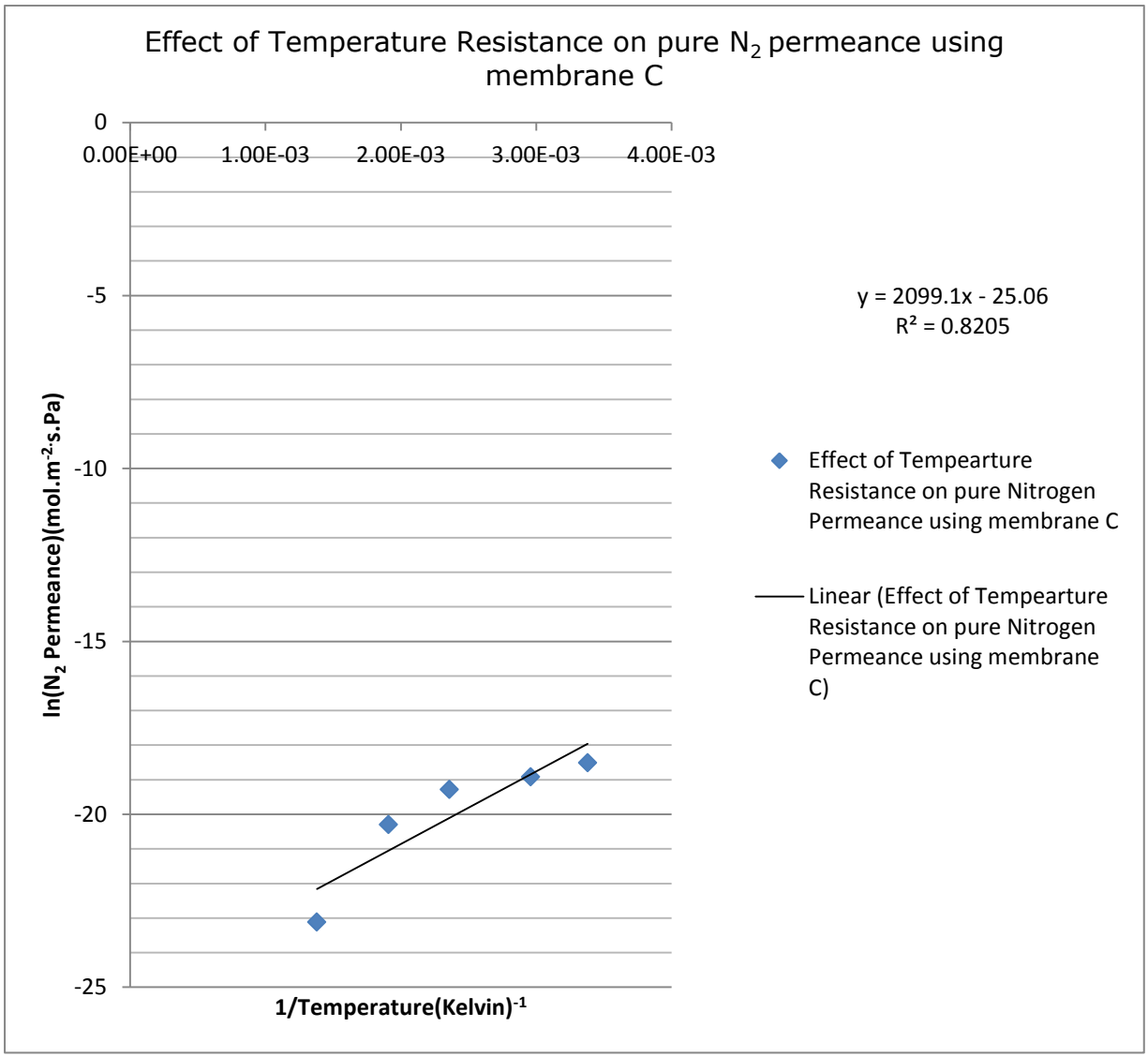

Figure 8:99: Pure N_2 Permeance at 10000 (Pascal) Pressure Drop and different temperatures using Membrane C

8.10 APPENDIX 10: ESTIMATION OF THE SURFACE FLOW

Table 8:174: Pure CO_2 permeance at 296K using Membrane C with retentate valve fully closed

Pure CO_2 Permeate Flow Rate (ml/min)	Pressure Drop(Pascal)
5.12	5000
15.20	6000
25.0	7000
40.56	8000
59.01	9000
70.40	10000

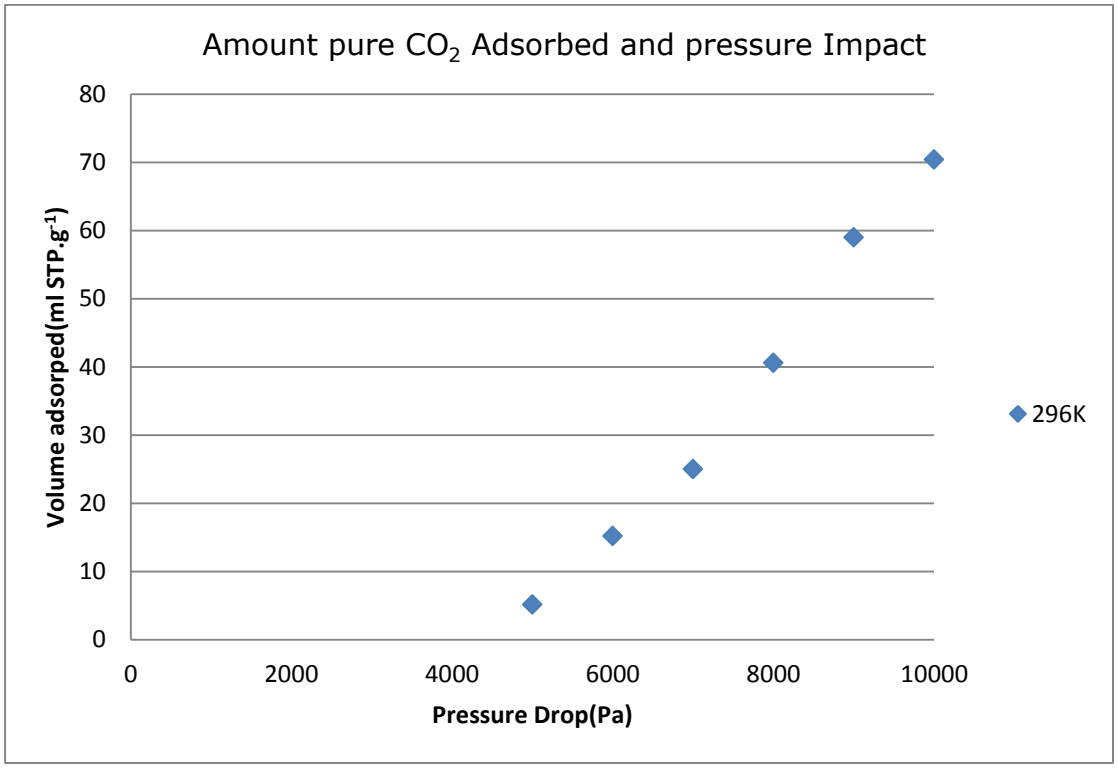

Figure 8:100: Figure: Amount of pure CO_2 adsorbed at 296K

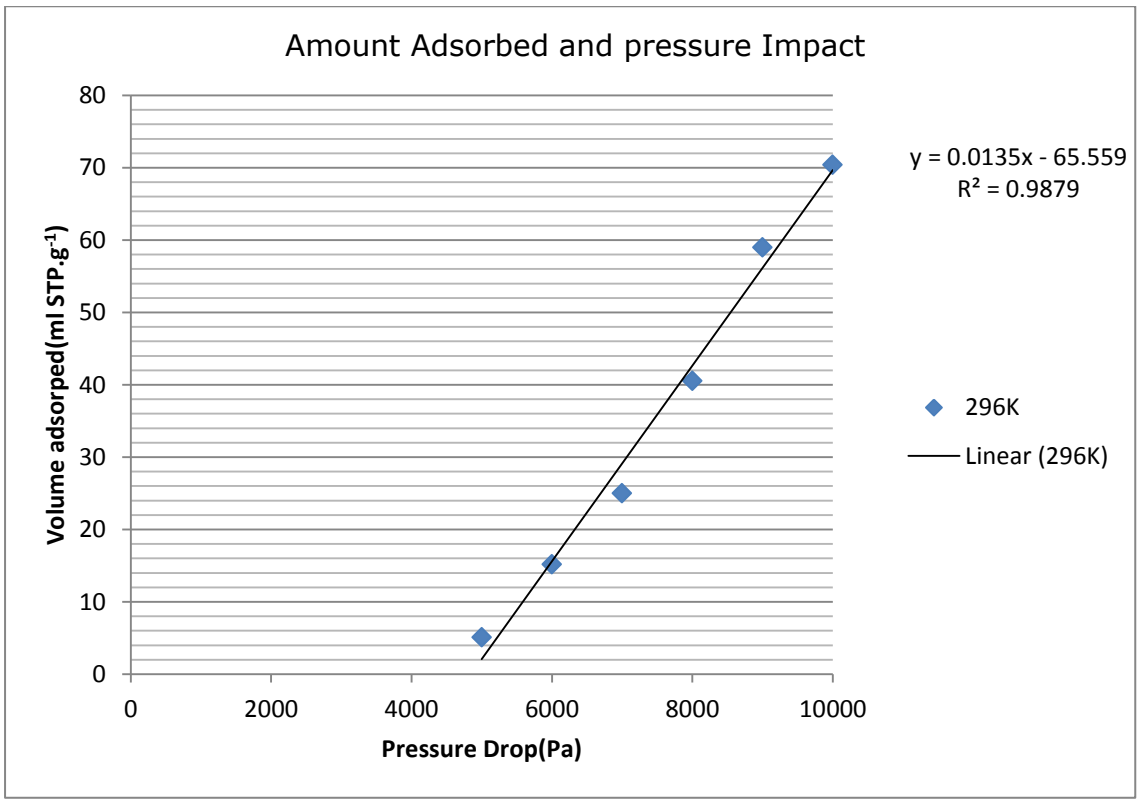

Figure 8:101: Amount of pure CO_2 adsorbed at 296K showing R^2

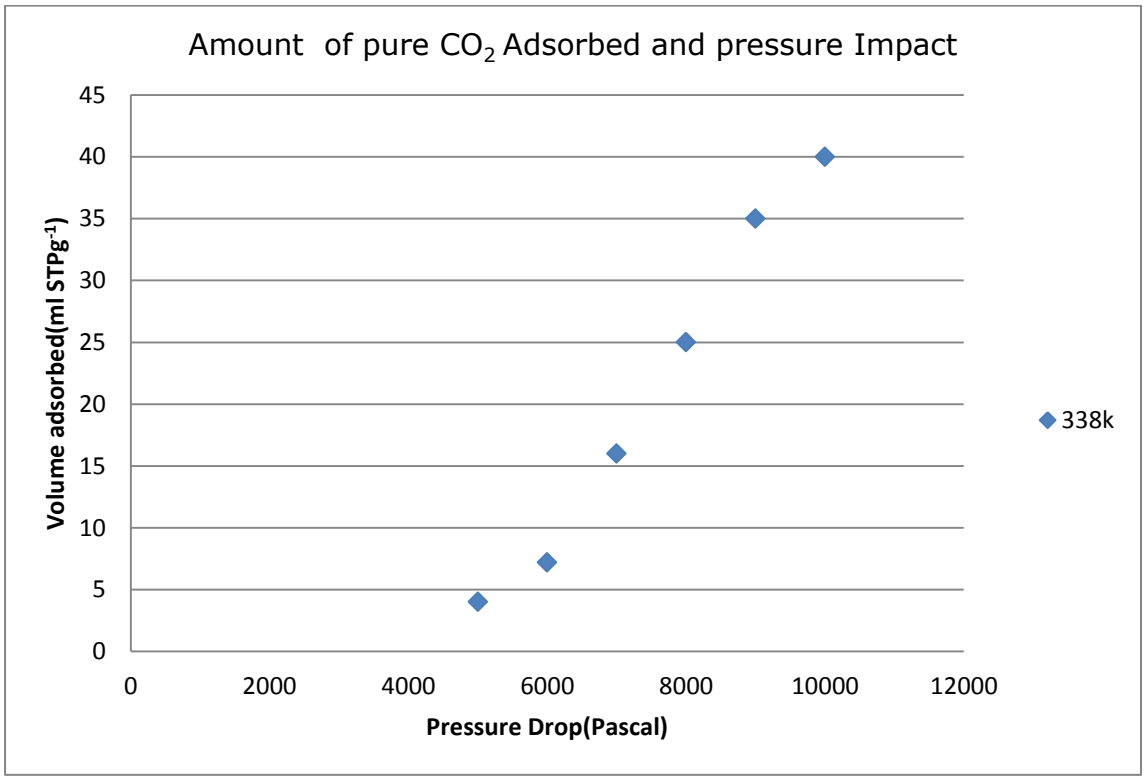

Figure 8:102: Amount of pure CO_2 adsorbed at 338K

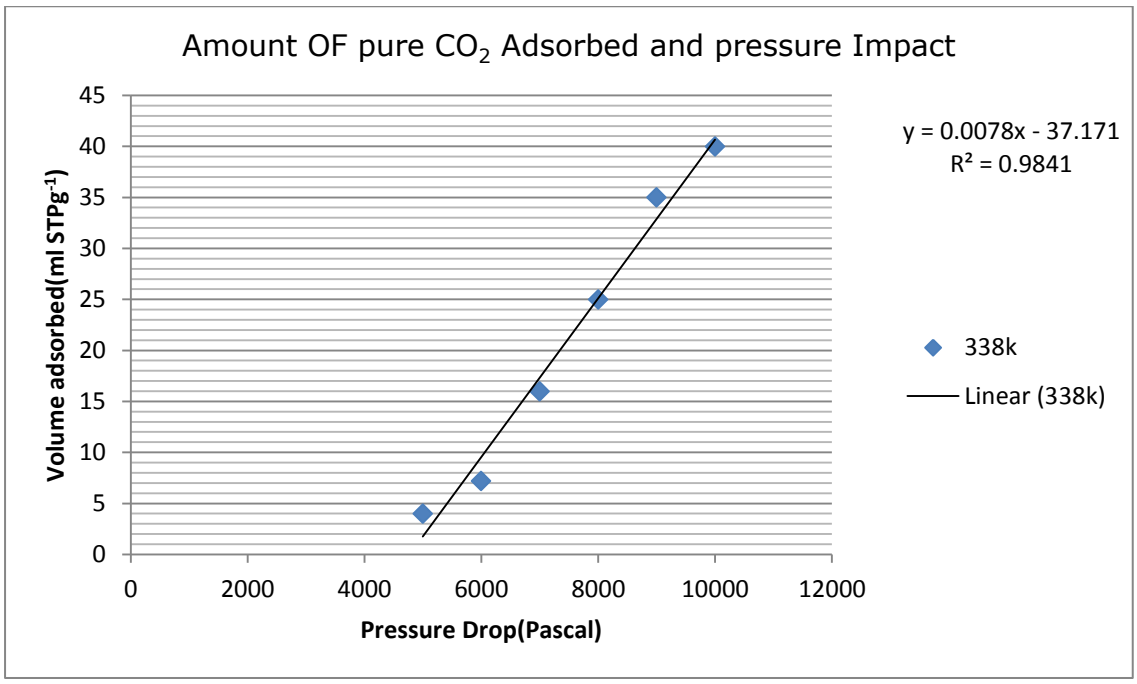

Figure 8:103: Amount of pure CO_2 adsorbed at 338K showing R^2

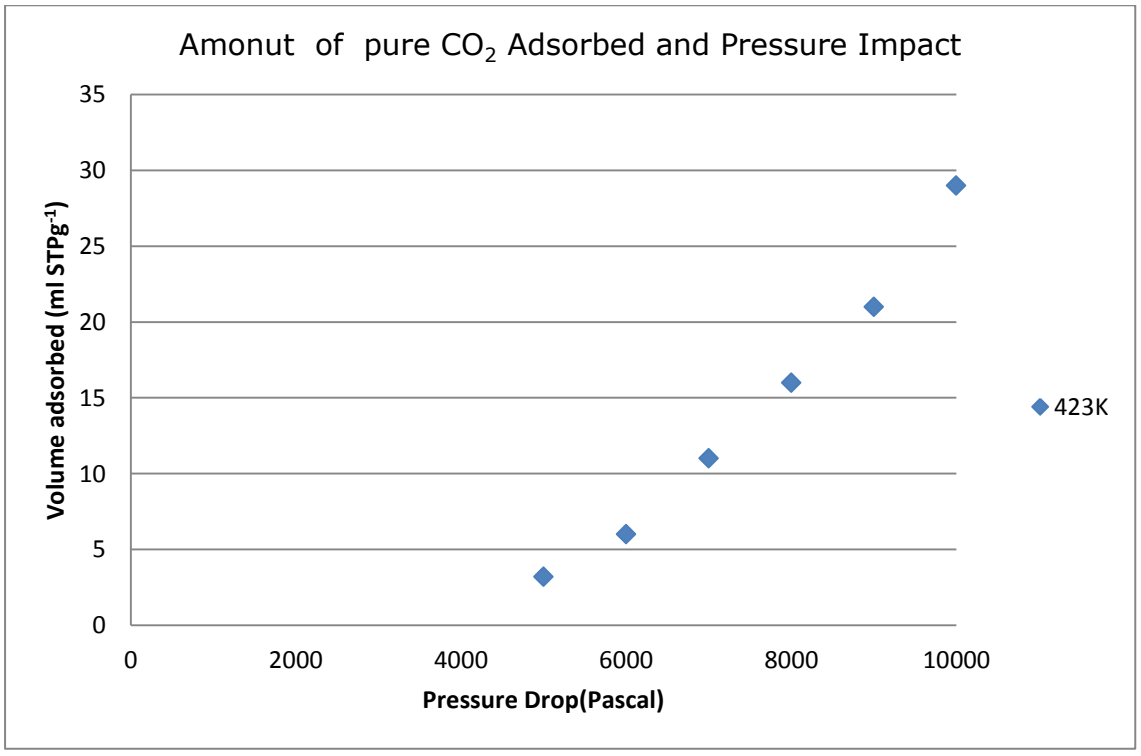

Figure 8:104: Amount of pure CO_2 adsorbed at 423K

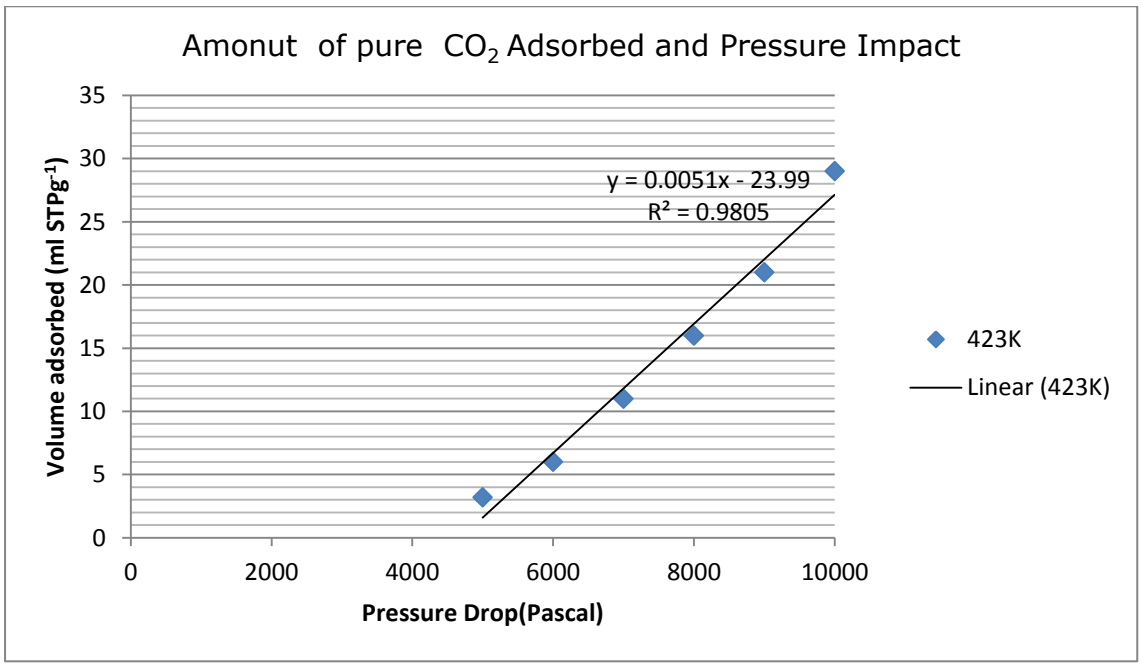

Figure 8:105: Amount of pure CO_2 adsorbed at 423K showing R^2

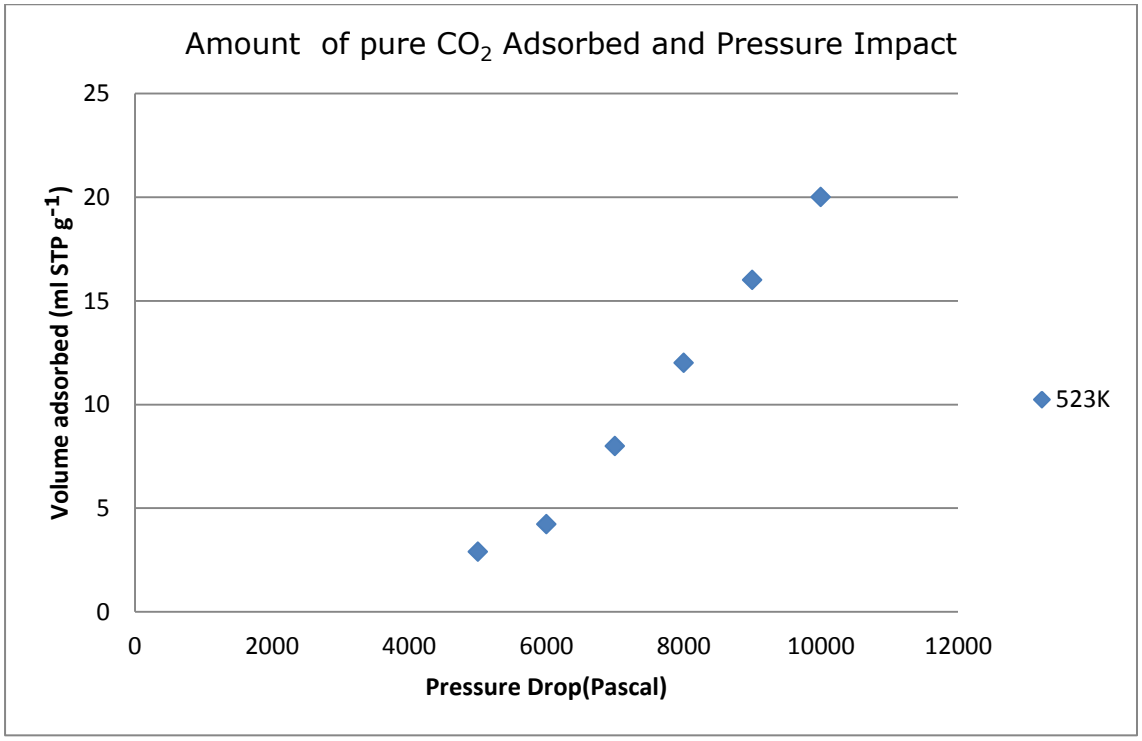

Figure 8:106: Amount of pure CO_2 adsorbed at 523K

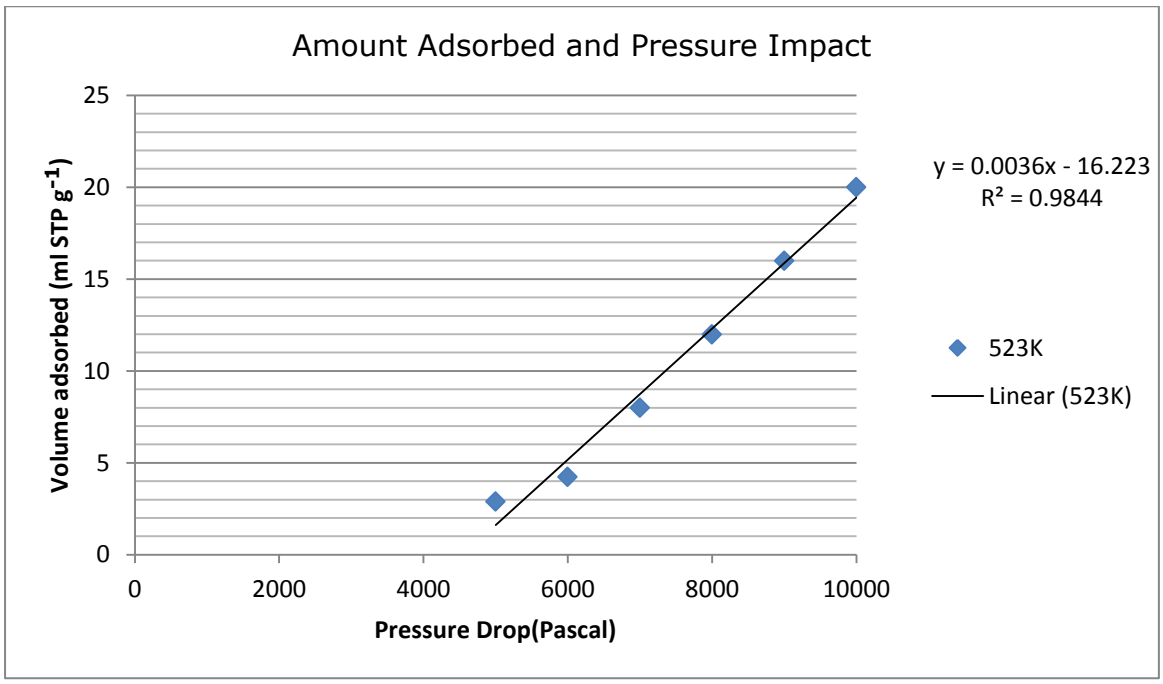

Figure 8:107: Amount of pure CO_2 adsorbed at 523K showing R^2

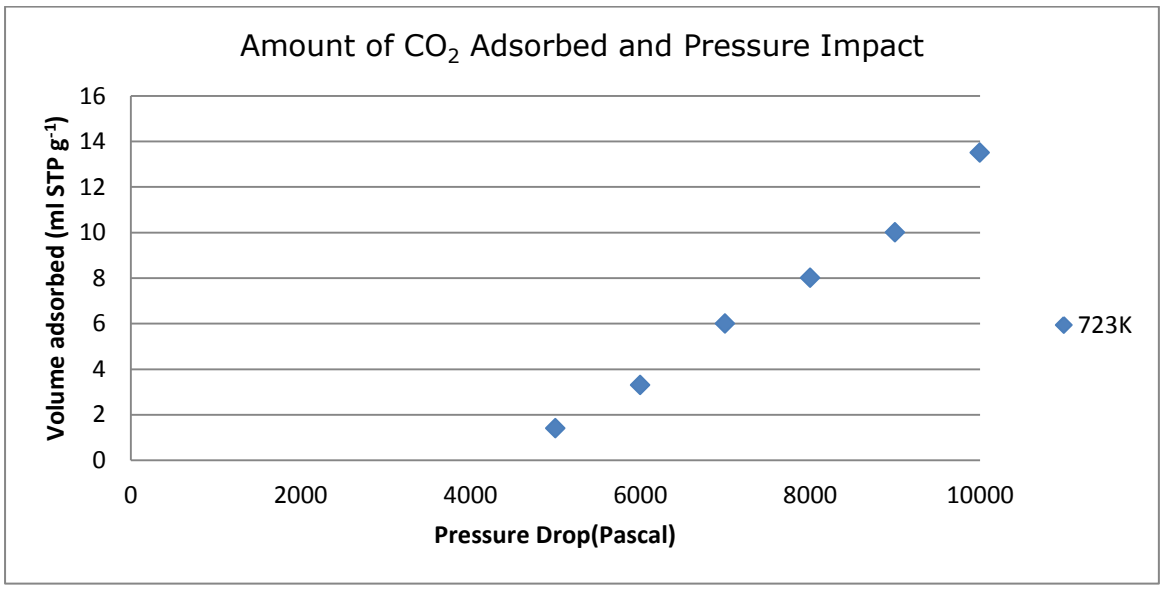

Figure 8:108: Amount of pure CO_2 adsorbed at 723k

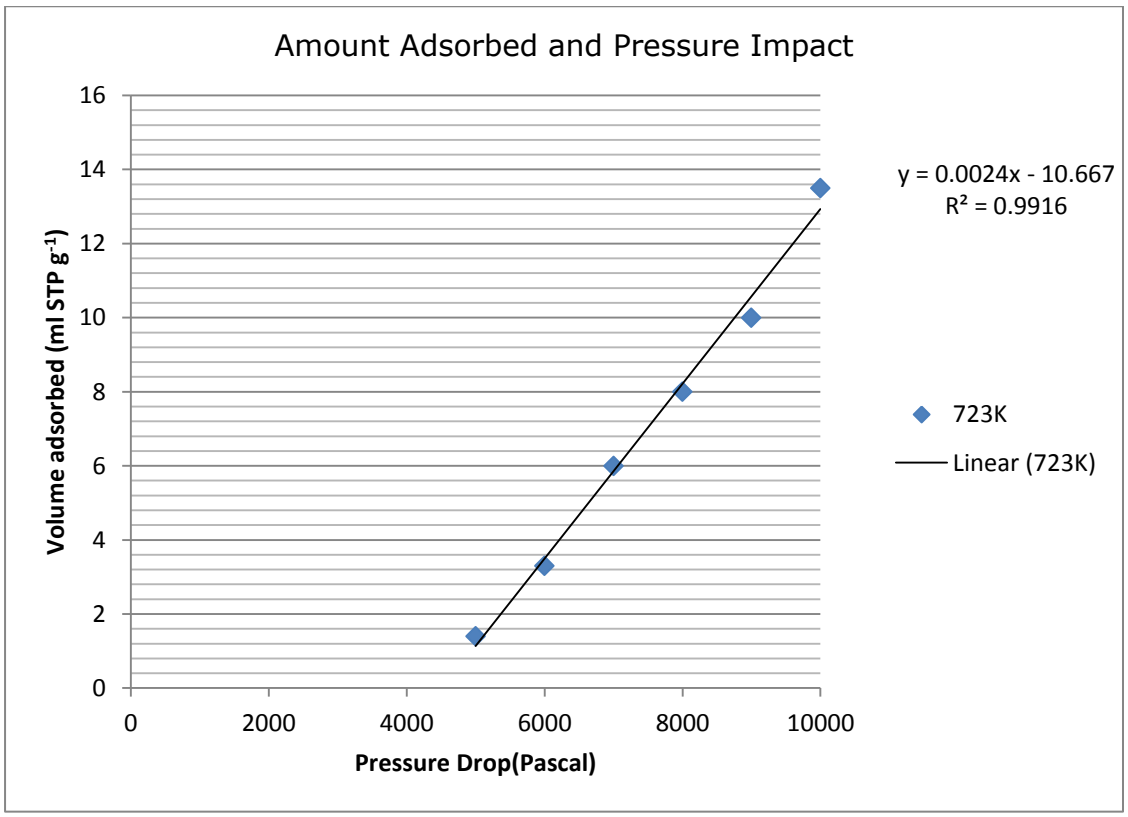

Figure 8:109: Amount of pure CO_2 adsorbed at 723k showing R^2

8.11 APPENDIX 11: EFFECT OF MEMBRANE THICKNESS ON PERMEANCE

Table 8:175: Pure CO_2 Permeance using membrane C of thickness 3.155E-04m

Permeance(mol.m^{-2}.s^{-1}.Pa^{-1})	Membrane Thickness(metres)
3.04E-08	3.155E-04
4.72E-08	3.155E-04
6.41E-08	3.155E-04
8.36E-08	3.155E-04
9.85E-08	3.155E-04
1.14E-07	3.155E-04

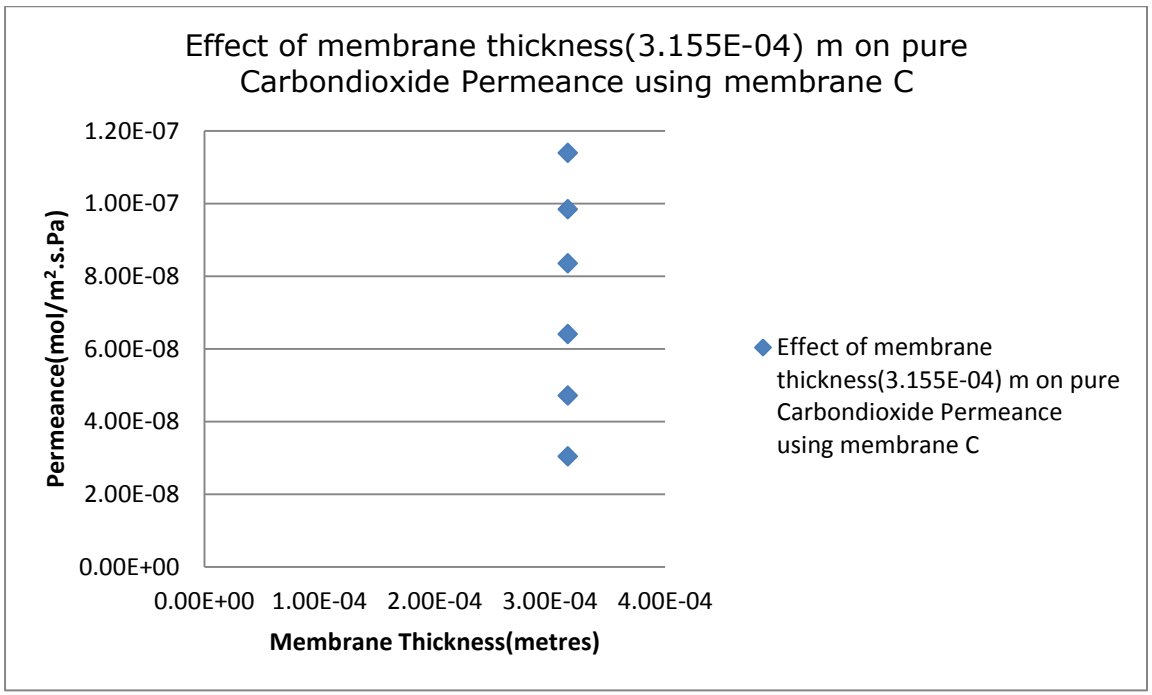

Figure 8:: Effect of membrane thickness (3.155E-04) m on Pure CO_2 Permeance using Membrane C

Table 8:176: Pure CO_2 Permeance using membrane C of thickness 1.926E-04m

Permeance(mol.m^{-2}.s^{-1}.Pa^{-1})	Membrane Thickness(metres)
2.60E-08	1.926E-04
3.44E-08	1.926E-04
4.64E-08	1.926E-04
6.27E-08	1.926E-04
6.98E-08	1.926E-04
7.73E-08	1.926E-04

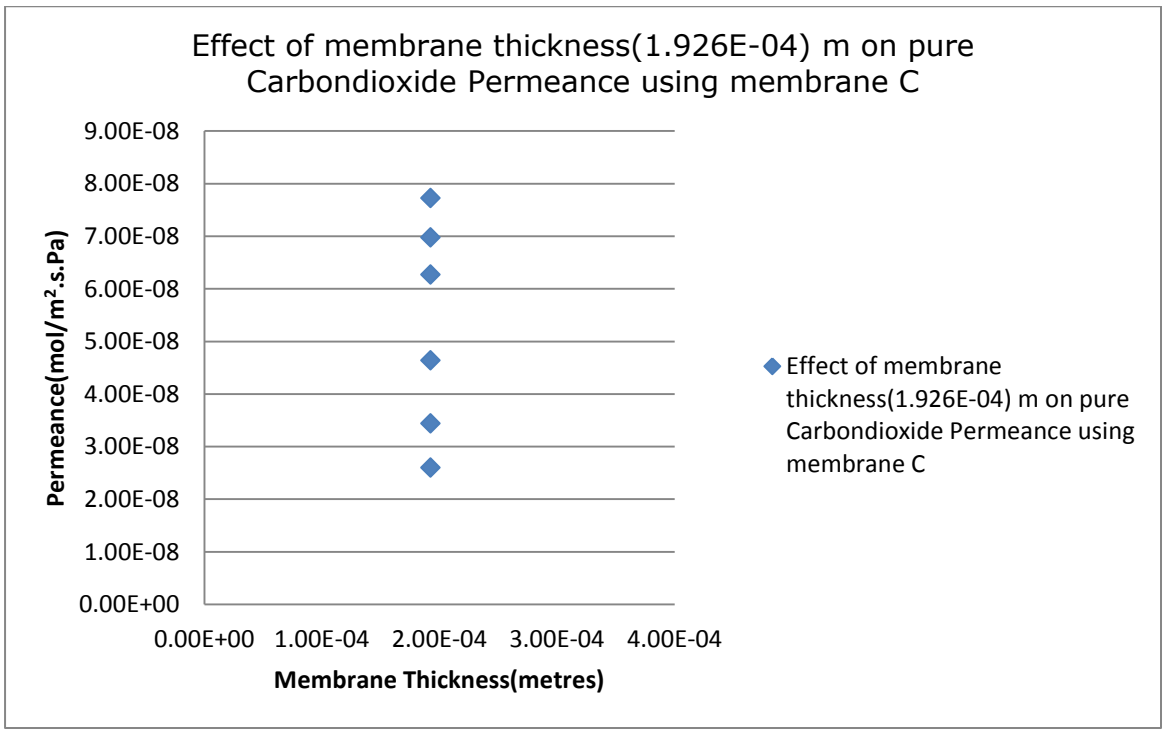

Figure 8:110: Effect of membrane thickness (1.926E-04) m on Pure CO_2 Permeance using membrane C

Table 8:177: Pure CO_2 Permeance using Membrane C of thickness 1.965E-04m

Permeance(mol.m^{-2}.s^{-1}.Pa^{-1})	Membrane Thickness(metres)
1.30E-08	1.965E-04
2.15E-08	1.965E-04
2.95E-08	1.965E-04
4.18E-08	1.965E-04
5.34E-08	1.965E-04
6.10E-08	1.965E-04

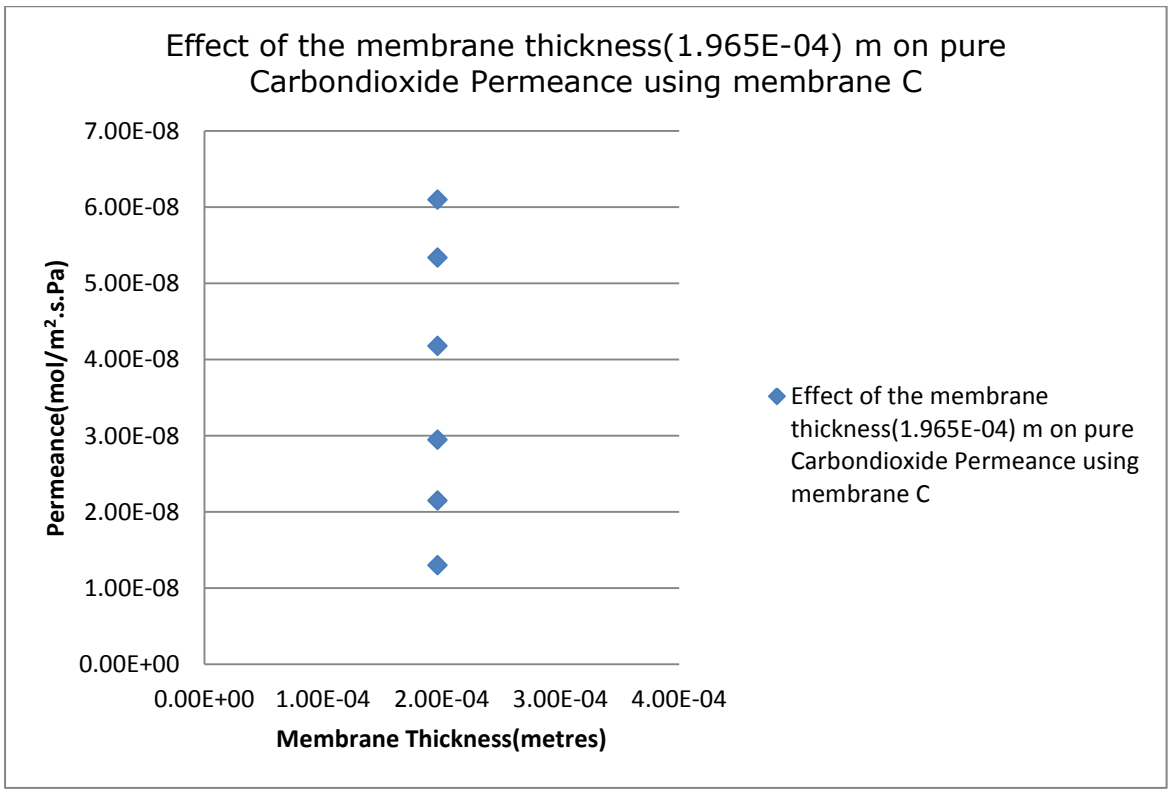

Figure 8:111: Effect of membrane thickness (1.965E-04) m on Pure CO_2 Permeance using Membrane C

Table 8:178: Pure CO_2 Permeance using Membrane C of thickness 2.00E-04m

Permeance(mol.m^{-2}.s^{-1}.Pa^{-1})	Membrane Thickness(metres)
2.60E-09	2.00E-04
6.88E-09	2.00E-04
1.01E-08	2.00E-04
1.59E-08	2.00E-04
2.05E-08	2.00E-04
2.85E-08	2.00E-04

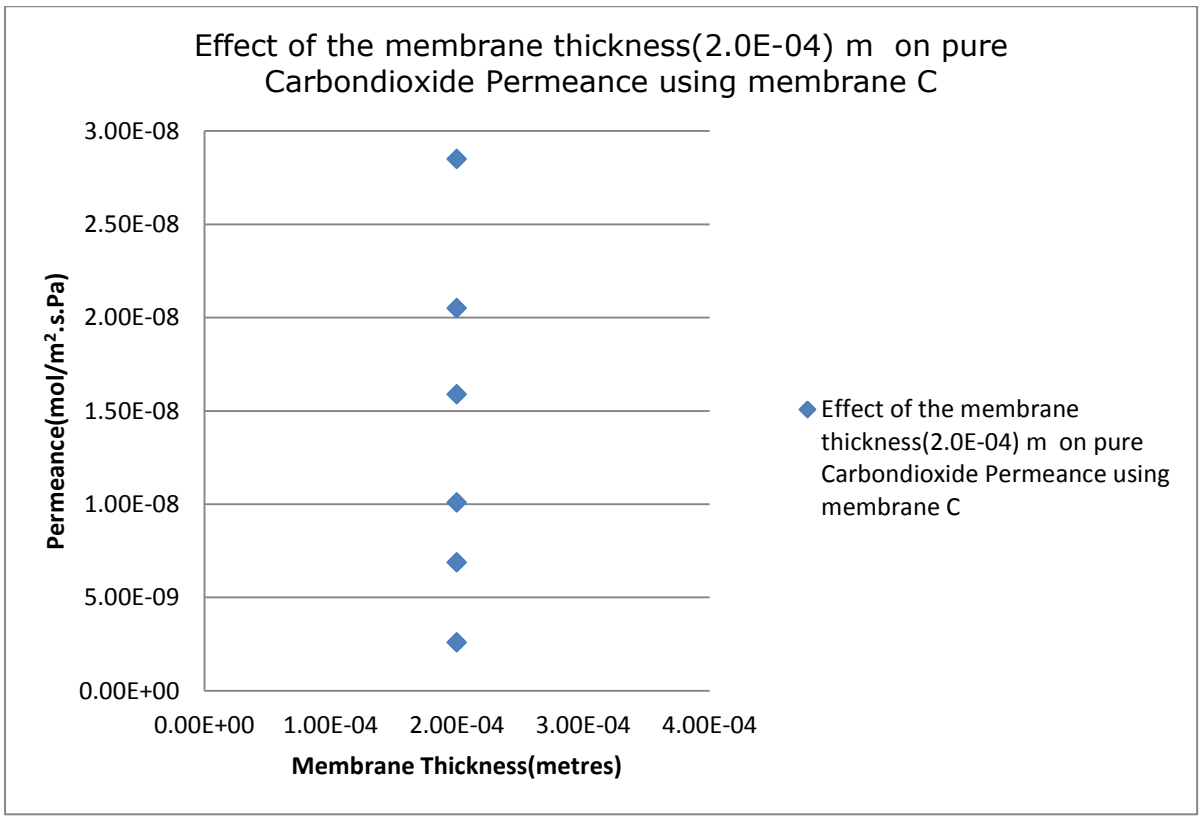

Figure 8:112: Effect of membrane thickness (2.00E-04) m on Pure CO_2 Permeance using Membrane C

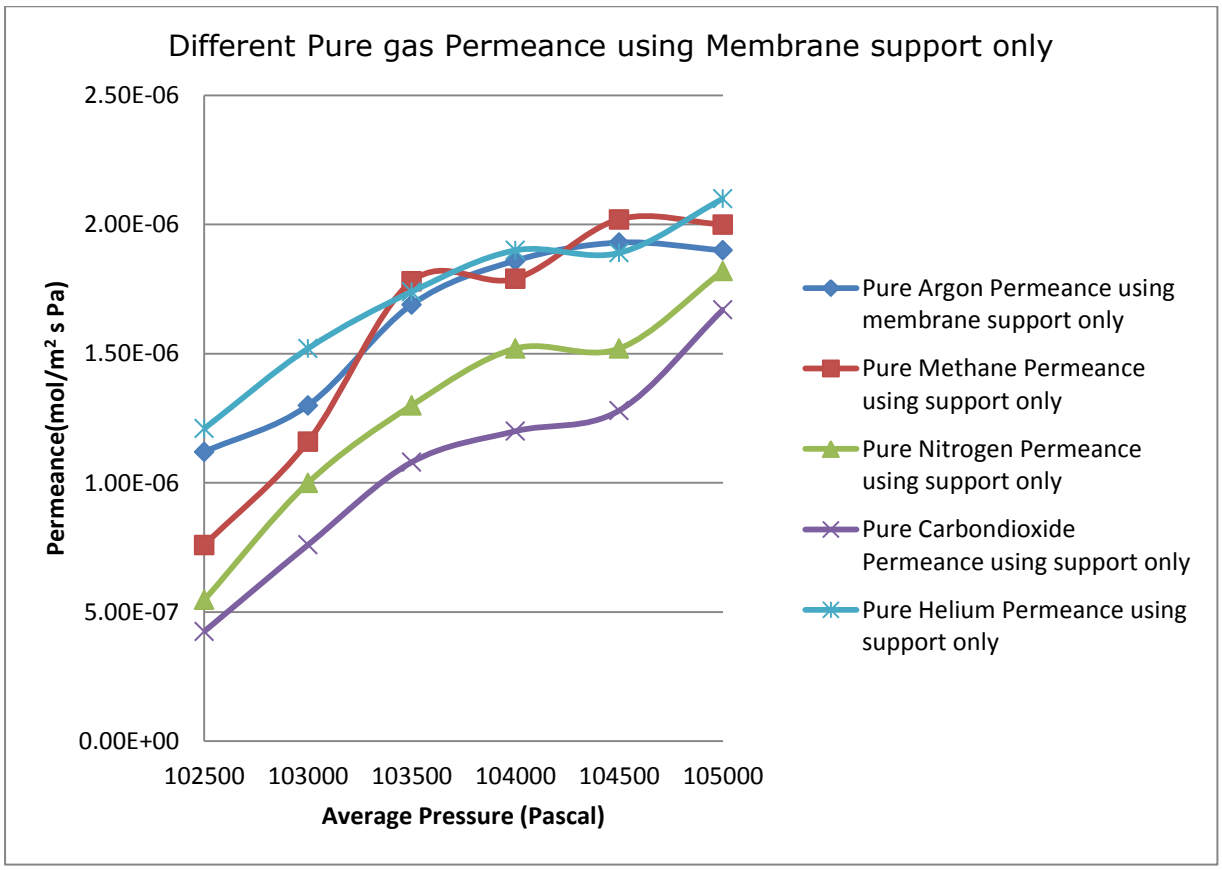

Figure 8:113: Different Pure Gas Permeance using Membrane support only

```
Workstation: RG02701                    Bus Address  : 44
Instrument : Varian Star #1             Sample Rate  : 10.00 Hz
Channel    : Front = TCD                Run Time     : 6.495 min

** GC Workstation Multi Instrument Version 6.41 ** 01141-2588-C69-24B5 **

Chart Speed =    3.27 cm/min   Attenuation = 62          Zero Offset = 2%
Start Time  =    0.000   min    End Time    = 6.495   min   Min / Tick  = 1.00
```

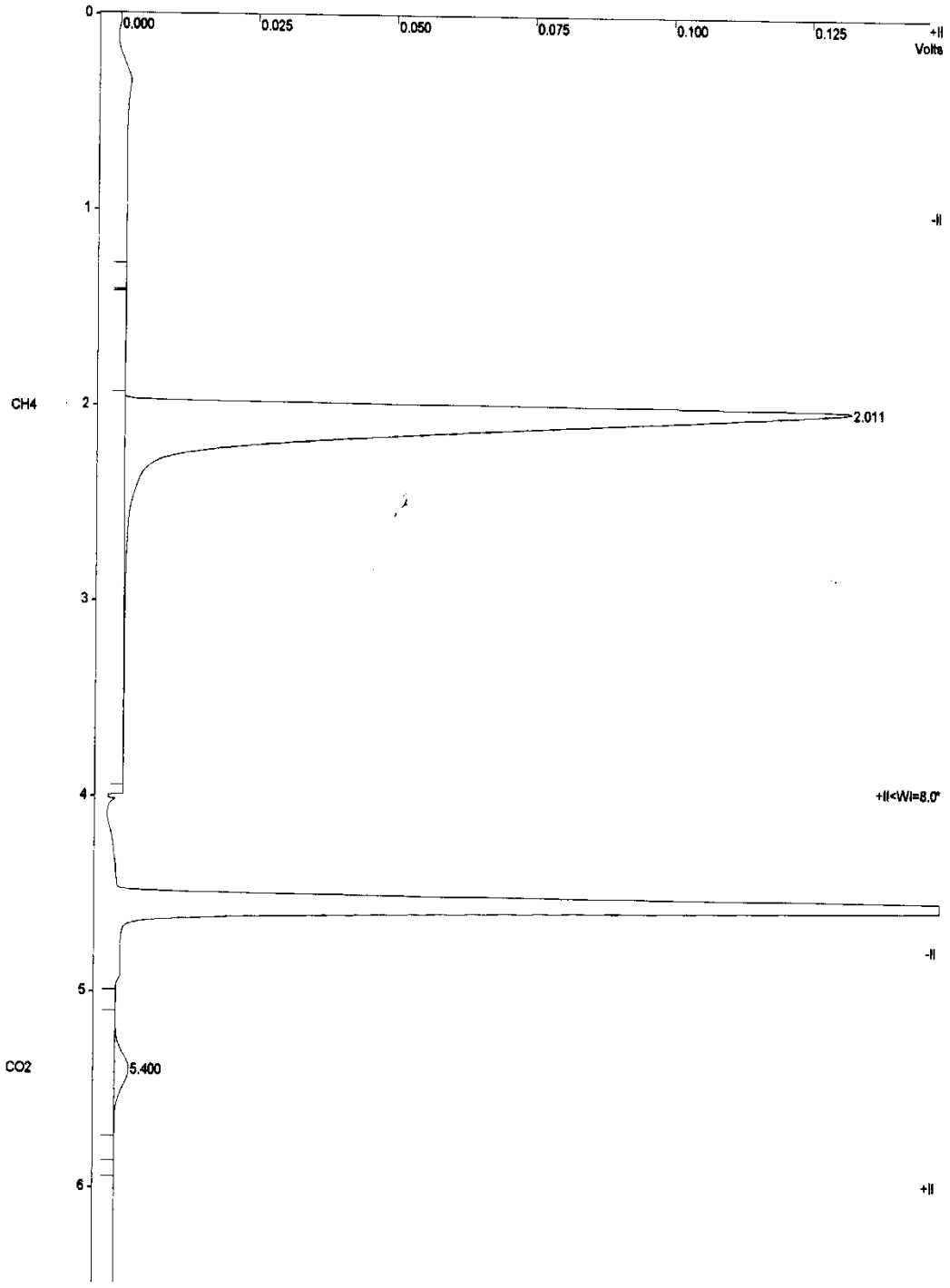

Figure 8:114: GC graph showing $C0_2$ and CH_4 peaks

Workstation: RG02701 Bus Address : 44
Instrument : Varian Star #1 Sample Rate : 10.00 Hz
Channel : Front = TCD Run Time : 8.493 min

** GC Workstation Multi Instrument Version 6.41 ** 01141-2588-C69-24B5 **

Chart Speed = 2.50 cm/min Attenuation = 16 Zero Offset = 4%
Start Time = 0.000 min End Time = 8.493 min Min / Tick = 1.00

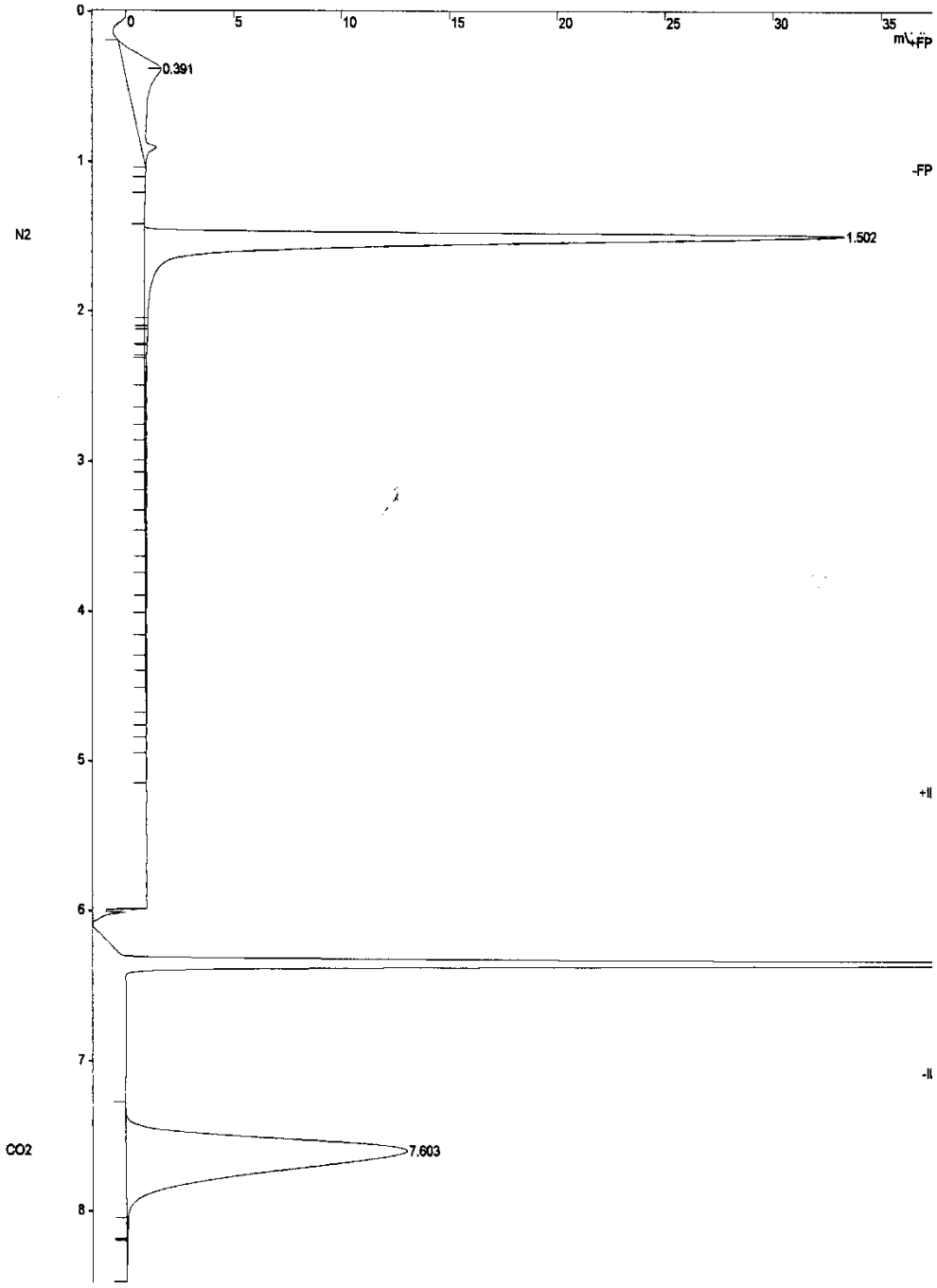

Figure 8:115: GC graph showing $C0_2$ and N_2 peaks

Table 8:179: GC results showing the $C0_2$ / CH_4 Recovery efficiency

Detector Type: 3800 (10 Volts)
Workstation: RG02701
Bus Address : 44
Instrument : Varian Star #1
Sample Rate : 10.00 Hz
Channel : Front = TCD
Run Time : 6.495 min

** GC Workstation Multi Instrument Version 6.41 ** 01141-2588-C69-24B5 **

Run Mode : Analysis
Peak Measurement: Peak Area
Calculation Type: External Standard

Peak No.	Peak Name	Result ()	Ret. Time (min)	Time Offset (min)	Area (counts)	Sep. Code	Width 1/2 (sec)	Group	Status Codes
1	CH4	80.9595	2.012	0.002	1057934	BB	7.7	0	
2		0.0000	4.934	0.000	4104	BP	9.4	0	
3	CO2	16.8680	5.379	-0.018	50790	PB	9.8	0	C
	Group 0	97.8275		-0.016	1112828				
	Totals:	97.8275		-0.016	1112828				

Status Codes:
C - Out of calibration range

Total Unidentified Counts : 4104 counts

Detected Peaks: 5 Rejected Peaks: 2 Identified Peaks: 2

Multiplier: 1 Divisor: 1 Unidentified Peak Factor: 0

Baseline Offset: -52 microVolts LSB: 1 microVolts

Noise (used): 3 microVolts - monitored before this run

Manual injection

Calib. out of range; No Recovery Action Specified

****

8.12 APPENDIX 12: SOURCES OF ERROR AND ANALYSES

8.12.1 Introduction

Errors are inevitable in our human activities, but they can be minimized. Several errors were encountered in different stages in this project. Some errors were unavoidable, avoidable and by oversight. Some of the errors were derived from different sources such as equipment poor calibration, data measurement, data assumptions, weather condition, and human factor.

8.12.2 Error from poor calibration of Equipment

The equipment calibrations were necessary to ensure accurate data being provided by all the equipment. Calibrations were always carried out before data measurement and analyses. This act definitely minimised the error due to equipment malfunction. Some of the equipment that were regularly calibrated included Gas chromatograph machines, Mass Flow Controller, Gas Flow meter, Digital Thermometers Carbolite $33O^0C$ Oven, Carbolite 1100^0C Furnace.

8.12.3 Human Factor

Human Error is known to be the main sources of error in any experimental work. In order to minimise this particular source of error, regular training of every new equipment was provided and also, data collections and reading were always done with extreme care with repeated procedure, to ensure correct data being reported.

8.12.4 Data Measurement

Measuring of experimental data is one of the major sources of error. Data measured and collated in this work were based on the average or mean values. This mean value was adopted to minimize the error.

8.12.5 Data Assumptions

Data assumption contributed to the errors in this work. Some data used in this work were assumed due to lack of possibility of determining the real membrane data for the project. This was shown clearly in comparing the theoretical permeability of the membrane to experimental permeability. The values showed that the experimental permeability values were found to be higher than the theoretical experimental values. This could be because in the surface flow model that was used to determine the theoretical permeability; DS, KS and ε values were assumed which had introduced deviation from the values determined experimentally.

8.12.6 Uncertainty Errors

These types of errors are caused by natural fluctuations or irregularities. For instance, the fluctuation introduced by weather condition might force experimental equipment to introduce error to the measurement. These cannot be eliminated due to their uncontrollable tendency.

8.13 EXPRESSING ERRORS

For each measured value, A, there is an estimated error, ΔA [62] [63]. The complete result is given by $A \pm \Delta A$. This shows that true values probably falls between a maximum values A+ΔA and a minimum value of A-ΔA. At times, the terms relative error and percentage error are used to estimate the errors. Hence,

$$\text{Relative Error} = \frac{\Delta A}{A} \qquad 3.8$$

and Percentage Error = Relative Error x 100%

Where ΔA represent an estimated Error and A, a measured value.

To demonstrate the error in the measured data using data from table 8:1. Assuming that the major source of the error in the experiment was from the

equipment. For instance, the flow meter used in the permeation measurement had a limited accuracy of +/- 0.05.This value shows that the true value measured lies between these limits. Applying this to the measured values in the table 8:1, we have relative and percentage errors shown in table 8:180 using numerical algorithm approach.

Table 8:180 Permeation results with the Relative and Percentage Errors Expression

$P_F$eed (Bar) Absolute	$P_{Permeate}$ (Bar) Absolute	ΔP(Bar) Pressure Drop Absolute (P_F - P_P)	Pure Methane Permeate Flow Rate (ml/min)	Maximum Methane Flow Rate (ml/min)	Minimum Methane Flow Rate (ml/min)	Relative Error	Percentage Error (X100)
1.05	1.00	0.05	100	100.05	99.95	5.00E-4	0.05
1.06	1.00	0.06	210	210.05	209.95	2.00E-4	0.02
1.07	1.00	0.07	310	310.05	309.95	1.61E-4	0.016
1.08	1.00	0.08	450	450.05	449.95	1.10E-4	0.011
1.09	1.00	0.09	550	550.05	549.95	9.09E-5	0.009
1.1	1.00	0.1	650	650.05	649.95	8.00E-5	0.008

From table 8:180 above, the degree of error decreases as the permeation data increases.